

# Wetting phenomena in electrolyte solutions

Von der Fakultät für Mathematik und Physik der Universität Stuttgart zur Erlangung der Würde einer Doktorin der Naturwissenschaften (Dr. rer. nat.) genehmigte Abhandlung

Vorgelegt von

**Ingrid Carolina Ibagon Pardo**

aus Choachí, Kolumbien

Hauptberichter: Prof. Dr. S. Dietrich

Mitberichter: Prof. Dr. C. Holm

Tag der mündlichen Prüfung: 24. November 2014

Max-Planck-Institut für Intelligente Systeme  
Stuttgart

und

IV. Institut für Theoretische Physik  
Universität Stuttgart

2014



This thesis is related to the following publications:

Ref. [169] :

I. Ibagon, M. Bier, S. Dietrich, *Wetting in electrolyte solutions*, J. Chem. Phys. **138**, 214703 (2013).

Ref. [139]:

M. Bier and I. Ibagon, *Density functional theory of electrowetting*, Phys. Rev. E **89**, 042409 (2014).

Ref. [226] :

I. Ibagon, M. Bier, S. Dietrich, *Order of wetting transitions in electrolyte solutions*, J. Chem. Phys. **140**, 174713 (2014).

I. Ibagon, M. Bier, S. Dietrich, *Three phase contact line and line tension of an electrolyte solution in contact with a charged substrate* in preparation for publication.



# Erklärung

Hiermit erkläre ich gemäß §6 Absatz (3) der Promotionsordnung der Universität Stuttgart, dass ich, abgesehen von den ausdrücklich bezeichneten Hilfsmitteln und den Ratschlägen von jeweils namentlich aufgeführten Personen, die Dissertation selbständig verfasst habe.

Stuttgart, 26.09.2014

Ingrid Carolina Ibagón Pardo



# Acknowledgments

I am really thankful to Prof. Dr. S. Dietrich for giving me the opportunity to perform my doctoral studies at his department at the Max-Planck Institut for Intelligent Systems in Stuttgart. I am grateful for all the scientific discussions we had and his crucial comments and ideas which contributed significantly to this project.

I am very grateful to my direct supervisor, Dr. Markus Bier, for his patience and guidance since the first day I arrived to Stuttgart. I also thank him for all the time he dedicated to this project, specially during the first year when he introduced me to classical DFT and theory of liquids, and for his careful proofreading of the manuscript of this thesis. Overall he has been an excellent advisor.

Thanks to Prof. Dr. C. Holm for co-refereeing this thesis.

I thank all my present and former colleagues at Prof. Dietrich's Department for the friendly work atmosphere.

Many thanks to Ms. Anke Geigle for her help with administrative and not administrative issues.

Gracias a mis padres porque sin su amor, sus esfuerzos y sus sacrificios yo no habría llegado hasta aquí. Gracias a mis hermanas por el amor y la amistad incondicional. Gracias a los cuatro por haber venido a visitarme haciendo más felices mis vacaciones.

Obrigada ao Thiaguim, meu marido, pelo amor, pela paciência, e por me animar e encorajar a terminar este doutorado. Obrigada também por ler e corrigir todos meus textos em português e em inglês várias vezes. Enfim, obrigada por fazer minha vida mais fácil ♡.

Thanks to Reka and Jorge, my (ex)neighbors, who let me in into their lives and introduced me to their nice friends: Birgit, Armando, Elena, Marco, Karen, Noreen, Rafael, Samira and Maxim which became our friends too. Thanks to all of them and to Yazil and Carlos, which became part of the group recently, for all the fun and the delicious food and drinks we have shared. Thanks also for having lovely children: Aazar, Leo, Samuel and Mariana which made our get-togethers more special.

Thanks to Carlos Parra, Sophia Hopp and Andreas Reindl for their valuable help with the German version of the summary.





# Contents

<b>Summary</b>	<b>13</b>
<b>Zusammenfassung</b>	<b>17</b>
<b>1 Introduction</b>	<b>21</b>
1.1 Bulk electrolyte solutions . . . . .	23
1.2 Fluids near planar charged surfaces . . . . .	24
1.3 Wetting behavior in systems with ions . . . . .	28
1.4 Line tension . . . . .	30
<b>2 General formalism</b>	<b>33</b>
2.1 Classical density functional theory . . . . .	33
2.2 Wetting . . . . .	36
2.2.1 Effective interface potential and the contact angle . . . . .	39
2.3 Line tension of a sessile liquid drop . . . . .	40
2.3.1 Substrate-fluid dividing interface . . . . .	41
2.3.2 Line tension of a liquid wedge . . . . .	41
2.3.3 Line tension of a sessile drop . . . . .	43
<b>3 Wetting in electrolyte solutions: a lattice model</b>	<b>47</b>
3.1 Model . . . . .	47
3.2 Density functional . . . . .	49
3.2.1 Wetting films . . . . .	54
3.2.2 Choice of parameters . . . . .	55
3.3 Bulk phase diagram . . . . .	55
3.4 Wetting . . . . .	57
3.4.1 Wetting in the salt-free solvent . . . . .	57
3.4.2 Wetting in electrolyte solution . . . . .	60

<b>4</b>	<b>Wetting in electrolyte solutions: a continuum model</b>	<b>65</b>
4.1	Model with short-ranged interactions . . . . .	65
4.1.1	Pure solvent . . . . .	76
4.1.2	Electrolyte solution . . . . .	77
4.2	Model with long-ranged interactions . . . . .	78
<b>5</b>	<b>Density functional theory of electrowetting</b>	<b>87</b>
5.1	Theoretical considerations . . . . .	87
5.1.1	Setting . . . . .	87
5.1.2	Contact angle and effective interface potential . . . . .	88
5.1.3	Density functional theory of wetting . . . . .	91
5.1.4	Electrowetting equation . . . . .	95
5.2	Discussion . . . . .	97
5.2.1	Electrowetting and electrocapillarity . . . . .	97
5.2.2	Electrowetting on uncoated metal electrodes . . . . .	99
5.2.3	Electrowetting of water on hydrophobic dielectrics in oil . . . . .	100
5.2.4	Electrowetting of water on hydrophilic dielectrics in oil . . . . .	101
5.2.5	Electrowetting of immiscible electrolyte solutions on dielectrics . . .	102
<b>6</b>	<b>Three phase contact line and line tension of an electrolyte solution in contact with a charged substrate</b>	<b>105</b>
6.1	Density functional . . . . .	106
6.2	Line tension calculation . . . . .	108
6.3	Pure solvent . . . . .	108
6.4	Electrolyte solution . . . . .	110
6.4.1	Density distributions close to the three phase contact line . . . . .	113
<b>7</b>	<b>Conclusions and outlook</b>	<b>117</b>
<b>A</b>	<b>Bulk correlation length of the pure solvent</b>	<b>121</b>
<b>B</b>	<b>Double parabola approximation for the pure solvent</b>	<b>123</b>
<b>C</b>	<b>First-order perturbation theory for including the long-ranged interactions</b>	<b>127</b>
<b>D</b>	<b>Coefficients for the effective interface potential in the presence of long-ranged interactions</b>	<b>129</b>

E Derivation of the effective interface potential for the model with long-ranged interactions	133
F Line tension calculation in the lattice model	145
Curriculum vitae	161



# Summary

The present study analyzes wetting phenomena in electrolyte solutions. They are investigated by means of classical density functional theory. First, the wetting of a charged substrate by an electrolyte solution is studied with emphasis on the influence of the substrate charge density and of the ionic strength on the wetting transition temperature and on the order of the wetting transition. The corresponding models consist of solvent particles, anions, and cations. Two mean field approaches are used: (1) A lattice model (Chap. 3) within which particles occupy the sites of a semi-infinite simple cubic lattice. Each site is either empty or occupied by a single particle and the particles interact among each other via an attractive nearest-neighbor interaction which is taken to be the same for all pairs of particles. In addition, ion pairs interact via the Coulomb potential. The substrate can carry a homogeneous surface charge density and additionally attracts particles in the first layer adjacent to it. (2) A continuum model (Chap. 4) with short- and long-ranged solvent-solvent and substrate-solvent interactions and with ions interacting among each other and with the wall only via the electrostatic field. The motivation to use a lattice model for this system is that this kind of model offers the possibility to study broad interfacial regions, which is important for wetting phenomena studies, with a lower computational cost in comparison to continuum models.

For the lattice model, the bulk phase behavior has been obtained (see Fig. 3.1) as a function of the ionic strength. Within this model the reduced critical temperature is independent of the ionic strength whereas the critical density depends linearly on it. The wetting phenomena are analyzed in terms of the effective interface potential, which is calculated numerically for this model. The pure, i.e., salt-free, solvent exhibits a second-order wetting transition for all strengths of the substrate-particle and the particle-particle interactions for which the wetting transition temperature is nonzero (Fig. 3.2). Depending on the value of the ratio between the strengths of the substrate-fluid and fluid-fluid interactions, the model can exhibit layering transitions when gas-liquid coexistence is approached along an isotherm (Fig. 3.3). Next, the influence of the substrate charge density and of the ionic strength on the wetting transition temperature and on the order

of the wetting transition are studied. If the substrate is neutral, the addition of salt to the solvent changes neither the order nor the transition temperature of the wetting transition of the system. On the other hand, if the surface charge is nonzero, upon adding salt this continuous wetting transition changes to first-order within the range of substrate surface charge densities and ionic strengths considered here (Fig. 3.4). As the substrate surface charge density is increased, for fixed ionic strength, the wetting transition temperature decreases. Moreover, the wetting transition temperature decreases when the ionic strength is decreased for fixed surface charge density  $\sigma$  (Fig. 3.5). When bulk coexistence is approached along an isotherm, in the case of a first-order wetting transition, i.e., if  $\sigma \neq 0$ , the model exhibits first-order layering transitions in addition to prewetting (Fig. 3.6). This leads to a series of triple points in the surface phase diagram (see Fig. 3.7). The prewetting line associated with the first-order wetting transition becomes longer as the surface charge density is increased (Fig. 3.8).

For the continuum model, expressions for the effective interface potential are derived analytically. The analysis of these expressions renders the conditions under which corresponding wetting transitions can be first- or second-order. Within mean field theory two cases are considered: One with only short-ranged solvent-solvent and substrate-solvent interactions and one with both short- and long-ranged solvent-solvent and solvent-wall interactions. The analytic results reveal in a transparent way that wetting transitions in electrolyte solutions, which occur far away from their critical point (i.e., the bulk correlation length is less than half of the Debye length), are always first-order if the solvent-solvent and solvent-wall interactions are short-ranged. In contrast, wetting transitions close to the bulk critical point of the solvent (i.e., the bulk correlation length is larger than the Debye length) exhibit the same wetting behavior as the pure, i.e., salt-free, solvent. If the salt-free solvent is governed by long-ranged solvent-solvent as well as long-ranged substrate-solvent interactions and exhibits critical wetting, adding salt can cause the occurrence of an ion-induced first-order thin-thick transition which precedes the subsequent continuous wetting as for the salt-free solvent (Fig. 4.1).

The phenomenon of electrowetting, i.e., the dependence of the macroscopic contact angle of a fluid on the electrostatic potential of the substrate, is studied in Chap. 5 for a vertical parallel plate capacitor in contact with two immiscible fluids, where at least one of the two fluids is an electrolyte solution (Fig. 5.1). This system is studied by using density functional theory applied to a continuum model similar to the one presented in Chap. 4. Here, the possibility of the formation of films of microscopic thickness on the substrates, widely ignored in the context of electrowetting, is taken into account (Fig. 5.2). This approach allows one to transparently derive the electrowetting equation (5.18). The

derivation shows that electrowetting is a consequence of the voltage-dependence of the depth of the effective interface potential. Moreover, it is shown that the traditional electrocapillarity approach to electrowetting, i.e., the assumption that electrowetting is a consequence of the voltage-dependence of the substrate-fluid interfacial tension, is a good approximation for the cases of metallic electrodes or electrodes coated with a hydrophobic dielectric in contact with an electrolyte solution and an ion-free oil. In contrast, a significantly reduced tendency for electrowetting is predicted for electrodes coated with a dielectric which is hydrophilic or which is in contact with two immiscible electrolyte solutions.

Finally, the line tension and the three-phase contact line structure of a drop of an electrolyte solution on a charged substrate are investigated within the lattice model in Chap. 6. For the pure, i.e., salt-free, solvent, the equilibrium liquid-gas interface profile approaches its asymptote from above, as expected for second-order wetting transitions (Fig. 6.2) and the line tension depends linearly on the contact angle the drop makes with the substrate (Fig. 6.3). For the electrolyte solution, the equilibrium liquid-gas interface profile approaches its asymptote from below as expected for first-order wetting transitions (Fig. 6.4). When the contact angle is changed by varying the temperature while keeping the surface charge fixed, the line tension increases as the temperature is increased, i.e., as the contact angle is decreased. For fixed temperature, the line tension is smaller for the larger ionic strength (Fig. 6.5). When the contact angle is changed by varying the surface charge density at fixed temperature, the line tension increases as the surface charge is increased. The increase of the line tension depends weakly on the ionic strength for very small surface charge. However, as the surface charge is increased, the increase of the line tension becomes more pronounced for the smaller ionic strength (Fig. 6.6). The equilibrium structure of the three-phase contact line for different charge densities has been calculated. For large surface charge densities, non-linear effects of the Poisson-Boltzmann theory are more important. This results in a different structure for the  $\pm$ -ions and for the electrostatic potential when compared with small surface charge densities (Figs. 6.7, 6.8 and 6.9).





# Zusammenfassung

In der vorliegenden Arbeit werden Benetzungsphänomene in Elektrolytlösungen mittels klassischer Dichtefunktionaltheorie untersucht. Zunächst wird der Einfluss der Oberflächenladungsdichte und der Ionenstärke auf die Übergangstemperatur und die Ordnung des Benetzungsübergangs beim Benetzen eines elektrisch geladenen Substrats durch eine Elektrolytlösung studiert. Die hier betrachteten Elektrolytlösungen bestehend aus drei Teilchensorten: Lösungsmittel, Anionen und Kationen. Es werden zwei verschiedene Molekularfeld-Näherungen verwendet:

- (1) Ein Gitter-Modell (Kapitel 3), in welchem die Gitterplätze eines halbunendlichen einfach-kubischen Gitters entweder leer oder von nur einem Teilchen besetzt sind. Alle direkt benachbarten Teilchen wechselwirken attraktiv miteinander. Zusätzlich wechselwirken Ionen durch das Coulomb-Potential miteinander. Das Substrat kann eine homogene Oberflächenladung tragen und zusätzlich wirkt es attraktiv auf die Fluid-Teilchen in der direkt angrenzenden Schicht.
- (2) Ein Kontinuum-Modell (Kapitel 4) mit kurz- und langreichweitigen Wechselwirkungen, in welchem die Ionen miteinander und mit der Wand ausschließlich mittels des elektrostatischen Felds wechselwirken.

Für das Gitter-Modell wurde das Phasenverhalten als Funktion der Ionenstärke bestimmt (Abb. 3.1). Innerhalb dieses Modells ist die reduzierte kritische Temperatur unabhängig von der Ionenstärke, wohingegen sich die kritische Dichte linear mit der Ionenstärke ändert. Die Analyse der Benetzungsphänomene wird mit Hilfe des effektiven Grenzflächenpotentials vorgenommen, welches für dieses Modell numerisch berechnet wurde. Die reine, d.h. salzfreie, Lösung zeigt einen Benetzungsübergang zweiter Ordnung bei allen Stärken der Substrat-Fluid- und der Fluid-Fluid-Wechselwirkung, bei denen die Benetzungstemperatur über dem absoluten Nullpunkt liegt (Abb. 3.2). In Abhängigkeit vom Wert des Verhältnisses zwischen den Stärken der Substrat-Fluid- und der Fluid-Fluid-Wechselwirkung kann das Modell bei isothermer Annäherung an die Gas-Flüssigkeits-Koexistenz sogenannte “layering transitions” zeigen (Abb. 3.3). Als nächstes wurde der Einfluss der Ladungsdichte des Substrats und der Ionenstärke auf die Tem-

peratur und die Ordnung des Benetzungsübergangs untersucht. Bei einem elektrisch neutralen Substrat ändert die Zugabe von Salz zur Lösung weder die Temperatur noch die Ordnung des Benetzungsübergangs. Ist das Substrat hingegen geladen, ändert sich für die hier betrachteten Ladungsdichten und Ionenstärken der kontinuierliche Benetzungsübergang in einen erster Ordnung (Abb. 3.4). Bei konstanter Ionenstärke sinkt die Benetzungstemperatur mit steigender Oberflächenladungsdichte. Außerdem sinkt die Benetzungstemperatur bei konstanter Oberflächenladungsdichte mit abnehmender Ionenstärke (Abb. 3.5). Bei isothermer Annäherung an die Koexistenz tritt bei einem Benetzungsübergang von erster Ordnung, d.h. bei geladenem Substrat, nicht nur das übliche Vorbenetzen (“prewetting”) auf, sondern auch zusätzlich “layering transitions” erster Ordnung (Abb. 3.6). Dies führt zu einer Folge von Tripelpunkten im Oberflächenphasendiagramm (Abb. 3.7). Die mit dem Benetzungsübergang erster Ordnung verbundene Vorbenetzungslinie wird länger, wenn die Oberflächenladung erhöht wird.

Innerhalb des Kontinuummodells wurden analytische Ausdrücke für das effektive Grenzflächenpotential hergeleitet. Eine Analyse dieser Ausdrücke gibt Aufschluss über die Bedingungen, unter welchen Benetzungsübergänge von erster Ordnung oder kontinuierlich sein können. Im Rahmen der Molekularfeldtheorie wurden zwei Fälle betrachtet: einerseits ausschließlich kurzreichweitige Wechselwirkungen und andererseits sowohl lang- als auch kurzreichweitige Wechselwirkungen. Die analytischen Ergebnisse zeigen, dass Benetzungsübergänge in Elektrolytlösungen weit entfernt vom kritischen Punkt (d.h. die Korrelationslänge beträgt weniger als die Hälfte der Debye-Länge) bei ausschließlich kurzreichweitigen Wechselwirkungen stets von erster Ordnung sind. Dagegen zeigen Benetzungsübergänge in der Nähe des kritischen Punkts (d.h. die Korrelationslänge ist größer als die Debye-Länge) dasselbe Benetzungsverhalten wie das reine, d.h. salzfreie, Lösungsmittel. Wenn das salzfreie Lösungsmittel durch langreichweitige Wechselwirkungen beschrieben wird und einen kritischen Benetzungsübergang aufweist, kann das Hinzufügen von Salz das Auftreten eines ioneninduzierten dünn-dick bergangs erster Ordnung bewirken, der anschließendem kontinuierlichem Benetzen vorausgeht, wie beim salzfreien Lösungsmittel (Abb. 4.1).

Das Phänomen “electrowetting”, d.h. die Abhängigkeit des makroskopischen Kontaktwinkels eines Fluids vom elektrostatischen Potential des Substrats, wird in Kapitel 5 für den Fall eines vertikalen Plattenkondensators in Kontakt mit zwei nicht mischbaren Fluiden untersucht, von denen mindestens eine eine elektrolytische Lösung ist (Abb. 5.1). Dieses System wird mittels Dichtefunktionaltheorie untersucht, die auf ein Kontinuummodell angewendet wird, welches dem in Kapitel 4 vorgestellten ähnlich ist. Dabei wird die weithin ignorierte Möglichkeit berücksichtigt, dass sich Benetzungsfilme

mikroskopischer Dicke auf dem Substrat bilden können (Abb. 5.2). Dieser Ansatz erlaubt es die sogenannte “electrowetting equation” (5.18) herzuleiten. Diese Herleitung zeigt, dass “electrowetting” eine Folge der Spannungsabhängigkeit der Tiefe des effektiven Grenzflächenpotentials ist. Außerdem wird gezeigt, dass der traditionelle Elektrokapillariätszugang, d.h. die Annahme, dass “electrowetting” eine Folge der Spannungsabhängigkeit der Substrat-Fluid Grenzflächenspannung ist, eine gute Näherung darstellt für die Fälle, dass metallische oder mit einem hydrophoben Dielektrikum beschichtete Elektroden in Kontakt mit einer Elektrolytlösung und einem salzfreien Öl vorliegen. Dagegen wird eine deutlich verringerte Tendenz für “electrowetting” bei hydrophil beschichteten Elektroden oder bei zwei nicht mischbaren Elektrolytlösungen vorausgesagt.

Schließlich wurden die Linienspannung und die Struktur der Dreiphasenkontaktlinie eines Tropfens elektrolytischer Lösung auf einem geladenen Substrat innerhalb des Gittermodells in Kapitel 6 untersucht. Im Falle des reinen, d.h. salzfreien, Lösungsmittels nähert sich das Grenzflächenprofil zwischen Flüssigkeit und Gas seiner Asymptoten “von oben” an, wie dies für kontinuierliche Benetzungsübergänge erwartet wird (Abb. 6.2), und die Linienspannung hängt linear vom Kontaktwinkel ab, den der Tropfen mit dem Substrat bildet (Abb. 6.3). Im Fall der elektrolytischen Lösung nähert sich das Grenzflächenprofil zwischen Flüssigkeit und Gas seiner Asymptoten “von unten” an, wie dies für Benetzungsübergänge erster Ordnung zu erwarten ist (Abb. 6.4). Wenn der Kontaktwinkel durch Temperaturerhöhung bei konstanter Oberflächenladung verringert wird, erhöht sich die Linienspannung. Bei konstanter Temperatur nimmt die Linienspannung mit steigender Ionenstärke ab (Abb. 6.5). Wenn der Kontaktwinkel durch Erhöhung der Oberflächenladungsdichte bei konstanter Temperatur verringert wird, erhöht sich die Linienspannung. Der Anstieg der Linienspannung hängt für sehr kleine Oberflächenladungen schwach von der Ionenstärke ab. Wird jedoch die Oberflächenladung erhöht, so ist der Anstieg der Linienspannung ausgeprägter bei kleinen Ionenstärken (Abb. 6.6). Die Gleichgewichtsstruktur der Dreiphasenkontaktlinie wurde für verschiedene Ladungsdichten berechnet. Bei großen Oberflächenladungsdichten sind nichtlineare Effekte der Poisson-Boltzmann-Theorie wichtig. Verglichen mit kleinen Oberflächenladungsdichten resultiert dies in einer andersartigen Struktur der Dichteprofile der Ionen und des elektrostatischen Potentials (Abb. 6.7, 6.8 und 6.9).



# Chapter 1

## Introduction

This thesis deals with wetting in electrolyte solutions, which are of great importance in physical chemistry and biophysical systems. They are ubiquitous in nature, e.g., physiological fluids and sea water are electrolyte solutions made of mixtures of sodium  $\text{Na}^+$ , chloride  $\text{Cl}^-$ , potassium  $\text{K}^+$ , and calcium  $\text{Ca}^{2+}$  ions mainly. Moreover, their susceptibility to electric fields, which can be easily controlled by electrodes, is crucial for several important processes such as electrolysis and electrowetting. These and many other relevant applications of electrolytes involve interfaces with solid media. Therefore understanding their interfacial properties is of great scientific and technological importance. Although experimental access to the interfacial structure of fluids is challenging in comparison to the bulk structure, interfacial properties such as the excess adsorption are experimentally accessible. Wetting phenomena can be addressed by analyzing the behavior of the excess adsorption in the vicinity of phase boundaries or when substrate-fluid or fluid-fluid interactions change due for example to modifications of the substrate chemistry or of the chemical composition of the fluid.

To a large extent, wetting studies have been devoted to fluids composed of electrically neutral molecules such as one-component fluids and binary liquid mixtures [1–5], whereas investigations of electrolyte solutions have been challenging due to their complexity, which arises from the long-ranged Coulomb interactions between ions and the fact that they are formed at least by three constituents: solvent, cations and anions. Nevertheless, the presence of ions is of crucial importance for wetting phenomena such as electrowetting [6] (see Sec. 1.3 and Chap. 5) which offers numerous applications such as “lab-on-a-chip” devices [7, 8], adjustable lenses [9] and electronic displays [10]. The presence of ions in wetting phenomena is also unavoidable because many substrates release ions once they are brought into contact with polar solvents and because in biological and industrial application water is, strictly speaking, an electrolyte solution [11].

Most of the studies dealing with wetting properties in the presence of ions have focused on the thickness of wetting films and on the behavior of the disjoining pressure [12–16]. Only recently theoretical investigations concerning wetting transitions at coexistence of electrolyte solutions close to charged solid substrates have emerged [17–20] (See Sec. 1.3 for a brief review concerning wetting phenomena in systems with ions). However, the models in Refs. [17–20] suffer from some limitations such as restrictions to small system sizes.

In this thesis, wetting transitions at coexistence of electrolyte solutions close to charged substrates are studied. To that end, a lattice and a continuum model are investigated by means of classical density functional theory. In Chap. 2 the foundations of classical density functional theory and the basic concepts of wetting phenomena are introduced. In order to overcome the problems of previous studies, in Chap. 3 the lattice model for an electrolyte exposed to a charged substrate is introduced (Sec. 3.1). This model takes into account all three constituents, i.e., solvent, anions and cations, via density functional theory (see Sec. 2.1) and offers the possibility to study significantly broader interfacial regions than the continuum models of Refs. [19, 20]. The bulk and wetting behavior of this model are studied.

Despite the differences between the models studied in Refs. [17–20] and in Chap. 3, agreement concerning the trend that electrostatic forces favor first-order wetting transitions is found between them. Consequently, a natural question which arises is whether this observation is accidental or whether there is a deeper reason for it. To answer this question, in Chap. 4 we derive an approximate expression for the effective interface potential (see Subsec. 2.2.1) of a suitable model for an electrolyte solution near a charged wall, which has been introduced and studied in Ref. [21]. The analysis of the effective interface potential provides a transparent understanding of the wetting behavior of electrolyte solutions.

In Chap. 5 the effective interface potential for the case of a vertical parallel plate capacitor in contact with two immiscible fluids is derived and used to obtain an electrowetting equation. The cases of uncoated metal electrodes and electrodes coated with hydrophobic and hydrophilic dielectrics with an electrolyte solution and an oil as fluids are studied. In addition, the case of metal electrodes coated with dielectrics with two immiscible electrolyte solutions as fluids is also considered.

Finally, in Chap. 6 the liquid-vapor-substrate three phase contact line (TPCL) of an electrolyte solution close to a charged planar substrate is studied within the lattice model presented in Chap. 3. In particular, the influence of surface charge and ionic strength on the equilibrium structure close to the TPCL and on the line tension, i.e., the free energy

per unit length associated with the contact line, is analyzed.

The remaining of this chapter is intended to provide a short review of general issues related to the present work .

## 1.1 Bulk electrolyte solutions

In 1887 Arrhenius proposed the dissociation of salts and acids into positive ions (cations) and negative ions (anions) when they are dissolved in water [22]. Assuming that ions were non-interacting particles Arrhenius calculated the osmotic pressure of electrolyte aqueous solutions using van't Hoff's law. While the theory was proved valid for weak electrolytes, i.e., electrolytes that form a small amount of ions, it failed for strong electrolytes such as NaCl. This problem remained unsolved until Debye and Hückel published their theory of strong electrolytes [23]. They realized that, although on average ions are randomly distributed and the electrostatic field inside the electrolyte is zero, there are positional correlations between anions and cations. Due to these correlations anions tend to distribute around a cation and vice versa. As a result the electrostatic potential of the central ion is exponentially screened. Debye-Hückel theory is correct in the limit of dilute solutions [24, 25] and works quite well for 1:1 electrolytes (e.g. NaCl or KCl).

Debye-Hückel theory is based on the linearization of the Poisson-Boltzmann equation which relates the average electrostatic potential with the average ion distribution. Gronwall et al. extended the theory to overcome this linearization for the case of symmetric electrolyte solutions [26], which was later extended to asymmetric electrolyte solutions by La Mer et al. [27]. Another important extension proposed by Bjerrum [28, 29], introduces the formation of ion pairs, i.e., ions that come close enough for the energy of the attractive electrostatic interaction to be larger than the thermal energy. Integral equations have also been used to obtain the structure and thermodynamic properties of electrolyte solutions. In these theories, the Ornstein-Zernike equation [30] is solved by using some closure relation between the pair correlation function and the direct correlation function [31]. Waisman and Lebowitz [32–34] solved analytically the corresponding integral equation theory for the primitive model, which assumes ions to be oppositely charged hard spheres in a continuum dielectric (when positive and negative ions have the same size the model is called restricted primitive model (RPM)), using the mean spherical approximation (MSA) [35]. The asymptotic behavior of the thermodynamic consistent generalization of the MSA, the GMSA proposed by Høye et al. [36], has been studied in Ref. [37]. The hypernetted chain approximation has also been applied to electrolyte solutions [38, 39]. Ionic systems have been also studied using field-theoretic approaches [40–44].

In this framework, Poisson-Boltzmann theory is proven to be the saddle-point approximation of the field-theoretic action [42] and corrections can be obtained by means of loop expansions.

Phase separation and critical behavior of ionic fluids has been the subject of multiple theoretical [45–48] and experimental investigations [49–52]. In 1976, after a systematic study of the RPM, Stell et al. concluded that this system should exhibit a liquid-gas coexistence curve with a critical point. Later investigations have shown that the critical point belongs to the Ising universality class [47]. While earlier experiments supported both Ising (e.g. [49,51]) and mean-field (e.g. [50,52]) criticality, more recent ones have confirmed Ising behavior (see the review in Ref. [53] and references therein). Computer simulation techniques have also been applied for obtaining the structure of electrolyte solutions. The results obtained by this methods are important to test the validity of different approaches and have contributed to clarify the character of criticality in these systems confirming the Ising behavior. Several Monte Carlo [54–58] and molecular dynamics [59–61] simulations have been reported. A review of simulations of phase transitions in ionic systems is available in Ref. [62].

## 1.2 Fluids near planar charged surfaces

Surfaces in polar solvents or electrolyte solutions usually become charged. This is due to the ionization or dissociation of surface chemical groups, or to the adsorption or chemical binding of ions from the solution onto the surface. The surface-solution interface structure is called *electric double layer*. This name arises from the first model for this interface due to Helmholtz. In his model, the surface charge was completely neutralized by a layer of counterions, known as the Helmholtz layer, which is located parallel to the surface. The structure formed by the layer of co-ions on the surface and the one of counterions in the solution is equivalent to a parallel-plate capacitor whose plates carry equal but opposite charges; therefore the name “double layer”. This model predicts a constant differential capacitance (i.e., a voltage-independent capacitance) which does not agree with experimental observations. An alternative approach based on the Poisson-Boltzmann equation was introduced by Gouy [63] and later by Chapman [64]. They proposed the diffuse double layer model in which the density of the ions is approximated by a Boltzmann distribution. Agreement between Gouy-Chapman theory predictions and experiments is found in dilute solutions only. The failure of the theory is, inter alia, due to the fact that ions are modeled as charged point particles that can approach the substrate arbitrarily close. In order to take into account the effect of the finite size of ions, Stern [65] introduced



a plane of closest approach for the center of the ions. Beyond this plane, a diffuse Gouy-Chapman layer is assumed. This theory, which combines Helmholtz and Gouy-Chapman models, gives results which are consistent with experiments [66]. However, there are still discrepancies which are handled by refinements of the Stern model that take into account e.g. the influence of the solvent or of specific adsorption (see Refs. [67,68] and references therein).

Improvement over the Gouy-Chapman theory has been achieved by theories such as the modified Poisson-Boltzmann (MPB) theory [69,70], density functional theories [71–77], and integral equation theories [70,78], which produce results that are in good agreement with Monte Carlo simulations [79–82]. A field-theoretic approach has also been used to study the counterion distribution at a charged plane [83,84]. Within this approach, Poisson-Boltzmann theory is shown to be reliable in the weak-coupling limit of low surface charge and low valence ions and invalid in the opposite limit (i.e., in the strong-coupling regime). This approach offers the possibility to derive a theory that becomes valid in the latter limit.

In recent years, there has been an increasing interest in room-temperature ionic liquids (RTILs), i.e., salts with melting points below 100 °C, due to their potential application as electrolytes for fuel cells and batteries, catalyst and lubricants, among others [85, 86]. For such applications their interaction with solid surfaces plays an important role. Accordingly, the structure of RTILs in contact with charged surfaces has been the subject of several theoretical [87–90] and experimental studies [91–98] to cite a few; a recent review of the subject can be found in Ref. [99]. In contrast to ordinary electrolyte solutions, Gouy-Chapman-Stern models are not applicable to RTILs. This is mainly due to the fact that RTILs are dense ionic systems with strongly correlated ions. In a feature article, Kornyshev [87] stressed this point and proposed an alternative mean-field approach to the problem consisting in a Poisson-Boltzmann lattice-gas model that takes into account constraints on the ion packing in RTILs. This theory suggested a more general form for the differential capacitance which contains the Gouy-Chapman result as a limiting case. From this formulation it follows that the capacitance versus voltage plot can have a bell-like shape with a maximum at the point of zero charge (PZC) or a double hump shape (called camel-shape in Ref. [87]) with a minimum at the PZC. This is in contrast to the Gouy-Chapman theory of dilute electrolyte for which the the capacitance versus voltage plot has U-shape with a minimum at the PZC. A similar expression for the differential capacitance has been derived for concentrated electrolyte solutions in Ref. [100]. The behavior of the differential capacitance predicted in Ref. [87] was confirmed by subsequent experiments [91–93] and simulations [88,89]. However both experiments [94–96] and simulations [88]

suggested an alternate charge layering structure which decays exponentially into the bulk liquid, which is not predicted by the simple mean-field theory in Ref. [87]. This structure, known as *overscreening* structure from theoretical studies of molten salts near charged walls [101], starts with a layer of counterions that overscreens the surface charge of the electrode, the net charge resulting from the difference between the charge of the electrode and the charge of the first layer is then overscreened by the coions in the second layer and so on for several layers until charge neutrality is reached. This layering arrangement is suggested to be a generic feature of RTILs at charged surfaces [94] and to be originated from strong correlations between ions which are not taken into account in Ref. [87]. In order to capture this feature, Bazant et al. [90] proposed a phenomenological theory based on a Landau-Ginzburg functional with an additional potential gradient term, similar to Cahn-Hilliard concentration gradient expansions [102]. For small voltages this theory predicts the overscreening structure described before. Increasing the voltage gradually weakens the overscreening and finally a condensed layer of counterions known as *crowding* [90] or *lattice saturation* [87] forms for large voltage. The predictions of this theory are in agreement with simulations in Ref. [88] and experiments in Refs. [94, 98]. More recent experiments [96, 97] have shown that the extension of the uncharged tails of the cations plays an important role in the interfacial behavior of RTILs. The experiments suggest a transition from alternating cation-anion monolayer structures to bilayer structures with tail to tail cations when the length of the cation chain is increased. Since the seminal paper by Kornyshev [87] there has been a growing number of studies of RTILs at charged walls; the models used vary from “coarse-grain” models, which used simple representations of the ions, to more sophisticated atomistic descriptions of them. The literature is too vast to be reviewed here and the interested reader is referred to Refs. [99, 103] and references therein.

Interactions between charged objects in contact with electrolyte solutions play an important role in biology and soft matter physics. Experiments [104, 105] and computer simulations [106–109] have shown an attraction between like-charged surfaces in the presence of solutions with multivalent ions. These results do not agree with predictions from Poisson-Boltzmann theories for which the interaction between like-charged surfaces is always repulsive [11]. This contradiction between observations and theory has been attributed to correlation effects [84, 110] and to other non-electrostatic interactions [111]. Interactions between charged objects have also been studied in binary liquid mixtures [21, 112–119] where additional effects such as the adsorption preferences of the surfaces for one of the components of the mixture play an important role. For instance the critical Casimir force emerges in binary liquid mixtures close to their criti-

cal point [120]. This force is attractive if the adsorption preferences of the surfaces are the same (symmetric boundary conditions (BC)) and repulsive if they are opposite (antisymmetric BC). Recently, the interaction potential between a colloidal particle and a planar surface immersed in a water-2,6-lutidine mixture has been measured directly in salt-free mixtures [114] and in mixtures with added salt [115]. For the salt-free case the experimental observations were interpreted assuming the superposition of the electrostatic force, which dominates far away from the critical temperature, and the critical Casimir force which dominates as the critical point is approached. However, the subsequent experimental observations in mixtures with added salt could not be explained by using this simple superposition and pointed towards a coupling between electrostatics and critical phenomena. It turns out that contrary to the salt-free case where critical Casimir forces are observed very close to the critical point, for symmetric BC in mixtures with added salt the attractive Casimir force starts to dominate several Kelvin away from it. In addition, for antisymmetric BC in mixtures with added salt a crossover from attractive to repulsive forces is observed upon approaching the critical point although both the electrostatic and Casimir forces are repulsive. Several mechanisms were suggested to explain the emergence of this attractions in the case of antisymmetric BC in mixtures with added salt [21, 116–119]. In Refs. [21, 116] the effective surface-surface interaction potential is derived approximately from a Ginzburg-Landau-like description. From this derivation it turns out that the leading correction to the simple superposition of Casimir and electrostatic interactions is due to the interaction between two electric double layers: One due to the unequal partitioning of ions, i.e, due to a difference of the solubility contrast of cations and anions in the mixture, in the non-uniform order parameter close to one wall and the other one due to the surface charge on the opposite wall. This interaction is expected to be important only when direct electrostatic interactions are weak, which is the case for antisymmetric BC. On the other hand, for symmetric BC with hydrophobic surfaces, direct electrostatic forces are strong and the effect of added salt is to reduce the Debye length weakening the the direct electrostatic repulsion. Accordingly, the Casimir attraction is observed at temperatures further away from the critical point than in the salt-free case. In Refs. [117, 118] a mechanism that is independent of differences in the solubility of ions was proposed. In this model anions and cations are considered to be hydrophilic. It has been suggested that the charged wall attracts ions which in turn attract water molecules to this wall due to their hydrophilic character. Accordingly, for a range of temperatures an actual hydrophobic wall might turn into and effectively hydrophilic one upon adding salt, leading to an effective wall-wall attraction. On the other hand, an actual hydrophilic wall will remain hydrophilic upon adding salt. However it has been

argued in Ref. [21] that this apparent hydrophilicity could be an artifact of the so called bilinear coupling approximation (BCA) used in these references. In Ref. [119], the effect of ion solvation and solvent adsorption in the interaction between surfaces was studied numerically using BCA in the nonlinear regime. It has been suggested that nonlinearities can strongly influence this interaction.

### 1.3 Wetting behavior in systems with ions

Theoretical studies of wetting films in systems with ions started back in 1938 when Langmuir developed a model to determine the equilibrium thickness of water films on planar surfaces in contact with undersaturated water vapor, based on the calculation of the repulsive force between two plates immersed in electrolyte solutions [12]. The typical values for the equilibrium film thickness as predicted by Langmuir's formula were confirmed experimentally [13] and the experimental data were used to analyze the effect of various contributions to the disjoining pressure onto the stability of the wetting films [14]. Some years later Kayser generalized Langmuir's model for the equilibrium thickness of wetting films to liquid mixtures of polar and non-polar components in contact with ionizable substrates [15]; in contact with the wetting liquid these substrates donate ions to the liquid which act as counterions to the emerging opposite charge left on the substrate with overall charge neutrality. This analysis was followed up by a study in which the effect of added salt, i.e., of ions which do not stem from the substrate [16]. These works did not address the issue of wetting transitions at coexistence but rather focused on the thickness of the wetting films and the behavior of the disjoining pressure. For wetting films of solvents without added salt, i.e., with counterions only, Langmuir [12] and Kayser [15] found that the film thickness  $l$  increases as  $l \sim (\Delta\mu)^{-1/2}$ , with  $\Delta\mu = \mu_{co} - \mu$ , as the chemical potential  $\mu$  approaches its value  $\mu_{co}$  at coexistence from the vapor side ( $\mu < \mu_{co}$ ). In contrast, wetting films without ions and at neutral substrates but with van der Waals interactions lead to  $l \sim (\Delta\mu)^{-1/4}$  or  $l \sim (\Delta\mu)^{-1/3}$ , depending on whether retardation effects are taken into account or not, respectively [2]. In the case that the effect of added salt dominates over van der Waals interactions, Kayser [16] found  $l \sim \ln(\Delta\mu)$  as it holds for short-ranged interactions.

Wetting transitions at two-phase coexistence of electrolyte solutions at charged solid substrates were analyzed in Refs. [17–20]. In Ref. [18] the effect of adding ions onto the wetting behavior of the pure solvent was studied by using Cahn's phenomenological theory [1–4] for the solvent combined with the Poisson-Boltzmann theory for the ions. This model does not take into account the solvent particles explicitly, neglecting the coupling

between solvent particles and ions. On the other hand, the model in Ref. [19] takes all three types of particles (i.e., solvent, cations, and anions) explicitly into account in terms of hard spheres of different diameters with a Yukawa attraction between all pairs and the Coulomb interaction between ions. The model was studied by using Rosenfeld’s density functional theory [121,122] combined with a mean-field approximation for the Yukawa and the electrostatic interactions. Within this model, the polar nature of the solvent molecules was ignored; it was included in a subsequent article by the same authors in which the solvent particles were represented by dipolar hard spheres [20]. However, for technical reasons, the numerical analyses of these continuum models in which all three types of particles are treated explicitly on a microscopic level were limited to small system sizes. Therefore Refs. [19,20] focused on the case of strong screening of the Coulomb interactions which is provided by large ionic strengths, i.e., large ion concentrations. However, the approaches used in Refs. [18–20] are not reliable for large ionic strengths due to the use of Poisson-Boltzmann theory for the electrostatic interactions which has been proved to be valid only for low ionic concentrations and low surface charge density [79].

All the studies mentioned before are focused on the equilibrium thickness of wetting films either at two-phase coexistence or when coexistence is approached along an isotherm from the vapor side ( $\mu < \mu_{co}$ ). This equilibrium thickness, as well as the contact angle, is set by the intermolecular forces and changes in the equilibrium thickness and the contact angle are achieved varying the temperature. However, the contact angle can also be changed by applying an electrostatic potential, which is known as electrowetting and can be used to control the wettability of a substrate by a fluid [123–125]. A typical electrowetting setup consists of a planar metal electrode (usually coated with a thin dielectric layer), a drop of a conductive liquid, and a thin wire immersed in the droplet as counter-electrode. When a potential difference is applied between the two electrodes the contact angle decreases with the voltage according a so-called electrowetting equation [6]. A summary of the classical approaches to derive this equation, which is then also called Young-Lippmann equation and which depends quadratically on the applied voltage, can be found in Ref. [6]. These approaches are based on the assumption that electrowetting is an electrocapillarity effect, i.e., it is assumed to hinge on the voltage-dependence of the substrate-fluid interfacial tension [6, 124–138]. A justification for this approach is frequently given in terms of the vast experimental evidence for systems of uncoated and hydrophobically coated electrodes. However, it turned out that the commonly given derivations of the electrowetting equation [6] are incorrect in that they express the contact angle in terms of fluid-substrate interfacial tensions, which are descriptors of the interfacial structure of a *single* fluid phase in thermodynamic contact with a substrate.

It has been overlooked that the interfacial structure, and thus interfacial quantities, of a fluid can change upon bringing it into contact with another fluid. An alternative derivation based on a density functional theory approach is presented in Chap. 5 (see also Ref. [139]). This approach shows that electrowetting *cannot* be consistently understood as an electrocapillarity effect. In addition, it has been shown experimentally that the electrowetting equation derived by using the electrocapillarity approach is only valid for voltages smaller than a critical value, called the saturation voltage, above which the contact angle has always been found to saturate, i.e., a voltage-induced wetting transition has not been observed yet. This phenomenon is called contact angle saturation and its origin is not fully clear yet (see Refs. [6, 140] for reviews of theories and mechanisms that have been proposed to explain such a contact angle saturation). Concerning the materials used in experiments, electrowetting has been reported to depend weakly on the liquid properties. The effect has been observed in deionized water [141], aqueous electrolyte solutions (with no significant influence due to salt type or concentration) [142], RTILs [143] and physiological fluids [7]. On the other hand, the effect depends significantly on the properties of the dielectric layer used to coat the metal electrode [6, 139]. The properties of this layer are crucial to achieve a large contact angle tuning range, to reduce contact angle hysteresis, and to ensure reproducibility. Reviews of electrowetting can be found in Refs. [6, 140, 144].

## 1.4 Line tension

The line tension is the free energy contribution per unit length associated with the contact line where three interfaces meet, e.g., for a sessile liquid drop surrounded by a gas phase on top of a solid substrate, the contact line corresponds to the periphery of the circle where the liquid-gas interface meets the substrate. Although its magnitude is small (theory predicts values of the order of  $10^{-12}$  to  $10^{-11}$  N while experimental values are in the range  $10^{-12}$  to  $10^{-5}$  N [145]), the line tension plays an important role for different systems and phenomena such as wetting in nanoporous surfaces [146], stability of emulsions and foams [147], drop size [148] and many others [145]. The line tension has been the subject of several theoretical and experimental investigations (see Refs. [145, 149–152] and references therein). Experimental arrangements to study line tensions include solid-liquid-gas systems such as drops or bubbles on solid substrates and particles at liquid-gas interfaces, and liquid-liquid-gas systems such as liquid lenses at liquid-gas interfaces and thin liquid film arrangements. Theoretical investigations include extensions of capillarity theory, which take into account line tension effects, microscopic theories, and molecular

dynamics and Monte Carlo simulations. Most of these investigations deal with simple fluids or binary liquid mixtures and only few studies had studied the influence of electrostatic interactions on the line tension [153–155]. However, the analysis in Ref. [154] only considers the electrostatic contribution to the free-energy based on a Poisson-Boltzmann theory. Therefore, only the electrostatic contribution to the line tension is analyzed. In Ref. [153] the theory of capillarity has been extended taking into account line contributions as well as electric charges at the interfaces and the TPCL. Within this approach electrowetting has been interpreted as a line tension effect, but some of its predictions are in disagreement with experiments [144]. In Ref. [155] an equation for the contact angle as a function of the electrostatic potential at the TPCL and an estimate for the electrostatic contribution to the line tension have been derived using a variational approach on a wedge like geometry. Recently, Dörr and Hardt [156] studied the electric double layer structure close to the TPCL by solving the linearized Poisson-Boltzmann equation in a wedge geometry without calculating the line tension. Following the method in Ref. [156], Das and Mitra calculated the Maxwell stress and contact angle variation of drops or bubbles on a charged substrate again without taking into account line effects [157]. More recently, Dörr and Hardt [158] computed the line tension of an electrolyte in contact with a charged substrate by considering a wedge geometry similar to Refs. [154, 156, 157]. Similarly to Ref. [154] they considered only the electrostatic contribution to the line tension. However, their model differs to the one in Ref. [154] in that it includes the interfacial deformation of the fluid-fluid interface. To my knowledge there are no microscopic calculations of line tensions in electrolyte solutions in which both solvent and ion contributions are taken into account simultaneously. The line tension of a lattice model for an electrolyte solution is considered in Chap. 6.





# Chapter 2

## General formalism

In this thesis, the wetting of charged substrates by electrolyte solutions is studied using a lattice and a continuum model. The general approach used to study both models is classical density functional theory (DFT), which is the appropriate framework to study inhomogeneous fluids. In this chapter, the DFT formalism and the basic concepts of wetting theory which are the common ingredients of the following chapters, are introduced. In the last section relevant aspects concerning microscopic calculations of the line tension are briefly reviewed.

### 2.1 Classical density functional theory

Classical DFT is a standard approach to calculate the structure, the thermodynamic properties and the phase behavior of fluids. It is particularly suitable for inhomogeneous fluids i.e., fluids for which the average one-body density  $\varrho(\mathbf{r})$ , is spatially varying. Such inhomogeneities in  $\varrho$  appear at interfaces between coexisting phases or in the vicinity of confining surfaces, which can be represented by external potentials. The theory has its origins in the density functional treatment for the ground state of an inhomogeneous electron gas developed by Hohenberg and Kohn [159] and Kohn and Sham [160] and the extension for non-zero temperatures derived by Mermin [161]. In this section, a brief introduction to the DFT formalism for the case of one-component fluids, which can be easily generalized to multicomponent fluids, is presented. Reviews and more rigorous treatments of classical DFT can be found in Refs. [162, 163].

The Hamiltonian for a one-component fluid of  $N$  particles in the presence of an arbi-

trary external potential  $V(\mathbf{r})$  is given by

$$H_N(\underline{\mathbf{r}}, \underline{\mathbf{p}}) = \sum_{i=1}^N \frac{\mathbf{p}_i^2}{2m} + U(\underline{\mathbf{r}}) + \sum_{i=1}^N V(\mathbf{r}_i) \quad (2.1)$$

where  $\mathbf{p}_i$  and  $\mathbf{r}_i$  are the momentum and the position of particle  $i \in \{1, \dots, N\}$ , respectively, the collection of which are abbreviated by  $\underline{\mathbf{p}} = (\mathbf{p}_1, \dots, \mathbf{p}_N)$  and  $\underline{\mathbf{r}} = (\mathbf{r}_1, \dots, \mathbf{r}_N)$ ,  $m$  is the mass of one particle and  $U(\underline{\mathbf{r}})$  is the total interatomic potential. For this system the equilibrium density is given by

$$\varrho_{eq}(\mathbf{r}) = \text{Tr} \left( f_N(\underline{\mathbf{r}}, \underline{\mathbf{p}}) \sum_{i=1}^N \delta(\mathbf{r} - \mathbf{r}_i) \right) \quad (2.2)$$

where  $\text{Tr}$  is the classical trace

$$\text{Tr} = \sum_{N=0}^{\infty} \frac{1}{h^{3N} N!} \int d\mathbf{r}_1 \cdots \int d\mathbf{r}_N \int d\mathbf{p}_1 \cdots \int d\mathbf{p}_N, \quad (2.3)$$

with the Planck constant  $h$ ,  $f_N(\underline{\mathbf{r}}, \underline{\mathbf{p}})$  is the equilibrium grand canonical probability density

$$f_N(\underline{\mathbf{r}}, \underline{\mathbf{p}}) = \Xi^{-1} \exp(-\beta(H_N(\underline{\mathbf{r}}, \underline{\mathbf{p}}) - \mu N)), \quad (2.4)$$

with the grand partition function  $\Xi = \text{Tr}(\exp(-\beta(H_N(\underline{\mathbf{r}}, \underline{\mathbf{p}}) - \mu N)))$ , where  $\beta = (k_B T)^{-1}$  is the inverse thermal energy with the Boltzman constant  $k_B$ , and  $\mu$  is the chemical potential.

For given interatomic potential energy  $U$  and temperature  $T$  there is an unique functional  $\mathcal{F}[\varrho]$ , independent of the external potential, defined by [164, 165]

$$\mathcal{F}[\varrho] = \min_{\tilde{f}_N | \varrho} \text{Tr} \left( \tilde{f}_N(\underline{\mathbf{r}}, \underline{\mathbf{p}}) \left( K(\underline{\mathbf{r}}) + U(\underline{\mathbf{r}}) + k_B T \ln \tilde{f}_N(\underline{\mathbf{r}}, \underline{\mathbf{p}}) \right) \right) \quad (2.5)$$

where  $K(\underline{\mathbf{r}}) = \sum_{i=1}^N \frac{\mathbf{p}_i^2}{2m}$  is the total kinetic energy and where  $\tilde{f}_N | \varrho$  denotes the set of all probability densities  $\tilde{f}_N$  which lead to the prescribed one-body density  $\varrho$  via

$$\text{Tr} \left( \tilde{f}_N(\underline{\mathbf{r}}, \underline{\mathbf{p}}) \sum_{i=1}^N \delta(\mathbf{r} - \mathbf{r}_i) \right) = \varrho(\mathbf{r}). \quad (2.6)$$

The grand canonical density functional  $\Omega[\varrho]$  is constructed via a Legendre transform of  $\mathcal{F}[\varrho]$

$$\Omega[\varrho] = \mathcal{F}[\varrho] + \int d\mathbf{r} \varrho(\mathbf{r}) (V(\mathbf{r}) - \mu). \quad (2.7)$$

The equilibrium density  $\varrho_{eq}(\mathbf{r})$  in Eq. (2.2) minimizes  $\Omega[\varrho]$  so that

$$\left. \frac{\delta\Omega[\varrho]}{\delta\varrho(\mathbf{r})} \right|_{\varrho=\varrho_{eq}} = \left. \frac{\delta\mathcal{F}[\varrho]}{\delta\varrho(\mathbf{r})} \right|_{\varrho=\varrho_{eq}} + V(\mathbf{r}) - \mu = 0. \quad (2.8)$$

Moreover, at the equilibrium density  $\varrho_{eq}(\mathbf{r})$ ,  $\Omega[\varrho_{eq}(\mathbf{r})]$  equals the grand potential  $\Omega = -k_B T \ln \Xi$ . Therefore, the knowledge of the functional  $\mathcal{F}[\varrho]$  reduces the problem of calculating the equilibrium density profile and the grand potential of inhomogeneous fluids to a functional minimization problem, representing a simplification over the direct evaluation of the grand partition function  $\Xi$ . Since the Helmholtz free energy functional is given by

$$\begin{aligned} F[\varrho] &= \Omega[\varrho] + \mu \int d\mathbf{r} \varrho(\mathbf{r}) \\ &= \mathcal{F}[\varrho] + \int d\mathbf{r} \varrho(\mathbf{r}) V(\mathbf{r}), \end{aligned} \quad (2.9)$$

the functional  $\mathcal{F}[\varrho]$  is known as the intrinsic Helmholtz free energy functional. This functional is divided into an ideal and an excess contribution, i.e.,  $\mathcal{F}[\varrho] = \mathcal{F}_{id}[\varrho] + \mathcal{F}_{ex}[\varrho]$ . The ideal gas contribution is exactly known as

$$\mathcal{F}_{id}[\varrho] = k_B T \int d\mathbf{r} \varrho(\mathbf{r}) (\ln(\Lambda^3 \varrho(\mathbf{r})) - 1) \quad (2.10)$$

were  $\Lambda = h/\sqrt{2\pi m k_B T}$  is the thermal de Broglie wavelength. On the other hand the excess contribution  $\mathcal{F}_{ex}[\varrho]$ , which accounts for the interaction among the fluid particles, is in general unknown and has to be approximated. A review of some approximations for  $\mathcal{F}[\varrho]$  can be found in Ref. [162]. The approximation used in the present work corresponds to a mean field theory (MFT) and will be described in detail for each of the models studied in Sec. 3.2 and Sec. 4.1.

When the interatomic potential energy  $U(\mathbf{r})$  is a sum of pair potentials  $u(\mathbf{r}_i, \mathbf{r}_j)$ , one has the following relation between  $\mathcal{F}_{ex}[\varrho]$  and the pair density  $\varrho^{(2)}(\mathbf{r}, \mathbf{r}')$  [31]

$$\frac{\delta\mathcal{F}_{ex}[\varrho]}{\delta u(\mathbf{r}, \mathbf{r}')} = \frac{1}{2} \varrho^{(2)}(\mathbf{r}, \mathbf{r}'). \quad (2.11)$$

Assuming that the pair potential can be decomposed into a reference part  $u_{ref}$  and a perturbation part  $u_{per}$  and integrating Eq. (2.11) at constant  $\varrho(\mathbf{r})$ , along a path in function space such that

$$u_\lambda(\mathbf{r}, \mathbf{r}') = u_{ref}(\mathbf{r}, \mathbf{r}') + \lambda u_{per}(\mathbf{r}, \mathbf{r}') \quad 0 \leq \lambda \leq 1, \quad (2.12)$$

yields

$$\mathcal{F}_{ex}[\varrho] = \mathcal{F}_{ex,ref}[\varrho] + \frac{1}{2} \int_0^1 d\lambda \int d\mathbf{r} \int d\mathbf{r}' \varrho^{(2)}(\mathbf{r}, \mathbf{r}'; \lambda) u_{per}(\mathbf{r}, \mathbf{r}'), \quad (2.13)$$

where  $\mathcal{F}_{ex,ref}[\varrho]$  is the excess free energy functional of the reference fluid with pair potential  $u_{ref}$  (i.e,  $\lambda = 0$ ) and  $\varrho^{(2)}(\mathbf{r}, \mathbf{r}'; \lambda)$  is the pair density of the system with pair potential  $u_\lambda(\mathbf{r}, \mathbf{r}')$ . Equation (2.13) is the starting point for perturbation theories in both bulk and inhomogeneous fluids [31]. The reference potential  $u_{ref}$  is usually taken to be the repulsive part of the full pair potential  $u(\mathbf{r}, \mathbf{r}')$  while the attractive part of it is treated as the perturbation  $u_{per}$ .

A mean-field-like approximation known as random phase approximation (RPA) corresponds to set

$$\varrho^{(2)}(\mathbf{r}, \mathbf{r}') \approx \varrho(\mathbf{r})\varrho(\mathbf{r}'). \quad (2.14)$$

In this case the excess free energy (Eq. (2.13)) reduces to

$$\mathcal{F}_{ex}[\varrho] \approx \mathcal{F}_{ex,ref}[\varrho] + \frac{1}{2} \int d\mathbf{r} \int d\mathbf{r}' \varrho(\mathbf{r})\varrho(\mathbf{r}') u_{per}(\mathbf{r}, \mathbf{r}'). \quad (2.15)$$

Another well known approximation is the square-gradient approximation [162] for which the intrinsic free energy functional follows from a gradient expansion

$$\mathcal{F}[\varrho] = \int d\mathbf{r} [f(\varrho(\mathbf{r})) + f_2(\varrho(\mathbf{r})) (\nabla\varrho(\mathbf{r}))^2 + \mathcal{O}((\nabla\varrho(\mathbf{r}))^4)]. \quad (2.16)$$

Truncating the expansion after the first term corresponds to the local density approximation (LDA), where  $f(\varrho)$  is the free energy density of a uniform fluid of density  $\varrho$ . The coefficient  $f_2$  is determined by requiring the functional  $\mathcal{F}[\varrho]$  to be consistent with linear-response theory [31]. In this case it is found that

$$\beta f_2(\varrho) = \frac{1}{12} \int d\mathbf{r} r^2 c^{(2)}(r) \quad (2.17)$$

where  $c^{(2)}(r)$  is the two-body direct correlation function.

## 2.2 Wetting

This section briefly introduces the concepts of wetting phenomena to the extent needed in the following chapters. The richness of these phenomena has been covered in great detail in various reviews [1–5].

Wetting transitions are surface phase transitions which occur whenever a phase C

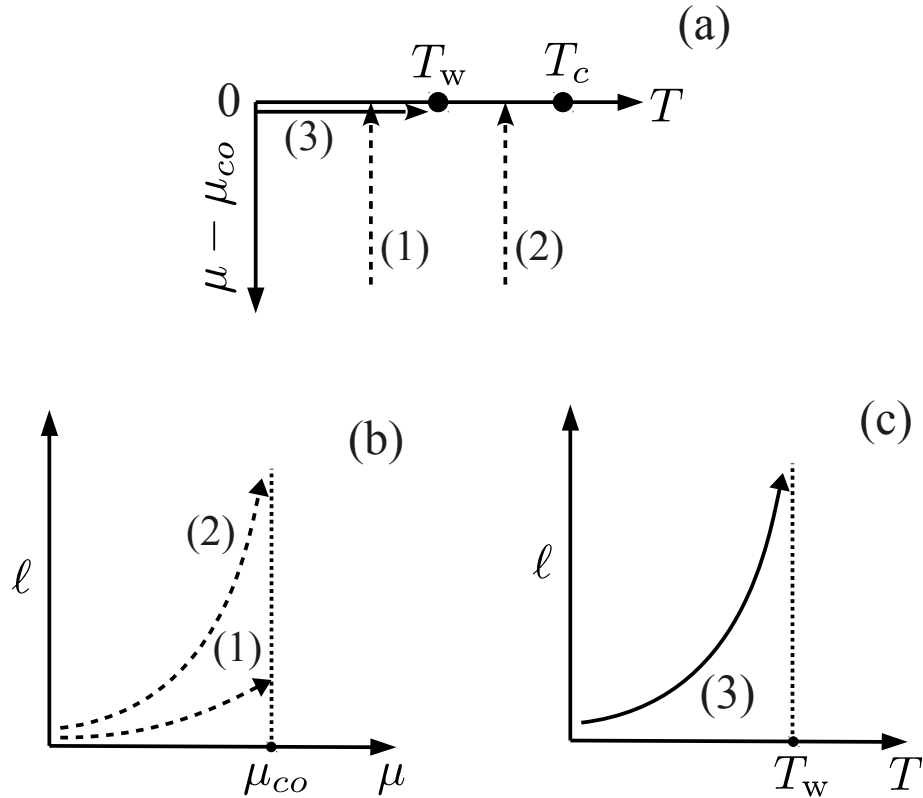


Figure 2.1: (a) Generic surface phase diagram for a continuous wetting transition at  $T_w$  (according to Refs. [2,3]). At liquid-gas coexistence  $\mu = \mu_{co}$  and  $T_t \leq T \leq T_c$  where  $T_t$  is the triple point. (b) Thickness of the intruding liquid film  $\ell$  as coexistence is approached from the gas phase ( $\mu < \mu_{co}$ ) along an isotherm (paths (1) and (2)). Incomplete or partial wetting occurs as coexistence is approached along path (1) whereas complete wetting occurs along path (2). At two-phase coexistence (path 3), the film thickness  $\ell$  diverges smoothly as  $T \rightarrow T_w$  (see (c)).

intrudes at the interface between two phases A and B, with either A, B, and C in thermodynamic coexistence or with A as a spectator phase and B and C in thermodynamic coexistence. As an example, consider the case in which A is an inert substrate and B and C are the gas and the liquid phase of a simple fluid, respectively. Upon approaching gas-liquid coexistence along an isotherm, the thickness of the intruding liquid film can be either finite (microscopic) (path (1) in Figs. 2.1 and 2.2), which is called incomplete or partial wetting, or macroscopically large (path (2) in Figs. 2.1 and 2.2), which is called complete wetting. The transition at two-phase coexistence (path (3) in Figs. 2.1 and 2.2) from incomplete to complete wetting occurs at the wetting transition temperature  $T = T_w$ . It can be either continuous (second-order), in which case the film thickness diverges smoothly as  $T \rightarrow T_w$  along two-phase coexistence (see Fig. 2.1 (c)), or discon-

tinuous (first-order), implying a macroscopically large jump of the film thickness from a finite value below  $T_w$  to a macroscopically large one above  $T_w$  (see Fig. 2.2 (c)). In the surface phase diagram a first-order wetting transition has a prewetting line associated with it, which is connected tangentially to the gas-liquid coexistence line at  $T_w$ , extends into the gas phase region, and ends at a critical point (see Fig. 2.2 (a)). This line marks the loci of a finite discontinuity in film thickness (see Fig. 2.2 (b)). This finite jump in film thickness becomes smaller as the system is brought further away from coexistence and vanishes at the prewetting critical point.

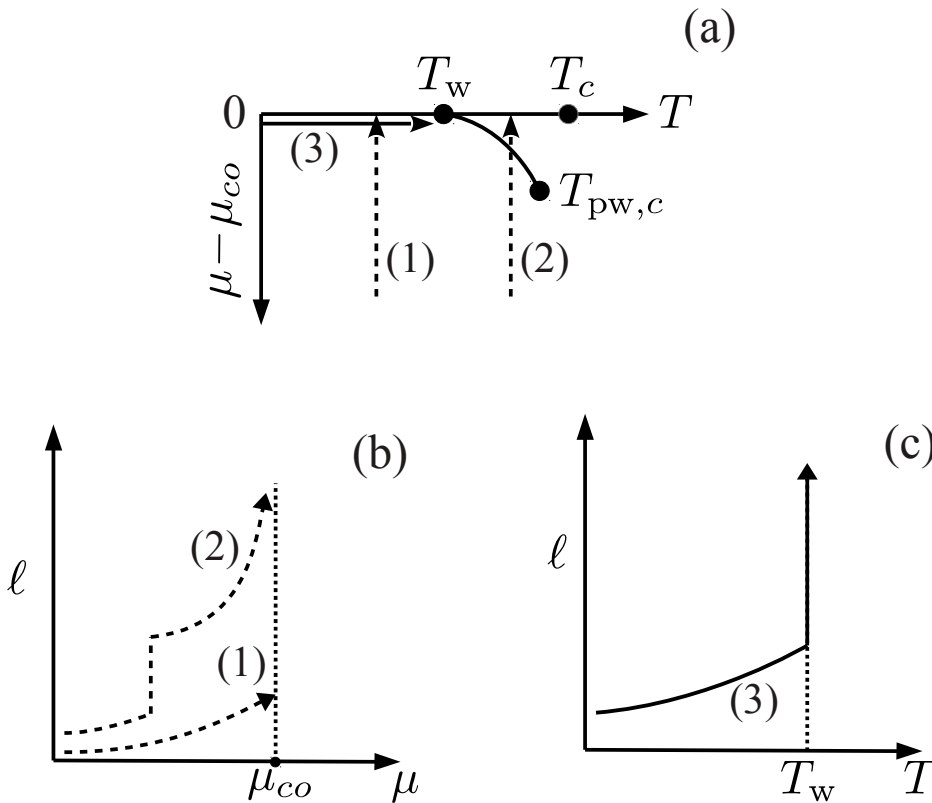


Figure 2.2: (a) Generic surface phase diagram for a first-order wetting transition at  $T_w$  (according to Refs. [2,3]), showing the prewetting line which starts at the wetting transition temperature  $T_w$ , extends into the gas phase region ( $\mu < \mu_{co}$ ) and ends at the prewetting critical point  $T_{pw,c}$ . (b) Film thickness  $\ell$  as coexistence is approached along paths (1) and (2). Incomplete wetting occurs along path (1) whereas complete wetting occurs along path (2). Additionally, there is a jump in film thickness  $\ell$  when the prewetting line is crossed by path (2). At coexistence (path 3), the film thickness  $\ell$  jumps discontinuously from a finite value below  $T_w$  to a macroscopic one above (see (c)).

## 2.2.1 Effective interface potential and the contact angle

The wetting behavior of fluids near substrates can be transparently studied by analyzing the effective interface potential  $\omega(\ell)$  [2]

$$\omega(\ell) = \Omega_s(\ell) - \gamma_{l,g} - \gamma_{s,l} \quad (2.18)$$

where  $\Omega_s(\ell)$  is the constrained surface contribution to the grand potential, i.e.,  $\Omega_s(\ell) := (\Omega[\{\rho^{(\ell)}\}] - \Omega_b V)/A$ ,  $\Omega_b$  is the bulk grand potential density,  $A$  is the substrate area and  $V$  is the system volume. The density profiles  $\rho^{(\ell)}$  are the solutions of the Euler-Lagrange equations (2.8) for a prescribed film thickness  $\ell$ . The film thickness  $\ell$  is defined by requiring the density profiles  $\rho(z)$  to fulfill a certain property at  $z = \ell$ , e.g,  $\phi(z) = (\phi_l + \phi_g)/2$  where  $\phi_l$  and  $\phi_g$  are the bulk number densities of the coexisting liquid and gas phases, respectively, or  $\left. \frac{d^2 \rho(z)}{dz^2} \right|_{z=\ell} = 0$ , etc.  $\gamma_{l,g}$  and  $\gamma_{s,l}$  are the liquid-gas and substrate-liquid interfacial tensions, respectively, such that by construction at two-phase coexistence one has  $\omega(\ell \rightarrow \infty) = 0$ . The equilibrium film thickness  $\ell_{eq}$  is given by the global minimum of the effective interface potential  $\omega(\ell_{eq}) \leq 0$ . At  $\ell_{eq}$ ,  $\Omega_s(\ell)$  renders the substrate-gas interfacial tension  $\gamma_{s,g}$ , which implies (see Eq. 2.18)

$$\gamma_{s,g} = \gamma_{l,g} + \gamma_{s,l} + \omega(\ell_{eq}). \quad (2.19)$$

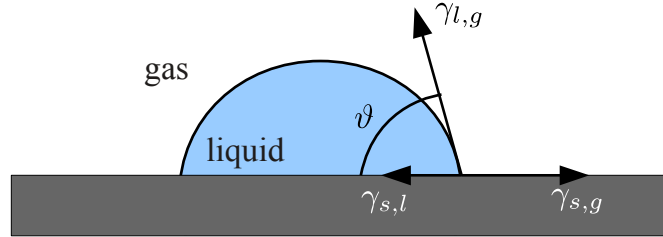


Figure 2.3: Sessile liquid drop forming a contact angle  $\vartheta$  with a homogeneous substrate.

The effective interface potential  $\omega(\ell_{eq})$  is related to the contact angle. Consider a liquid drop on a homogeneous substrate in equilibrium with its vapor, as shown schematically in Fig. 2.3. The relation between the equilibrium contact angle  $\vartheta$  the drop makes with the substrate and the three interfacial tensions associated with the liquid-gas, substrate-liquid and substrate-gas interfaces meeting at the three phase contact line, is given by Young's equation

$$\gamma_{s,g} = \gamma_{s,l} + \gamma_{l,g} \cos \vartheta. \quad (2.20)$$

Combining Eqs. (2.19) and (2.20) one obtains [2]

$$\cos \vartheta = 1 + \frac{\omega(\ell_{eq})}{\gamma_{l,g}}. \quad (2.21)$$

Comparing the description in terms of the contact angle with the description of wetting transition given before in terms of the thickness of the microscopic liquid film that intrudes between the substrate and the vapor phase, one can see that incomplete or partial wetting corresponds to non-zero contact angle  $0 < \vartheta < \pi$  and complete wetting to  $\vartheta = 0$ , i.e.,  $\omega(\ell \rightarrow \infty) = 0$ . Moreover,  $\omega(\ell_{eq}) \leq 0$  vanishes continuously as  $T \rightarrow T_w$  so that the thicker the microscopic liquid film the smaller the contact angle.  $\vartheta = \pi$  corresponds to complete drying. In this case, a macroscopically thick film of gas intrudes between the liquid phase and the substrate.

### 2.3 Line tension of a sessile liquid drop

The grand canonical energy  $\Omega$  of a sessile drop on a solid substrate (see Fig. 2.3) decomposes into volume contributions associated with the gas, liquid, and solid bulk phases; surface contributions due to the substrate-liquid, substrate-gas, and liquid-gas interfaces; and a line contribution associated with the contact line along which the three phases (solid, gas and liquid) meet, i.e.,

$$\Omega = \sum_{i=g,l,s} V_i \Omega_i + A_{s,g} \gamma_{s,g} + A_{s,l} \gamma_{s,l} + A_{l,g} \gamma_{l,g} + \tau L + \dots, \quad (2.22)$$

where  $V_i$  is the volume of the phase  $i$  with  $i \in \{g, l, s\}$  and  $\Omega_i$  is the bulk free energy density of this phase.  $\gamma_{s,g}$ ,  $\gamma_{s,l}$ , and  $\gamma_{l,g}$  are the interfacial tensions and  $A_{s,g}$ ,  $A_{s,l}$ , and  $A_{l,g}$  the corresponding interfacial areas of the substrate-gas, substrate-liquid and liquid-gas interfaces, respectively.  $L$  is the length of the three phase contact line,  $\tau$  is the line tension and  $\dots$  denotes subleading terms that vanish for infinitely long contact line  $L \rightarrow \infty$ .

The decomposition in Eq. (2.22) enables the evaluation of the line tension provided that the bulk free energy densities and the interfacial tensions are calculated consistently in separated steps. However, as pointed out in Ref. [149] for a sessile drop on an inert solid substrate which is a spectator phase, two different definitions of the line tension are possible: one which depends on the choice of dividing interfaces and one that is independent. Therefore, care has to be taken when calculating the line tension of a sessile drop on an inert substrate. A relation between the two definitions was derived in



Ref. [149]. The results of Ref. [149] relevant to this work are reviewed in the following.

### 2.3.1 Substrate-fluid dividing interface

First, the influence of the choice of the dividing interface in the values of the substrate-liquid and substrate-gas interfacial tension  $\gamma_{s,l}$  and  $\gamma_{s,g}$ , respectively, was considered (see Sec. II in Ref. [149]). If an inert substrate is exposed to the liquid or gas phase of a fluid  $f$ , the substrate-fluid interfacial tension is defined as

$$\gamma_{s,f} = \lim_{V_s, V_f, A_{s,f} \rightarrow \infty} = \frac{\Omega - V_f \Omega_f - V_s \Omega_s}{A_{s,f}} \quad (2.23)$$

where  $\Omega$  is the grand potential of the fluid plus the substrate,  $\Omega_f$  and  $\Omega_s$  are the grand canonical free energy densities of the fluid and the substrate, respectively,  $V_f$  is the volume of the fluid,  $V_s$  is the volume of the substrate, and  $A_{s,f}$  is the area of the planar substrate-fluid interface. If two parallel dividing interfaces separated by a distance  $\Delta h$  are considered, the fluid and substrate volume corresponding to each choice of dividing interface are related by  $V_s^{(2)} = V_s^{(1)} + \Delta h A_{s,f}$  and  $V_f^{(2)} = V_f^{(1)} - \Delta h A_{s,f}$ . Consequently, it follows from Eq. (2.23) that the values of  $\gamma_{s,f}$  associated with these two choices of the dividing interface differ by

$$\gamma_{s,f}^{(2)} - \gamma_{s,f}^{(1)} = (\Omega_f - \Omega_s) \Delta h. \quad (2.24)$$

Accordingly, the values of  $\gamma_{s,l}$  and  $\gamma_{s,g}$  depend on the choice of the substrate-fluid dividing interface. If the substrate-liquid and the substrate-gas dividing interfaces are chosen to be at the same height above the substrate, the difference  $\gamma_{s,g} - \gamma_{s,l}$  which enters Young's equation (Eq. 2.20) does not depend on the choice of the dividing interface.

Note that the value of the liquid-gas interfacial tension  $\gamma_{l,g}$  is independent of the choice of the liquid-gas dividing interface because at two-phase coexistence the grand canonical free energy densities of the gas and the liquid phase are equal, i.e.,  $\Omega_g = \Omega_l$ .

### 2.3.2 Line tension of a liquid wedge

The subsequent question is whether or not the choice of the solid-fluid dividing interface affects the value of the line tension  $\tau$ . In order to answer this question, in Ref. [149] (see Sec. II and VI in Ref. [149]) the line tension in a wedge geometry in which three planar interfaces meet along an infinitely long contact line  $L \rightarrow \infty$  and the liquid-gas interface meets the substrate with a contact angle  $\vartheta$  was considered. Again, the effect of shifting the dividing interface by a distance  $\Delta h$  is investigated. Using Eq. (2.22) the difference

in the value of the line tension corresponding to these two different dividing interfaces is given by,

$$\begin{aligned} \tau^{(2)} - \tau^{(1)} = \frac{1}{L} & \left( - (V_s^{(2)} - V_s^{(1)}) \Omega_s - (V_g^{(2)} - V_g^{(1)}) \Omega_g - (V_l^{(2)} - V_l^{(1)}) \Omega_l \right. \\ & \left. - (A_{s,g}^{(2)} \gamma_{s,g}^{(2)} - A_{s,g}^{(1)} \gamma_{s,g}^{(1)}) - (A_{s,l}^{(2)} \gamma_{s,l}^{(2)} - A_{s,l}^{(1)} \gamma_{s,l}^{(1)}) - (A_{l,g}^{(2)} \gamma_{l,g}^{(2)} - A_{l,g}^{(1)} \gamma_{l,g}^{(1)}) \right). \end{aligned} \quad (2.25)$$

The volume changes can be written as:

$$\begin{aligned} V_s^{(2)} - V_s^{(1)} &= \Delta h \left( A_{s,l}^{(2)} + A_{s,g}^{(2)} \right) = \Delta h \left( A_{s,l}^{(1)} + A_{s,g}^{(1)} \right) \\ V_l^{(2)} + V_g^{(2)} - (V_l^{(1)} + V_g^{(1)}) &= - \left( V_s^{(2)} - V_s^{(1)} \right). \end{aligned} \quad (2.26)$$

The substrate-liquid and substrate-gas surface tensions transform according to Eq. (2.24) as:

$$\begin{aligned} \gamma_{s,l}^{(2)} - \gamma_{s,l}^{(1)} &= (\Omega_l - \Omega_s) \Delta h \\ \gamma_{s,g}^{(2)} - \gamma_{s,g}^{(1)} &= (\Omega_g - \Omega_s) \Delta h. \end{aligned} \quad (2.27)$$

As explained before the value of the liquid-gas interfacial tension is independent of the choice of the dividing interface, i.e.,  $\gamma_{l,g}^{(1)} = \gamma_{l,g}^{(2)} = \gamma_{l,g}$ .

The changes in area can be written in terms of the contact angle  $\vartheta$  and the length of the contact line  $L$  as:

$$\begin{aligned} A_{s,g}^{(2)} - A_{s,g}^{(1)} &= \frac{\Delta h}{\tan \vartheta} L \\ A_{s,l}^{(2)} - A_{s,l}^{(1)} &= -\frac{\Delta h}{\tan \vartheta} L \\ A_{l,g}^{(2)} - A_{l,g}^{(1)} &= -\frac{\Delta h}{\sin \vartheta} L \end{aligned} \quad (2.28)$$

Inserting Eqs. (2.26)-(2.28) into Eq. (2.25) and using the fact that at two-phase

coexistence  $\Omega_g = \Omega_l = \Omega_b$ , renders

$$\begin{aligned}
\tau^{(2)} - \tau^{(1)} &= \frac{1}{L} \left( \Delta h \left( A_{s,l}^{(1)} + A_{s,g}^{(1)} \right) (\Omega_b - \Omega_s) \right. \\
&\quad - \left( \left( \frac{\Delta h}{\tan \vartheta} L + A_{s,g}^{(1)} \right) \left( (\Omega_b - \Omega_s) \Delta h + \gamma_{s,g}^{(1)} \right) - A_{s,g}^{(1)} \gamma_{s,g}^{(1)} \right) \\
&\quad - \left( \left( -\frac{\Delta h}{\tan \vartheta} L + A_{s,l}^{(1)} \right) \left( (\Omega_b - \Omega_s) \Delta h + \gamma_{s,l}^{(1)} \right) - A_{s,l}^{(1)} \gamma_{s,l}^{(1)} \right) \\
&\quad \left. + \left( \frac{\Delta h}{\sin \vartheta} L \right) \gamma_{l,g} \right) \\
&= \frac{1}{L} \left( \frac{\Delta h}{\tan \vartheta} L \left( \gamma_{s,l}^{(1)} - \gamma_{s,g}^{(1)} \right) + \left( \frac{\Delta h}{\sin \vartheta} L \right) \gamma_{l,g} \right) \\
&= \frac{\gamma_{l,g} + \left( \gamma_{s,l}^{(1)} - \gamma_{s,g}^{(1)} \right) \cos \vartheta}{\sin \vartheta} \Delta h.
\end{aligned} \tag{2.29}$$

Using Young's equation (Eq. 2.20) one obtains:

$$\tau^{(2)} - \tau^{(1)} = \gamma_{l,g} \Delta h \sin \vartheta. \tag{2.30}$$

Therefore, the change in the value of the line tension is proportional to the distance  $\Delta h$  between the two different choices of substrate-fluid dividing interface. As a consequence of this result, in order to compare values of line tensions obtained from calculations in a wedge geometry, in addition to the line tension value one has to provide the definition of the substrate-fluid dividing interface. The dependence of the line tension on the position of the substrate-fluid dividing interface is in conflict with the invariance of the line tension with respect to notional changes of the system, i.e, variations that leave the grand canonical potential unchanged, which is derived using as a reference system a sessile liquid drop surrounded by gas on top of an inert substrate.

### 2.3.3 Line tension of a sessile drop

In this section, the line tension of a sessile droplet in contact with an undeformable inert substrate is considered. For small droplets gravity can be neglected and the grand canonical energy can be decomposed as follows (see Eq. 2.22)

$$\Omega = -p_l V_l - p_g V_g + \Omega_s V_s + A_{l,g} \gamma_{l,g}(R) + \pi r^2 \gamma_{s,l} + (A - \pi r^2) \gamma_{s,g} + 2\pi r \tau, \tag{2.31}$$

where the liquid-gas dividing interface is chosen to be a spherical cap which is extrapolated into the three-phase contact line.  $r$  is the radius of the contact circle and  $R$  is the radius

of the sphere forming the spherical cap. The area of the substrate-gas dividing interface in the absence of the drop is  $A$  and the area of the substrate-liquid interface is  $A_{s,l} = \pi r^2$ . The substrate-liquid and substrate-gas dividing interfaces are chosen to be in the same plane. Subleading contributions to  $\tau$  in Eq. (2.31) are disregarded so that the definitions of the line tension in Eqs. (2.22) and (2.31) agree. The pressure inside the droplet  $p_l$  deviates from the pressure in the gas phase  $p_g = p$  by  $\Delta p$ , i.e.,  $p_l = p + \Delta p$ .  $\gamma_{l,g}(R)$  is the surface tension of a spherical liquid drop surrounded by gas. With these considerations Eq. (2.31) holds for two scenarios: one in which the liquid drop exchanges matter with the surrounding gas phase (therefore the chemical potentials in both phases are the same) and a second one in which the volume of the liquid drop is prescribed so that pressure in the liquid phase is determined by the amount of liquid.

In Ref. [149] two procedures to derive an equation which relates the contact angle  $\vartheta$  to the radius  $r$  were used. In the first one the requirement that the grand canonical potential must be invariant with respect to notional changes was exploited. The notional changes consist of a change in the liquid-gas dividing interface by  $[dR]$  and a common shift of the substrate-liquid and substrate-gas dividing interfaces by  $[dh]$ . (The square brackets were used in Ref. [149] to characterize notional changes). In the second procedure the equation is derived from a variational procedure at fixed volume of the liquid drop  $V_l$ . Both procedures lead to the same equation for the contact angle:

$$\gamma_{l,g} \cos \vartheta + (\gamma_{s,l} - \gamma_{s,g}) = -\frac{\tau}{r} - \left. \frac{d\tau}{dr} \right| - \frac{\sin \vartheta \cos \vartheta}{r} \left. \frac{d\tau}{d\vartheta} \right|, \quad (2.32)$$

where  $\left. \frac{d\tau}{dr} \right|$  and  $\left. \frac{d\tau}{d\vartheta} \right|$  are stiffness coefficients which describe the cost in free energy resulting from variational changes of  $r$  and  $\vartheta$  at fixed thermodynamic conditions. Moreover, the stiffness coefficients are equal to the notional derivatives of the line tension, i.e,

$$\left. \frac{d\tau}{d\vartheta} \right| = \left[ \frac{d\tau}{d\vartheta} \right] \quad \text{and} \quad \left. \frac{d\tau}{dr} \right| = \left[ \frac{d\tau}{dr} \right]. \quad (2.33)$$

It was also found that the line tension in Eq. (2.31) with the substrate-gas surface tension  $\gamma_{s,g}$  and substrate-liquid surface tension  $\gamma_{s,l}$  evaluated at the pressure  $p$ , is independent of the choice of the dividing interfaces within the leading order. However, if on the other hand in Eq. (2.31) the substrate-liquid surface tension  $\gamma_{s,l}(p_l)$  is evaluated at the pressure  $p_l = p + \Delta p$  and the substrate-liquid surface tension  $\gamma_{s,l}(p_g)$  at the pressure  $p_g = p$ , one obtains an alternative definition of the line tension. It turns out that this alternative definition is equivalent to the definition using the planar interfaces (see Subsec. 2.3.2) and its value depends on the choice of solid-fluid dividing interface as in Eq.

(2.30). In order to distinguish the two definitions of the line tension, the line determined using Eq. (2.31) with  $\gamma_{s,l}(p)$  and  $\gamma_{s,g}(p)$  is called  $\tau$ , whereas the second definition with  $\gamma_{s,l}(p + \Delta p)$  and  $\gamma_{s,g}(p)$  is called  $\tau_w$ . The relation between the two definitions is given by

$$\tau = \tau_w + \frac{r}{2} (\gamma_{s,l}(p + \Delta p) - \gamma_{s,l}(p)), \quad (2.34)$$

which can be written for one-component fluids as

$$\tau = \tau_w - \frac{\Gamma_{s,l}}{\varrho_l} \gamma_{l,g} \sin \vartheta, \quad (2.35)$$

where  $\Gamma_{s,l}$  is the excess adsorption at the planar substrate-liquid interface and  $\varrho_l$  is the bulk density of the liquid phase. Using Eq. (2.35) the line tension determined from a microscopic density functional theory calculation in a wedge geometry can be related to the line tension of sessile droplet.



# Chapter 3

## Wetting in electrolyte solutions: a lattice model

### 3.1 Model

In this chapter a lattice model for an electrolyte solution in contact with a charged wall is studied. The solution consists of three components: solvent (0), anions ( $-$ ), and cations ( $+$ ). The coordinate perpendicular to the wall is  $z$ . The region above the wall, accessible to the electrolyte components, is divided into a set of cells the centers of which form a simple cubic lattice  $\{\mathbf{r}\}$  with lattice constant  $a$ . The volume  $a^3$  of a cell corresponds roughly to the volumes of the particles, which are assumed to be of similar size. The centers of the molecules in the top layer of the substrate form the plane  $z = 0$ . At closest approach the centers of the solvent molecules and ions are at  $z = a$ . The plane  $z = a/2$  is taken to be the surface of the planar wall. Each cell is either empty or occupied by a single particle. This mimics the steric hard core repulsion between all particles. Particles at different sites interact among each other via an attractive nearest-neighbor interaction of strength  $u$  which is taken to be the same for all pairs of particles. In addition, ion pairs interact via the Coulomb potential. The solvent particles are taken to carry a dipole moment.

The wall attracts particles only in the first adjacent layer via an interaction potential of strength  $u_w$  which is the same for all species. In addition it can carry a homogeneous surface charge density  $\tilde{\sigma} = \sigma ea^{-2}$  which is taken to be localized in the plane  $z = a/2$  and which interacts electrostatically with the ions;  $e > 0$  is the elementary charge. Since the focus of this chapter is the influence of ions onto wetting phenomena, the more realistic, long-ranged van der Waals forces which are known to be relevant for wetting transitions [2] are not considered.

The corresponding lattice-gas Hamiltonian for this system reads

$$\begin{aligned}
H = & \frac{1}{2} \sum_{\substack{\mathbf{r}, \mathbf{r}' \\ \mathbf{r} \neq \mathbf{r}'}} \sum_{i,j} n_i(\mathbf{r}) n_j(\mathbf{r}') w(|\mathbf{r} - \mathbf{r}'|) + \frac{1}{2} \sum_{\substack{\mathbf{r}, \mathbf{r}' \\ \mathbf{r} \neq \mathbf{r}'}} \sum_{i,j} \frac{e^2 q_i q_j n_i(\mathbf{r}) n_j(\mathbf{r}')}{4\pi\epsilon_0 |\mathbf{r} - \mathbf{r}'|} \\
& + \sum_{\substack{\mathbf{r}, \mathbf{r}' \\ \mathbf{r} \neq \mathbf{r}'}} \sum_{i,j} \frac{e q_i n_i(\mathbf{r}) \mathbf{m}_j(\mathbf{r}') \cdot (\mathbf{r} - \mathbf{r}')}{4\pi\epsilon_0 |\mathbf{r} - \mathbf{r}'|^3} \\
& + \frac{1}{2} \sum_{\substack{\mathbf{r}, \mathbf{r}' \\ \mathbf{r} \neq \mathbf{r}'}} \sum_{i,j} \left[ \frac{\mathbf{m}_i(\mathbf{r}) \cdot \mathbf{m}_j(\mathbf{r}')}{4\pi\epsilon_0 |\mathbf{r} - \mathbf{r}'|^3} - \frac{3(\mathbf{m}_i(\mathbf{r}) \cdot (\mathbf{r} - \mathbf{r}')) (\mathbf{m}_j(\mathbf{r}') \cdot (\mathbf{r} - \mathbf{r}'))}{4\pi\epsilon_0 |\mathbf{r} - \mathbf{r}'|^5} \right] \\
& - \sum_{\mathbf{r}} \sum_i u_w \delta_{z,a} n_i(\mathbf{r}) - \frac{\tilde{\sigma}}{2\epsilon_0} \sum_{\mathbf{r}} \sum_i q_i n_i(\mathbf{r}) z - \frac{\tilde{\sigma}}{2\epsilon_0} \sum_{\mathbf{r}} \sum_i \mathbf{m}_i(\mathbf{r}) \cdot \hat{\mathbf{e}}_z
\end{aligned} \tag{3.1}$$

where  $n_i(\mathbf{r})$  are occupation number variables, which are either 0 or 1 according to whether the cell at the discrete position  $\mathbf{r} = (\mathbf{r}_{||}, z \geq a) = (x, y, z \geq a) = (ma, na, pa)$  with  $m, n \in \mathbb{Z}$ ,  $|m| \leq \bar{M}/2$  and  $|n| \leq \bar{N}/2$ , and  $p = 1, 2, 3, \dots, \bar{L}$  is empty or occupied by a particle (there is no double occupancy);  $i, j = 0, +, -$ ,  $e q_i$  is the particle charge with  $q_0 = 0$  and  $q_{\pm} = \pm 1$ ;  $\mathbf{m}_i(\mathbf{r})$  is the particle dipole moment at  $\mathbf{r}$  (the typical situation of a polar solvent and of ions without permanent electric dipoles, i.e.,  $\mathbf{m}_{\pm} = 0$ , is considered here);  $w(|\mathbf{r} - \mathbf{r}'|) = -u$  for nearest neighbors ( $u > 0$  corresponds to attraction) and  $w(|\mathbf{r} - \mathbf{r}'|) = 0$  beyond;  $-u_w$  is the strength of the attractive ( $u_w > 0$ ) substrate potential acting on the first layer  $z = a$ . For the charge density  $\tilde{\rho}(\mathbf{r}) = \tilde{\sigma} \delta(z - a/2)$  on a substrate with radial extension  $R_0$  the electrostatic potential is given by  $\tilde{\phi}(\mathbf{r}) = \int d^3 r' \frac{\tilde{\rho}(\mathbf{r}')}{4\pi\epsilon_0 |\mathbf{r} - \mathbf{r}'|} = \frac{\tilde{\sigma}}{2\epsilon_0} (\sqrt{R_0^2 + (z - a/2)^2} - |z - a/2|) \rightarrow -\frac{\tilde{\sigma}}{2\epsilon_0} z + \text{const.}$  for  $R_0 \gg |z - a/2|$  and  $z > a/2$ . In this regime of being close to the charged wall the electric field is uniform [176]. Therefore the actual position of the charged wall enters the electrostatic potential, and thus the Hamiltonian in Eq. (3.1), only via an irrelevant additive constant. The potential energy of a dipole moment  $\mathbf{m}_i(\mathbf{r})$  in the electric field  $\tilde{\mathbf{E}}(\mathbf{r}) = -\tilde{\nabla} \tilde{\phi}(\mathbf{r}) \rightarrow \frac{\tilde{\sigma}}{2\epsilon_0} \hat{\mathbf{e}}_z = \text{const.}$  of the surface charge is given by  $-\mathbf{m}_i(\mathbf{r}) \cdot \tilde{\mathbf{E}}$ . In Eq. (3.1) only charge neutral configurations  $\{n_i(\mathbf{r})\}$ , i.e.,  $\sum_{\mathbf{r}} (n_+(\mathbf{r}) - n_-(\mathbf{r})) = -\bar{M}\bar{N}\sigma$  with  $\mathbf{r} \in V = \bar{M}\bar{N}\bar{L}a^3$ , are considered.

For weak external electric fields the polarization is expected to exhibit a linear response behavior [176]. In this case, it has been shown that the relative permittivity  $\epsilon$  of microscopic models like the one in Eq. (3.1) can be expressed in terms of molecular properties such as the dipole moment and the polarizability [177, 178]. In order to simplify the model, the polar nature of the solvent is taken into account effectively via the relative permittivity  $\epsilon$  of the electrolyte solution which is assumed to depend on the solvent configuration  $n_0(\mathbf{r})$  but not on the configuration of the ions  $n_{\pm}(\mathbf{r})$  because the orientational



polarization, i.e., the polarization due to the permanent dipoles of the solvent molecules, is the dominant contribution to the total polarization. In this case Eq. (3.1) reduces to (see, c.f., Eqs. (3.7) and (3.9))

$$H = \frac{1}{2} \sum_{\substack{\mathbf{r}, \mathbf{r}' \\ \mathbf{r} \neq \mathbf{r}'}} \sum_{i, j} n_i(\mathbf{r}) n_j(\mathbf{r}') w(|\mathbf{r} - \mathbf{r}'|) - \sum_{\mathbf{r}} \sum_i u_w \delta_{z, a} n_i(\mathbf{r}) + \frac{1}{2} \int_V d^3 r^* \tilde{\phi}(\mathbf{r}^*) \tilde{Q}(\mathbf{r}^*) \quad (3.2)$$

where  $\tilde{Q}(\mathbf{r}^*) = \frac{e}{a^3} \sum_i q_i n_i^*(\mathbf{r}^*) + \tilde{\sigma} \delta(z^* - a/2)$  is the local charge density where  $n_i^*(\mathbf{r}^*) = n_i(\mathbf{r})$  for all  $\mathbf{r}^* \in (a\mathbb{R})^3$  and  $\mathbf{r} \in (a\mathbb{Z})^3$  with  $\max(|x^* - x|, |y^* - y|, |z^* - z|) \leq a/2$ ;  $\tilde{\phi}(\mathbf{r}^*)$  is the electrostatic potential which can be obtained by solving the Poisson equation

$$-\varepsilon_0 \tilde{\nabla} \cdot [\varepsilon(n_0^*(\mathbf{r}^*)) \tilde{\nabla} \tilde{\phi}(\mathbf{r}^*)] = \tilde{Q}(\mathbf{r}^*, [n_{\pm}^*]), \quad \mathbf{r}^* \in (a\mathbb{R})^3 \cap V, \quad (3.3)$$

where  $V$  is the volume of the fluid. For general permittivity profiles  $\varepsilon(n_0^*(\mathbf{r}^*))$  no closed solution  $\tilde{\phi}(\mathbf{r}^*)$  of Eq. (3.3) as a functional of  $\varepsilon(n_0^*(\mathbf{r}^*))$  and  $\tilde{Q}(\mathbf{r}^*)$  is known, i.e., for each configuration  $\{n_i(\mathbf{r})\}$  the evaluation of Eq. (3.2) requires to solve the differential equation (3.3) anew. It has been proven, that models including charges as in Eq. (3.2) possess a proper thermodynamic limit for sequences of finite-sized systems, which is independent of the shape of the container, provided that globally charge neutral configurations  $\{n_i(\mathbf{r})\}$  are considered [179, 180]. Since the thermodynamic limit is performed for sequences of finite-sized systems the electrostatic potential  $\tilde{\phi}(\mathbf{r}^*)$  in Eq. (3.3) vanishes at infinity ( $|\mathbf{r}^*| \rightarrow \infty$ ) [176].

## 3.2 Density functional

With a given expression for  $\varepsilon(n_0(\mathbf{r}))$  (see, c.f., Eq. (3.15)), Eq. (3.2) can be used directly for numerical analyses such as Monte Carlo simulations, provided an efficient method to determine the electrostatic potential  $\tilde{\phi}(\mathbf{r}^*)$  for arbitrary permittivity profiles  $\varepsilon(n_0(\mathbf{r}))$  becomes available (see for example Ref. [181] for recent efforts in this direction). In this work, a suitable mean field approximation is considered. This approximation can be formulated as to minimize a grand canonical density functional  $\Omega[\{\varrho_i(\mathbf{r})\}]$  [162] of continuous and dimensionless occupation number distributions  $\varrho_i(\mathbf{r})$  such that at the minimum  $\varrho_i(\mathbf{r}) = \varrho_i^{eq}(\mathbf{r})$  approximates the thermal average  $\langle n_i(\mathbf{r}) \rangle$ .

Application of the Bragg-Williams Approximation [184–187] to the model Hamiltonian in Eq. (3.2) leads to the following grand canonical density functional:

$$\begin{aligned}
\beta\Omega[\{\varrho_i(\bar{\mathbf{r}})\}] &= \sum_{\bar{\mathbf{r}}} \left[ \sum_i \varrho_i(\bar{\mathbf{r}}) \ln \varrho_i(\bar{\mathbf{r}}) + \left(1 - \sum_i \varrho_i(\bar{\mathbf{r}})\right) \ln \left(1 - \sum_j \varrho_j(\bar{\mathbf{r}})\right) \right] \\
&+ \frac{1}{2} \beta \sum_{\substack{\bar{\mathbf{r}}, \bar{\mathbf{r}}' \\ \bar{\mathbf{r}} \neq \bar{\mathbf{r}}'}} \sum_{i,j} \varrho_i(\bar{\mathbf{r}}) \varrho_j(\bar{\mathbf{r}}') w(|\bar{\mathbf{r}} - \bar{\mathbf{r}}'|) - \beta \sum_{\bar{\mathbf{r}}} \sum_i u_w \delta_{z,1} \varrho_i(\bar{\mathbf{r}}) \\
&- \beta \sum_{\bar{\mathbf{r}}} \sum_i \mu_i \varrho_i(\bar{\mathbf{r}}) + 2\pi l_B \int_V d^3 \bar{\mathbf{r}}^* \frac{(\mathbf{D}(\bar{\mathbf{r}}^*, [\varrho_{\pm}^*]))^2}{\varepsilon(\varrho_0^*(\bar{\mathbf{r}}^*))},
\end{aligned} \tag{3.4}$$

where  $\beta = (k_B T)^{-1}$  is the inverse thermal energy and  $\mu_i$  is the chemical potential of species  $i$ ,  $\tilde{l}_B = l_B a = e^2 \beta / (4\pi \varepsilon_0)$  is the Bjerrum length in vacuum,  $\bar{\mathbf{r}} = \mathbf{r}/a$  are the dimensionless lattice positions,  $\bar{\mathbf{r}}^* = \mathbf{r}^*/a$ ,  $\varrho_i^*(\bar{\mathbf{r}}^*) = \varrho_i(\bar{\mathbf{r}})$  for all  $\bar{\mathbf{r}}^* \in \mathbb{R}^3$  and  $\bar{\mathbf{r}} \in \mathbb{Z}^3$  with  $\max(|\bar{x}^* - \bar{x}|, |\bar{y}^* - \bar{y}|, |\bar{z}^* - \bar{z}|) \leq 1/2$ . The actual number densities of the components are given by  $\tilde{\varrho}_i(\bar{\mathbf{r}}) = \varrho_i(\bar{\mathbf{r}}) a^{-3}$ . Charge neutrality demands  $\sum_{\bar{\mathbf{r}}} [\varrho_+(\bar{\mathbf{r}}) - \varrho_-(\bar{\mathbf{r}})] = -\bar{A}\sigma$  where  $A = MN = \bar{A}a^2 = \bar{M}\bar{N}a^2$  is the substrate area and  $\sigma = \tilde{\sigma}/(ea^{-2})$ ; this constraint is implemented via a boundary condition for  $\mathbf{D}$  (see, c.f., Eq. (3.14)). The first two terms of Eq. (3.4) represent the ideal gas or entropic contribution  $\mathcal{F}_{id}$  to the intrinsic Helmholtz free energy functional  $\mathcal{F}[\{\varrho_i(\bar{\mathbf{r}})\}] = \mathcal{F}_{id}[\{\varrho_i(\bar{\mathbf{r}})\}] + \mathcal{F}_{ex}[\{\varrho_i(\bar{\mathbf{r}})\}]$  (see Sec. 2.1); the third and the fourth term represent the non-electrostatic contribution to  $\mathcal{F}_{ex}[\{\varrho_i(\bar{\mathbf{r}})\}]$ , which follows from the first and second term in Eq. (3.2) and turns out to be equal to the random phase approximation (RPA) within density functional theory [162]. This approximation is justified because it has turned out that RPA is reliable in the present situation of vanishing contrast between the non-electrostatic interactions of the three species [21]. The last term is the electrostatic energy. Using SI units, the electrostatic field energy density, which enters into Eq. (3.4), is given by [176]

$$\frac{1}{2} \tilde{\mathbf{E}} \cdot \tilde{\mathbf{D}} = -\frac{1}{2} \frac{\tilde{\mathbf{D}}^2}{\varepsilon_0 \varepsilon} = \frac{1}{2} \frac{\mathbf{D}^2 e^2}{\varepsilon_0 \varepsilon a^4} = 2\pi k_B T l_B \frac{\mathbf{D}^2}{\varepsilon a^3} \tag{3.5}$$

and

$$\frac{1}{2} \tilde{\mathbf{E}} \cdot \tilde{\mathbf{D}} = -\frac{1}{2} \tilde{\nabla} \tilde{\phi} \cdot \tilde{\mathbf{D}} = \frac{1}{2} \tilde{\phi} \left( \tilde{\nabla} \cdot \tilde{\mathbf{D}} \right) - \frac{1}{2} \tilde{\nabla} \cdot \left( \tilde{\phi} \tilde{\mathbf{D}} \right), \tag{3.6}$$

where  $\tilde{\mathbf{E}} = -\tilde{\nabla} \tilde{\phi} = \frac{\tilde{\mathbf{D}}}{\varepsilon_0 \varepsilon}$  is the actual electric field,  $\tilde{\phi}$  is the electrostatic potential and  $\tilde{\mathbf{D}} = \mathbf{D} e a^{-2}$  is the actual electric displacement generated by the ions and the surface charge density  $\tilde{\sigma} = \sigma e a^{-2}$ , satisfying Gauß's law [176]

$$\tilde{\nabla} \cdot \tilde{\mathbf{D}} = \tilde{Q}(\mathbf{r}^*), \tag{3.7}$$

so that ( $\nabla = a\tilde{\nabla}$ )

$$\nabla \cdot \mathbf{D}(\bar{\mathbf{r}}^*, [\varrho_{\pm}^*]) = \sum_i q_i \varrho_i^*(\bar{\mathbf{r}}^*) + \sigma \delta(\bar{z} - 1/2). \quad (3.8)$$

Due to Eq. (3.6), the electrostatic contribution to the functional can be written as

$$\mathcal{F}_{el} = \frac{1}{2} \int d^3r^* \left[ \tilde{\phi}(\mathbf{r}^*) \left( \tilde{\nabla} \cdot \tilde{\mathbf{D}} \right) - \tilde{\nabla} \cdot \left( \tilde{\phi} \tilde{\mathbf{D}} \right) \right], \quad (3.9)$$

where the last term leads to a vanishing surface contribution [176], because the thermodynamic limit is performed for sequences of finite-sized systems. Using Eq. (3.7) renders the last term in Eq. (3.2).

Because the substrate potential depends only on  $\bar{z}$ , the minimum of  $\beta\Omega[\{\varrho_i(\bar{\mathbf{r}})\}]$  lies in the subspace of distributions  $\varrho_i(\bar{\mathbf{r}})$  which depend on  $\bar{z}$  only. Therefore Eq. (3.4) can be written for the special case  $\varrho_i(\bar{\mathbf{r}}) = \varrho_i(\bar{z})$ , i.e.,

$$\begin{aligned} \frac{\beta\Omega[\{\varrho_i(\bar{z})\}]}{A} &= \sum_{\bar{z}=1}^{\bar{L}_z} \left\{ \sum_i \varrho_i(\bar{z}) \ln \varrho_i(\bar{z}) + \left(1 - \sum_i \varrho_i(\bar{z})\right) \ln \left(1 - \sum_j \varrho_j(\bar{z})\right) \right. \\ &\quad - \beta u \sum_{ij} (\varrho_i(\bar{z}) \varrho_j(\bar{z}+1) + 2\varrho_i(\bar{z}) \varrho_j(\bar{z})) - \beta u_w \sum_i \varrho_i(\bar{z}) \delta_{\bar{z},1} \\ &\quad \left. - \beta \sum_i \mu_i \varrho_i(\bar{z}) \right\} + 2\pi l_B \int_{1/2}^{\bar{L}_z+1/2} d\bar{z}^* \frac{(D(\bar{z}^*, [\varrho_{\pm}^*]))^2}{\varepsilon(\varrho_0^*(\bar{z}))}, \end{aligned} \quad (3.10)$$

where  $A = \bar{A}a^2$  is the substrate area so that  $AL_z$  is the volume of the fluid ( $L_z = \bar{L}_za$ ), and  $\varrho_i(\bar{L}_z+1) = 0$ .

Gauß's law (Eq. (3.8)) reduces to

$$\frac{dD(\bar{z}^* > 1/2, [\varrho_{\pm}^*])}{d\bar{z}^*} = \sum_i q_i \varrho_i^*(\bar{z}^*) = \varrho_+^*(\bar{z}^*) - \varrho_-^*(\bar{z}^*), \quad (3.11)$$

where the last term in Eq. (3.8) appears as a boundary condition to Eq. (3.11):

$$D(\bar{z}^* = 1/2, [\varrho_{\pm}^*]) = \sigma. \quad (3.12)$$

Since  $\varrho_{\pm}^* \in [0, 1]$  are bounded, i.e., the densities  $\varrho_{\pm}^*$  do not exhibit  $\delta$ -like singularities, the boundary condition is determined entirely by the surface charge.

The density profiles  $\varrho_{\pm}(\bar{z})$  have to fulfill global charge neutrality, i.e.,

$$\sum_{\bar{z}=1}^{\bar{L}_z} [\varrho_+(\bar{z}) - \varrho_-(\bar{z})] + \sigma = 0, \quad (3.13)$$

which according to the integrated Eq. (3.11) is equivalent to

$$D(\bar{z}^* = \bar{L}_z + 1/2, [\varrho_{\pm}^*]) = 0. \quad (3.14)$$

The relative permittivity  $\varepsilon(\bar{z}^*)$  is taken to depend locally on the solvent density  $\varrho_0^*(\bar{z}^*)$  (see Subsec. 3.1) through the Clausius-Mossotti expression [176]

$$\varepsilon(\varrho_0^*(\bar{z}^*)) = \frac{1 + \frac{2\alpha}{3\varepsilon_0}\varrho_0(\bar{z}^*)}{1 - \frac{\alpha}{3\varepsilon_0}\varrho_0^*(\bar{z}^*)}, \quad (3.15)$$

where  $\alpha$  is an effective polarizability of the solvent molecules. In the following its value is chosen such that  $\varepsilon = 60$  for  $\varrho_0 = 1$ ; this choice corresponds to a mean value for liquid water along the liquid-vapor coexistence curve.

As for a lattice model Eqs. (3.2) and (3.10) do not include the kinetic energy. The latter requires an off-lattice description which leads to a density independent contribution to the chemical potential of species  $i$  so that

$$\begin{aligned} \mu_{i,phys} &= k_B T \ln(\tilde{\varrho}_i \Lambda_i^3) + \mu_{ex}, \\ &= k_B T \ln\left(\frac{\varrho_i}{a^3} \Lambda_i^3\right) + \mu_{ex}, \\ &= k_B T \ln(\varrho_i) + \mu_{ex} + 3k_B T \ln(\Lambda_i/a), \\ &= \mu_i + 3k_B T \ln(\Lambda_i/a), \end{aligned} \quad (3.16)$$

where  $\Lambda_i = h/\sqrt{2\pi m_i k_B T}$  is the thermal wavelength,  $m_i$  is the particle mass, and  $\mu_{ex}$  is the excess chemical potential over the ideal gas contribution. This gives rise to a density independent difference between the actual physical chemical potential  $\mu_{i,phys}$  and the chemical potential  $\mu_i$  of the lattice-gas model:  $\mu_{i,phys} - \mu_i = 3k_B T \ln(\Lambda_i/a)$ .

In order to obtain the equilibrium configuration, the density functional in Eq. (3.10) has to be minimized under the constraints given by Eq. (3.12) and Eq. (3.14) [162]. The variation of Eq. (3.10) reads:

$$\begin{aligned}
\frac{\beta\delta\Omega[\{\varrho_i(\bar{z})\}]}{A} &= \sum_{\bar{z}=1}^{\bar{L}} \left\{ \sum_i \delta\varrho_i(\bar{z}) \left[ \ln \varrho_i(\bar{z}) - \beta\mu_i - \ln \left( 1 - \sum_j \varrho_j(\bar{z}) \right) \right] \right. \\
&\quad - \beta u \sum_{ij} \left( \delta\varrho_i(\bar{z})\varrho_j(\bar{z}+1) + \varrho_i(\bar{z})\delta\varrho_j(\bar{z}+1) + 2\delta\varrho_i(\bar{z})\varrho_j(\bar{z}) + 2\varrho_i(\bar{z})\delta\varrho_j(\bar{z}) \right) \\
&\quad - 2\pi l_B \int_{\bar{z}-1/2}^{\bar{z}+1/2} d\bar{z}^* \frac{(D(\bar{z}^*, [\varrho_{\pm}^*]))^2}{(\varepsilon(\varrho_0^*(\bar{z}^*)))^2} \varepsilon'(\varrho_0^*(\bar{z}^*)) \sum_i \delta_{i,0} \delta\varrho_i^*(\bar{z}^*) \\
&\quad \left. + 4\pi l_B \int_{\bar{z}-1/2}^{\bar{z}+1/2} d\bar{z}^* \frac{D(\bar{z}^*, [\varrho_{\pm}^*])}{\varepsilon(\varrho_0^*(\bar{z}^*))} \delta D(\bar{z}^*) - \beta u_w \sum_i \delta_{\bar{z},1} \delta\varrho_i(\bar{z}) \right\} \\
&= \sum_{\bar{z}=1}^{\bar{L}} \left\{ \sum_i \delta\varrho_i(\bar{z}) \left[ \ln \varrho_i(\bar{z}) - \beta\mu_i - \ln \left( 1 - \sum_j \varrho_j(\bar{z}) \right) \right] \right. \\
&\quad - \beta u \sum_j \left( \varrho_j(\bar{z}+1) + \sum_{\bar{z}'=1}^{\bar{L}} \varrho_j(\bar{z}') \delta_{\bar{z},\bar{z}'+1} + 2\varrho_j(\bar{z}) + 2\varrho_j(\bar{z}) \right) - \beta u_w \delta_{\bar{z},1} \left. \right] \\
&\quad - 2\pi l_B \int_{\bar{z}-1/2}^{\bar{z}+1/2} d\bar{z}^* \frac{(D(\bar{z}^*, [\varrho_{\pm}^*]))^2}{(\varepsilon(\varrho_0^*(\bar{z}^*)))^2} \varepsilon'(\varrho_0^*(\bar{z}^*)) \delta_{i,0} \delta\varrho_i^*(\bar{z}^*) \\
&\quad \left. - \int_{\bar{z}-1/2}^{\bar{z}+1/2} d\bar{z}^* \phi'(\bar{z}^*) \delta D(\bar{z}^*) \right\}
\end{aligned} \tag{3.17}$$

where  $\phi(\bar{z}^*) = \beta e \tilde{\phi}(z^*)$  is the dimensionless electrostatic potential which fulfills

$$\begin{aligned}
\tilde{D}(z^*) &= \varepsilon_0 \varepsilon \tilde{E}(z^*) = -\varepsilon_0 \varepsilon \frac{d\tilde{\phi}(z^*)}{dz^*}, \\
ea^{-2}D(\bar{z}^*) &= -\varepsilon_0 \varepsilon \frac{1}{a} \frac{d}{d\bar{z}^*} \left( \frac{\phi(\bar{z}^*)}{\beta e} \right), \\
D(\bar{z}^*) &= -\frac{\varepsilon}{4\pi l_B} \phi'(\bar{z}^*).
\end{aligned} \tag{3.18}$$

Upon integrating by parts the last term in Eq. (3.17), by using Eq. (3.12) so that  $\delta D(\bar{z}^* = 1/2) = 0$  and Eq. (3.14) so that  $\delta D(\bar{z}^* = \bar{L} + 1/2) = 0$ , with  $\delta D'(\bar{z}^*) = \sum_i q_i \delta\varrho_i^*(\bar{z}^*)$  due to Eq. (3.11), and  $\delta\varrho^*(\bar{z}^*) = \delta\varrho_i(\bar{z})$  for all  $\bar{z}^* \in \mathbb{R}$  and  $\bar{z} \in \mathbb{Z}$  with  $\max(|\bar{z}^* - \bar{z}| \leq 1/2)$  one obtains the following three coupled Euler-Lagrange equations for  $\bar{z} \in \{1, \dots, \bar{L}\}$

$$\ln \varrho_i(\bar{z}) - \mu_i^* - \beta u_w \delta_{\bar{z},1} - \ln \left( 1 - \sum_j \varrho_j(\bar{z}) \right) - \frac{1}{3T^*} \sum_j (4\varrho_j(\bar{z}) + \varrho_j(\bar{z}+1) + \varrho_j(\bar{z}-1))$$

$$+ q_i \int_{\bar{z}-1/2}^{\bar{z}+1/2} d\bar{z}^* \phi(\bar{z}^*) - 2\pi l_B \int_{\bar{z}-1/2}^{\bar{z}+1/2} d\bar{z}^* \frac{(D(\bar{z}^*, [\varrho_{\pm}^*]))^2}{(\varepsilon(\varrho_0^*(\bar{z}^*)))^2} \varepsilon'(\varrho_0^*(\bar{z}^*)) \delta_{i,0} = 0 \quad (3.19)$$

with  $i, j = 0, +, -$ , where  $q_i e$  is the electric charge of component  $i$  and  $T^* = \frac{1}{3\beta u}$  is the reduced temperature and  $\mu_i^* = \beta\mu_i$ . At the wall the convention  $\varrho_j(0) = 0$  is used. The integrals in Eq. (3.19) are approximated by

$$\int_{\bar{z}-1/2}^{\bar{z}+1/2} d\bar{z}^* f(\bar{z}^*) \approx ((\bar{z} + 1/2) - (\bar{z} - 1/2)) f\left(\frac{(\bar{z} + 1/2) + (\bar{z} - 1/2)}{2}\right) = f(\bar{z}). \quad (3.20)$$

For given chemical potentials  $\mu_i$  these coupled equations can be solved numerically by an iterative algorithm. The values of the chemical potentials  $\mu_i$  considered here correspond to those for the bulk gas phase of the system. For each iteration the electrostatic potential  $\phi(\bar{z}^*)$  must be calculated by solving Poisson's equation (see Eqs. (3.11) and (3.18))

$$\frac{d}{d\bar{z}^*}(\varepsilon(\varrho_0^*(\bar{z}^*))\phi'(\bar{z}^*)) = -4\pi l_B \sum_i q_i \varrho_i^*(\bar{z}^*), \quad (3.21)$$

ensuring global charge neutrality at each step.

### 3.2.1 Wetting films

The wetting behavior can be transparently inferred from the effective interface potential  $\omega(\ell)$  introduced in Subsec. 2.2.1. Here, in order to obtain  $\Omega_s(\ell)$ ,  $\Omega[\varrho_i(z)]$  (Eq. 3.10) has been minimized under the constraint

$$\sum_{\bar{z}=1}^{\infty} (\varrho_0(\bar{z}) - \varrho_{0,b}) = \Gamma = \ell(\varrho_{0,l} - \varrho_{0,g}), \quad (3.22)$$

where  $\varrho_{0,b}$  is the number density of the bulk gas phase in units of  $a^{-3}$  and  $\tilde{\ell} = \ell a$  is the film thickness defined as

$$\ell = \frac{\Gamma}{\varrho_{0,l} - \varrho_{0,g}}, \quad (3.23)$$

where  $\tilde{\Gamma} = \int_0^\infty dz (\tilde{\varrho}_0(z) - \tilde{\varrho}_0(\infty)) = \Gamma a^{-2}$  is the excess adsorption (or coverage) of the substrate by the solvent and  $\varrho_{0,l}$  and  $\varrho_{0,g}$  are the corresponding bulk number densities of the liquid and the gas phase, respectively.

### 3.2.2 Choice of parameters

If one chooses the lattice constant  $a$  to be equal to  $4\text{\AA}$ , the maximal density  $1/a^3$  lies between the densities for liquid water at the triple point and at the critical point. Accordingly, the choice  $l_B = 400$  corresponds to  $T \approx 417$  K. This temperature lies between the triple point temperature of 273 K and the critical point temperature of 647 K for water. In the units used in this chapter  $1 \text{ mM} = 10^{-3} \text{ mol/L}$  corresponds to  $\varrho_i = \tilde{\varrho}_i a^3 = 3.9 \times 10^{-5}$ .

For the present calculation values for the reduced surface charge density  $\sigma$  in the range between 0 and  $10^{-2}$  have been used. For  $a = 4\text{\AA}$  the latter value corresponds to  $1 \mu\text{C}/\text{cm}^2$ . Such values are within the range of measured surface charge densities of silicon nitride at two different concentrations of the background electrolyte NaCl (1 mM, 10 mM) determined by potentiometric pH titration [188], which is a common method to determine the unknown concentration of an identified substance and to estimate the surface charge of a solid by comparing the titration of the solution with solid against the titration of the same solution without solid.

These consideration indicate that the values of the reduced substrate surface charge densities  $\sigma$  and ionic strengths  $I$  considered in the following are within the range of values for which Poisson-Boltzmann theory, i.e., mean-field theory for the electrostatic interaction, shows quantitative agreement with corresponding Monte Carlo simulations [79]. The former is essentially identical to the theory used to describe the ions in Eq. (3.10) if one neglects the effect of nonzero ion size, which is weak for the considered dilute electrolyte solutions.

### 3.3 Bulk phase diagram

In the bulk, the number densities  $\varrho_i$  of the fluid are spatially constant and from the requirement of local charge neutrality it follows that  $\varrho_+ = \varrho_- = I$ , where  $I$  is the so-called ionic strength for monovalent ions. Under these conditions the density functional given by Eq. (3.10) reduces to

$$\begin{aligned} \frac{\beta\Omega[\{\varrho_i\}]}{\bar{V}} = & \varrho_0(\ln \varrho_0 - \mu_0^*) + I(2 \ln I - \mu_I^*) \\ & + (1 - \varrho_0 - 2I) \ln (1 - \varrho_0 - 2I) - \frac{1}{T^*}(\varrho_0 + 2I)^2, \end{aligned} \quad (3.24)$$

where  $\mu_I^* = \mu_+^* + \mu_-^*$  and  $\bar{V} = V/a^3$  ( $V$  is the volume of the fluid). The last term in Eq. (3.10) vanishes because in the bulk  $D = 0$  due to Eq. (3.11). The Euler Lagrange

equations (3.19) read

$$\begin{aligned} \ln \varrho_0 - \mu_0^* - \ln(1 - \varrho_0 - 2I) - \frac{2}{T^*}(\varrho_0 + 2I) &= 0 \\ 2 \ln I - \mu_I^* - 2 \ln(1 - \varrho_0 - 2I) - \frac{4}{T^*}(\varrho_0 + 2I) &= 0. \end{aligned} \quad (3.25)$$

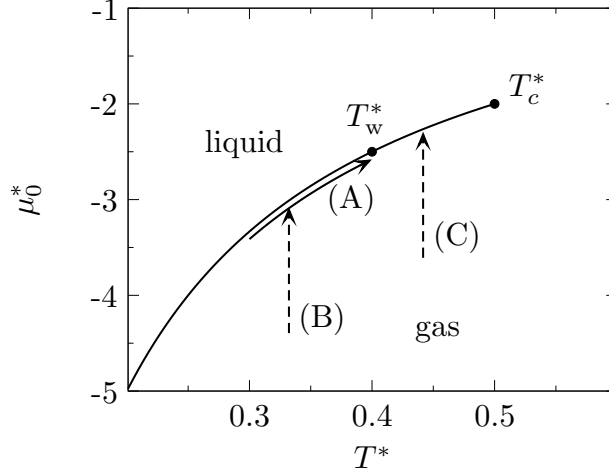


Figure 3.1: Bulk phase diagram  $\mu_{0,co}(T)$  of liquid-gas coexistence according to Eq. (3.24) in the  $\mu_0^* - T^*$  plane for the salt-free ( $I = 0$ ) case of a pure solvent. If the wetting transition temperature  $T_w^*$  is above the triple point  $T_t^* \simeq 0.21$  (for water), three types of paths (A), (B), and (C) are used to study the wetting behavior of the present model. (A) is a path along gas-liquid coexistence on the gas side whereas along the paths (B) and (C) two-phase coexistence is approached along isotherms leading to incomplete (B) and complete (C) wetting, respectively.

For a given ionic strength  $I = \varrho_{\pm}^{(1)}$  in the liquid phase of the solution, the liquid-gas coexistence curves, i.e., the solvent density in the liquid phase of the solution and the coexisting densities of the ions and of the solvent in the gas phase of the solution, are determined by the equality of the chemical potentials  $\mu_0$  and  $\mu_I$  and of the pressure  $p$ :

$$\begin{aligned} \mu_0[\{\varrho_{i,g}\}, T^*] &= \mu_0[\{\varrho_{i,l}\}, T^*], \\ \mu_I[\{\varrho_{i,g}\}, T^*] &= \mu_I[\{\varrho_{i,l}\}, T^*], \\ p[\{\varrho_{i,g}\}, T^*] &= p[\{\varrho_{i,l}\}, T^*]. \end{aligned} \quad (3.26)$$

For  $I = 0$  the resulting phase diagram can be determined analytically and is plotted in Fig. 3.1. The reduced critical temperature is  $T_c^*(I = 0) = 0.5$  and the critical number density is  $\varrho_{0,c}(I = 0) = 0.5$ . For  $I \neq 0$  the binodal curves are determined numerically and the critical points are obtained by determining the maximum of the corresponding



spinodal curves. Within the present model the reduced critical temperature  $T_c^*$  is independent of  $I$  whereas  $\varrho_{0,c}(I) = 0.5 - 2I$ . In agreement with experimental evidence [189] the shift of the binodal curves is negligibly small for ionic strengths up to 10 mM, i.e.,  $I \leq 3.9 \times 10^{-4}$ .

## 3.4 Wetting

### 3.4.1 Wetting in the salt-free solvent

In this section the wetting behavior in the case  $I = 0$  is considered. Under this condition, the model described in Sec. 3.1 reduces to the lattice-gas model studied by Pandit et al. [190, 191]. In that case, the Euler-Lagrange equations in Eq. (3.19) reduce to

$$\ln \varrho_0(\bar{z}) - \ln [1 - \varrho_0(\bar{z})] - \mu_0^* - \beta u_w \delta_{1,\bar{z}} - \frac{1}{3T^*} [4\varrho(\bar{z}) + \varrho(\bar{z} + 1) + \varrho(\bar{z} - 1)] = 0, \quad (3.27)$$

and the ratio  $u_w/u = 3T^*\beta u_w$  controls the wetting and drying transitions. For  $u_w/u > 1$  the substrate is so strong that it is already wet at  $T^* = 0$ ; in the range  $0.5 < u_w/u < 1$  there is a wetting transition at  $T_w^* > 0$ ; and in the parameter range  $0 \leq u_w/u < 0.5$  a drying transition occurs. Depending on the value of the ratio  $u_w/u$  one observes layering transitions, i.e., one can distinguish the number of discrete layers which are forming upon reaching thick films. The transition from  $n$  to  $n + 1$  layers is first order and shows up as a jump in the film thickness  $\ell$ . The loci of these discontinuities are layering transition lines, each ending at a critical point  $T_{c,n}^*$ . For large  $n$ ,  $T_{c,n}^*$  approaches the roughening transition. However, within the present mean-field theory  $T_{c,n}^*$  approaches  $T_c^*$ . Since layering transitions should only occur along or near the melting curve or the sublimation line, these layering transitions are a special feature of the lattice-gas model used to describe the liquid and gas phases [2].

Calculations in the parameter range  $0.5 < u_w/u < 1$  were carried out. A wider range of the parameter  $u_w/u$  was studied thoroughly by Pandit et al. [190, 191]. Figure 3.2 shows the effective interface potential  $\omega(\ell) = \Omega_s(\ell) - \gamma_{g,l} - \gamma_{l,s}$  for three different temperatures along a path at coexistence [path (A) in Fig. 3.1] for the rather arbitrarily chosen values  $u_w/u = 0.81$  and  $u_w/u = 0.69$ . Here  $\gamma_{g,l}$  and  $\gamma_{l,s}$  are the gas-liquid and liquid-substrate interfacial tensions, respectively, such that by construction at two-phase coexistence  $\omega(\ell \rightarrow \infty) = 0$ . The equilibrium thickness of the liquid film is given by the position of the global minimum of  $\omega(\ell)$ . If  $\ell = \infty$  is the global minimum of  $\Omega_s(\ell)$  the system is wet. In this case, the gas-substrate surface tension is given by  $\gamma_{g,s} = \Omega_s(\ell = \infty) = \gamma_{g,l} + \gamma_{l,s}$ .

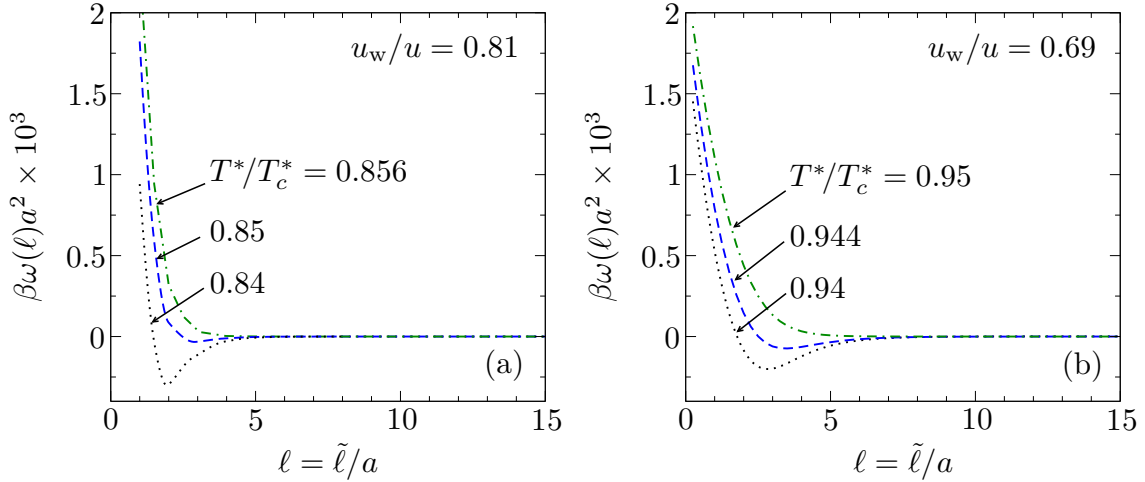


Figure 3.2: Effective interface potential  $\omega(\ell) = \Omega_s(\ell) - \gamma_{g,l} - \gamma_{l,s}$  at two-phase coexistence as a function of the thickness  $\ell = \tilde{\ell}a$  of the adsorbed liquid film for three temperatures in the salt-free case ( $I = 0$ ) for  $u_w/u = 0.81$  (a) and  $u_w/u = 0.69$  (b). In both cases  $\omega(\ell)$  exhibits only a single minimum, the position of which diverges continuously as  $T^* \rightarrow T_w^*$ . Accordingly, the system undergoes critical wetting at  $T_w^* \simeq 0.856T_c^*$  for  $u_w/u = 0.81$  and at  $T_w^* \simeq 0.95T_c^*$  for  $u_w/u = 0.69$ .

In the two cases which were considered in Fig. 3.2,  $\omega(\ell)$  exhibits only a single minimum, the position of which diverges continuously or via steps of finite size as  $T^* \rightarrow T_w^*$ . For  $T^* > T_w^*$  the position of the minimum is  $\ell = \infty$  and the system is wet. The wetting transition is second order and occurs at the temperature  $T_w^* \simeq 0.856T_c^*$  for  $u_w/u = 0.81$  and at  $T_w^* \simeq 0.95T_c^*$  for  $u_w/u = 0.69$ . Within the present model, in which all interactions are of the nearest-neighbor type only for the pure solvent, the system exhibits a second-order wetting transition in the entire parameter range  $0.5 < u_w/u < 1$ . This observation is compatible with corresponding Monte Carlo simulations of the Ising model on a cubic lattice [192, 193]. However, the order of wetting transitions depends sensitively on the range of interactions as well as on whether a continuous or a lattice model is considered. For a continuous analogue of the present model, Pandit et al. [191] found a second-order wetting transition only for  $0.5 < u_w/u \lesssim 0.7$  but a first-order one for  $u_w/u \gtrsim 0.7$ .

Moreover, lattice-gas models with short-ranged particle-particle interactions and long-ranged substrate potentials were studied by de Oliveira and Griffiths [194] and Ebner [195, 196]. In Ref. [194] complete wetting in a system with  $T_w = 0$  was studied within mean field theory. Ebner reported  $T_w = 0$  or a first-order wetting transition depending on the strength of the substrate potential [195] and studied the same interaction potentials as the ones used in Refs. [194, 195] applying Monte Carlo simulations [196]. Finally,

in systems in which both the particle-particle interactions and the substrate potentials are long-ranged, critical (i.e., second-order) and first-order wetting can occur for suitable choices of the interaction potentials [197, 198].

The film thickness  $\ell = \tilde{\ell}/a$  as function of  $\mu_{0,co}^*(T^*) - \mu_0^*$ , when bulk coexistence  $\mu_{0,co}(T^*)$  (see Fig. 3.1) is approached along four isotherms from the gas phase [paths of type (B) and (C) in Fig. 3.1], is plotted in Fig. 3.3. In the case  $u_w/u = 0.81$  (Fig. 3.3(a)) the isotherms exhibit vertical steps at the aforementioned layering transitions. Above  $T_w^*$ , i.e., when the substrate is completely wet at coexistence, the isotherms exhibit an unlimited number of such steps as  $\mu_{0,co}^*(T^*) - \mu_0^*$  approaches zero, while for  $T^* < T_w^*$  there is only a finite number of steps. For  $u_w/u = 0.69$  (Fig. 3.3(b)) layering transitions do not occur and the film thickness diverges logarithmically for  $T^* > T_w^*$ , while for  $T^* < T_w^*$  it reaches a finite value at coexistence.

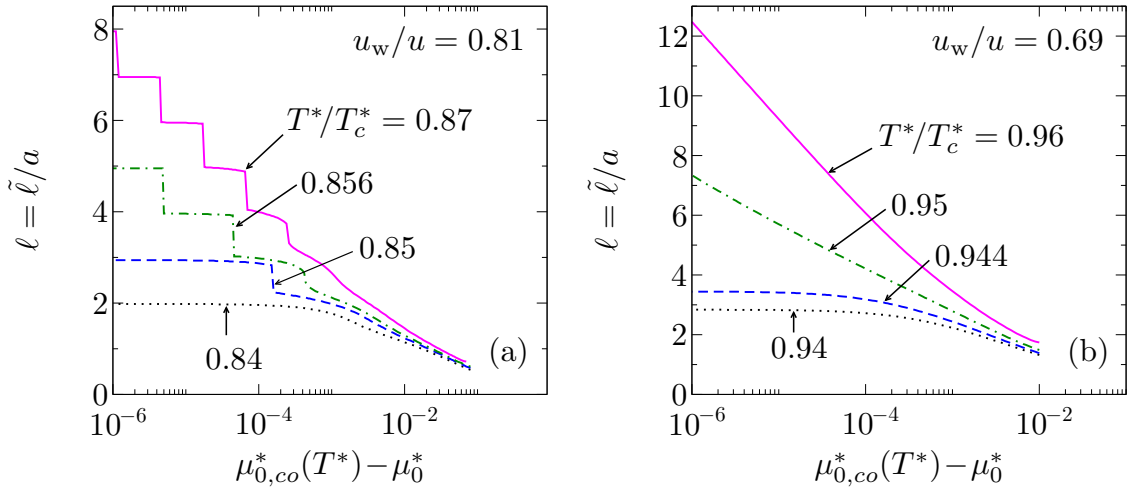


Figure 3.3: Film thickness  $\ell = \tilde{\ell}/a$  in units of the lattice constant  $a$  as a function of undersaturation  $\mu_{0,co}^*(T^*) - \mu_0^*$  for the salt-free case ( $I = 0$ ). Gas-liquid coexistence  $\mu_{0,co}^*(T^*)$  is approached from the gas phase. (a)  $u_w/u = 0.81$ : for  $T^* < T_w^* = 0.856T_c^*$  the system is partially wet and, if at all, there is a finite number of layering transitions; for  $T^* > T_w^*$  the isotherms exhibit an unlimited number of layering transitions as  $\mu_{0,co}^*(T^*) - \mu_0^* \rightarrow 0$  and the first few layering transitions are rounded because for this temperature  $T^* > T_{c,n}^*$ . (b)  $u_w/u = 0.69$ : the film thickness diverges logarithmically for  $T^* > T_w^* = 0.95T_c^*$ , while it reaches a finite value at coexistence for  $T^* < T_w^*$ . In (b) there are no layering transitions. Note that with  $T_c^*(I) = \frac{1}{2}$  one has  $\mu_{0,co}^*(T^*) - \mu_0^* = \frac{2/3}{T^*/T_c^*} \left[ \frac{\mu_{0,co}(T^*) - \mu_0}{u} \right]$ .

### 3.4.2 Wetting in electrolyte solution

Within the above concepts this section focuses on the influence of the ionic strength  $\tilde{I} = Ia^{-3}$  and of the surface charge density  $\tilde{\sigma} = \sigma ea^{-2}$  on the wetting behavior of systems with  $u_w/u = 0.81$  or  $u_w/u = 0.69$ . If the substrate is neutral ( $\sigma = 0$ ), the addition of salt changes neither the order nor the transition temperature of the wetting transition, i.e., there is a second-order wetting transition at the wetting temperature  $T_w^*$  as discussed in the previous Subsubsec. 3.4.1. This is expected because within the present model all particles have the same size, the ions have the same absolute charge, and the strength of the particle-particle and of the substrate-particle nearest-neighbor interactions are the same for all three species. Hence local charge neutrality ( $\rho_+(\bar{z}) = \rho_-(\bar{z})$ ) holds due to the exchange symmetry with respect to the ionic components. This implies that there is no electric field ( $D(\bar{z}) = 0$ ). If the surface charge becomes non-zero, the order of the wetting transition changes from second order ( $\sigma = 0$ ) to first order ( $\sigma \neq 0$ ) for all values of the charge density  $\sigma$  and ionic strength  $I$  studied here, with  $\sigma = 2 \times 10^{-5}$  (i.e.,  $\tilde{\sigma} \approx 0.002 \mu\text{C}/\text{cm}^2$ ) as the smallest non-zero value considered. This result is in agreement with previous studies. The influence of ionic solutes on the order of the wetting transition was studied in Ref. [18] by using Cahn's phenomenological theory and in Ref. [19] by using density functional theory for an explicit solvent model for an ionic solution. Both studies suggest that electrostatic interactions favor first-order wetting.

Figure 3.4 shows examples of the effective interface potential  $\omega(\ell)$  in the case of non-zero surface charge densities,  $\sigma = 2 \times 10^{-3}$  and  $\sigma = 2 \times 10^{-4}$ , for two temperatures and at bulk coexistence [see path (A) in Fig. 3.1]. In both cases,  $\omega(\ell)$  has two local minima. For  $T^* < T_w^*$  the global minimum corresponds to a thin film whereas for  $T^* > T_w^*$  the film is macroscopically thick. At the wetting transition temperature  $T_w^*$  the two minima correspond to the same value of the effective interface potential  $\omega(\ell)$ . Accordingly, at  $T_w^*$  the film thickness jumps discontinuously from a finite value below  $T_w^*$  to a macroscopic one above  $T_w^*$  so that the system undergoes a first-order wetting transition. If  $\sigma$  is decreased the height of the barrier in  $\omega(\ell)$  at the wetting temperature  $T_w^*$  decreases and the minimum close to the wall is shifted to larger thicknesses (Fig. 3.4(b)). In the case  $\sigma = 0$ ,  $\omega(\ell)$  has only a single minimum, like in the salt-free case (see Fig. 3.2), corresponding to a second-order wetting transition.

In Fig. 3.5 the wetting transition temperature is plotted as function of the surface charge density for two values of the ionic strength and for  $u_w/u = 0.81$  (Fig. 3.5 (a)) and  $u_w/u = 0.69$  (Fig. 3.5 (b)). As  $\sigma = \tilde{\sigma}a^2/e$  is increased, the wetting transition temperature  $T_w^*$  decreases due to the strengthening of the substrate-fluid attraction as the substrate is charged up. For  $\sigma \neq 0$  the system with a smaller ionic strength  $I$  has always the lower

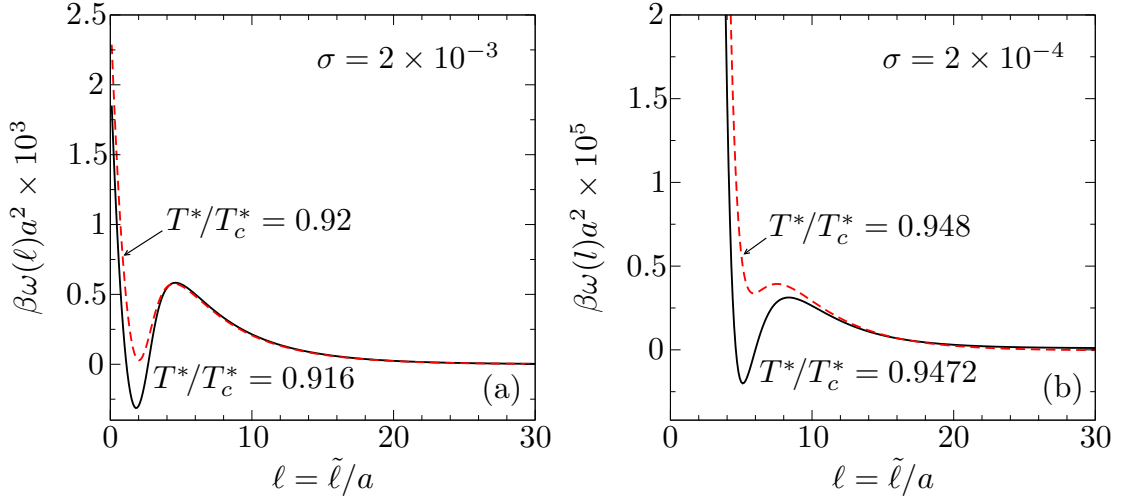


Figure 3.4: Effective interface potential  $\omega(\ell)$  at gas-liquid coexistence as function of the thickness  $\ell = \tilde{\ell}/a$  of the liquid film for  $u_w/u = 0.69$ ,  $I = 3.9 \times 10^{-5}$  ( $\tilde{I} = 1\text{mM}$ ), and  $\sigma = 2 \times 10^{-3}$  ( $\tilde{\sigma} = 0.2\mu\text{C}/\text{cm}^2$ ) in (a) and  $\sigma = 2 \times 10^{-4}$  ( $\tilde{\sigma} = 0.02\mu\text{C}/\text{cm}^2$ ) in (b) for two temperatures in each case. The effective interface potential  $\omega(\ell)$  has two local minima (one at  $\ell < \infty$  and one at  $\ell = \infty$ ) which have the same depth at  $T_w^*$ . Accordingly, for both surface charge densities  $\sigma$  the system undergoes a first-order wetting transition.

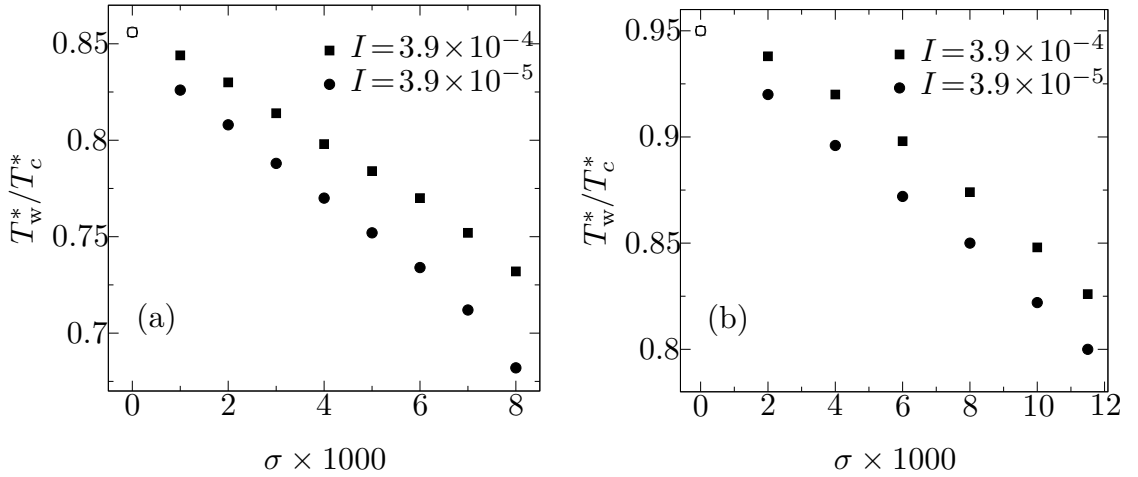


Figure 3.5: Wetting transition temperature  $T_w^*$  as a function of the substrate surface charge density  $\sigma = \tilde{\sigma}a^2/e$  for  $u_w/u = 0.81$  in (a) and for  $u_w/u = 0.69$  in (b). The two types of symbols correspond to distinct values of the ionic strength  $I = \tilde{I}a^3$  in the bulk liquid phase ( $\bullet$  for  $I = 3.9 \times 10^{-5}$  ( $\tilde{I} = 1\text{mM}$ ) and  $\blacksquare$  for  $I = 3.9 \times 10^{-4}$  ( $\tilde{I} = 10\text{mM}$ )). Filled symbols correspond to first-order wetting transitions, while the empty one at  $\sigma = 0$  corresponds to a second-order wetting transition, with the corresponding wetting transition temperature being independent of  $I$ .

wetting transition temperature  $T_w^*$  because in this case the screening of the electrostatic forces of the substrate is reduced making them effectively stronger which favors wetting. As already mentioned above, within the present model for  $\sigma = 0$  the wetting transition temperature is independent of the ionic strength  $\tilde{I} = Ia^{-3}$ . In the case of first-order wetting transitions these results are in qualitative agreement with Ref. [19]. However, the off-lattice model used therein exhibits also second-order wetting transitions (see the discussion above in Subsubsec. 3.4.1), for which  $T_w^*$  is a non-monotonic function of  $\sigma$ .

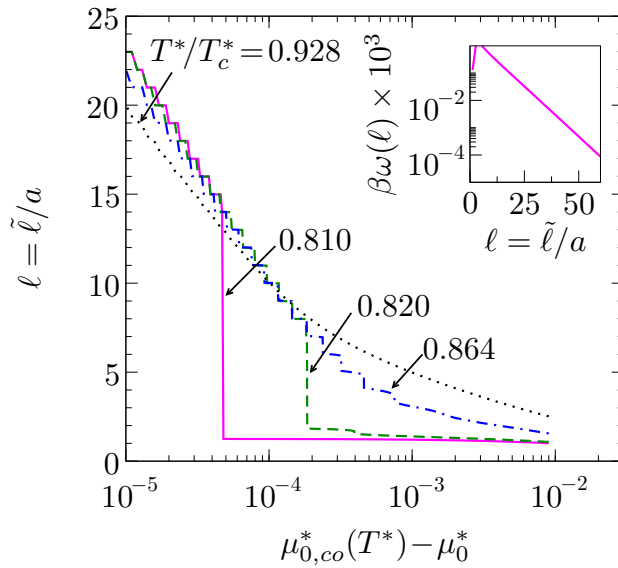


Figure 3.6: The film thickness  $\ell = \tilde{\ell}a$  (Eq. (3.23)) as a function of undersaturation  $\mu_{0,co}^*(T^*) - \mu_0^*$  along four different isotherms for  $u_w/u = 0.81$ ,  $I = 3.9 \times 10^{-5}$  ( $\tilde{I} = 1\text{mM}$ ), and  $\sigma = 2 \times 10^{-3}$  ( $\tilde{\sigma} = 0.2\mu\text{C}/\text{cm}^2$ ) exhibits a large but finite jump (corresponding to more than one monolayer) when the prewetting line is crossed and small jumps when the various layering transition lines are crossed. The film thickness increases for small undersaturation as  $\ell \sim \ln(\mu_{0,co}^*(T^*) - \mu_0^*)$  where  $\mu_{0,co}^*(T^*) - \mu_0^* = \frac{2/3}{T^*/T_c^*} \left[ \frac{\mu_{0,co}(T^*) - \mu_0}{u} \right]$ . The inset displays the corresponding asymptotic behavior of the effective interface potential  $\omega(\ell) \sim \exp(-2\kappa\ell)$  where  $\kappa = \sqrt{8\pi l_B I / (\epsilon(\rho_0^{(l)}))}$  is the inverse Debye length.

Since the wetting transitions for  $\sigma \neq 0$  are first order, there is a prewetting line associated with them. The prewetting line is attached tangentially to the gas-liquid coexistence line at the wetting temperature  $T_w^*$  and bends away from coexistence, marking the loci of a finite discontinuity in film thickness  $\ell = \tilde{\ell}a$ . The discontinuity upon crossing the prewetting line gets smaller as one moves further away from coexistence and it vanishes at the prewetting critical point. Figure 3.6 shows the film thickness  $\ell = \tilde{\ell}a$  for four different isotherms as a function of undersaturation  $\mu_{0,co}^*(T^*) - \mu_0^*$  for  $u_w/u = 0.81$  and

$\sigma = 2 \times 10^{-3}$  ( $\tilde{\sigma} = 0.2 \mu\text{C}/\text{cm}^2$ ). The film thickness increases for small undersaturation as  $\ell \sim \ln(\mu_{0,co}^*(T^*) - \mu_0^*)$ . Accordingly,  $\omega(\ell) \sim \exp(-2\kappa\ell)$ , where  $\kappa = \sqrt{8\pi l_B I / \varepsilon(\varrho_0^l)}$  is the inverse Debye length (see inset of Fig. 3.6). This is in agreement with Refs. [16] and [18] for wetting of solvents with added salt. In contrast, for wetting films of solvents without addition of salt, i.e., with counterions only, one has  $\ell \sim (\mu_{co} - \mu)^{-1/2}$  and  $\omega(\ell) \sim \ell^{-1}$  [12, 14, 15, 18]. In order to obtain this result, Eqs. (3.2) and (3.10) have to be modified to consider only solvent particles and counterions but leaving out coions. In addition to the finite thin-thick jumps in film thickness  $\ell$  when crossing the prewetting line first-order layering transitions similar to those found in the salt-free case for  $u_w/u = 0.81$  (see Fig. 3.3) are observed. The addition of the electrostatic interaction leads to a series of triple points where the layering transition lines meet the prewetting line, as shown in the surface phase diagram in Fig. 3.7. A similar phase diagram was found by Ebner [195] using a lattice-gas model for a one-component fluid in which the fluid particles interact among each other via a Lennard-Jones (6-12) potential and a fluid particle interacts with the substrate via a (9-3) potential. This is also in line with the prediction by Pandit et al. [190] for a substrate of intermediate strength, i.e., for  $0.5 < u_w/u < 1$ , with interactions ranging beyond nearest neighbors.

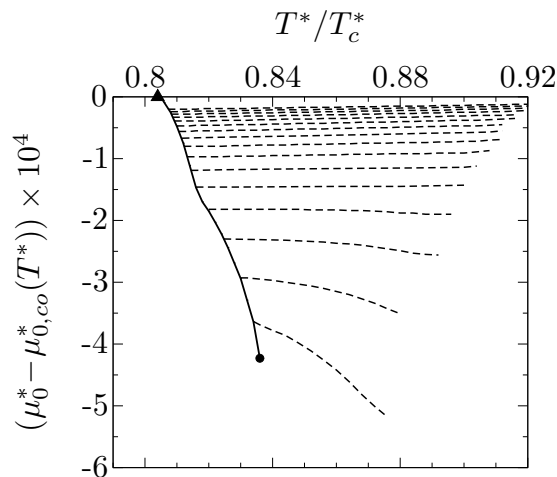


Figure 3.7: Surface phase diagram for  $u_w/u = 0.81$  and  $\sigma = 2 \times 10^{-3}$  ( $\tilde{\sigma} = 0.2 \mu\text{C}/\text{cm}^2$ ). The full line is the prewetting line attached to  $T_w^* = 0.864 T_c^*$  (▲) and ending at the prewetting critical point (●). The dashed lines correspond to layering transition lines. They end at layering critical points  $T_{c,n}^*$  (located at the end of the dashed lines without being indicated separately), which within the present mean-field theory accumulate for  $n \rightarrow \infty$  at  $T_c^*$  instead of at the roughening transition temperature of the gas-liquid interface on the lattice.

Figure 3.8 shows the prewetting lines for ionic strength  $I = 3.9 \times 10^{-5}$  ( $\tilde{I} = 1\text{mM}$ )

and for four values of  $\sigma$  in the case  $u_w/u = 0.81$ . One can see clearly that as  $\sigma$  decreases, the wetting temperature  $T_w^*$  rises and the prewetting line becomes shorter. This is in agreement with the fact that in the limit  $\sigma \rightarrow 0$  the wetting transition turns second order. The values of the prewetting critical points for the lines shown in Fig. 3.8 are given in Table 3.1.

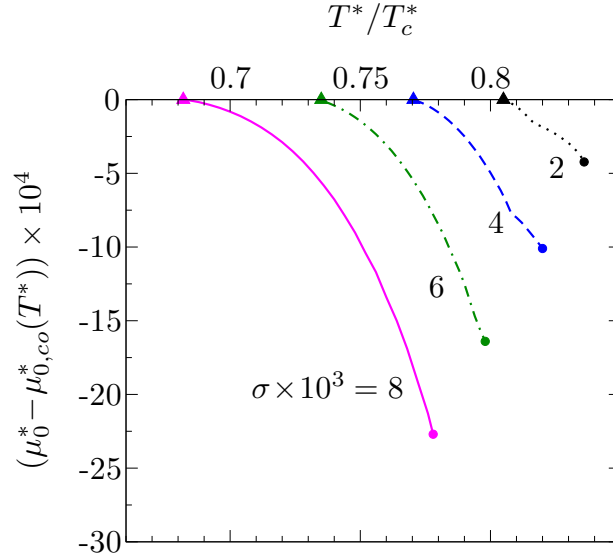


Figure 3.8: Prewetting lines for four values of the surface charge density  $\sigma = \tilde{\sigma}a^2/e$  with ionic strength  $I = 3.9 \times 10^{-5}$  ( $\tilde{I} = 1\text{mM}$ ) in the bulk liquid phase and for  $u_w/u = 0.81$ . The locations of the wetting transitions ( $\blacktriangle$ ) and of the prewetting critical points ( $\bullet$ ) are given in Table 3.1.

$\sigma = \tilde{\sigma}a^2/e$	$T_w^*/T_c^*$	$T_{pw,c}^*/T_c^*$	$\mu_{0,co}^*(T_{pw,c}^*) - \mu_{0,pw,c}^*$
$2 \times 10^{-3}$	0.804	0.836	$4.23 \times 10^{-4}$
$4 \times 10^{-3}$	0.77	0.82	$1.01 \times 10^{-3}$
$6 \times 10^{-3}$	0.734	0.798	$1.60 \times 10^{-3}$
$8 \times 10^{-3}$	0.682	0.778	$2.27 \times 10^{-3}$

Table 3.1: Prewetting critical points  $(T_{pw,c}^*, \mu_{0,pw,c}^*)$  for the prewetting lines shown in Fig. 3.8. The ionic strength in the liquid phase is  $I = 3.9 \times 10^{-5}$  ( $\tilde{I} = 1\text{mM}$ ).  $T_w^*$  is the transition temperature for first-order wetting. Note that  $\mu_{0,co}^*(T_{pw,c}^*) - \mu_{0,pw,c}^* = \frac{2/3}{T_{pw,c}^*/T_c^*} \left[ \frac{\mu_{0,co}(T_{pw,c}^*) - \mu_{0,pw,c}}{u} \right]$ .



# Chapter 4

## Wetting in electrolyte solutions: a continuum model

### 4.1 Model with short-ranged interactions

In this chapter a continuum model [21] for an electrolyte solution in three spatial dimensions consisting of solvent molecules (0), anions (-), and cations (+) close to a charged planar wall is studied. Solvent particles are assumed to have a non-vanishing volume  $a^3$  whereas the ions are considered to be point-like particles. The wall under consideration is the  $\tilde{x}-\tilde{y}$  plane at  $\tilde{z} = 0$ , i.e.,  $\tilde{\mathbf{r}} = (\tilde{\mathbf{r}}_{||} = (\tilde{x}, \tilde{y}), \tilde{z} = 0)$  which can carry a surface charge density  $\tilde{\sigma} = \sigma ea^{-2}$ , where  $e > 0$  is the elementary charge. The starting point is the following variational grand canonical functional, which is a modification of the one introduced in Ref. [21]:

$$\begin{aligned} \beta\Omega_0[\varrho_0(\mathbf{r}), \varrho_{\pm}(\mathbf{r})] = & \int d^3r \left\{ \varrho_0(\mathbf{r})(\ln(\varrho_0(\mathbf{r})) - \beta\mu_0) + (1 - \varrho_0(\mathbf{r})) \ln(1 - \varrho_0(\mathbf{r})) \right. \\ & \left. + \chi(T)\varrho_0(\mathbf{r})(1 - \varrho_0(\mathbf{r})) + \frac{\chi(T)}{6}(\nabla\varrho_0(\mathbf{r}))^2 \right\} \\ & - \beta h_1 \int d^2r_{||} \varrho_0(\mathbf{r}_{||}, z = 0) + \beta \frac{g}{2} \int d^2r_{||} \varrho_0(\mathbf{r}_{||}, z = 0)^2 \\ & + \int d^3r \left\{ \sum_{i=\pm} \varrho_i(\mathbf{r}) (\ln \varrho_i(\mathbf{r}) - 1 - \beta\mu_i + V_i(\varrho_0(\mathbf{r}))) \right. \\ & \left. + \frac{2\pi l_B}{\varepsilon(\varrho_0(\mathbf{r}))} (\mathbf{D}(\mathbf{r}, [\varrho_{\pm}]))^2 \right\}, \end{aligned} \quad (4.1)$$

where  $\beta = (k_B T)^{-1}$  is the inverse thermal energy,  $\mu_0$  is the chemical potential of the solvent,  $\mu_{\pm}$  are the chemical potentials of the  $\pm$ -ions,  $\tilde{l}_B = l_B a = e^2 \beta / (4\pi \varepsilon_0)$  is the

Bjerrum length in vacuum, and  $\mathbf{r} = \tilde{\mathbf{r}}/a$  are dimensionless positions. The actual number density of the solvent is given by  $\tilde{\varrho}_0(\mathbf{r}) = \varrho_0(\mathbf{r})a^{-3}$  with  $\varrho_0(\mathbf{r}) \in [0, 1]$ , whereas the number densities of anions and cations are given by  $\tilde{\varrho}_{\pm}(\mathbf{r}) = \varrho_{\pm}(\mathbf{r})a^{-3}$ . In the following the fluid solvent at position  $\mathbf{r}$  with  $\varrho_0(\mathbf{r}) < 1/2$  is referred to as a “gas”, whereas for  $\varrho_0(\mathbf{r}) > 1/2$  it is called a “liquid”. The first and the last integral are taken over the half-space  $\mathbf{r} = (x, y, z \geq 0)$  whereas the second and the third integral run over the surface  $z = 0$ ;  $\varrho_{\pm}(\ln \varrho_{\pm} - 1 - \beta\mu_{\pm})$  is the bulk grand potential density of the  $\pm$ -ions in the low number density limit. The Flory-Huggins parameter  $\chi(T) > 0$  describes the effective interaction between solvent particles [170]. The excess free energy of the solvent  $\beta F_{ex}^{sol}[\varrho_0(\mathbf{r})] = \int d^3r [\chi(T)\varrho_0(\mathbf{r})(1-\varrho_0(\mathbf{r})) + \frac{\chi(T)}{6}(\nabla\varrho_0(\mathbf{r}))^2]$  is taken into account using the square-gradient approximation. The ratio 1/6 of the coefficients in the two terms of  $\beta F_{ex}^{sol}[\varrho_0(\mathbf{r})]$  follows from considering nearest neighbors only [171]. Within this model the interaction of the solvent with the wall is captured by the parameters  $h_1$  and  $g$ . This implicitly assumes that the fluid-wall interactions are sufficiently short ranged so that their contributions to  $\Omega_0$  depend only on the solvent density  $\varrho_0(\mathbf{r}_{\parallel}, z=0)$  in the vicinity of the wall. This parametrization has been used by Nakanishi and Fisher [172] in order to analyze the global surface phase diagram of the Landau-Ginzburg theory for wetting.  $V_{\pm}(\varrho_0)$  is the solvation free energy per  $k_B T$  of a  $\pm$ -ion in the solvent of number density  $\varrho_0$ . Whereas more realistic expressions of  $V_{\pm}(\varrho_0)$  are discussed in the literature [21], here a simple piece-wise constant expression is used  $V_{\pm}(\varrho_0 < 1/2) = V_g$  and  $V_{\pm}(\varrho_0 > 1/2) = V_l$  with  $V_g - V_l \gg 1$ . This choice guarantees a vanishingly small ionic strength in the gas ( $\varrho_0 < 1/2$ ) as compared to the ionic strength in the liquid ( $\varrho_0 > 1/2$ ). Without restriction of generality  $V_l := 0$  is chosen, which can be achieved by a redefinition of the ionic chemical potentials ( $\beta\mu_{\pm} - V_l \mapsto \beta\hat{\mu}_{\pm}$ ; in the following the hat  $\hat{\cdot}$  is dropped). The discontinuity of  $V_{\pm}(\varrho_0)$  at  $\varrho_0 = 1/2$  is expected to not affect the results significantly because only thermodynamic states of liquid-gas coexistence well below the critical point are considered, for which  $\varrho_0 = 1/2$  is deep inside the unstable region of the bulk phase diagram. Note that here no unequal partitioning of ions in a non-uniform solvent occurs due to  $V_+(\varrho_0) - V_-(\varrho_0) = 0$ , i.e., due to a vanishing difference of solubility contrasts of anions and cations between the two phases in the sense of Ref. [21]. Moreover, no specific adsorption of ions at interfaces is considered here, i.e., there are no surface fields acting on  $\varrho_{\pm}$ .  $\tilde{\mathbf{D}} = \mathbf{D}ea^{-2}$  is the electric displacement generated by the ions and by the surface charge density as related according to Gauß’s law  $\nabla \cdot \mathbf{D}(\mathbf{r}, [\varrho_{\pm}]) = \varrho_+(\mathbf{r}) - \varrho_-(\mathbf{r}) + \sigma\delta(z)$ . (Note that Gauß’s law is an ingredient of the theory in addition to Eq. (4.1).) Within the present model, ions interact among each other and with the wall only electrostatically (besides the hard core repulsion of the wall which prevents the ions to penetrate the wall). Here, this is expressed in terms of the

energy density of the electric field (see Sec. 3.2) where  $\varepsilon(\varrho_0)$  is the local permittivity of the solvent of density  $\varrho_0$  divided by the vacuum permittivity  $\varepsilon_0$ . Various empirical expressions for  $\varepsilon(\varrho_0)$  are in use [173]. However, for the sake of simplicity a simple piece-wise constant expression is considered here  $\varepsilon(\varrho_0 < 1/2) = 1$  and  $\varepsilon(\varrho_0 > 1/2) = \varepsilon_l$  with the relative permittivity  $\varepsilon_l$  of the liquid solvent. For the same reasons as for the case of the piece-wise constant expressions  $V_{\pm}(\varrho_0)$  (see above), the discontinuity of  $\varepsilon(\varrho_0)$  at  $\varrho_0 = 1/2$  is expected to be irrelevant for the present purposes.

The bulk grand canonical potential density per  $k_B T$  following from Eq. (4.1) is given by

$$\beta\Omega_b(\varrho_0, \varrho) = f_{sol}(\varrho_0) + f_{ion}^{(+)}(\varrho) + f_{ion}^{(-)}(\varrho) + \varrho(V_+(\varrho_0) + V_-(\varrho_0)) \quad (4.2)$$

with  $\varrho_+ = \varrho_- := \varrho$  due to local charge neutrality in the bulk, and with the abbreviations  $f_{sol}(\varrho_0) := \varrho_0(\ln(\varrho_0) - \beta\mu_0) + (1 - \varrho_0)\ln(1 - \varrho_0) + \chi(T)\varrho_0(1 - \varrho_0)$  and  $f_{ion}^{(\pm)}(\varrho_{\pm}) := \varrho_{\pm}(\ln \varrho_{\pm} - 1 - \beta\mu_{\pm})$ . As a consequence of local charge neutrality  $\Omega_b$  depends on  $\mu_+$  and  $\mu_-$  only via the combination  $\mu_+ + \mu_- \equiv \mu_I$ . Accordingly, the ionic chemical potentials  $\mu_{\pm}$  are of no individual importance but only their sum is of physical relevance. In the bulk  $D = 0$  due to local charge neutrality so that the last term in Eq. (4.1) does not contribute to Eq. (4.2). Equilibrium bulk states  $(\varrho_0, \varrho)$  minimize  $\beta\Omega_b(\varrho_0, \varrho; \mu_0, \mu_I, T)$ , i.e., they fulfill the Euler-Lagrange equations

$$\frac{\partial\Omega_b}{\partial\varrho_0} = 0 \quad (4.3)$$

and

$$\frac{\partial\Omega_b}{\partial\varrho} = 0. \quad (4.4)$$

Equations (4.3) and (4.4) render two solutions, i.e., minima:

$$[\varrho_{0,l}(\mu_0, \mu_I, T), \varrho_l(\mu_0, \mu_I, T) \equiv I] \quad (4.5)$$

and

$$[\varrho_{0,g}(\mu_0, \mu_I, T), \varrho_g(\mu_0, \mu_I, T)]. \quad (4.6)$$

Coexistence between these two minima occurs if upon inserting these two solutions into  $\Omega_b$  the minima are equally deep:

$$\begin{aligned} & \Omega_b(\varrho_0 = \varrho_{0,l}(\mu_0, \mu_I, T), \varrho = \varrho_l(\mu_0, \mu_I, T); \mu_0, \mu_I, T) \\ &= \Omega_b(\varrho_0 = \varrho_{0,g}(\mu_0, \mu_I, T), \varrho = \varrho_g(\mu_0, \mu_I, T); \mu_0, \mu_I, T). \end{aligned} \quad (4.7)$$

This renders a relation  $\mu_0 = \mu_0^{co}(\mu_I, T)$  which describes a two-dimensional manifold in the three-dimensional parameter space  $(\mu_0, \mu_I, T)$  where gas-liquid coexistence

occurs. Inserting these relations into the solutions renders  $[\varrho_{0,l}^{co}(\mu_I, T), \varrho_l^{co}(\mu_I, T)]$  and  $[\varrho_{0,g}^{co}(\mu_I, T), \varrho_g^{co}(\mu_I, T)]$  with  $\varrho_{0,\{l,g\}}^{co}(\mu_I, T) = \varrho_{0,\{l,g\}}(\mu_0 = \mu_0^{co}(\mu_I, T), \mu_I, T)$  and  $\varrho_{l,g}^{co}(\mu_I, T) = \varrho_{l,g}(\mu_0 = \mu_0^{co}(\mu_I, T), \mu_I, T)$  where  $\varrho_l^{co} = I$ . In the following the superscript *co* in  $\varrho_{0,l}^{co}$ ,  $\varrho_{0,g}^{co}$ , and  $\varrho_g^{co}$  is dropped in order to avoid a clumsy notation so that, if not stated otherwise,  $\varrho_{0,l}$ ,  $\varrho_{0,g}$ ,  $I$ , and  $\varrho_g$  correspond to the coexisting densities.

Equation (4.4) can be used to express the bulk ionic strength as

$$\varrho = \exp\left(\frac{1}{2}(\beta\mu_I - V_+(\varrho_0) - V_-(\varrho_0))\right). \quad (4.8)$$

Due to the choice  $V_{\pm}(\varrho_0 < 1/2) = V_g$  and  $V_{\pm}(\varrho_0 > 1/2) = V_l = 0$  one obtains for the ionic strength in the gas ( $\varrho_0 = \varrho_{0,g} < 1/2$ )  $\varrho = \varrho_g = \exp(\beta\mu_I/2 - V_g)$  and in the liquid ( $\varrho_0 = \varrho_{0,l} > 1/2$ )  $\varrho = \varrho_l = \exp(\beta\mu_I/2)$  (see Eq. (4.8)). In the following it is assumed that  $V_g \gg 1$  such that one can set  $\varrho_g = 0$ , and  $I = \varrho_l = \exp(\beta\mu_I/2)$ . Accordingly, by using  $\mu_I = 2k_B T \ln I$  the densities discussed above can be expressed as functions of  $I$  and  $T$ . Note that Eq. (4.8) is independent of the Flory-Huggins parameter  $\chi(T)$ . For the choice of the ion potential  $V_{\pm}(\varrho_0)$  (such that  $V'_{\pm}(\varrho_0 \neq 1/2) = V''_{\pm}(\varrho_0 \neq 1/2) = 0$ ) the binodal  $T_{bi}(\varrho_0)$  is determined via the implicit relation

$$\chi(T) = \frac{\ln(\varrho_0) - \ln(1 - \varrho_0)}{2\varrho_0 - 1}, \quad (4.9)$$

where the temperature dependence of  $\chi(T)$  is often taken to be  $\chi(T) \cong \chi_S + \chi_H/T$ , where  $\chi_S$  and  $\chi_H/T$  are referred to as the entropic and the enthalpic part of  $\chi(T)$ , respectively [170]. From Eq. (4.9) one infers the critical point to be located at  $(\varrho_{0,c} = 1/2, \chi(T_c) = 2)$ . Note that within the present approximation the binodal (and hence the critical point) is independent of the ionic strength  $I$ .

In the presence of walls,  $\varrho_0$  and  $\varrho_{\pm}$  vary spatially in normal direction  $z$ . Their equilibrium profiles minimize the full functional  $\Omega_0[\varrho_0(\mathbf{r}), \varrho_{\pm}(\mathbf{r})]$  in Eq. (4.1) and thus render the equilibrium state. This procedure can be performed numerically. However, for the present purpose, analytic expressions are sought. In order to achieve this goal a Taylor expansion of the local part in Eq. (4.1) around the sharp-*k*-ink reference density profiles [2]

$$\bar{\varrho}_0(z) = \varrho_{sk,0}(z) = \begin{cases} \varrho_{0,l}, & 0 \leq z \leq \ell \\ \varrho_{0,g}, & z > \ell \end{cases} \quad (4.10)$$

and

$$\bar{\varrho}_{\pm}(z) = \varrho_{sk,\pm}(z) = \begin{cases} I, & 0 \leq z \leq \ell \\ 0, & z > \ell \end{cases} \quad (4.11)$$

is performed, where  $\ell$  is the position of the discontinuity of the sharp-kink profile  $\varrho_{sk,0}(z)$ , and  $\varrho_{0,l}$  and  $\varrho_{0,g}$  are, respectively, the equilibrium bulk densities of the solvent in the liquid and gas phase for a bulk ionic strength  $I$  in the liquid phase. This Taylor expansion renders an approximate variational functional  $\hat{\Omega}_0$  which up to quadratic order is given by

$$\begin{aligned} \frac{\beta \hat{\Omega}_0[\varrho_0(z), \varrho_{\pm}(z)]}{A} &= \ell f_{sol}(\varrho_{0,l}) + (L - \ell) f_{sol}(\varrho_{0,g}) + \int_0^L dz \left\{ f'_{sol}(\bar{\varrho}_0(z)) (\varrho_0(z) - \bar{\varrho}_0(z)) \right. \\ &\quad \left. + \frac{1}{2} f''_{sol}(\bar{\varrho}_0(z)) (\varrho_0(z) - \bar{\varrho}_0(z))^2 + \frac{\chi(T)}{6} \left( \frac{d\varrho_0(z)}{dz} \right)^2 \right\} \\ &\quad - \beta h_1 \varrho_0(0) + \beta \frac{g}{2} (\varrho_0(0))^2 \\ &\quad + \int_0^{\ell} dz \left\{ \sum_{i=\pm} \left[ f_{ion}^{(i)}(I) + f_{ion}^{(i)'}(I) (\varrho_i(z) - I) \right. \right. \\ &\quad \left. \left. + \frac{1}{2} f_{ion}^{(i)''}(I) (\varrho_i(z) - I)^2 \right] + \frac{2\pi l_B}{\varepsilon_l} (D(z, [\varrho_{\pm}]))^2 \right\}, \end{aligned} \quad (4.12)$$

where  $\tilde{A} = Aa^2$  is the wall area and  $\tilde{V} = ALa^3$  is the volume of the system. In order to obtain Eq. (4.12) it has been used that  $\varrho_{\pm}(z > \ell) = 0$ ,  $V_{\pm}(\varrho_0(z \leq \ell)) = V_l = 0$  because  $\varrho_0(z \leq \ell) > 1/2$ , and  $\varepsilon(\varrho_0 \leq \ell) = \varepsilon_l$ . Therefore Eq. (4.12) does not apply very close to the critical point where the actual spatial variation of  $V_{\pm}(\varrho_0(z))$  and  $\varepsilon(\varrho_0(z))$  matters. Moreover,  $D(z > \ell) = 0$  because the gas phase contains no ions and  $D(z \rightarrow \infty) \rightarrow 0$  due to the constraint of global charge neutrality.

The Euler-Lagrange equation for  $\varrho_0(z)$ , which follows from Eq. (4.12) for fixed  $\ell$ , is given by

$$\frac{\chi(T)}{3} \frac{d^2 \varrho_0(z)}{dz^2} = f'_{sol}(\bar{\varrho}_0(z)) + f''_{sol}(\bar{\varrho}_0(z)) (\varrho_0(z) - \bar{\varrho}_0(z)) \quad (4.13)$$

with the boundary conditions

$$\frac{\chi(T)}{3} \frac{d\varrho_0(z)}{dz} \Big|_{z=0} = -\beta h_1 + \beta g \varrho_0(0) \quad \text{and} \quad \frac{d\varrho_0(z)}{dz} \Big|_{z=L} = 0. \quad (4.14)$$

Similarly, the Euler-Lagrange equations for  $\varrho_{\pm}(z)$ ,  $0 \leq z \leq \ell$ , read (using Eq. (4.16) and

$\frac{d}{dz} \frac{\delta D(z)}{\delta \varrho_i(z')} = \frac{\delta}{\delta \varrho_i(z')} \frac{dD(z)}{dz} = q_i \delta(z - z')$  due to Gauß's law)

$$f_{ion}^{(i)'}(I) + f_{ion}^{(i)''}(I)(\varrho_i(z) - I) = -q_i \phi(z), \quad (4.15)$$

where  $e q_{\pm}$  is the ion charge with  $q_{\pm} = \pm 1$  and  $\tilde{\phi}(z) = \phi(z)/(\beta e)$  is the electrostatic potential such that

$$D(z) = -\frac{\varepsilon_l}{4\pi l_B} \phi'(z) \quad \text{for } 0 \leq z \leq \ell. \quad (4.16)$$

The variation leading to Eq. (4.15) generates also boundary terms  $\phi(z) \delta D(z, [\varrho_{\pm}]) / \delta \varrho_i(z')$  at  $z = 0$  and  $z = \ell$  which, however, vanish because of the boundary conditions  $D(z = 0) = \sigma$  and  $D(z = \ell) = 0$ . The latter holds due to  $D \equiv 0$  in the gas and the continuity of  $D(z)$  at  $z = \ell$  in the absence of a surface charge at  $z = \ell$ . Due to Eq. (4.4), in Eq. (4.15) one has  $f_{ion}^{(i)'} = 0$ . For the particular choice of  $\bar{\varrho}_0(z)$  in Eq. (4.10) one has  $f'_{sol}(\bar{\varrho}_0(z < \ell)) = f'_{sol}(\varrho_{0,l}) = 0$  and  $f'_{sol}(\bar{\varrho}_0(z > \ell)) = f'_{sol}(\varrho_{0,g}) = 0$  due to Eq. (4.3) and the Euler-Lagrange equation (4.13) can be written as

$$\frac{d^2}{dz^2} \Delta \varrho_0(z) = \begin{cases} \frac{1}{\xi_l^2} \Delta \varrho_0(z), & 0 \leq z < \ell \\ \frac{1}{\xi_g^2} \Delta \varrho_0(z), & z > \ell \end{cases} \quad (4.17)$$

with

$$\frac{1}{\xi_{g,l}^2} = \frac{3}{\chi(T)} \left( \frac{1}{\varrho_{0,\{g,l\}}} + \frac{1}{1 - \varrho_{0,\{g,l\}}} - 2\chi(T) \right), \quad (4.18)$$

where  $\xi_{g,l}$  can be identified with the bulk correlation length of the solvent in the gas and in the liquid phase, respectively (see Appendix A), and where  $\Delta \varrho_0(z) = \varrho_0(z) - \bar{\varrho}_0(z) = \varrho_0(z) - \varrho_{0,l}$  for  $0 \leq z < \ell$  and  $\Delta \varrho_0(z) = \varrho_0(z) - \varrho_{0,g}$  for  $z > \ell$ . In addition to the boundary conditions in Eq. (4.14), Eq. (4.13) requires the density profile  $\varrho_0(z)$  and its first derivative  $\frac{d\varrho_0(z)}{dz}$  to be continuous at  $z = \ell$ , i.e.,

$$\begin{aligned} \varrho_{0,l} + \Delta \varrho_0(\ell^-) &= \varrho_{0,g} + \Delta \varrho_0(\ell^+) \\ \left. \frac{d}{dz} \Delta \varrho_0(z) \right|_{z=\ell^-} &= \left. \frac{d}{dz} \Delta \varrho_0(z) \right|_{z=\ell^+} \end{aligned} \quad (4.19)$$

because the right-hand side of Eq. (4.13) is discontinuous; otherwise the left-hand side of Eq. (4.13) would be more singular at  $z = \ell$  than the right-hand side. Similarly, for  $\Delta \varrho_{\pm}(z)$  one obtains (see Eqs. (4.4) and (4.15))

$$\Delta \varrho_{\pm}(z) = -q_{\pm} \phi(z) I, \quad (4.20)$$

where  $\Delta\rho_{\pm}(z) = \rho_{\pm}(z) - \bar{\rho}_{\pm}(z) = \rho_{\pm}(z) - I$  for  $0 \leq z < \ell$  and zero otherwise (see Eq. (4.11) and  $\rho_{\pm}(z > \ell) = 0$ ). The dependences of Eqs. (4.13) and (4.20) on  $\mu_0$  and  $\mu_I$  enter via the equilibrium values of  $I$ ,  $\varrho_{0,g}$ , and  $\varrho_{0,l}$  (Eqs. (4.2)-(4.7)).

The Poisson equation, which relates the dimensionless electrostatic potential  $\phi = \beta e \tilde{\phi}$  to the dimensionless number densities  $\varrho_{\pm}$  of the ions, can be written as (see Eqs. (4.16) and (4.20) and Gauß's law)

$$\begin{aligned}
\phi''(z) &= -\frac{4\pi\lambda_B}{\varepsilon_l} \frac{dD}{dz} = -\frac{4\pi l_B}{\varepsilon_l} \sum_{i=\pm} q_i \varrho_i(z) \\
&= -\frac{4\pi l_B}{\varepsilon_l} \sum_{i=\pm} q_i (\Delta\varrho_i + I) \\
&= -\frac{4\pi l_B}{\varepsilon_l} \sum_{i=\pm} q_i I (1 - q_i \phi(z)) \\
&= \frac{8\pi I l_B}{\varepsilon_l} \phi(z) \\
&= \kappa^2 \phi(z)
\end{aligned} \tag{4.21}$$

which is the linearized Poisson-Boltzmann equation with

$$\kappa = \sqrt{8\pi I l_B / \varepsilon_l} \tag{4.22}$$

as the inverse Debye length. This equation must be solved subject to the boundary conditions

$$\phi'(z=0) = -\frac{4\pi l_B \sigma}{\varepsilon_l} \quad \text{and} \quad \phi'(z=\ell) = 0 \tag{4.23}$$

which corresponds to  $D(z=0) = \sigma$  and  $D(z=\ell) = 0$ ; the latter follows from the overall charge neutrality (see Eqs. 3.13 and 3.14) and the assumption that there are no ions in the vapor phase. Equations (4.17) and (4.21) can be solved analytically, yielding the constrained equilibrium profiles

$$\Delta\varrho_0^{(\ell)}(z) = \begin{cases} \hat{A}_l \exp(z/\xi_l) + \hat{B}_l \exp(-z/\xi_l), & 0 \leq z \leq \ell \\ \hat{B}_g \exp(-z/\xi_g), & z > \ell \end{cases} \tag{4.24}$$

where (see Eqs. (4.19) and (4.14))

$$\begin{aligned}
\hat{A}_l &= \frac{1}{N} \left[ \left( \beta g + \frac{\chi(T)}{3\xi_l} \right) (\varrho_{0,g} - \varrho_{0,l}) + \beta(h_1 - g\varrho_{0,l}) \left( \frac{\xi_g}{\xi_l} - 1 \right) \exp(-\ell/\xi_l) \right], \\
\hat{B}_l &= \frac{1}{N} \left[ \left( \frac{\chi(T)}{3\xi_l} - \beta g \right) (\varrho_{0,g} - \varrho_{0,l}) + \beta(h_1 - g\varrho_{0,l}) \left( 1 + \frac{\xi_g}{\xi_l} \right) \exp(\ell/\xi_l) \right], \\
\hat{B}_g &= \frac{\xi_g}{\xi_l} \left( B_l \exp\left(\frac{\ell}{\xi_g} - \frac{\ell}{\xi_l}\right) - \hat{A}_l \exp\left(\frac{\ell}{\xi_g} + \frac{\ell}{\xi_l}\right) \right), \\
\hat{N} &= \left( \beta g + \frac{\chi(T)}{3\xi_l} \right) \left( \frac{\xi_g}{\xi_l} + 1 \right) \exp(\ell/\xi_l) - \left( \beta g - \frac{\chi(T)}{3\xi_l} \right) \left( 1 - \frac{\xi_g}{\xi_l} \right) \exp(-\ell/\xi_l),
\end{aligned} \tag{4.25}$$

and (see Eq. (4.20))  $\Delta\varrho_{\pm}^{(\ell)}(z) = -q_{\pm}I\phi^{(\ell)}(z)$  with

$$\phi^{(\ell)}(z) = A_I \exp(\kappa z) + B_I \exp(-\kappa z), \tag{4.26}$$

where (see Eq. (4.23))

$$\begin{aligned}
A_I &= \frac{4\pi l_B \sigma}{\varepsilon_l \kappa} \frac{1}{\exp(2\kappa\ell) - 1}, \\
B_I &= A_I \exp(2\kappa\ell).
\end{aligned} \tag{4.27}$$

Note that because  $\varrho_{\pm}(z) \geq 0$ ,  $|\Delta\varrho_{\pm}(z)|$  has an upper limit given by (see Eq. (4.20))

$$|\Delta\varrho_{\pm}(z)| \leq I, \text{ i.e., } |\phi(z)| \leq 1, \tag{4.28}$$

Since  $\phi(z)$  is monotonic (see Eqs. (4.26) and (4.27)) one requires

$$\begin{aligned}
|\phi(0)| &\leq 1 \\
\Rightarrow \frac{4\pi l_B |\sigma|}{\varepsilon_l \kappa} \coth(\kappa\ell) &\leq 1,
\end{aligned} \tag{4.29}$$

which implies that there is an upper limit for the absolute value  $|\sigma|$  surface charge density:

$$|\sigma| \leq \frac{\varepsilon_l \kappa}{4\pi l_B q_{\pm}} \tanh(\kappa\ell) =: \sigma_{sat}(\kappa\ell). \tag{4.30}$$

In case the real surface charge  $|\sigma|$  is larger than the saturation value  $\sigma_{sat}(\kappa\ell)$  the latter has to be used instead in order to ensure  $\varrho_{\pm}(z) \geq 0$ . This is the analogue of the well-known charge renormalization in the linearized Poisson-Boltzmann theory of semi-infinite electrolyte solutions [182].

Within the present model, at two-phase coexistence  $\varrho_{0,g} = 1 - \varrho_{0,l}$  so that  $\xi_g = \xi_l = \xi$



and that Eq. (4.25) reduces to

$$\begin{aligned}
A_l &= \frac{1}{N} \left( \beta g + \frac{\chi(T)}{3\xi} \right) (\varrho_{0,g} - \varrho_{0,l}), \\
B_l &= \frac{1}{N} \left[ \left( \frac{\chi(T)}{3\xi} - \beta g \right) (\varrho_{0,g} - \varrho_{0,l}) + 2\beta(h_1 - g\varrho_{0,l}) \exp(\ell/\xi) \right], \\
B_g &= (B_l - A_l \exp(2\ell/\xi)), \\
N &= 2 \left( \beta g + \frac{\chi(T)}{3\xi} \right) \exp(\ell/\xi).
\end{aligned} \tag{4.31}$$

The solvent density profiles at two-phase coexistence — obtained by expanding  $\Omega_0$  up to quadratic order around the sharp-kink profiles (see Eqs. (4.24) and (4.31)) — are similar but not identical to the ones obtained by using the so-called double parabola approximation (DPA) (see Appendix B). A difference between the two approaches arises because the boundary conditions and the definition of the thickness of the liquid film differ in both approaches. Within the present approach the thickness  $\ell_{film}$  of the liquid film is defined as the position  $z > 0$  in which the magnitude of the derivative  $|\varrho'_0(z)|$  of the solvent profile is maximal. This definition of the film thickness  $\ell_{film}$  is convenient within the present approach because Eq. (4.24) shows that it coincides with the position  $\ell$  of the discontinuity of the sharp-kink profile  $\varrho_{sk,0}(z)$ , i.e.,  $\ell_{film} = \ell$ . Alternative definitions of the film thickness are possible but lead to more complicated expressions of the effective interface potential introduced below. Moreover, the present solvent profile and its derivative are continuous everywhere (see Eq. (4.19)), whereas within the DPA the solvent profile is continuous everywhere but its derivative is discontinuous at the position  $z = \ell_{DP}$  where  $\varrho_{0,DP}(\ell_{DP}) = \frac{1}{2}(\varrho_{0,g} + \varrho_{0,l})$  (see Eq. (B.7)). This equation defines the liquid film thickness  $\ell_{DPA}$  within the DPA. However, the discontinuity  $\varrho'_{0,DPA}(\ell_{DPA}^+) - \varrho'_{0,DPA}(\ell_{DPA}^-) = \mathcal{O}(\exp(-\ell_{DPA}/\xi))$  is exponentially small for large film thicknesses ( $\ell_{DPA} \gg \xi$ ) (see Eqs. (B.7) and (B.8)). Moreover, in Appendix B it is shown that the relative difference between the coefficients of the profiles in Eq. (4.24) and those in Eq. (B.7) is also exponentially small for  $\ell = \ell_{DPA} \gg \xi$  (see Eq. (B.9)).

At the functional minimum the integrations in Eq. (4.12) can be performed analytically with the first integrand (see Eqs. (4.17) and (4.18))

$$\begin{aligned}
&\frac{\chi(T)}{6} \left( \frac{d}{dz} \Delta\varrho_0(z) \right)^2 + \frac{1}{2} (\Delta\varrho_0(z))^2 \left( \frac{1}{\varrho_{0,\{g,l\}}} + \frac{1}{1 - \varrho_{0,\{g,l\}}} - 2\chi(T) \right) \\
&= \frac{\chi(T)}{6} \left( \frac{(\Delta\varrho_0(z))^2}{\xi_{g,l}^2} + \left( \frac{d}{dz} \Delta\varrho_0(z) \right)^2 \right)
\end{aligned}$$

$$\begin{aligned}
&= \frac{\chi(T)}{6} \left( \frac{(\Delta\varrho_0(z))^2}{\xi_{g,l}^2} + \frac{d}{dz} \left( \Delta\varrho_0(z) \frac{d}{dz} \Delta\varrho_0(z) \right) - \Delta\varrho_0(z) \frac{d^2}{dz^2} (\Delta\varrho_0(z)) \right) \\
&= \frac{\chi(T)}{6} \frac{d}{dz} \left( \Delta\varrho_0(z) \frac{d}{dz} \Delta\varrho_0(z) \right), \tag{4.32}
\end{aligned}$$

and with the second the integrand (see Eqs. (4.16), (4.20), and (4.21) and  $f_{ion}^{(i)'}(I) = 0$ )

$$\begin{aligned}
\frac{1}{2I} \sum_{i=\pm} (\Delta\varrho_i(z))^2 + \frac{2\pi l_B}{\varepsilon_l} (D(z, [\Delta\varrho_{\pm}]))^2 &= \frac{I}{\kappa^2} \left( \kappa^2 (\phi(z))^2 + (\phi'(z))^2 \right) \\
&= \frac{I}{\kappa^2} \left( \phi(z)\phi''(z) + (\phi'(z))^2 \right) \\
&= \frac{I}{\kappa^2} (\phi(z)\phi'(z))'. \tag{4.33}
\end{aligned}$$

By exploiting the boundary conditions in Eqs. (4.14), (4.19), and (4.23) one obtains for the surface contribution to the constrained grand potential

$$\begin{aligned}
\beta\Omega_s(\ell) &:= \frac{\beta\hat{\Omega}_0[\varrho_0^{(\ell)}(z), \varrho_{\pm}^{(\ell)}(z)] - V\beta\Omega_b(\varrho_{0,g}, \varrho_g = 0)}{A} \\
&= \beta\ell[\Omega_b(\varrho_{0,l}, I) - \Omega_b(\varrho_{0,g}, 0)] \\
&\quad + \frac{\chi(T)}{6} (\Delta\varrho_0^{(\ell)'(\ell)}(\varrho_{0,g} - \varrho_{0,l}) - \Delta\varrho_0^{(\ell)'(0)}\Delta\varrho_0^{(\ell)}(0)) \\
&\quad - \beta h_1(\varrho_{0,l} + \Delta\varrho_0^{(\ell)}(0)) + \frac{\beta g}{2}(\varrho_{0,l} + \Delta\varrho_0^{(\ell)}(0))^2 + \frac{1}{2}\sigma\phi^{(\ell)}(0) \tag{4.34}
\end{aligned}$$

where  $\Delta\varrho_0^{(\ell)'(\ell)} = \left( \frac{d}{dz} \Delta\varrho_0^{(\ell)}(z) \right) \Big|_{z=\ell}$ . Finally, inserting the solutions given by Eqs. (4.24)-(4.27) into Eq. (4.34) and using Eqs. (4.14) and (4.23) leads to

$$\begin{aligned}
\beta\Omega_s(\ell) &= \beta\ell[\Omega_b(\varrho_{0,l}, I) - \Omega_b(\varrho_{0,g}, 0)] \\
&\quad + \frac{\chi(T)}{6}(\varrho_{0,g} - \varrho_{0,l}) \left[ \frac{\hat{A}_l}{\xi_l} \exp(\ell/\xi_l) - \frac{\hat{B}_l}{\xi_l} \exp(-\ell/\xi_l) \right] \\
&\quad + \frac{\beta(g\varrho_{0,l} - h_1)}{2}(\hat{A}_l + \hat{B}_l) - \beta h_1\varrho_{0,l} + \frac{\beta g}{2}\varrho_{0,l}^2 \\
&\quad + \frac{2\pi l_B \sigma^2}{\varepsilon_l \kappa} \coth(\kappa\ell). \tag{4.35}
\end{aligned}$$

The first term is the difference between the grand canonical potentials per volume of the (potentially metastable) liquid and the gas bulk phase, respectively, multiplied by the film thickness  $\ell$ . This contribution linear in  $\ell$  vanishes at two-phase coexistence due to Eq. (4.7). The other terms provide the free energy associated with the emergence of the liquid-gas and the liquid-wall interfaces as well as their effective interaction for  $\ell < \infty$ .

These expressions are valid also off two-phase coexistence.

At two-phase coexistence and in the limit  $\ell \gg 1/\kappa$  the surface contribution (Eq. (4.35)) can be written as

$$\begin{aligned}
\beta\Omega_s(\ell) \simeq & \frac{\chi(T)}{12} \frac{(\varrho_{0,g} - \varrho_{0,l})^2}{\xi} - \frac{\beta^2(h_1 - g\varrho_{0,l})^2}{2\left(\beta g + \frac{\chi(T)}{3\xi}\right)} - \beta h_1 \varrho_{0,l} + \frac{\beta g}{2} \varrho_{0,l} \\
& + (\varrho_{0,l} - \varrho_{0,g}) \frac{\chi(T)}{3\xi} \frac{\beta(h_1 - g\varrho_{0,l})}{\beta g + \frac{\chi(T)}{3\xi}} \exp(-\ell/\xi) \\
& - (\varrho_{0,l} - \varrho_{0,g})^2 \frac{\chi(T)}{12\xi} \frac{\frac{\chi(T)}{3\xi} - \beta g}{\beta g + \frac{\chi(T)}{3\xi}} \exp(-2\ell/\xi) \\
& + \frac{2\pi l_B \sigma^2}{\varepsilon_l \kappa} (1 + 2 \exp(-2\kappa\ell)),
\end{aligned} \tag{4.36}$$

where only the last term in Eq. (4.35) has been expanded for  $\kappa\ell \gg 1$ . Note that within the present theory the ions enter into  $\Omega_s(\ell)$  only via the last term. Therefore, if the surface charge  $\sigma$  is zero, the ions do not modify the wetting behavior of the solvent. This is due to the fact that  $\sigma = 0$  implies that there are no surface fields acting on  $\varrho_{\pm}$ . The first term in Eq. (4.36) is the liquid-gas surface tension  $\gamma_{l,g} = \frac{\chi(T)}{12} \frac{(\varrho_{0,g} - \varrho_{0,l})^2}{\xi}$ , within the present approach. As expected, within mean field theory (MFT)  $\varrho_{0,l} - \varrho_{0,g}$  vanishes  $\propto |\chi - \chi_c|^\beta$  with  $\beta = 1/2$  upon approaching the critical point ( $\varrho_{0,c} = \frac{1}{2}, \chi_c = 2$ ) (see Eq. (4.9)) and from Eq. (4.18) one has  $\xi \propto |\chi - \chi_c|^{-\nu}$  with  $\nu = 1/2$ , so that  $\gamma_{l,g} \propto |\chi - \chi_c|^\mu$  with  $2\beta + \nu = \mu = 3/2$ ; in general  $\mu = (d - 1)\nu$  where  $d$  is the spatial dimension with  $d = 4$  corresponding to MFT [3]. The wall-liquid surface tension is  $\gamma_{w,l} = -\frac{\beta^2(h_1 - g\varrho_{0,l})^2}{2(\beta g + \frac{\chi(T)}{3\xi})} - \beta h_1 \varrho_{0,l} + \frac{\beta g}{2} \varrho_{0,l} + \frac{2\pi l_B \sigma^2}{\varepsilon_l \kappa}$ . These two contributions are independent of the film thickness  $\ell$ . The remaining terms carry the dependence on  $\ell$ , generated by the effective interaction between the emerging liquid-vapor and wall-liquid interfaces.

Accordingly, the effective interface potential  $\omega(\ell) = \Omega_s(\ell) - \Omega_s(\infty)$  at two-phase coexistence is given by

$$\begin{aligned}
\beta\omega(\ell \gg 1/\kappa) \simeq & (\varrho_{0,l} - \varrho_{0,g}) \frac{\chi(T)}{3\xi} \frac{\beta(h_1 - g\varrho_{0,l})}{\beta g + \frac{\chi(T)}{3\xi}} \exp(-\ell/\xi) \\
& - (\varrho_{0,l} - \varrho_{0,g})^2 \frac{\chi(T)}{12\xi} \frac{\frac{\chi(T)}{3\xi} - \beta g}{\beta g + \frac{\chi(T)}{3\xi}} \exp(-2\ell/\xi) \\
& + \frac{4\pi l_B \sigma^2}{\varepsilon_l \kappa} \exp(-2\kappa\ell).
\end{aligned} \tag{4.37}$$

This effective potential captures the dependence of the grand canonical potential on the

film thickness and determines whether or not the wall-gas interface is wetted by the liquid. Moreover, the order of the wetting transition can be inferred from its functional form [2].

The property  $\xi_l = \xi_g$  at coexistence is a special feature of the present model. In general  $\xi_l \neq \xi_g$  so that in this case an expansion of the effective interface potential  $\omega(\ell)$  similar to Eq. (4.37) contains products of powers of  $\exp(-\ell/\xi_l)$  and  $\exp(-\ell/\xi_g)$  (see Eq. (4.35)).

### 4.1.1 Pure solvent

First the case of a pure solvent (i.e.,  $I = 0$ ) near a neutral wall (i.e.,  $\sigma = 0$ ) and at gas-liquid coexistence is considered. For such a system the effective interface potential in Eq. (4.37) reduces to

$$\beta\omega(\ell) = a_0(T) \exp(-\ell/\xi) + b_0(T) \exp(-2\ell/\xi) \quad (4.38)$$

with

$$a_0(T) = (\varrho_{0,l} - \varrho_{0,g}) \frac{\chi(T)}{3\xi} \frac{\beta(h_1 - g\varrho_{0,l})}{\beta g + \frac{\chi(T)}{3\xi}} \quad (4.39)$$

and

$$b_0(T) = -(\varrho_{0,l} - \varrho_{0,g})^2 \frac{\chi(T)}{12\xi} \frac{\frac{\chi(T)}{3\xi} - \beta g}{\beta g + \frac{\chi(T)}{3\xi}}. \quad (4.40)$$

For second-order wetting to occur at  $T = T_w$ , the coefficient  $a_0(T)$  must be negative for  $T < T_w$ , vanish at  $T = T_w$ , and be positive for  $T > T_w$ . As  $\varrho_{0,l} > \varrho_{0,g}$ , and because  $\varrho_{0,l}$  can vary only between its value at the triple point  $\varrho_{0,l}(T_t)$  and the critical density  $\varrho_{0,c} = \varrho_{0,l}(T_c)$ ,  $a_0(T)$  fulfills the above mentioned conditions if

$$\varrho_{0,c} < \frac{h_1}{g} < \varrho_{0,l}(T_t). \quad (4.41)$$

Here and the following  $h_1 > 0$  and  $g > 0$  are considered. The order of the transition is determined by the higher-order coefficients in the expansion of  $\omega(\ell)$  [2]. If  $b_0(T_w) < 0$ , the transition will be first order while second-order wetting can occur if  $b_0(T_w) > 0$ . Only in the latter case  $a_0(T_w) = 0$  determines the wetting transition temperature, so that

$$\varrho_{0,l}(T_w) = \frac{h_1}{g}. \quad (4.42)$$

Within the present approach, the wetting transition can be second order if

$$\beta g > \frac{\chi(T_w)}{3\xi}, \quad (4.43)$$

and first order if the inequality is reversed. The separatrix between first- and second-order wetting (i.e., the loci of tricritical wetting [172]) is given by

$$\beta g = \frac{\chi(T_w)}{3\xi(T_w)}, \quad (4.44)$$

where  $\chi(T_w)$  follows from Eqs. (4.9) and (4.42):

$$\chi(T_w) = \frac{\ln(h_1/g) - \ln(1 - h_1/g)}{2h_1/g - 1}. \quad (4.45)$$

## 4.1.2 Electrolyte solution

In the case of an electrolyte solution close to a charged wall the effective interface potential given by Eq. (4.37) has the generic form studied by Aukrust and Hauge [174] for a model in which both the wall-fluid and the fluid-fluid interaction potentials decay exponentially but on distinct scales. The information about the wetting behavior is extracted in an analogous procedure to the pure solvent case in Subsec. 4.1.1. Note that the electrostatic term  $a_I(T) \exp(-2\kappa\ell)$  with

$$a_I(T) = \frac{4\pi l_B \sigma^2}{\varepsilon_I \kappa} \quad (4.46)$$

has a coefficient which is always positive. (Equation (4.37) shows that the coefficients  $a_0(T)$  (Eq. (4.39)) and  $b_0(T)$  (Eq. (4.40)) do not change upon adding ions.) Accordingly, the wetting behavior will depend on the competition between the Debye length  $1/\kappa$  and the correlation length  $\xi$ :

- (i)  $1/\kappa < \xi$ : In this case the electrostatic term decays faster than the remaining two terms in Eq. (4.37). Therefore one obtains the same wetting behavior as for the pure solvent (see Subsec. 4.1.1).
- (ii)  $\xi < 1/\kappa < 2\xi$ : In this case the electrostatic term is the dominant subleading contribution in the expansion. Moreover, because  $a_I(T) > 0$  for all temperatures, the transition can be second order if  $a_0(T)$  satisfies the conditions given by Eq. (4.41).
- (iii)  $1/\kappa > 2\xi$ : In this case, the electrostatic term is the leading contribution. As a result, if in the pure solvent the wetting transition is second order, due to adding ions and due to a nonzero surface charge density at the wall it turns first order or the wall becomes wet at all temperatures  $T > T_t$ .

As discussed in Subsec. 4.1.1, for the pure solvent it is possible to determine the separatrix between first- and second-order wetting in terms of the surface parameters  $h_1$

and  $g$  only. Accordingly, the phase diagram is of the type shown in Fig. 2(a) of Ref. [172] for  $g > 0$  and of the type shown there in Fig. 2(b) for  $g = 0$ . On the other hand, for electrolyte solutions this separatrix depends also on the surface charge density, the ionic strength, and the competition between the Debye and the correlation lengths. As mentioned before our approach neglects the interaction between ions so that it can be used only for low ion concentrations, e.g.,  $I \lesssim 10\text{mM}$ , which corresponds to a Debye length  $1/\kappa \gtrsim 3\text{nm}$  in water at room temperature. Thus one typically ends up with case (iii) ( $1/\kappa > 2\xi$ ) except in close proximity to the critical point, where one can reach case (ii) ( $\xi < 1/\kappa < 2\xi$ ) and ultimately case (i) ( $1/\kappa < \xi$ ). Therefore, for  $g > 0$  the phase diagram for  $\sigma \neq 0$  is of the type shown in Fig. 2(a) of Ref. [172], as for the pure solvent case with  $g > 0$ , but the separatrix between first- and second-order wetting is shifted closer to the critical point upon increasing the Debye length, i.e., upon decreasing the ionic strength.

The wetting behavior will be richer if  $\xi_l \neq \xi_g$  (see the discussion below Eq. (4.37)). In this case, the possible wetting scenarios will depend on the competition between the Debye length  $1/\kappa$ , the correlation length  $\xi_g$  of the gas, and the correlation length  $\xi_l$  of the liquid. This creates additional cases compared to the ones discussed above (see (i)-(iii)). Nevertheless, in the present context, far from the critical point case (iii) is still the typical one with the distinction that here  $1/(2\kappa)$  competes with the maximum of  $\xi_l$  and  $\xi_g$ .

In the limit  $\sigma \rightarrow 0$  one has  $a_I(T) \rightarrow 0$  so that in this case there is no contribution to the effective interface potential due to the ions. This is due to the fact that within the present theory there are no surface fields acting on  $\varrho_{\pm}$  if  $\sigma = 0$ . For considering instead the limit  $I \rightarrow 0$ , i.e.,  $\kappa \rightarrow 0$ , in the expression for  $a_I(T)$  one has to use the saturation value  $|\sigma| = \sigma_{sat}(\kappa\ell)$  given by Eq. (4.30), which implies  $a_I(T) \sim \kappa^3$ . Accordingly,  $a_I(T) \rightarrow 0$  when  $\kappa \rightarrow 0$  so that, as expected, in the limit  $I \rightarrow 0$  the pure solvent case is recovered.

## 4.2 Model with long-ranged interactions

In this section systems in which the solvent exhibits attractive long-ranged interaction potentials among the solvent particles as well as between the wall and the solvent particles are considered. As in the previous section, the goal is to obtain an analytic expression for the effective interface potential  $\omega(\ell)$ . Following Ref. [175] the attractive part of the pair potential between the solvent particles, as it enters the density functional, is modeled as

$$\bar{w}(r) = \frac{A_f}{(1+r^2)^3} \quad (4.47)$$

with  $A_f < 0$  and the substrate potential as

$$V(z > 0) = - \sum_{i \geq 3} \frac{u_i}{z^i} \quad (4.48)$$

with  $u_3 > 0$  corresponding to an asymptotically attractive interaction. The contribution  $\sim u_4$  is generated, inter alia, by the discrete lattice structure of the substrate or by a thin overlayer [2] and thus it can be tuned. The substrate potential  $V(z)$  diverges for  $z \rightarrow 0$ . Therefore the solvent density  $\varrho_0(z)$  must vanish for  $z \rightarrow 0$ . In the following this effect is taken into account approximately by replacing the short-ranged part of  $V(z)$  in Eq. (4.48) by a hard-wall potential positioned at  $z = d_w$ ; the distances  $z$  are still measured from  $z = 0$ . (Beyond this sharp-kink approximation for the wall-liquid interfacial profile,  $d_w$  is replaced by the moment  $d_{wl}^{(1)}$  (Eq. D.9) of the profile  $\varrho_{0,wl}(z)$ .) This implies that in the present section the short-ranged description of the surface-fluid interaction given in terms of the surface parameters  $h_1$  and  $g$  in the previous section has to be shifted from  $z = 0$  to  $z = d_w$  (see Eq. (4.1)). On the other hand, in order to account for the long-ranged attractive part of  $V(z)$  (i.e., for  $z \gg d_w$ ), here only the first two terms of the sum in Eq. (4.48) are considered. The functional form in Eq. (4.47) facilitates to carry out subsequent integrals analytically. These long-ranged interactions are treated as a perturbation of the grand canonical functional in Eq. (4.1):

$$\Omega[\varrho_0(\mathbf{r}), \varrho_{\pm}(\mathbf{r})] = \Omega_0[\varrho_0(\mathbf{r}), \varrho_{\pm}(\mathbf{r})] + \Delta\Omega[\varrho_0(\mathbf{r})] \quad (4.49)$$

where  $\Omega_0[\varrho_0(\mathbf{r}), \varrho_{\pm}(\mathbf{r})]$  is given by Eq. (4.1) and

$$\Delta\Omega[\varrho_0(\mathbf{r})] = \frac{1}{2} \int d^3r \int d^3r' \bar{w}(|\mathbf{r} - \mathbf{r}'|) \varrho_0(\mathbf{r}) \varrho_0(\mathbf{r}') + \int d^3r \varrho_w V(\mathbf{r}) \varrho_0(\mathbf{r}). \quad (4.50)$$

The integrations run over the half space  $\{\mathbf{r} = (x, y, z \geq d_w)\}$ ,  $\bar{w}(r)$  is given by Eq. (4.47), and  $V(\mathbf{r})$  is given by Eq. (4.48);  $\varrho_w$  is the particle number density of the substrate. Concerning the interaction between the solvent particles, it turns out that it is most suitable captured by the quantity [2],

$$t(z) := \int_z^\infty dz' \int d^2r'_\parallel \bar{w} \left( (r'^2_\parallel + z'^2)^{1/2} \right). \quad (4.51)$$

For large distances and non-retarded van der Waals forces one has

$$t(z \rightarrow \infty) = - \left( \frac{t_3}{z^3} + \frac{t_4}{z^4} + \dots \right), \quad (4.52)$$

which defines the coefficients  $t_3 > 0$  and  $t_4$ . For the present model this implies

$$t_3 = -\frac{\pi A_f}{6}, \quad (4.53)$$

$$t_4 = 0. \quad (4.54)$$

The addition of the long-ranged pair potential between solvent particles (Eq. (4.47)) modifies the bulk grand canonical potential per  $k_B T$  of the pure solvent (i.e.,  $\varrho_{\pm} = 0$ ) (see Eq. (4.2)). Accordingly, in this system the bulk densities  $\varrho_{0,l}$  and  $\varrho_{0,g}$  minimize the modified bulk grand canonical potential density given by

$$\beta\Omega_{b,lr}(\varrho_0, \varrho = 0) = \varrho_0(\ln(\varrho_0) - \beta\tilde{\mu}_0) + (1 - \varrho_0)\ln(1 - \varrho_0) + \tilde{\chi}(T)\varrho_0(1 - \varrho_0) \quad (4.55)$$

with the shifted solvent chemical potential  $\tilde{\mu}_0 = \mu_0 - \pi^2 A_f/8$  and the modified Flory-Huggins parameter  $\tilde{\chi}(T) = \chi_S + \chi_H/T - \pi^2\beta A_f/8$ , i.e., the RPA-like perturbation  $\Delta\Omega[\varrho_0(\mathbf{r})]$  in Eq. (4.50) changes only the enthalpic part of the Flory-Huggins parameter. The binodal  $T_{bi,lr}(\varrho_0)$  is again of the form given in Eq. (4.9) but with  $\chi(T)$  replaced by  $\tilde{\chi}(T)$ . Hence the critical point is located at  $(\varrho_{0,c} = 1/2, \tilde{\chi}(T_c) = 2)$ , i.e.,

$$T_c = \frac{\chi_H - \pi^2 A_f/(8k_B)}{2 - \chi_S}. \quad (4.56)$$

The bulk correlation length is now given by (see Appendix A)

$$\frac{1}{\xi^2} = \frac{3}{\tilde{\chi}(T)} \left( \frac{1}{\varrho_0} + \frac{1}{1 - \varrho_0} - 2\tilde{\chi}(T) \right) \frac{1}{1 + \frac{\pi^2\beta A_f}{8\tilde{\chi}(T)}}. \quad (4.57)$$

In a first-order perturbative theory approach (see Appendix C) the influence of  $\Delta\Omega[\varrho_0(\mathbf{r})]$  on the wetting behavior of the electrolyte solution can be determined by inserting into Eq. (4.49) the solutions  $\varrho_0^{(0)}(\mathbf{r})$  and  $\varrho_{\pm}^{(0)}(\mathbf{r})$  as obtained from  $\Omega_0[\varrho_0(\mathbf{r}), \varrho_{\pm}(\mathbf{r})]$  (see Sec. 4.1). The superscript (0) denotes these solutions as the ones obtained from the unperturbed functional  $\Omega_0$ .

Following the same procedure as described in Sec. 4.1, i.e., expanding the local part of the grand canonical functional in Eq. (4.49) around the sharp-kink density profiles in Eqs. (4.10) and (4.11), for  $\ell \rightarrow \infty$  one obtains the following form for the effective interface



potential (see Appendix E):

$$\beta\omega(\ell \rightarrow \infty) \simeq \frac{a_1(T)}{\ell^2} + \frac{b_1(T)}{\ell^3} + \dots + a_0(T) \exp(-\ell/\xi) + b_0(T) \exp(-2\ell/\xi) + a_I(T) \exp(-2\kappa\ell), \quad (4.58)$$

where ellipses stand for further subdominant terms as powers of  $1/\ell$ . As in the absence of long-ranged interactions the ions enter into  $\omega(\ell)$  only via the last term. The analytic expressions for the coefficients  $a_1(T)$  and  $b_1(T)$  are given in Appendix D,  $a_0(T)$  and  $b_0(T)$  are given by Eqs. (4.39) and (4.40), respectively, and  $a_I(T)$  is given by Eq. (4.46). Corrections to the coefficients  $a_0(T)$  and  $b_0(T)$  due to the long-ranged interactions (Eqs. (4.47) and (4.48)) are neglected because these long-ranged interactions are treated as a small perturbation to the model with short-ranged interactions only. The sign of the coefficients  $a_1(T)$ ,  $b_1(T)$ ,  $a_0(T)$ , and  $b_0(T)$  can change with  $T$  while  $a_I(T)$  is always positive (see Appendix D). As discussed for short-ranged interactions in the previous Sec. 4.1, the order of the wetting transition can be inferred from the analysis of these coefficients. They depend on seven parameters:  $\chi_S$ ,  $\chi_H$ ,  $A_f$ ,  $u_3\varrho_w$ ,  $u_4\varrho_w$ ,  $h_1$ , and  $g$ . The value of  $\chi_S$  is typically much smaller than unity [170] so that  $\chi_S = 0$  is considered in the following. Moreover, in the discussion below, the amplitude  $A_f$  is chosen to be in the range  $(0.04 - 0.15) \times 10^{-19}$  J, which corresponds to typical strengths of the van der Waals interaction in condensed phases (see Ref. [11]) and  $\chi_H$  is determined via of Eq. (4.56) using the critical temperature  $T_c = 647$  K of water. Finally,  $u_3\varrho_w$  is fixed by specifying the temperature  $T^{(a_1)}$  at which  $a_1(T^{(a_1)}) = 0$  given by the implicit relation (see Eq. D.1)  $\varrho_{0,l}(T^{(a_1)}) = u_3\varrho_w/t_3 = -6u_3\varrho_w/(\pi A_f)$  ( $u_3 > 0$ ,  $A_f < 0$ ); in the case of a critical wetting transition this temperature coincides with the wetting transition temperature  $T_w = T^{(a_1)}$ . With these choices the only remaining free parameters in the following analysis are  $u_4\varrho_w$ ,  $h_1$ , and  $g$ . However, their values are constrained by the condition  $b_1(T_w) > 0$  for critical wetting (see Eq. (D.2)). Due to the additional presence of the parameters  $A_f$ ,  $u_3\varrho_w$ , and  $u_4\varrho_w$  of the long-ranged interactions, in that case the corresponding discussion is slightly more difficult than the one for short-ranged interactions only as studied in the previous section.

First the pure solvent case, i.e.,  $a_I = 0$  is analyzed. In this case, the necessary conditions for the occurrence of critical wetting are (Eq. (4.58) and Ref. [2])

$$a_1(T_w) = 0, \quad a_1(T < T_w) < 0, \quad \text{and} \quad b_1(T_w) > 0 \quad (4.59)$$

i.e.,  $T^{(a_1)} = T_w$ , and, as before, one obtains conditions for the parameters of the pair

potentials (see Eqs. (D.1) and (D.2)):

$$\varrho_{0,c}/\varrho_w < u_3/t_3 < \varrho_{0,l}(T_t)/\varrho_w \quad (4.60)$$

and

$$\varrho_w u_4 - 3t_3 \varrho_{0,l}(T_w) \left[ d_w + d_{wl}^{(1)} \right] > 0, \quad (4.61)$$

with  $d_{wl}^{(1)}$  given by Eq. (D.9) and  $\varrho_{0,l}(T_w) = u_3 \varrho_w / t_3$ .

Although necessary, these conditions are not sufficient for critical wetting to occur. Large negative values of the coefficient  $a_0(T)$  of the exponentially decaying contribution can still lead to a first-order wetting transition even if  $b_1(T^{(a_1)}) > 0$ . Within the present model one has  $a_0(T) > 0$  for  $h_1/g > \varrho_{0,l}(T)$  (see Eq. (4.39)). If  $b_1(T^{(a_1)}) < 0$  the wetting transition is always first order. However, in the case of a first-order wetting transition all details of  $\omega(l)$ , and not only its leading contributions, matter for a reliable description of the character of the transition and for determining the corresponding wetting transition temperature. Hence, an asymptotic expansion of  $\omega(\ell)$  as in Eq. (4.58) is not conclusive in the case of first-order wetting.

For wetting of a wall by a one-component fluid with short- and long-ranged interactions and based on a Cahn type theory, in Refs. [199,200] a wetting scenario has been predicted which involves a succession of two interfacial phase transitions upon increasing  $T$ . The first of these two transitions is a discontinuous jump between two finite values  $\ell_1$  and  $\ell_2 > \ell_1$  of the film thickness  $\ell$  at two-phase coexistence and is referred to as a “thin-thick transition”. The second one is the standard second-order wetting transition at  $T = T_w$ . (In Refs. [199,200] the possibility of a thin-thick transition preceding a first-order wetting transition has not been discussed). This wetting scenario can be explained in terms of the competition between the short- and long-ranged interactions. Such a thin-thick transition precedes the critical wetting transition only if the short-ranged interactions would give rise to a first-order wetting transition in the case that the long-ranged interactions were negligible. Because the present theory involves both short- and long-ranged interactions, the occurrence of this wetting scenario can be checked for the pure solvent case. In this case, the separatrix between first- and second-order wetting is given by Eq. (4.44) for the model with short-ranged interactions only (e.g., for  $g = 1$  the transition will be first order in the pure solvent case without long-ranged interaction if  $h_1 > 0.49$ ). By choosing a proper set of parameters (see the discussion above) the occurrence of this two-stage transition for the pure solvent has been observed within the present model for  $\pi^2 A_f \lesssim 0.55 \times 10^{-19}$  J,  $\varrho_{0,l}(T_w) = u_3 \varrho_w / t_3 = 0.7$ ,  $u_4 = 2.3 \times t_3$ ,  $g = 1$ , and  $h_1 = 0.76$ , such that the condition for second-order wetting given by Eq. (4.61) is satisfied.

This thin-thick transition has also been observed for wetting of a wall by a one-component fluid in models with short-ranged interactions only [201–203] and with long-ranged interactions only [197]. Furthermore it has been observed experimentally for wetting of hexane on water [204]. In Ref. [201] this thin-thick transition has been observed for a generalization of the Sullivan model [205], in which in addition to the exponentially decaying wall-fluid potential a square-well attraction has been included. A thin-thick transition was also analyzed in Ref. [202] for a Landau theory of wetting which includes an extra surface term  $h_3(\varrho_0(0))^3$  linked to the substrate potential (see Ref. [172] and Eq. (4.1)). In Ref. [203] it has been shown that the behavior of the model in Ref. [201] can be mapped onto that used in Ref. [202]. With that it turns out that the thin-thick transition predicted in Refs. [201] and [202] involves short-ranged forces only and is due to the competition between two opposing (effective) surface fields at the same surface, one favoring wetting and the other favoring drying. Such a competition between surface fields is not considered here. Therefore within the present model a thin-thick transition does not occur in the pure solvent case with short-ranged interactions only (see Sec. 4.1).

The influence of ions and of surface charges on the wetting behavior of electrolytes with solvents governed by short- and long-ranged forces differs qualitatively from the one discussed in Subsec. 4.1.2, because in this case the leading contributions to  $\omega(\ell \rightarrow \infty)$  decay algebraically as function of the film thickness  $\ell$ . Accordingly, the contribution due to the ions and the charged wall can enter at most as the leading non-algebraic term in the expansion for  $\ell \rightarrow \infty$ ; this is the case if the Debye length  $1/\kappa$  is larger than (twice) the bulk correlation length  $\xi$  (see Subsec 4.1.2).

Various parameter sets  $(h_1, g, u_4, T^{(a_1)})$  have been chosen such that the pure solvent with short- and long-ranged interactions near a charge neutral wall (i.e., for  $a_I(T) = 0$ ) exhibits a second-order wetting transition at  $T_w(I = 0, \sigma = 0)$  without being preceded by a thin-thick transition (i.e., different from the above scenario). For fixed ionic strength  $I \neq 0$  and upon increasing the surface charge density  $\sigma$ , due to  $a_I(T) \sim \sigma^2/\sqrt{I}$  (Eq. 4.46)  $\omega(\ell)$  rises at finite film thickness  $\ell$  to the effect that the wetting transition temperature  $T_w(I, \sigma)$  decreases for increasing surface charge density  $\sigma$  (see Fig. 3.5). Moreover, for fixed surface charge density  $\sigma$  the wetting transition temperature  $T_w(I, \sigma)$  decreases upon decreasing the ionic strength  $I$  (i.e., increasing the amplitude  $\sigma^2/\sqrt{I}$  and the Debye length  $1/\kappa \sim 1/\sqrt{I}$ ) (see Fig. 3.5). In addition, the positive and monotonically decreasing (as a function of increasing  $\ell$ ) contribution  $a_I(T) \exp(-2\kappa\ell)$  to  $\omega(\ell)$  does lead to a thin-thick transition preceding the critical wetting transition which is absent without ions. Figure 4.1 shows the curves for  $\omega(\ell)$  corresponding to the temperatures  $T_1 = 0.918 \times T_c$ ,  $T_2 = 0.919 \times T_c$ ,  $T_3 = 0.92 \times T_c$ ,  $T_4 = 0.932 \times T_c$ , and  $T_w = 0.944 \times T_c$  with  $T_1 < T_2 \lesssim$

$T_{t-t,w} < T_3 < T_4 < T_w$ , i.e., the *thin-thick* transition occurs in between the temperatures  $T_2$  and  $T_3$ , whereas the critical wetting transition takes place at the wetting temperature  $T_w$ .

However, in the case that the pure solvent exhibits a second-order wetting transition, which is preceded by a thin-thick wetting transition, the effect of the term due to the ions and to the surface charge density ( $a_I(T) \neq 0$ ), in the case  $1/\kappa > 2\xi$ , is to decrease the thin-thick wetting transition temperature  $T_{t-t,w}$  and to increase the value of the jump in film thickness.

The case of  $a_I(T) \neq 0$  for a system in which a pure solvent with short- and long-ranged interactions near a charge neutral wall exhibits a first-order wetting transition is not discussed here, because within the present approach only the leading contributions of the effective interface potential for  $\ell \rightarrow \infty$  are analytically accessible (see Eq. (4.58)) and reliable knowledge of the behavior of  $\omega(\ell)$  for small  $\ell$ , which is particularly important for first-order wetting transitions, is lacking. Therefore, in order to be able to analyze the effect of the ions and of the surface charge density on solvents which without ions exhibit first-order wetting transitions, more details of the effective interface potential are needed.

The thin-thick wetting transition at two-phase coexistence, which precedes a standard second-order wetting scenario, has been discussed in the context of wetting in electrolytes in Ref. [18] for a model of an ionic solution close to a charged wall in which the solvent-solvent and solvent-wall interactions are short-ranged only and the contribution of the ions to the effective interface potential is calculated by solving the full Poisson-Boltzmann equation instead of the linearized one as in the present study (see Sec. 4.1). The thin-thick transition in Ref. [18] occurs in a restricted region of the parameter space, provided that the transition in the pure solvent is first order and that  $1/\kappa < 2\xi$ , i.e, for large ionic strength.

In contrast, within the present approach the *combined* presence of short- *and* long-ranged interactions is taken into account. As discussed above for the case of a pure solvent with short- *and* long-ranged interactions, a thin-thick transition will precede a long-ranged critical wetting transition only if the short-ranged interactions alone would give rise to a first-order wetting transition in the case that the long-ranged interactions were negligible [199, 200]. This is precisely the case that is encountered in the present context for the electrolyte solution when solvent-solvent and solvent-wall long-ranged interactions are taken into account: In the absence of these long-ranged interactions the transition is first-order if  $1/\kappa > 2\xi$  (see Subsec. 4.1.2), such that  $\ell$  jumps from  $\ell_1$  to  $\ell_2 = \infty$  (see Fig. 4.1). Once the long-ranged interactions are taken into account they block the jump of  $\ell$  to  $\ell_2 = \infty$  and limit this jump to one with a finite value

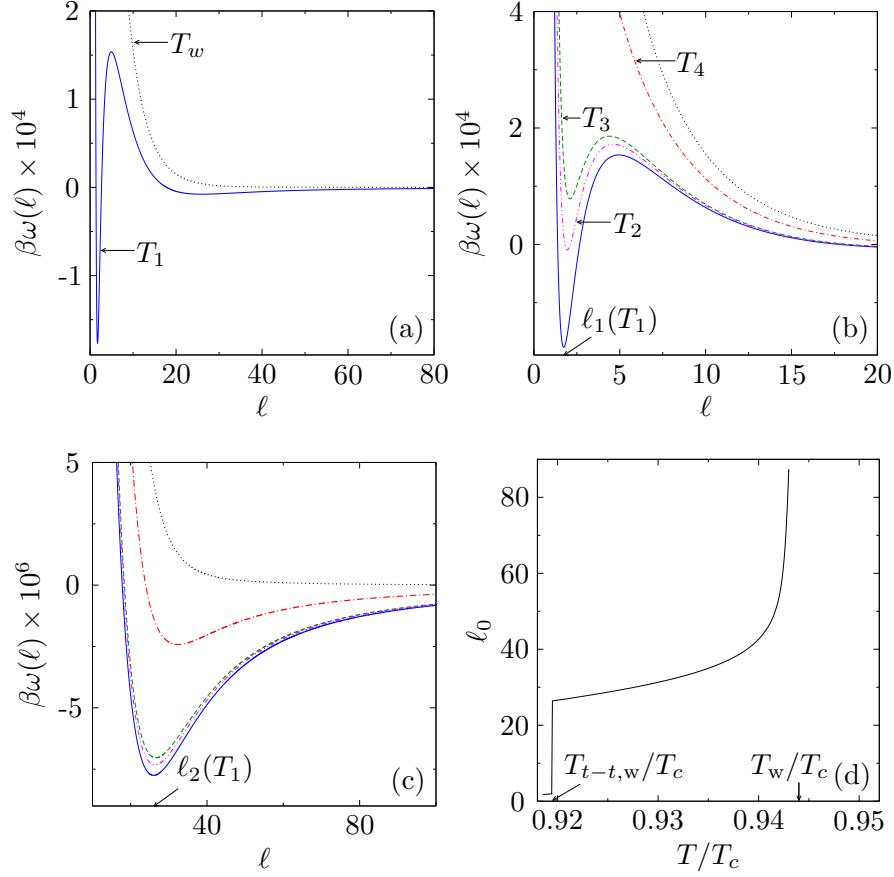


Figure 4.1: Effective interface potential  $\omega(\ell)$  for systems governed by short- and long-ranged interactions as function of the thickness  $\ell$  of the liquid film at gas-liquid coexistence in the presence of ions for the case that the pure, i.e., salt-free, solvent exhibits a critical wetting transition (without being preceded by a thin-thick transition). The parameters used are  $A_f/k_B = -1013\text{K}$ ,  $u_3 = 0.7 \times t_3$  (i.e.,  $\varrho_{0,l}(T^{(a_1)} = T_w) = 0.7$ ),  $u_4 = 2.28 \times t_3$ ,  $g = 1$ ,  $h_1 = 0.76 \times g$ ,  $I = 1mM$ , and  $\sigma = 0.1\mu\text{C}/\text{cm}^2$  (see main text). The effective interface potential  $\omega(\ell)$  has two local minima (at  $\ell_1(T)$  (see (a) and (b)) and  $\ell_2(T)$  (see (c)) with  $\ell_1 < \ell_2 < \infty$ ), one of the two being the global one at a given temperature (see (a)). They have the same depth at  $T = T_{t-t,w} \approx 0.919 \times T_c$  (not apparently visible). For  $T > T_{t-t,w}$  the film thickness  $\ell_2(T)$  is the global minimum and diverges continuously  $1/(T_w - T)$  as  $T \rightarrow T_w \approx 0.944 \times T_c$  (see (c)). The global minimum  $\ell_0(T)$  as a function of temperature is plotted in (d). At  $T_{t-t,w}$  the film thickness exhibits a finite jump and subsequently diverges smoothly for  $T \nearrow T_w$ . Accordingly, the system undergoes a thin-thick wetting transition at  $T_{t-t,w}$ , followed by a continuous one at  $T_w$ . Five different temperatures,  $T_1 \approx 0.918 \times T_c$ ,  $T_2 \approx 0.919 \times T_c$ ,  $T_3 \approx 0.92 \times T_c$ ,  $T_4 = 0.932 \times T_c$  and  $T_w$  are displayed in (a), (b), and (c) (using a common color code) with  $T_1 < T_2 \lesssim T_{t-t,w} < T_3 < T_4 < T_w$ . (Note the different scales of the axes.) The film thickness  $\ell$  is measured in units of  $a$  such that  $a^3$  is the volume of a solvent particle. Densities are measured in units of  $a^3$ .

$\ell_2 < \infty$ . Once  $\ell$  has reached the value  $\ell_2$  a further increase in temperature leads to the unfolding of the standard wetting scenario under the aegis of long-ranged interactions at  $T_w > T_{t-t,w}$ . Therefore, the thin-thick wetting transition is the remnant of the first-order wetting transition that would occur in the electrolyte solution if the long-ranged solvent-solvent and solvent-wall interactions were negligible (see Subsec. 4.1.2).

# Chapter 5

## Density functional theory of electrowetting

In this chapter, the phenomenon of electrowetting, i.e., the dependence of the macroscopic contact angle of a fluid on the electrostatic potential of the substrate, is analyzed by using a density functional theory approach. The effective interface potential (see Subsec. 2.2.1) for Pellat's classical setup of a vertical parallel plate capacitor [124, 125] is determined and used to derive an electrowetting equation.

### 5.1 Theoretical considerations

#### 5.1.1 Setting

Consider Pellat's classical setup [124, 125] depicted in Fig. 5.1. A vertical parallel plate capacitor of width  $L$  is in contact with two immiscible fluids  $F_1$  and  $F_2$  of mass densities  $\varrho_{m1}$  and  $\varrho_{m2}$ , respectively. At least one of the fluids  $F_1$  and  $F_2$  is assumed to be an electrolyte solution. It is further assumed that  $\varrho_{m1} > \varrho_{m2}$  so that both fluids are separated in the gravitational field with  $F_1$  being the lower and  $F_2$  being the upper phase (see Fig. 5.1). Provided the capacitor width  $L$  is smaller than the capillary length [208–210]

$$\lambda = \sqrt{\frac{\gamma_{12}}{(\varrho_{m1} - \varrho_{m2})g}} \quad (5.1)$$

with the  $F_1$ - $F_2$  interfacial tension  $\gamma_{12}$  and the acceleration due to gravity  $g$ , the contact angles  $\vartheta_+$  and  $\vartheta_-$  of phase  $F_1$  are related to the meniscus height  $h$  by [208–210]

$$\cos \vartheta_+ + \cos \vartheta_- \simeq \frac{hL}{\lambda^2} \quad \text{for } L \ll \lambda. \quad (5.2)$$

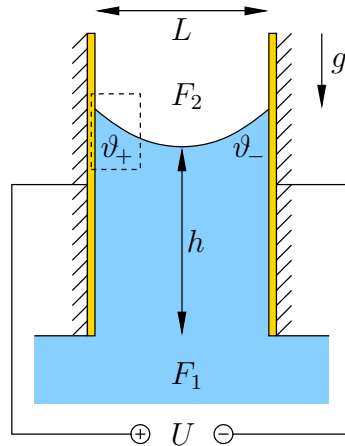


Figure 5.1: Pellat's setup [124,125] of electrocapillary rise of a fluid  $F_1$  in a vertical parallel plate capacitor of width  $L$  initially filled with a fluid  $F_2$ . The meniscus height  $h$  is related to the contact angles  $\vartheta_+$  and  $\vartheta_-$  by Eq. (5.2). Electrowetting corresponds to a dependence of  $\vartheta_+$  and  $\vartheta_-$ , and hence of  $h$ , on the voltage  $U$  between the plate electrodes. A closeup of the three-phase contact region marked by the dashed box is depicted in Fig. 5.2.

Depending on the interactions of the fluids  $F_1, F_2$  and the substrates  $S_+, S_-$ , which are metal electrodes (represented by the hatched parts in Fig. 5.1) possibly coated with some dielectric (represented by yellow layers on top of the electrodes in Fig. 5.1), the respective contact angles  $\vartheta_+$  and  $\vartheta_-$  can be smaller or larger than  $\pi/2$ , which corresponds to positive or negative contributions to the meniscus height  $h$ . Electrowetting can be detected as the dependence of the contact angles  $\vartheta_+(U)$  and  $\vartheta_-(U)$ , and in turn, via Eq. (5.2), of the meniscus height  $h(U)$ , on the electrostatic potential difference  $U = \Phi_+ - \Phi_-$  applied between the electrodes.

### 5.1.2 Contact angle and effective interface potential

The contact angles  $\vartheta_+$  and  $\vartheta_-$  in Fig. 5.1 provide a macroscopic description of the fluid-fluid-substrate three-phase contact region (highlighted by the dashed box in Fig. 5.1 for the anodic substrate  $S_+$ ). According to the chemical properties of the fluids and the substrates, the contact of substrate  $S_\pm$  with one fluid, henceforth denoted by fluid  $A$ , is more preferable than with the other fluid, henceforth denoted by fluid  $B$ . Here it is assumed that both substrates are chemically equal such that either fluid  $F_1$  or fluid  $F_2$  is preferred by both substrates  $S_+$  and  $S_-$ . Consequently, if substrate  $S_\pm$  is macroscopically in contact with the bulk of the less preferred fluid  $B$  and if the thermodynamic state is away from wetting transitions such that the substrate is only partially wet by phase  $A$ , a film of microscopic extension  $\ell_\pm > \xi$  composed of the preferred fluid  $A$  forms in between



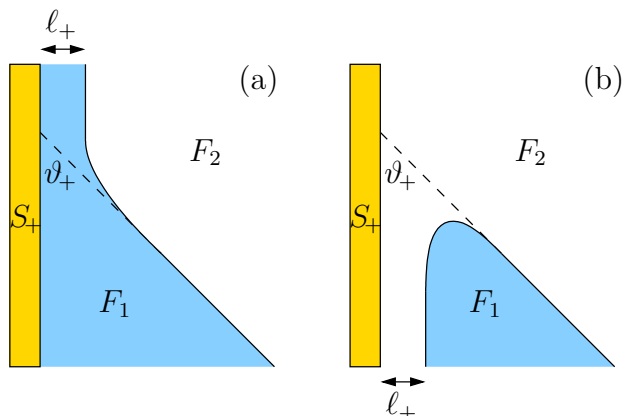


Figure 5.2: Closeup of the possible geometries of the three-phase contact region formed by the anodic substrate  $S_+$  (and similarly for the the cathodic substrate  $S_-$ ) and two immiscible fluids  $F_1$  and  $F_2$  marked by the dashed box in Fig. 5.1. The fluid which is preferred by the substrates  $S_{\pm}$  is denoted by  $A$ , whereas the other, less preferred fluid is called  $B$ . Panel (a) corresponds to the case of an  $F_1$ -philic ( $A = F_1$ ) substrate  $S_+$ , while panel (b) displays the case of an  $F_2$ -philic ( $A = F_2$ ) substrate  $S_+$ . Here it is assumed that both substrates  $S_+$  and  $S_-$  prefer the same fluid. The macroscopic contact angle  $\vartheta_+$  ( $\vartheta_-$ ) shown in Fig. 5.1 describes the asymptotic inclination of the  $F_1$ - $F_2$  interface far away from the substrate  $S_+$  ( $S_-$ ), whereas close to the substrate  $S_+$  ( $S_-$ ) a film of microscopic thickness  $\ell_+$  ( $\ell_-$ ) of the preferred fluid  $A$  is formed.

substrate  $S_{\pm}$  and the bulk of fluid  $B$  [2], where  $\xi$  denotes the bulk correlation length, which is of the order of the particle size if the thermodynamic state is away from critical points. Then the fluid structure is similar to that of a composition of an  $S_{\pm}$ - $A$  interface at the substrate surface and a free  $A$ - $B$  interface at a distance  $\ell_{\pm}$  away from the substrate, both being of typical extension  $\xi$  [2]. This structure leads to a surface contribution  $\Omega_{s,\pm B}(\ell_{\pm}) = \gamma_{\pm A} + \gamma_{12} + \omega_{\pm}(\ell_{\pm})$  to the grand potential of the system, where  $\gamma_{\pm A}$  and  $\gamma_{12}$  denote the  $S_{\pm}$ - $A$  and  $F_1$ - $F_2$  interfacial tensions, respectively, and where  $\omega_{\pm}(\ell_{\pm})$  is the effective interface potential [2]. It is important to distinguish  $\Omega_{s,\pm B}$  from the interfacial tension  $\gamma_{\pm B}$  of an  $S_{\pm}$ - $B$  interface in the *absence* of phase  $A$ . Here  $\Omega_{s,\pm B} \neq \gamma_{\pm B}$  because the presence of the preferred phase  $A$  leads to a structural change, i.e., the formation of  $A$ -films, as compared to the situation in the absence of phase  $A$ . Ignoring the difference between  $\Omega_{s,\pm B}$  and  $\gamma_{\pm B}$  is equivalent to ignoring the formation of  $A$ -films and it is this crucial misconception which underlies the electrocapillarity approach to electrowetting. In contrast, if substrate  $S_{\pm}$  is in contact with the bulk of the preferred fluid  $A$ , the fluid is non-uniform only close to the substrate surfaces up to distances  $\xi$ , and this interfacial structure is not modified by the presence of fluid  $B$ , hence  $\Omega_{s,\pm A} = \gamma_{\pm A}$ . Depending on whether the preferred fluid  $A$  is fluid  $F_1$  or fluid  $F_2$  the substrates  $S_{\pm}$  are referred to

as  $F_1$ -philic or  $F_2$ -philic, respectively. A closeup of the fluid-fluid-substrate three-phase contact region close to substrate  $S_+$  marked by the dashed box in Fig. 5.1 is sketched respectively in Figs. 5.2(a) and (b) for an  $F_1$ -philic ( $A = F_1$ ) and an  $F_2$ -philic ( $A = F_2$ ) substrate.

The macroscopic contact angle  $\vartheta_{\pm}$  (see Fig. 5.2) is related to the surface contributions  $\Omega_{s,\pm 1}$ ,  $\Omega_{s,\pm 2}$  and the interfacial tension  $\gamma_{12}$  of the  $S_{\pm}$ - $F_1$ ,  $S_{\pm}$ - $F_2$ , and  $F_1$ - $F_2$  interface, respectively, by Young's equation [208–210]

$$\Omega_{s,\pm 2} = \Omega_{s,\pm 1} + \gamma_{12} \cos \vartheta_{\pm}. \quad (5.3)$$

It is common to assume  $\Omega_{s,\pm\alpha} = \gamma_{s,\pm\alpha}$ ,  $\alpha \in \{F_1, F_2\}$ , but this misconception to ignore the structural differences of a macroscopic  $S_{\pm}$ - $\alpha$  contact in the presence and in the absence of additional phases can have significant consequences. The surface contributions  $\Omega_{s,\pm 1}$  and  $\Omega_{s,\pm 2}$  are related to the depth of the effective interface potential  $\omega_{\pm}(\ell)$  evaluated at the equilibrium film thickness  $\ell = \ell_{\pm}$  by [2]

$$\begin{aligned} \Omega_{s,\pm 1} &= \gamma_{\pm 1} \\ \Omega_{s,\pm 2} &= \gamma_{\pm 1} + \gamma_{12} + \omega_{\pm}(\ell_{\pm}) \end{aligned} \quad (5.4)$$

for  $F_1$ -philic substrates  $S_{\pm}$  (see above the three-phase contact region in Fig. 5.2(a)) and by

$$\begin{aligned} \Omega_{s,\pm 1} &= \Omega_{s,\pm 2} + \gamma_{12} + \omega_{\pm}(\ell_{\pm}) \\ \Omega_{s,\pm 2} &= \gamma_{s,\pm 2} \end{aligned} \quad (5.5)$$

for  $F_2$ -philic substrates  $S_{\pm}$  (see below the three-phase contact region in Fig. 5.2(b)). Hence, one obtains [2]

$$\cos \vartheta_{\pm} = \frac{\Omega_{s,\pm 2} - \Omega_{s,\pm 1}}{\gamma_{12}} = p \left( 1 + \frac{\omega_{\pm}(\ell_{\pm})}{\gamma_{12}} \right), \quad (5.6)$$

where  $p = +1$  for  $F_1$ -philic and  $p = -1$  for  $F_2$ -philic substrates  $S_{\pm}$ . This equation connects the macroscopic contact angle  $\vartheta_{\pm}$  with the microscopic structure represented by the effective interface potential  $\omega_{\pm}(\ell)$  of  $A$ -films at substrate  $S_{\pm}$  in macroscopic contact with bulk fluid  $B$ .

The next Sec. 5.1.3 describes an approximate calculation of the effective interface potentials  $\omega_{\pm}(\ell)$  for the setting of Fig. 5.1. The dependence of  $\omega_{\pm}(\ell_{\pm}; U)$  on the electrostatic potential difference  $U$  between the electrodes, together with Eq. (5.6), then leads to the

electrowetting equations derived in Sec. 5.1.4.

However, already without explicit expressions for the effective interface potentials, one can draw an important conceptual conclusion from Eq. (5.6): Electrowetting is *not* an electrocapillarity effect, since *no*  $U$ -dependent substrate–fluid interfacial tensions, which describe the contact of the substrate with *one* fluid, occur on the right-hand side. Instead, electrowetting is related to the depth of the effective interface potential, which describes the  $U$ -dependence of the microscopic fluid structure close to the substrate in the presence of *two* fluids.

### 5.1.3 Density functional theory of wetting

In order to obtain the effective interface potential  $\omega_{\pm}(\ell)$  of an  $A$ -film of thickness  $\ell$  at substrate  $S_{\pm}$  in Fig. 5.1, whose value for the equilibrium film thicknesses  $\ell = \ell_{\pm}$  is related to the contact angle  $\vartheta_{\pm}$  via Eq. (5.6), one may represent the structure in Fig. 5.1 far above (for an  $F_1$ -philic substrate  $S_{\pm}$ , see Fig. 5.2(a)) or below (for an  $F_2$ -philic substrate  $S_{\pm}$ , see Fig. 5.2(b)) the three-phase contact region by the quasi-one-dimensional slab depicted in Fig. 5.3(a). The chemically identical substrates  $S_+$  and  $S_-$ , which comprise metal electrodes coated with dielectric layers of thickness  $d$ , are separated by a distance  $L$  and covered with films of thicknesses  $\ell_+$  and  $\ell_-$ , respectively, of the preferred fluid  $A$ . Moreover, the electrodes are assumed to be ideally polarized, i.e., electrochemical reactions do not occur. Even under these conditions the film thicknesses  $\ell_+$  and  $\ell_-$  can differ, if unequal partitioning of ions at the film–bulk fluid interfaces takes place. This is expected to occur in general due to generic differences in solubility contrasts [21]. The macroscopic distance  $L$  between the substrates is typically the largest length scale such that only the limit  $L \rightarrow \infty$  is considered in the following. Hence the effective interface potentials  $\omega_+(\ell)$  and  $\omega_-(\ell)$  at the substrates  $S_+$  and  $S_-$ , respectively, are those of semi-infinite systems. For each substrate  $S_{\pm}$  a coordinate axis in normal direction with the origin  $z = 0$  at the substrate surface and the fluid at  $z > 0$  is introduced (see Fig. 5.3(b)). The interface between the  $A$ -film and the bulk of phase  $B$  is located at position  $z = \ell_{\pm}$  and the electrode is at  $z = -d$ , where the electrostatic potential is  $\Phi_{\pm}$  and the surface charge density is  $\sigma_{\pm}$ .

Considering the two bulk phases of fluids  $F_1$  and  $F_2$  outside the capacitor in Fig. 5.1 as particle reservoirs, one is naturally led to a grand-canonical description of the thermodynamic state. A starting point for the derivation of the effective interface potential  $\omega_{\pm}(\ell)$  is the grand potential functional per thermal energy  $k_B T = 1/\beta$  and per area  $\mathcal{A}$  of

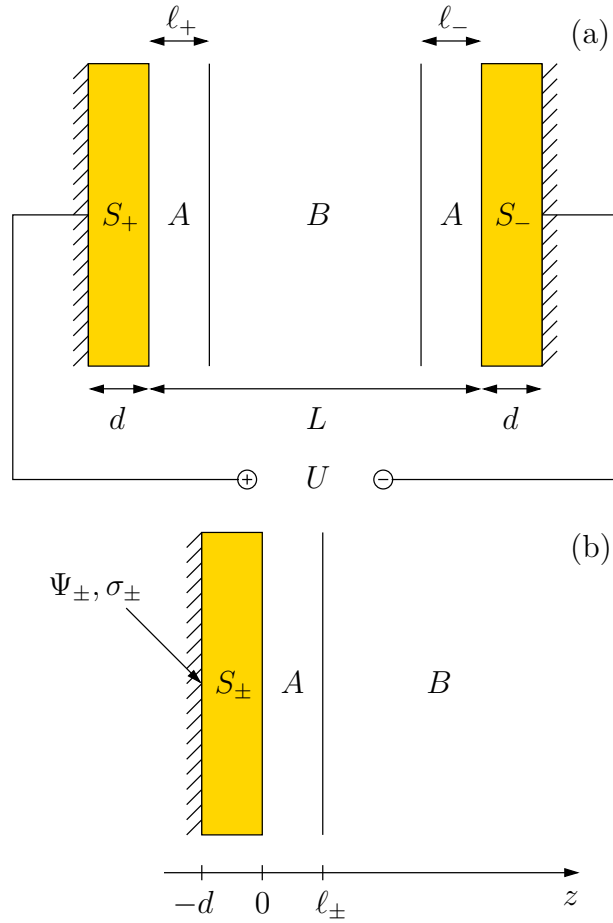


Figure 5.3: (a) Far above (Fig. 5.2(a)) or below (Fig. 5.2(b)) the three-phase contact regions (see Fig. 5.1) the dielectric substrates  $S_+$  and  $S_-$  of thickness  $d$  and distance  $L$  are covered by films of the preferred fluid  $A$  of microscopic thicknesses  $\ell_{\pm}$ , which separate the substrates from the bulk of the less preferred fluid  $B$ . (b) Since the separation  $L$  between the substrates  $S_+$  and  $S_-$  is typically the largest length scale, one can consider the limit  $L \rightarrow \infty$ , which renders the effective interface potential  $\omega_{\pm}(\ell)$  at substrate  $S_{\pm}$  that of a semi-infinite system. A coordinate axis normal to each substrate is introduced with the origin  $z = 0$  at the surface and the fluids in the range  $z > 0$ . The interface between the  $A$ -film and the bulk fluid  $B$  is located at  $z = \ell_{\pm}$  and the electrode is at position  $z = -d$ , where the electrostatic potential is  $\Phi_{\pm}$  and the surface charge density is  $\sigma_{\pm}$ .

the electrode

$$\begin{aligned}
 \frac{\beta\Omega_1[\varrho_0, \varrho_{\pm}]}{\mathcal{A}} &= \frac{\beta\Omega_0[\varrho_0]}{\mathcal{A}} + \frac{\beta d D(0)^2}{2\varepsilon_{\text{vac}}\varepsilon_S} - \beta\Phi_{\pm}D(0) \\
 &+ \int_0^{\infty} dz \left[ \sum_{i=\pm} \varrho_i(z) \left( \ln \frac{\varrho_i(z)}{\zeta_i} - 1 + \beta V_i(\varrho_0(z)) \right) + \frac{\beta D(z)^2}{2\varepsilon_{\text{vac}}\varepsilon(\varrho_0(z))} \right] \quad (5.7)
 \end{aligned}$$

in terms of the solvent composition profile  $\varrho_0$  and the  $\pm$ -ion number density profiles  $\varrho_{\pm}$ . Here the permittivity  $\varepsilon_{\text{vac}}$  of the vacuum, the relative permittivity  $\varepsilon_S$  of the substrate  $S_{\pm}$ , and the fugacities  $\zeta_{\pm}$  of  $\pm$ -ions are used. The density functional  $\Omega_0[\varrho_0]$  describes the grand potential of the pure, i.e., salt-free fluids. The electric displacement  $D(z)$  is determined by Gauß's law and the boundary condition of global charge neutrality:

$$D'(z) = \sum_{i=\pm} q_i e \varrho_i(z), \quad D(\infty) = 0. \quad (5.8)$$

Here  $q_{\pm} = \pm 1$  denotes the valency of  $\pm$ -ions and  $e$  is the elementary charge. Since the substrate  $S_{\pm}$  is free of ions the electrode surface charge density is given by  $\sigma_{\pm} = D(-d^+) = D(0^-)$  (see Fig. 5.3(b)). In the absence of specific adsorption of ions at the substrate surface, the electric displacement is continuous at  $z = 0$ , i.e.,  $D(0^-) = D(0^+) = D(0)$ , so that  $\sigma_{\pm} = D(0)$ . The electric displacement  $D(z)$  is related to the electrostatic potential  $\phi(z)$  by  $D(z) = -\varepsilon_{\text{vac}}\varepsilon(\varrho_0(z))\phi'(z)$ . The electrostatic potential of the electrode is given by  $\Phi_{\pm} = \phi(-d)$  (see Fig. 5.3(b)). The second term on the right-hand side and the term in the last line of Eq. (5.7) account for the electrostatic field energy inside the substrate and the fluids, respectively, whereas the last term in the first line represents the internal energy of the voltage source sustaining the electrostatic potential  $\phi(-d) = \Phi_{\pm}$  of the electrode (see Fig. 5.3(b)). The expressions  $V_{\pm}(\varrho_0(z))$  and  $\varepsilon(\varrho_0(z))$  denote respectively the local solvation free energy of a  $\pm$ -ion and the relative permittivity at a position  $z > 0$  where the solvent composition is given by  $\varrho_0(z)$  [21]. Finally, the second line of Eq. (5.7) describes the grand potential of the ions, where the ion number densities are assumed to be sufficiently small such that ions interact with each other only via the electrostatic field.

The equilibrium bulk state  $(\bar{\varrho}_0, I)$  with the bulk solvent composition  $\bar{\varrho}_0$  and the bulk ionic strength  $I$  minimizes the bulk grand potential density  $\Omega_b(\bar{\varrho}_0, I)/\mathcal{V}$ , which can be derived from Eq. (5.7) by inserting uniform profiles  $\varrho_0(z) = \bar{\varrho}_0$  and  $\varrho_{\pm}(z) = I$ , omitting all surface terms, and noting  $D = 0$  in the bulk. The two immiscible fluids  $A$  and  $B$  at co-existence in Fig. 5.3(a) correspond to two equilibrium bulk states  $(\bar{\varrho}_{0,A}, I_A)$  and  $(\bar{\varrho}_{0,B}, I_B)$ , respectively, with equal bulk grand potential density:  $\Omega_b(\bar{\varrho}_{0,A}, I_A)/\mathcal{V} = \Omega_b(\bar{\varrho}_{0,B}, I_B)/\mathcal{V}$ .

Since the present analysis is concerned with films of thicknesses  $\ell_{\pm} > \xi$  but not with interfacial structures on length scales less than  $\xi$  it is natural to approximate the solvent composition profile  $\varrho_0$  in Eq. (5.7) within the so-called sharp-kink approximation [2]

$$\varrho_{sk,0}\ell(z) := \begin{cases} \bar{\varrho}_{0,A}, & z < \ell \\ \bar{\varrho}_{0,B}, & z > \ell. \end{cases} \quad (5.9)$$

Furthermore, in view of the small ionic strengths  $I_A$  and  $I_B$  to be considered here and for sufficiently small surface potential  $|\phi(0) - \phi(\infty)|$ , the term in the second line of Eq. (5.7) can be expanded up to quadratic order in the ion number density deviations  $\Delta\rho_i(z) := \rho_i(z) - I_\alpha, i = \pm$ , with  $\alpha = A$  for  $z < \ell$  and  $\alpha = B$  for  $z > \ell$  if  $I_\alpha > 0$ . This leads to an approximate grand potential functional

$$\begin{aligned} \frac{\beta\Omega(\ell, [\Delta\rho_\pm])}{\mathcal{A}} &= \frac{\beta\Omega_0[\rho_{sk,0}]}{\mathcal{A}} + \frac{\beta dD(0)^2}{2\varepsilon_{\text{vac}}\varepsilon_S} - \beta\Phi_\pm D(0) \\ &+ \int_0^\ell dz \left[ f_A(\Delta\rho_+(z), \Delta\rho_-(z)) + \frac{\beta D(z)^2}{2\varepsilon_{\text{vac}}\varepsilon_A} \right] \\ &+ \int_\ell^\infty dz \left[ f_B(\Delta\rho_+(z), \Delta\rho_-(z)) + \frac{\beta D(z)^2}{2\varepsilon_{\text{vac}}\varepsilon_B} \right] \end{aligned} \quad (5.10)$$

with

$$f_\alpha(\Delta\rho_+, \Delta\rho_+) = \begin{cases} \sum_{i=\pm} \left[ I_\alpha \left( \ln \frac{I_\alpha}{\zeta_i} - 1 + \beta V_i(\bar{\rho}_{0,\alpha}) \right) \right. \\ \quad \left. + \left( \ln \frac{I_\alpha}{\zeta_i} + \beta V_i(\bar{\rho}_{0,\alpha}) \right) \Delta\rho_i + \frac{\Delta\rho_i^2}{2I_\alpha} \right], & I_\alpha > 0 \\ 0, & I_\alpha = 0. \end{cases} \quad (5.11)$$

By minimizing  $\beta\Omega(\ell, [\Delta\rho_\pm])/\mathcal{A}$  in Eq. (5.10) with respect to the profiles  $\Delta\rho_\pm$  one obtains the equilibrium profiles  $\Delta\rho_\pm^{(\ell)}$ . Inserting  $\Delta\rho_\pm^{(\ell)}$  into Eq. (5.10) and subtracting the bulk contribution  $\beta\Omega_b(\bar{\rho}_{0,B}, I_B)/\mathcal{A}$  leads to the surface contribution to the grand potential [2]

$$\Omega_s(\ell) = \frac{\Omega(\ell, [\Delta\rho_\pm^{(\ell)}]) - \Omega_b(\bar{\rho}_{0,B}, I_B)}{\mathcal{A}}. \quad (5.12)$$

Finally, the effective interface potential at substrate  $S_\pm$  is given by  $\omega_\pm(\ell) = \Omega_s(\ell) - \Omega_s(\infty)$  [2], which, in the present context, can be written in the form

$$\omega_\pm(\ell) = \omega_0(\ell) + \frac{A(\ell)}{2}(\Phi_\pm - \bar{\phi}_A)^2 + B(\ell)(\Phi_\pm - \bar{\phi}_A) + C(\ell). \quad (5.13)$$

Here  $\omega_0(\ell)$  denotes the effective interface potential corresponding to the grand potential functional  $\Omega_0[\rho_0]$  of the pure fluids,  $\bar{\phi}_\alpha := -(k_B T \ln(I_\alpha/\zeta_+) + V_+(\bar{\rho}_{0,\alpha}))/e = (k_B T \ln(I_\alpha/\zeta_-) + V_-(\bar{\rho}_{0,\alpha}))/e$  is the Galvani potential of phase  $\alpha \in \{A, B\}$ , and

$$\begin{aligned}
A(\ell) &= \frac{\varepsilon_{\text{vac}}}{Q(\ell)\lambda_B} \frac{\lambda_B - \lambda_A}{\lambda_S + \lambda_A} \exp\left(-\frac{\lambda_\ell}{\lambda_A}\right) \\
B(\ell) &= -\frac{\varepsilon_{\text{vac}}}{Q(\ell)\lambda_B} (\bar{\phi}_A - \bar{\phi}_B) \\
C(\ell) &= \frac{\varepsilon_{\text{vac}}}{2Q(\ell)\lambda_B} \frac{\lambda_S - \lambda_A}{\lambda_B + \lambda_A} \exp\left(-\frac{\lambda_\ell}{\lambda_A}\right) (\bar{\phi}_A - \bar{\phi}_B)^2 \\
Q(\ell) &= \cosh\left(\frac{\lambda_\ell}{\lambda_A}\right) \left(1 + \frac{\lambda_S}{\lambda_B}\right) + \sinh\left(\frac{\lambda_\ell}{\lambda_A}\right) \left(\frac{\lambda_A}{\lambda_B} + \frac{\lambda_S}{\lambda_A}\right)
\end{aligned} \tag{5.14}$$

with the length scales  $\lambda_A := 1/(\kappa_A \varepsilon_A)$ ,  $\lambda_B := 1/(\kappa_B \varepsilon_B)$ ,  $\lambda_S := d/\varepsilon_S$ , and  $\lambda_\ell := \ell/\varepsilon_A$ , where  $\kappa_\alpha^2 := 2\beta e^2 I_\alpha / (\varepsilon_{\text{vac}} \varepsilon_\alpha)$  is the square of the inverse Debye length in the bulk of phase  $\alpha \in \{A, B\}$ . In addition, the electrode charge density can be written as

$$\sigma_\pm = D(0) = F(\ell_\pm)(\Phi_\pm - \bar{\phi}_A) - B(\ell_\pm) \tag{5.15}$$

with

$$F(\ell) = \frac{\varepsilon_{\text{vac}}}{Q(\ell)} \left( \frac{1}{\lambda_A} \sinh\left(\frac{\lambda_\ell}{\lambda_A}\right) + \frac{1}{\lambda_B} \cosh\left(\frac{\lambda_\ell}{\lambda_A}\right) \right) \tag{5.16}$$

The Galvani potential difference (Donnan potential) between the phases  $A$  and  $B$ ,  $\bar{\phi}_A - \bar{\phi}_B = ((V_-(\bar{\rho}_{0,A}) - V_+(\bar{\rho}_{0,A})) - (V_-(\bar{\rho}_{0,B}) - V_+(\bar{\rho}_{0,B}))) / (2e)$ , can be inferred from the solubility of the  $\pm$ -ions in the solvents  $A$  and  $B$  [207, 211–213]. Moreover,  $\Phi_\pm - \bar{\rho}_{0,A}$  is determined by the potential difference  $U = \Phi_+ - \Phi_-$  and the fact that no chemical reactions take place at the electrodes so that the total charge of both electrodes vanishes:  $\sigma_+ + \sigma_- = 0$ . Using Eq. (5.15) leads to

$$\begin{aligned}
\Phi_+ - \bar{\phi}_A &= \frac{F(\ell_-)U + B(\ell_+) + B(\ell_-)}{F(\ell_+) + F(\ell_-)} \\
\Phi_- - \bar{\phi}_A &= \frac{-F(\ell_+)U + B(\ell_+) + B(\ell_-)}{F(\ell_+) + F(\ell_-)}
\end{aligned} \tag{5.17}$$

#### 5.1.4 Electrowetting equation

The equilibrium film thicknesses  $\ell_+$  and  $\ell_-$  are both similar in magnitude ( $\ell_+ \approx \ell_-$ ) of the order of a few bulk correlation lengths  $\xi$  away from wetting transitions. Hence, Eq. (5.17) leads to  $\Phi_\pm - \bar{\phi}_A \approx \pm U/2 + (B(\ell_+) + B(\ell_-)) / (F(\ell_+) + F(\ell_-))$ , i.e., the  $U$ -dependent part of  $\Phi_\pm - \bar{\phi}_A$  is rather insensitive to a variation of  $\ell_+ \approx \ell_-$ . Moreover, the film thicknesses  $\ell_+$  and  $\ell_-$  are typically much smaller than the Debye length  $1/\kappa_A$  in the  $A$ -

film. Consequently, the leading  $U$ -dependent contribution  $\sim U^2$  to the effective interface potential  $\omega_{\pm}(\ell)$  in Eq. (5.13), which decays exponentially with  $\ell$  on the length scale of half of a Debye length,  $1/(2\kappa_A)$  (see Eq. (5.14)), does not significantly shift the equilibrium film thickness  $\ell_{\pm}$  but it merely lifts the depth  $\omega_{\pm}(\ell_{\pm}; U)$  of the effective interface potential. Therefore, in the following, the film thicknesses  $\ell_{\pm}$  are considered as independent of the applied voltage  $U$ .

Hence, Eq. (5.6) can be written as [6]

$$\cos \vartheta_{\pm}(U) = \cos \vartheta_{\pm}(0) + \eta_{\pm}(U) \quad (5.18)$$

with the electrowetting number

$$\eta_{\pm}(U) := p \frac{\omega_{\pm}(\ell_{\pm}; U) - \omega_{\pm}(\ell_{\pm}; 0)}{\gamma_{12}}. \quad (5.19)$$

Inserting Eq. (5.17) into Eq. (5.13) leads to

$$\eta_{\pm}(U) = \frac{p}{\gamma_{12}} \left\{ \frac{A(\ell_{\pm})F(\ell_{\mp})^2}{2(F(\ell_{+}) + F(\ell_{-}))^2} U^2 \pm \left( \frac{A(\ell_{\pm})F(\ell_{\mp})(B(\ell_{+}) + B(\ell_{-}))}{(F(\ell_{+}) + F(\ell_{-}))^2} + \frac{B(\ell_{\pm})F(\ell_{\mp})}{F(\ell_{+}) + F(\ell_{-})} \right) U \right\}. \quad (5.20)$$

This equation is expected to be valid for sufficiently small voltages  $|U|$  such that the quadratic approximation Eq. (5.11) is applicable. The electrowetting number  $\eta_{\pm}(U)$  in Eq. (5.20) differs from those in the literature [6] in a number of aspects, as is discussed in the next section. The most obvious difference is the occurrence of a correction term  $\sim U$ , which vanishes exactly only if  $B(\ell) = 0$  due to a vanishing Donnan potential (Galvani potential difference)  $\bar{\phi}_A - \bar{\phi}_B$ . For  $\bar{\phi}_A - \bar{\phi}_B \neq 0$ , i.e.,  $B(\ell) \neq 0$ , the electrowetting number  $\eta_{\pm}(U)$  in Eq. (5.20) is not minimal at and not symmetric with respect to  $U = 0$ . However, for a sufficiently large voltage  $|U|$  the subleading term  $\sim U$  is dominated by the leading term  $\sim U^2$ .

Whereas the full expression for the electrowetting number  $\eta_{\pm}(U)$  in Eq. (5.20) depends on the five possibly largely different length scales  $\lambda_A$ ,  $\lambda_B$ ,  $\lambda_S$ ,  $\lambda_{\ell_{+}}$ , and  $\lambda_{\ell_{-}}$ , the latter two, corresponding to the thicknesses of the  $A$ -films at the substrates  $S_{+}$  and  $S_{-}$ , respectively, are typically of similar magnitude:  $\ell_{+} \approx \ell_{-}$ , i.e.,  $\lambda_{\ell_{+}} \approx \lambda_{\ell_{-}}$ . This case  $\ell_{+} = \ell_{-} =: \ell$  is discussed in detail in the next section, for which the electrowetting number  $\eta_{\pm}(U)$  in



Eq. (5.20) simplifies to

$$\eta_{\pm}(U) = \frac{p}{\gamma_{12}} \left( \frac{A(\ell)}{8} U^2 \pm \frac{B(\ell)}{2} \left( \frac{A(\ell)}{F(\ell)} + 1 \right) U \right). \quad (5.21)$$

Moreover, the film thicknesses  $\ell_+$  and  $\ell_-$  are typically smaller than the Debye lengths  $1/\kappa_A$  and  $1/\kappa_B$  so that the limiting case  $\lambda_\ell \ll \lambda_A, \lambda_B$  is considered throughout, within which

$$A(\ell) \simeq \frac{\varepsilon_{\text{vac}}}{Q(\ell)} \frac{\lambda_B - \lambda_A}{\lambda_B(\lambda_S + \lambda_A)} \quad (5.22)$$

$$B(\ell) = -\frac{\varepsilon_{\text{vac}}}{Q(\ell)} \frac{\bar{\phi}_A - \bar{\phi}_B}{\lambda_B} \quad (5.23)$$

$$F(\ell) \simeq \frac{\varepsilon_{\text{vac}}}{Q(\ell)} \left( \frac{\lambda_\ell}{\lambda_A^2} + \frac{1}{\lambda_B} \right) \quad (5.24)$$

$$Q(\ell) \simeq 1 + \frac{\lambda_S}{\lambda_B} + \frac{\lambda_\ell \lambda_S}{\lambda_A^2}. \quad (5.25)$$

## 5.2 Discussion

### 5.2.1 Electrowetting and electrocapillarity

Before discussing the electrowetting number in Eq. (5.21) obtained within the present density functional analysis, the traditional approach based on the assumption of electrowetting being an electrocapillarity effect [6, 124–138] is repeated. Here only the classical method based on Lippmann’s equation is presented. However, calculations using alternative methods, e.g., based on Maxwell’s stress tensor [6, 214], suffer from the same misconceptions.

The starting point is Young’s equation (5.3) but with the *incorrect* assumption  $\Omega_{s,\pm\alpha} = \gamma_{\pm\alpha}$ ,  $\alpha \in \{F_1, F_2\}$ . In order to obtain the  $U$ -dependence of the interfacial tension  $\gamma_{\pm\alpha}$  one considers a semi-infinite fluid  $\alpha$  bound by a planar substrate  $S_{\pm}$ . The interfacial tension  $\gamma_{\pm\alpha}$  changes upon changing the electrostatic potential  $\phi_{\pm\alpha}$  of substrate  $S_{\pm}$  with respect to that of the bulk of phase  $\alpha$  according to Lippmann’s equation [123, 206]

$$\frac{\partial \gamma_{\pm\alpha}}{\partial \phi_{\pm\alpha}} = -\sigma_{\pm\alpha}, \quad (5.26)$$

where  $\sigma_{\pm\alpha}$  is the surface charge density of substrate  $S_{\pm}$  in contact with phase  $\alpha$ . Describing the  $S_{\pm}$ - $\alpha$  interface by means of the potential-independent differential capacitance  $C_{S\alpha} = \partial \sigma_{\pm\alpha} / \partial \phi_{\pm\alpha}$ , which is assumed to not depend on  $S_{\pm}$  for chemically identical sub-

strates, and integrating twice with respect to the electrostatic substrate potential  $\phi_{\pm\alpha}$  using Lippmann's equation (5.26) leads to

$$\gamma_{\pm\alpha}(\phi_{\pm\alpha}) = \gamma_{\pm\alpha}(0) - \frac{C_{S\alpha}}{2}\phi_{\pm\alpha}^2. \quad (5.27)$$

Young's equation (5.3) in conjunction with the assumption  $\Omega_{s,\pm\alpha} = \gamma_{\pm\alpha}$  reads

$$\begin{aligned} \gamma_{\pm 2}(\phi_{\pm 2}) &= \gamma_{\pm 2}(0) - \frac{C_{S2}}{2}\phi_{\pm 2}^2 \\ &= \gamma_{\pm 1}(\phi_{\pm 1}) + \gamma_{12} \cos \vartheta_{\pm} \\ &= \gamma_{\pm 1}(0) - \frac{C_{S1}}{2}\phi_{\pm 1}^2 + \gamma_{12} \cos \vartheta_{\pm}. \end{aligned} \quad (5.28)$$

Noting  $\gamma_{\pm 2}(0) - \gamma_{\pm 1}(0) = \gamma_{12} \cos \vartheta_{\pm}(0)$  leads to

$$\cos \vartheta_{\pm} - \cos \vartheta_{\pm}(0) = \frac{C_{S1}}{2\gamma_{12}}\phi_{\pm 1}^2 - \frac{C_{S2}}{2\gamma_{12}}\phi_{\pm 2}^2. \quad (5.29)$$

Using  $\sigma_{\pm\alpha} = C_{S\alpha}\phi_{\pm\alpha}$ , one obtains the analog of Eq. (5.17) from  $U = \phi_{+\alpha} - \phi_{-\alpha}$  and  $\sigma_{+\alpha} + \sigma_{-\alpha} = 0$  as  $\phi_{\pm\alpha} = \pm U/2$ . This leads to the commonly used form of the electrowetting equation [6, 124–138]

$$\cos \vartheta_{\pm}(U) - \cos \vartheta_{\pm}(0) = \frac{C_{S1} - C_{S2}}{8\gamma_{12}}U^2 =: \eta_{ec}(U) \quad (5.30)$$

with the differential capacitances  $C_{S\alpha}$  being those of a substrate in macroscopic contact with only one fluid phase  $\alpha$ . These differential capacitances  $C_{S\alpha}$  can typically be interpreted as those of a capacitor of capacitance  $C_S = \varepsilon_{\text{vac}}\varepsilon_S/d$ , representing substrate  $S_{\pm}$ , connected *in series* with a capacitor of capacitance  $C_{\alpha}$ , representing fluid  $\alpha$ :  $1/C_{S\alpha} = 1/C_S + 1/C_{\alpha}$ . If fluid  $\alpha$  is an electrolyte solution the fluid capacitance is that of the electric double layer in a semi-infinite system,  $C_{\alpha} = \varepsilon_{\text{vac}}\kappa_{\alpha}\varepsilon_{\alpha}$ , whereas for a non-conducting dielectric fluid  $C_{\alpha} = \lim_{L \rightarrow \infty} \varepsilon_{\text{vac}}\varepsilon_{\alpha}/L = 0$ . Using the length scales defined after Eq. (5.14), this leads to

$$C_{S\alpha} = \begin{cases} \frac{\varepsilon_{\text{vac}}}{\lambda_S + \lambda_{\alpha}}, & \alpha \text{ electrolyte solution} \\ 0, & \alpha \text{ non-conducting fluid.} \end{cases} \quad (5.31)$$

Equations (5.30) and (5.31) represent the interpretation of electrowetting as an electrocapillarity effect [6]. However, the crucial misconception underlying this interpretation is to use the approximation  $\Omega_{s,\pm\alpha} = \gamma_{\pm\alpha}$  and hence the differential capacitance  $C_{S\alpha}$ , which

corresponds to a semi-infinite system of a single phase  $\alpha$  bound by substrate  $S_{\pm}$ , instead of accounting for the actual fluid structure at the substrate. The interfacial structure, and therefore surface quantities such as the surface contribution to the grand potential as well as the differential capacitance, of substrate  $S_{\pm}$  in macroscopic contact with the bulk fluid  $B$  depend significantly on whether the preferred fluid  $A$  is present or not because an  $A$ -film forms in between the substrate  $S_{\pm}$  and the bulk fluid  $B$  in the former case whereas it does not in the latter case. In contrast, these structural properties are naturally accounted for within the present density functional approach, which relates the contact angle to the effective interface potential (see Eq. (5.6)), a quantity which correctly describes the contact of a substrate with *both* fluids  $A$  and  $B$ .

## 5.2.2 Electrowetting on uncoated metal electrodes

The early investigations of electrocapillarity by Lippmann [123] and Pellat [124, 125] have been performed for metal electrodes without any dielectric coating. At that time for some decades mercury electrodes became the experimental standard for investigations of the electric double layer [206]. Pure metal electrodes can be considered as substrates with thickness  $d$  being the smallest length scale:  $\lambda_S \ll \lambda_{\ell} \ll \lambda_A, \lambda_B$ . Within this limit one obtains  $Q(\ell) \simeq 1$  from Eq. (5.25) and subsequently from Eqs. (5.22)–(5.24)

$$A(\ell) \simeq \varepsilon_{\text{vac}} \left( \frac{1}{\lambda_A} - \frac{1}{\lambda_B} \right) \quad (5.32)$$

$$B(\ell) \simeq -\frac{\varepsilon_{\text{vac}}}{\lambda_B} (\bar{\phi}_A - \bar{\phi}_B) \quad (5.33)$$

$$F(\ell) \simeq \varepsilon_{\text{vac}} \left( \frac{\lambda_{\ell}}{\lambda_A^2} + \frac{1}{\lambda_B} \right). \quad (5.34)$$

For the case  $\lambda_A \ll \lambda_B$ , which is typically the case for hydrophilic substrates, an aqueous electrolyte solution  $F_1 = A$  (i.e.,  $p = +1$ ), and an oil  $F_2 = B$ , one obtains for the the electrowetting number Eq. (5.21)

$$\begin{aligned} \eta_{\pm}(U) &\simeq \frac{\varepsilon_{\text{vac}}}{8\gamma_{12}\lambda_A} U^2 \mp \frac{\varepsilon_{\text{vac}}(\bar{\phi}_A - \bar{\phi}_B)}{2\gamma_{12}(\lambda_A + \lambda_{\ell}\lambda_B/\lambda_A)} U \\ &\simeq \frac{\varepsilon_{\text{vac}}}{8\gamma_{12}\lambda_A} U^2, \quad \text{for } |U| \gg 4|\bar{\phi}_A - \bar{\phi}_B|. \end{aligned} \quad (5.35)$$

Hence, if the voltage  $|U|$  is much larger than the Donnan potential (Galvani potential difference)  $|\bar{\phi}_A - \bar{\phi}_B|$ , the electrowetting number  $\eta_{\pm}(U)$  agrees with that in Eq. (5.30), where  $C_{S1} \simeq \varepsilon_{\text{vac}}/\lambda_A$ ,  $C_{S2} = 0$  due to Eq. (5.31).

Similarly, for the case  $\lambda_A \gg \lambda_B$ , which is typically the case for hydrophobic substrates,

an oil  $F_2 = A$  (i.e.,  $p = -1$ ), and an aqueous electrolyte solution  $F_1 = B$ , one obtains for the electrowetting number Eq. (5.21)

$$\begin{aligned}\eta_{\pm}(U) &\simeq \frac{\varepsilon_{\text{vac}}}{8\gamma_{12}\lambda_B}U^2 \pm \frac{\varepsilon_{\text{vac}}(\bar{\phi}_A - \bar{\phi}_B)}{2\gamma_{12}\lambda_A}U \\ &\simeq \frac{\varepsilon_{\text{vac}}}{8\gamma_{12}\lambda_B}U^2, \quad \text{for } |U| \gg 4|\bar{\phi}_A - \bar{\phi}_B|.\end{aligned}\quad (5.36)$$

Again, if the voltage  $|U|$  is much larger than the Donnan potential (Galvani potential difference)  $|\bar{\phi}_A - \bar{\phi}_B|$ , the electrowetting number  $\eta_{\pm}(U)$  again agrees with that in Eq. (5.30), where  $C_{S1} \simeq \varepsilon_{\text{vac}}/\lambda_B$ ,  $C_{S2} = 0$  due to Eq. (5.31).

Therefore, the present formalism (Eqs. (5.21)–(5.25)) confirms the electrocapillarity-based form of the electrowetting number for the case of uncoated metal electrodes ( $\eta_{\pm}(U) \simeq \eta_{\text{ec}}(U)$ ), provided the voltage  $|U|$  is sufficiently large as compared to the Donnan potential (Galvani potential difference)  $|\bar{\phi}_A - \bar{\phi}_B|$ . Interestingly, for uncoated metal electrodes it is irrelevant whether they are  $F_1$ -philic (hydrophilic) or  $F_2$ -philic (hydrophobic).

However, a small voltage  $|U| \ll |\bar{\phi}_A - \bar{\phi}_B|$  or  $\lambda_A \approx \lambda_B$ , e.g., for two immiscible electrolyte solutions, leads to electrowetting numbers  $\eta_{\pm}(U) \sim U$ , in contrast to  $\eta_{\text{ec}}(U) \approx 0$  in Eq. (5.30) due to  $C_{S1} \approx C_{S2}$  according to Eq. (5.31). Since these conditions are rather special, this scenario is not expected to be of practical relevance, but it might provide a test for the present approach.

### 5.2.3 Electrowetting of water on hydrophobic dielectrics in oil

In the last few decades most electrowetting settings used electrodes coated with an isolating dielectric for technical advantage [128]. Almost all of these studies used drops of an aqueous electrolyte solution  $F_1$  placed on a hydrophobic dielectric and an oil  $F_2$  as the environmental fluid in order to achieve large contact angle ranges being covered by electrowetting [6]. Within the present notation this situation corresponds to  $A = F_2$  (i.e.,  $p = -1$ ) and  $B = F_1$ . Since the thickness  $\ell$  of the microscopic oil film on the substrates  $S_{\pm}$  is typically smaller than the the Debye length  $1/\kappa_B$  of the dilute electrolyte solution  $B = F_1$ , which in turn is typically much smaller than the thickness  $d$  of the dielectric substrates  $S_{\pm}$ , one identifies the case  $\lambda_{\ell} \ll \lambda_B \ll \lambda_S \ll \lambda_A$ , where a (practically) ion-free oil  $A = F_2$  ( $I_A \approx 0$ ) is assumed. For this regime Eqs. (5.22)–(5.25) read

$$Q(\ell) \simeq \frac{\lambda_S}{\lambda_B} \quad (5.37)$$

$$A(\ell) \simeq -\frac{\varepsilon_{\text{vac}}}{\lambda_S} \quad (5.38)$$

$$B(\ell) \simeq -\frac{\varepsilon_{\text{vac}}}{\lambda_S}(\bar{\phi}_A - \bar{\phi}_B) \quad (5.39)$$

$$F(\ell) \simeq \frac{\varepsilon_{\text{vac}}}{\lambda_S} \quad (5.40)$$

and hence Eq. (5.21) is given by

$$\begin{aligned} \eta_{\pm}(U) &\simeq \frac{\varepsilon_{\text{vac}}}{8\gamma_{12}\lambda_S}U^2 \pm \frac{\varepsilon_{\text{vac}}(\bar{\phi}_A - \bar{\phi}_B)}{2\gamma_{12}\lambda_A}U \\ &\simeq \frac{\varepsilon_{\text{vac}}}{8\gamma_{12}\lambda_S}U^2, \quad \text{for } |U| \gg 4\frac{\lambda_S}{\lambda_A}|\bar{\phi}_A - \bar{\phi}_B|. \end{aligned} \quad (5.41)$$

Since  $\lambda_S/\lambda_A \ll 1$ , the approximation in the second line of the previous equation almost always applies. It shows that the electrowetting number  $\eta_{\pm}(U)$  for water on a hydrophobic dielectric in oil is also in agreement with  $\eta_{\text{ec}}(U)$  in Eq. (5.30) with  $C_{S1} \simeq \varepsilon_{\text{vac}}/\lambda_S$ ,  $C_{S2} = 0$  due to Eq. (5.31).

## 5.2.4 Electrowetting of water on hydrophilic dielectrics in oil

Replacing the hydrophobic dielectric substrate of the previous Sec. 5.2.3 by a hydrophilic one leads to the case  $A = F_1$  (i.e.,  $p = +1$ ),  $B = F_2$ , and  $\lambda_{\ell} \ll \lambda_A \ll \lambda_S \ll \lambda_B$ , where again a (practically) ion-free oil  $B = F_2$  ( $I_B \approx 0$ ) is assumed. For this regime Eqs. (5.22)–(5.25) read

$$Q(\ell) \simeq 1 + \frac{\lambda_{\ell}\lambda_S}{\lambda_A^2} = 1 + \frac{\varepsilon_A}{\varepsilon_S} \kappa_A \ell \kappa_A d \quad (5.42)$$

$$A(\ell) \simeq \frac{\varepsilon_{\text{vac}}}{Q(\ell)} \frac{1}{\lambda_S} \quad (5.43)$$

$$B(\ell) = -\frac{\varepsilon_{\text{vac}}}{Q(\ell)} \frac{\bar{\phi}_A - \bar{\phi}_B}{\lambda_B} \quad (5.44)$$

$$F(\ell) \simeq \frac{\varepsilon_{\text{vac}}}{Q(\ell)} \left( \frac{\lambda_{\ell}}{\lambda_A^2} + \frac{1}{\lambda_B} \right), \quad (5.45)$$

which leads to Eq. (5.21) of the form

$$\begin{aligned} \eta_{\pm}(U) &\simeq \frac{1}{Q(\ell)} \left( \frac{\varepsilon_{\text{vac}}}{8\gamma_{12}\lambda_S}U^2 \mp \frac{\varepsilon_{\text{vac}}(\bar{\phi}_A - \bar{\phi}_B)}{2\gamma_{12}\lambda_B} \right. \\ &\quad \left. \times \left( \frac{1}{\lambda_S(\lambda_{\ell}/\lambda_A^2 + 1/\lambda_B)} + 1 \right) U \right) \\ &\simeq \frac{1}{Q(\ell)} \frac{\varepsilon_{\text{vac}}}{8\gamma_{12}\lambda_S}U^2, \quad \text{for } |U| \gg 4|\bar{\phi}_A - \bar{\phi}_B|. \end{aligned} \quad (5.46)$$

Within the electrocapillarity approach one again expects, as in the previous Sec. 5.2.3, an electrowetting number  $\eta_{ec}(U) = \varepsilon_{vac}U^2/(8\gamma_{12}\lambda_S)$  (see Eqs. (5.30) and (5.31)). However, the electrowetting number  $\eta_{\pm}(U)$  within the present density functional approach in Eq. (5.46), for sufficiently large voltage  $|U| \gg 4|\bar{\phi}_A - \bar{\phi}_B|$ , is actually smaller than  $\eta_{ec}(U)$  by a factor  $1/Q(\ell)$ :  $\eta_{\pm}(U) \simeq \eta_{ec}(U)/Q(\ell)$ .

It is apparent from Eq. (5.42) that  $Q(\ell)$  is *not* necessarily close to unity, because the typically small value  $\kappa_A\ell \ll 1$  is multiplied with the typically large value  $\kappa_Ad\varepsilon_A/\varepsilon_S \gg 1$ . Assuming typical values of, e.g., dielectric layers of thicknesses  $d = 1 \mu\text{m}$  and dielectric constant  $\varepsilon_S = 2$ , a Debye length  $1/\kappa_A = 10 \text{ nm}$  in the aqueous ( $\varepsilon_A = 80$ ) electrolyte solution  $F_1 = A$ , and thicknesses  $\ell = 1 \text{ nm}$  of the electrolyte films on the substrates, Eq. (5.42) leads to  $Q(\ell) \approx 400$ . Hence, for this example of electrowetting on a hydrophilic dielectric, the analysis leads to electrowetting numbers  $\eta_{\pm}(U)$  which are more than two orders of magnitude smaller than expected within the electrocapillarity approach:  $\eta_{\pm}(U) \approx 0.0025\eta_{ec}(U) \ll \eta_{ec}(U)$ .

It appears as if no experimental studies of electrowetting on hydrophilic substrates have been reported so far. This is remarkable since the preparation of hydrophilic substrates is standard in surface science.

### 5.2.5 Electrowetting of immiscible electrolyte solutions on dielectrics

Whereas the previous two Secs. 5.2.3 and 5.2.4 considered an electrolyte solution and an oil, here the case of two immiscible electrolyte solutions is discussed. This situation is characterized by  $\lambda_{\ell} \ll \lambda_A, \lambda_B \ll \lambda_S$ , which leads to Eqs. (5.22)–(5.25) of the form

$$Q(\ell) \simeq \frac{\lambda_S}{\lambda_A} \left( \frac{\lambda_A}{\lambda_B} + \frac{\lambda_{\ell}}{\lambda_A} \right) = \frac{\varepsilon_B}{\varepsilon_S} \kappa_B d + \frac{\varepsilon_A}{\varepsilon_S} \kappa_A \ell \kappa_A d \quad (5.47)$$

$$A(\ell) \simeq \frac{\varepsilon_{vac}}{Q(\ell)} \frac{\lambda_B - \lambda_A}{\lambda_S \lambda_B} \quad (5.48)$$

$$B(\ell) = -\frac{\varepsilon_{vac}}{Q(\ell)} \frac{\bar{\phi}_A - \bar{\phi}_B}{\lambda_B} \quad (5.49)$$

$$F(\ell) \simeq \frac{\varepsilon_{vac}}{Q(\ell)} \left( \frac{\lambda_{\ell}}{\lambda_A^2} + \frac{1}{\lambda_B} \right). \quad (5.50)$$

If electrolyte solutions  $F_1$  and  $F_2$  are defined by  $\lambda_{F_1} \leq \lambda_{F_2}$ , i.e.,  $\varepsilon_{F_1}I_{F_1} \geq \varepsilon_{F_2}I_{F_2}$ , the following three cases have to be distinguished: (i)  $A = F_1$  (i.e.,  $p = +1$ ) and  $B = F_2$  with  $\lambda_A \ll \lambda_B$ , (ii)  $A = F_2$  (i.e.,  $p = -1$ ) and  $B = F_1$  with  $\lambda_A \gg \lambda_B$ , and (iii)  $\lambda_A \approx \lambda_B$ .

Case (i) leads to the electrowetting number Eq. (5.21)

$$\begin{aligned}\eta_{\pm}(U) &\simeq \frac{1}{Q(\ell)} \left( \frac{\varepsilon_{\text{vac}}}{8\gamma_{12}\lambda_S} U^2 \mp \frac{\varepsilon_{\text{vac}}(\bar{\phi}_A - \bar{\phi}_B)}{2\gamma_{12}\lambda_B} U \right) \\ &\simeq \frac{1}{Q(\ell)} \frac{\varepsilon_{\text{vac}}}{8\gamma_{12}\lambda_S} U^2, \quad \text{for } |U| \gg 4 \frac{\lambda_S}{\lambda_B} |\bar{\phi}_A - \bar{\phi}_B|.\end{aligned}\tag{5.51}$$

Hence  $\eta_{\pm}(U) \simeq \eta_{ec}/Q(\ell)$ , where, however, the depression factor  $1/Q(\ell)$  here is typically much smaller than that of the previous Sec. 5.2.4 because typically  $\varepsilon_B \kappa_B d / \varepsilon_S \gg 1$  (see Eqs. (5.42) and (5.47)).

The electrowetting number of case (ii) is given by

$$\begin{aligned}\eta_{\pm}(U) &\simeq \frac{\lambda_A}{\lambda_S} \left( \frac{\varepsilon_{\text{vac}}}{8\gamma_{12}\lambda_S} U^2 \pm \frac{\varepsilon_{\text{vac}}(\bar{\phi}_A - \bar{\phi}_B)}{2\gamma_{12}\lambda_A} U \right) \\ &\simeq \frac{\lambda_A}{\lambda_S} \frac{\varepsilon_{\text{vac}}}{8\gamma_{12}\lambda_S} U^2, \quad \text{for } |U| \gg 4 \frac{\lambda_S}{\lambda_A} |\bar{\phi}_A - \bar{\phi}_B|.\end{aligned}\tag{5.52}$$

This expression bears some resemblance to Eq. (5.41) except of the typically very small prefactor  $\lambda_A/\lambda_S \ll 1$  here.

Therefore, electrowetting is also expected to be strongly suppressed for two immiscible electrolyte solutions with  $\varepsilon_{F_1} I_{F_1} \not\approx \varepsilon_{F_2} I_{F_2}$ , a condition which is typically fulfilled.

For completeness the rather special case (iii) is mentioned, for which the electrowetting number reads

$$\eta_{\pm}(U) \simeq \mp \frac{p\varepsilon_{\text{vac}}(\bar{\phi}_A - \bar{\phi}_B)}{2\gamma_{12}\lambda_S} U.\tag{5.53}$$





## Chapter 6

# Three phase contact line and line tension of an electrolyte solution in contact with a charged substrate

In this chapter, the equilibrium density distribution of an electrolyte solution near the three-phase contact line (TPCL) is calculated within classic density functional theory for the lattice model presented in Sec. 3.1. As discussed in Chaps. 3 and 4, if the substrate potential depends only on the direction perpendicular to the wall  $z$ , the equilibrium density profiles do not depend on the lateral coordinate, say  $x$ . However, this translational invariance in the lateral direction can be broken by imposing appropriate boundary conditions. In order to do so, the thermodynamic state of the system has to be chosen at two-phase coexistence and below the wetting transition temperature  $T < T_w$ . In this case, depending on the boundary conditions in the bulk, i.e., at  $z \rightarrow \infty$ , two different equilibrium density distributions are possible. If the boundary condition imposes the liquid phase in the bulk, i.e.  $\tilde{\varrho}_i(z \rightarrow \infty) = \tilde{\varrho}_{i,l}$ , a substrate-liquid interface is formed. On the other hand, if the boundary condition imposes the gas phase in the bulk, i.e.  $\tilde{\varrho}_i(z \rightarrow \infty) = \tilde{\varrho}_{i,g}$ , a substrate-gas interface, which can be decomposed into substrate-liquid and liquid-gas interfaces separated by a liquid-like layer of thickness  $\tilde{\ell}_0(T)$ , is formed (see Sec. 2.2 and Chaps. 3 and 4). Imposing these two different boundary conditions at  $x = \pm\infty$  for  $z \rightarrow \infty$ , i.e.  $\tilde{\varrho}_i(x \rightarrow \infty, z \rightarrow \infty) = \tilde{\varrho}_{i,l}$  and  $\tilde{\varrho}_i(x \rightarrow -\infty, z \rightarrow \infty) = \tilde{\varrho}_{i,g}$ , leads to an equilibrium density distribution  $\tilde{\varrho}_i(x, y)$  which interpolates smoothly between a substrate-gas interface at  $x \rightarrow -\infty$  and a substrate-liquid interface at  $x \rightarrow \infty$ . A particular definition of the local position of the liquid-gas interface renders a curve  $z = \tilde{\ell}(x)$  (see Eq. (6.7)) such that  $\tilde{\ell}(x \rightarrow -\infty) = \tilde{\ell}_0(T)$  and that  $\tilde{\ell}(x \rightarrow \infty) = \tilde{\ell}_0(T) + x \tan \vartheta$ , where  $\vartheta$  is the contact angle given by Young's equation (Eq. 2.20) (see Fig. 6.1). This arrangement

leads to the formation of a TPCL where the liquid-gas, substrate-gas and substrate-liquid interfaces meet.

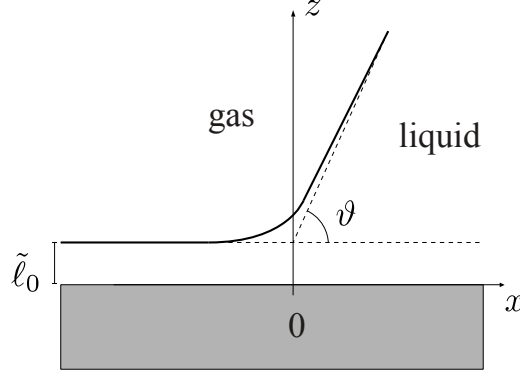


Figure 6.1: Typical shape of the liquid-gas interface  $z = \tilde{\ell}(x)$  (full line) near the three-phase contact line (TPCL) on a homogeneous planar surface.  $\tilde{\ell}_0$  is the equilibrium thickness of the microscopic liquid-like film for  $T < T_w$  and at two-phase coexistence. The dashed lines represent the asymptotes of  $z = \tilde{\ell}(x)$  for  $x \rightarrow \infty$  and  $x \rightarrow -\infty$ . The position  $x = 0$  is defined as the point at which the asymptotes intersect. The asymptote  $z = \tilde{\ell}(x \rightarrow \infty)$  intersects the substrate with the contact angle  $\vartheta$ . The density distribution is assumed to be translationally invariant in the  $y$  direction.

## 6.1 Density functional

The density functional in Eq. (3.4) can be written for the special case  $\varrho_i(\mathbf{r}) = \varrho_i(\bar{x}, \bar{z})$  considered in this chapter, i.e.,

$$\begin{aligned}
\frac{\beta\Omega[\{\varrho_i(\bar{x}, \bar{z})\}]}{\bar{L}} &= \sum_{\bar{x}=-\bar{L}_x/2}^{\bar{L}_x/2} \sum_{\bar{z}=1}^{\bar{L}_z} \left\{ \sum_i \varrho_i(\bar{z}) \ln \varrho_i(\bar{x}, \bar{z}) + \left(1 - \sum_i \varrho_i(\bar{x}, \bar{z})\right) \ln \left(1 - \sum_j \varrho_j(\bar{x}, \bar{z})\right) \right. \\
&\quad - \beta u \sum_{ij} \varrho_i(\bar{x}, \bar{z}) (\varrho_j(\bar{x} + 1, \bar{z}) + \varrho_j(\bar{x}, \bar{z} + 1) + \varrho_j(\bar{x}, \bar{z})) \\
&\quad \left. - \beta u_w \sum_i \varrho_i(\bar{x}, \bar{z}) \delta_{\bar{z},1} - \beta \sum_i \mu_i \varrho_i(\bar{x}, \bar{z}) \right\} \\
&\quad + 2\pi l_B \int_{-\bar{L}_x/2}^{\bar{L}_x/2} \int_{1/2}^{\bar{L}_z+1/2} d\bar{x}^* d\bar{z}^* \frac{(\mathbf{D}(\bar{x}^*, \bar{z}^*, [\varrho_{\pm}^*]))^2}{\varepsilon(\varrho_0^*(\bar{x}, \bar{z}))},
\end{aligned} \tag{6.1}$$

where  $\bar{L} = L/a$  is the contact line length and the fluid volume is  $V = L_x L_z L$ ;  $i, j = 0, +, -$ ; and  $\bar{x} = x/a$  and  $\bar{z} = z/a$  are dimensionless lattice coordinates (see Sec. 3.1 for the details of the model and Sec. 3.2 for details on the density functional).

Gauß's Law (Eq. 3.8) can be written as

$$\nabla \cdot \mathbf{D}(\bar{x}^*, \bar{z}^*, [\varrho_{\pm}^*]) = \sum_i q_i \varrho_i^*(\bar{x}^*, \bar{z}^*). \quad (6.2)$$

with the boundary conditions

$$\begin{aligned} D_z(\bar{x}^*, \bar{z}^*, [\varrho_{\pm}^*])|_{\bar{z}^*=1/2} &= \sigma, \\ D_z(\bar{x}^*, \bar{z}^*, [\varrho_{\pm}^*])|_{\bar{z}^*=\bar{L}_z+1/2} &= 0, \\ D_x(\bar{x}^*, \bar{z}^*, [\varrho_{\pm}^*])|_{\bar{x}^*=-\bar{L}_x/2} &= 0, \\ D_x(\bar{x}^*, \bar{z}^*, [\varrho_{\pm}^*])|_{\bar{x}^*=\bar{L}_x/2} &= 0, \end{aligned} \quad (6.3)$$

which follow from the overall charge neutrality (see Eqs. (3.13) and (3.14)).

The relative permittivity (see Eq. (3.15)) is given by

$$\varepsilon(\varrho_0^*(\bar{x}^*, \bar{z}^*)) = \frac{1 + \frac{2\alpha}{3\varepsilon_0} \varrho_0(\bar{x}^*, \bar{z}^*)}{1 - \frac{\alpha}{3\varepsilon_0} \varrho_0^*(\bar{x}^*, \bar{z}^*)}, \quad (6.4)$$

The Euler-Lagrange equations which follow from the minimization of Eq. (6.1) are given by (the derivation of this equations is analogous to the one presented in Sec. 3.2)

$$\begin{aligned} \ln \varrho_i(\bar{x}, \bar{z}) - \mu_i^* - \beta u_w \delta_{\bar{z},1} - \ln \left( 1 - \sum_j \varrho_j(\bar{x}, \bar{z}) \right) \\ - \frac{1}{3T^*} \sum_j (2\varrho_j(\bar{x}, \bar{z}) + \varrho_j(\bar{x}+1, \bar{z}) + \varrho_j(\bar{x}-1, \bar{z}) + \varrho_j(\bar{x}, \bar{z}+1) + \varrho_j(\bar{x}, \bar{z}-1)) \\ + q_i \int_{\bar{z}-1/2}^{\bar{z}+1/2} d\bar{z}^* \phi(\bar{x}^*, \bar{z}^*) - 2\pi l_B \int_{\bar{z}-1/2}^{\bar{z}+1/2} d\bar{z}^* \frac{(\mathbf{D}(\bar{x}^*, \bar{z}^*, [\varrho_{\pm}^*]))^2}{(\varepsilon(\varrho_0^*(\bar{x}^*, \bar{z}^*)))^2} \varepsilon'(\varrho_0^*(\bar{x}^*, \bar{z}^*)) \delta_{i,0} = 0. \end{aligned} \quad (6.5)$$

For given chemical potential at coexistence  $\mu_{i,co}$  (see Sec. 3.3), these coupled equations are solved numerically by an iterative algorithm. The electrostatic potential  $\phi(\bar{x}^*, \bar{z}^*)$  is calculated by solving Poisson's Equation (see Eq. 3.21)

$$\nabla \cdot (\varepsilon(\varrho_0^*(\bar{x}^*, \bar{z}^*)) \nabla \phi(\bar{x}^*, \bar{z}^*)) = -4\pi l_B \sum_i q_i \varrho_i^*(\bar{x}^*, \bar{z}^*). \quad (6.6)$$

The parameters for this calculation are the same used in Chap. 3 (see Subsec. 3.2.2).

## 6.2 Line tension calculation

Line tension values are calculated from the density profiles  $\{\varrho_i(\bar{x}, \bar{z})\}$  using the definition for the line tension introduced in Eq. (2.22) (see also Eq. (F.4)). The plane  $\bar{z} = 0$  is chosen as the substrate-fluid dividing interface. In Ref. [149] it has been proposed that in order to determine the line tension  $\tau$  unambiguously from microscopic calculations in a finite box, its boundaries have to be chosen such that the interfaces are cut perpendicularly and that its edges are placed inside the homogeneous regions of the system. Here in order to calculate the line tension, the integration box proposed in Ref. [149] was used (see Fig. 7 in Ref. [149] and Fig. F.1). However, in a lattice model this type of box introduces practical difficulties in the integration procedure which lead to numerical errors (see Appendix F for more details). Therefore, in order to verify the consistency of the results, the line tension has been calculated for various sizes of the integration box as described in Appendix F.

## 6.3 Pure solvent

First, the case  $I = 0$  is considered. As explained in Subsec. 3.4.1, in this case the ratio  $u_w/u = 3T^*\beta u_w$  controls the wetting and drying transitions. Here the liquid-gas interfaces near the TPCL and the line tension are studied for the particular choice  $u_w/u = 0.69$ , for which the system undergoes a second-order wetting transition (see Fig. 3.2) at  $T_w^* \simeq 0.95T_c^*$ . Fig. 6.2 shows the temperature dependence of the liquid-gas interface  $\ell(\bar{x})$  defined as

$$\ell(\bar{x}) = \frac{\sum_{\bar{z}=1}^{\bar{L}_z} (\varrho_0(\bar{x}, \bar{z}) - \varrho_{0,g})}{\varrho_{0,l} - \varrho_{0,g}}. \quad (6.7)$$

In the case of second-order wetting transitions, the curve  $\bar{z} = \ell(\bar{x})$  approaches the asymptotes for  $\bar{x} \rightarrow \infty$  and  $\bar{x} \rightarrow -\infty$  from above (Fig. 6.2). This result is in qualitative agreement with the results obtained for second order wetting in Refs. [150, 175, 224, 225].

The line tension as a function of the contact angle is presented in Fig. 6.3. The contact angle has been changed by varying the temperature  $T^*$ . The results for the line tension are compatible with the prediction of the interface displacement model (IDM) [150] for a system with short-ranged interactions approaching a second-order wetting transition at two-phase coexistence. In this case, the line tension  $\tau$  is negative and vanishes as  $\tau \sim -\vartheta$ . The order of magnitude of  $\tau$  ( $\beta\tau a = 0.1$  corresponds to  $\tau \approx 1.4 \times 10^{-12}$  N) is also comparable with values from other theoretical calculations for one-component fluids and with experimental results [145].

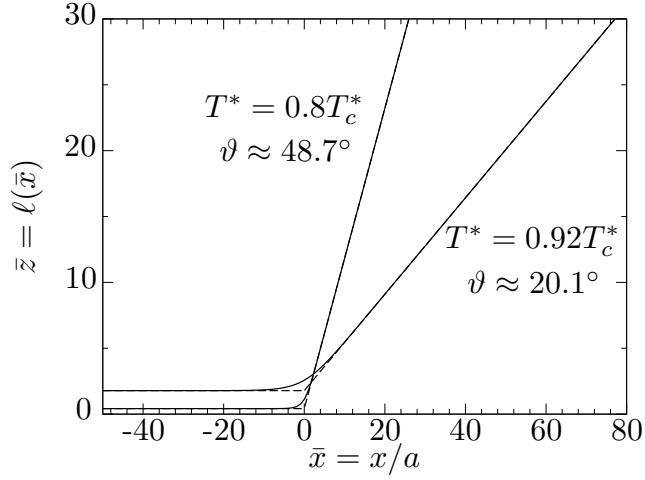


Figure 6.2: Liquid-gas interfaces for two different temperatures for  $u_w/u = 0.69$  in the pure solvent case. The system undergoes a second-order wetting transition at  $T_w^* \simeq 0.95T_c^*$  (see Fig. 3.2 (b)). The liquid-gas interface  $\bar{z} = \ell(\bar{x})$  (full lines) was calculated from the density profiles  $\rho_0(\bar{x}, \bar{z})$  using Eq. (6.7). For both  $\bar{x} \rightarrow \infty$  and  $\bar{x} \rightarrow -\infty$ , the curve  $\bar{z} = \ell(\bar{x})$  approaches the asymptotes (dashed lines) from above. The position  $\bar{x} = 0$  is defined as the point at which the asymptotes intersect.

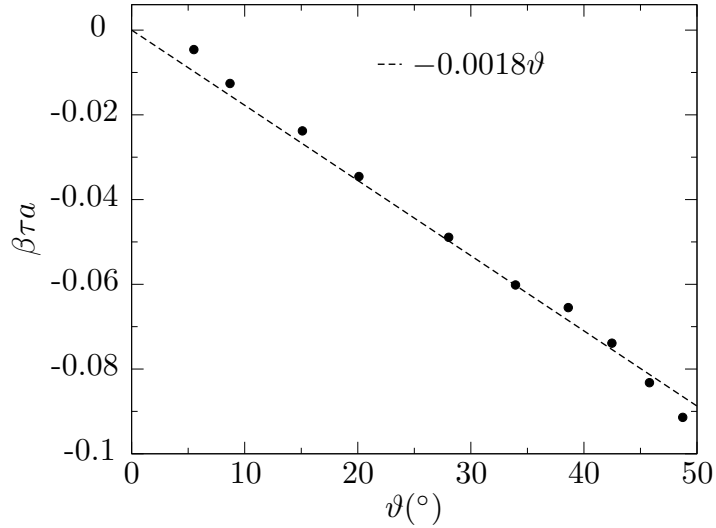


Figure 6.3: Contact angle dependence of the line tension  $\tau$  for the same system as in Fig. 4.1.1. The numerical results for the line tension ( $\bullet$ ) are consistent with the prediction of Ref. [150] for second-order wetting in systems with short-ranged interactions, i.e.,  $\tau$  is negative and it vanishes as  $\tau \sim -\vartheta$ . For details concerning the calculation of the line tension, see Appendix F.

## 6.4 Electrolyte solution

In this section the influence of the ionic strength  $\tilde{I} = Ia^{-3}$  and of the surface charge density  $\tilde{\sigma} = \sigma ea^{-2}$  on the TPCL and the line tension are studied. As discussed in Subsec. 3.4.2, within the lattice model for an electrolyte solution, if  $\sigma \neq 0$  and  $I \neq 0$  the system undergoes a first-order wetting transition (see Fig. 3.4). In this case, the wetting transition temperature  $T_w^*$  decreases with increasing surface charge density of the substrate  $\sigma$  for fixed ionic strength  $I$  or with decreasing ionic strength  $I$  for fixed surface charge density  $\sigma$  (see Fig. 3.5). Therefore, there are three different routes to achieve a change in the contact angle: (i) By changing the effective temperature  $T^*$  keeping the surface charge density  $\sigma$  and the ionic strength  $I$  fixed, (ii) by changing the surface charge density of the substrate  $\sigma$  keeping the temperature  $T^*$  and the ionic strength  $I$  fixed, and (iii) by changing the ionic strength  $I$  keeping the temperature  $T^*$  and surface charge density  $\sigma$  fixed. Here routes (i) and (ii) are employed for two values of the ionic strength  $I = 3.9 \times 10^{-5}$  ( $\tilde{I} = 1\text{mM}$ ) and  $I = 3.9 \times 10^{-4}$  ( $\tilde{I} = 10\text{mM}$ ) with  $u_w/u = 0.69$ .

Figure 6.4 shows the liquid-gas interface calculated using Eq. (6.7) for fixed temperature  $T^* = 0.8T_c^*$  and ionic strength  $I = 3.9 \times 10^{-5}$  ( $\tilde{I} = 1\text{mM}$ ) and for three different values of the surface charge density  $\sigma$ . When the wetting transition is first-order, the curve  $\bar{z} = \ell(\bar{x})$  approaches the asymptote from below for  $\bar{x} \rightarrow \infty$  and from above for  $\bar{x} \rightarrow -\infty$ . For large contact angles, i.e., for small values of  $\sigma$ ,  $\bar{z} = \ell(\bar{x})$  in Fig. 6.4 follows the asymptote closely. The deviation from the asymptotes increases for small contact angles. The behavior of the liquid-gas interface is similar for the case in which the contact angle is changed using route (i). These results for the interface profile are in agreement with those of Refs. [150, 175, 224, 225] for first-order wetting.

Figure 6.5 shows the line tension for the case in which the contact angle was changed using route (i) for two different values of the ionic strength and constant surface charge density  $\sigma = 1 \times 10^{-3}$  ( $\tilde{\sigma} = 0.1\mu\text{C}/\text{cm}^2$ ). The line tension is negative and increases with decreasing contact angle which is in agreement with the prediction from the IDM [150] for the case of first-order wetting transitions with short-range interactions. The line tension is smaller for the larger value of ionic strength  $I = 3.9 \times 10^{-4}$  ( $\tilde{I} = 10\text{mM}$ ) for fixed temperature. Smaller contact angles were not considered because they require bigger boxes and therefore higher computational cost. According to Ref. [150], the line tension in the case of first-order transitions should change its sign from negative to positive as  $\vartheta$  decreases and should be positive at the wetting transition temperature  $T_w^*$ , i.e., for  $\vartheta = 0$ . From the present calculations this prediction can not be confirmed, but one can see from the available data that such a change in sign is highly plausible. The asymptotic behavior for  $\vartheta \rightarrow 0$  predicted in Ref. [150] in this case is given by  $\tau \sim \tau_w + c_1\vartheta \ln \vartheta + c_2\vartheta + \mathcal{O}(\vartheta^2)$ .

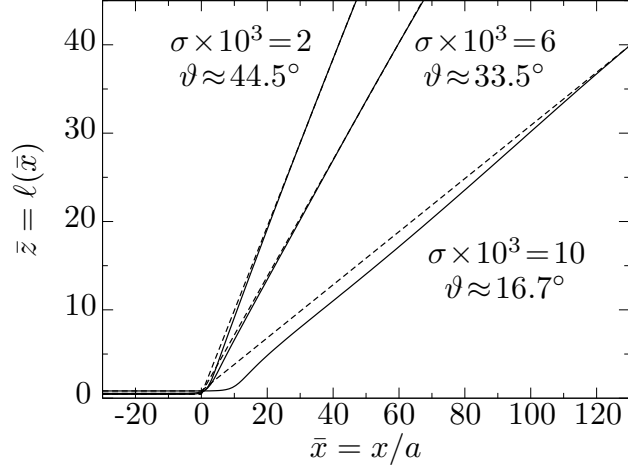


Figure 6.4: Liquid-gas interfaces for an electrolyte solution, which exhibits a first-order wetting transition (see Sec. 3.4.2) for various surface charge densities  $\tilde{\sigma} = \sigma e a^{-2}$ , fixed temperature  $T^* = 0.8T_c^*$ ,  $u_w/u = 0.69$  and  $I = 3.9 \times 10^{-5}$  ( $\tilde{I} = 1$  mM). Note that for the electrolyte solution the wetting temperature  $T_w$  is a function of the surface charge density (see Fig. 3.5).  $\ell(x)$  (full lines) was calculated from the density profiles  $\varrho_0(\bar{x}, \bar{z})$  using Eq. (6.7). For first-order wetting, the curves  $\bar{z} = \ell(\bar{x})$  approach the asymptotes (dashed lines) from above for  $\bar{x} \rightarrow -\infty$  and from below for  $\bar{x} \rightarrow \infty$ . The position  $\bar{x} = 0$  is defined as the point at which the asymptotes intersect.

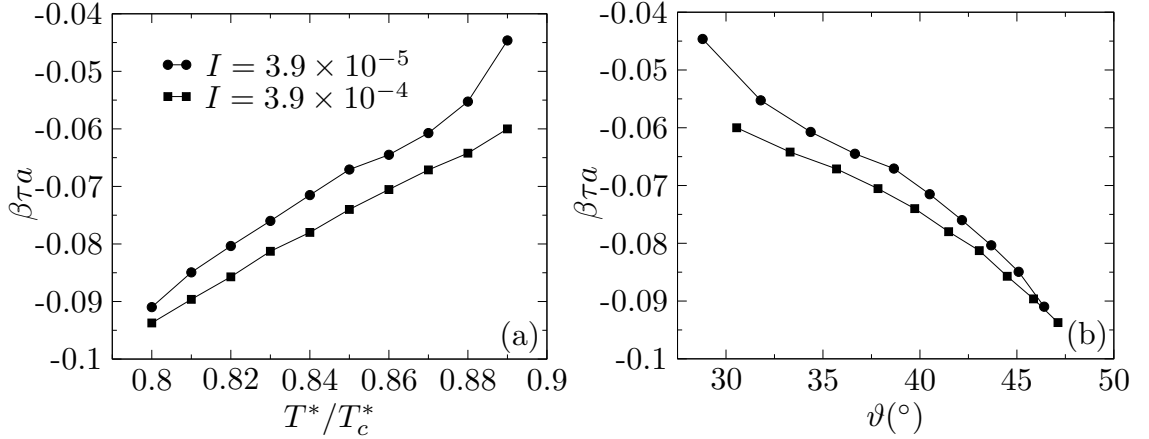


Figure 6.5: Line tension  $\tau$  as a function of the temperature  $T^*$  in (a) and of the contact angle  $\vartheta$  in (b) for  $\sigma = 1 \times 10^{-3}$  and  $u_w/u = 0.69$ . The two types of symbols correspond to distinct values of the ionic strength  $I = \tilde{I}a^3$  in the bulk liquid phase ( $\bullet$  for  $I = 3.9 \times 10^{-5}$  ( $\tilde{I} = 1$  mM) and  $\blacksquare$  for  $I = 3.9 \times 10^{-4}$  ( $\tilde{I} = 10$  mM)). See Appendix F for details of the line tension calculation.

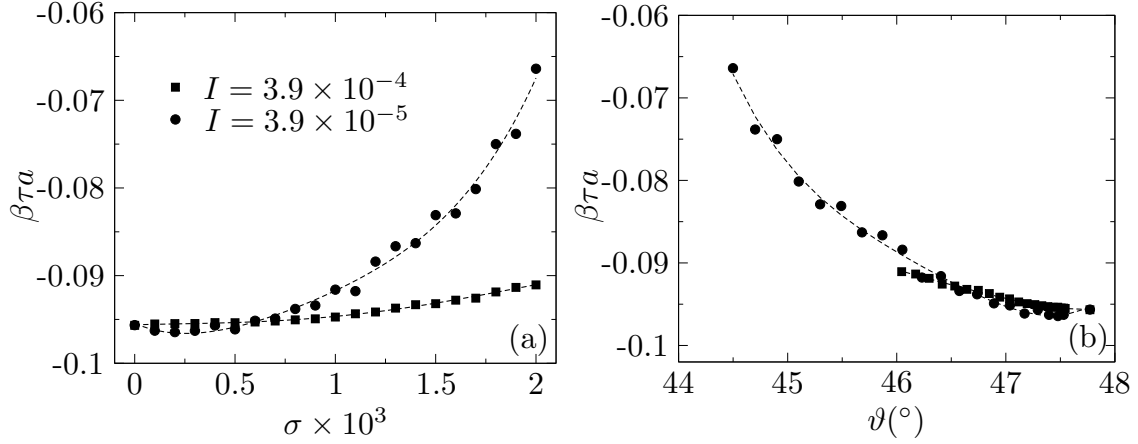


Figure 6.6: Line tension  $\tau$  as a function of the surface charge density  $\sigma = \tilde{\sigma}a^2/e$  in (a) and of the contact angle  $\vartheta$  in (b) for  $T^* = 0.8T_c^*$  and  $u_w/u = 0.69$ . The two types of symbols correspond to distinct values of the ionic strength  $I = \tilde{I}a^3$  in the bulk liquid phase ( $\bullet$  for  $I = 3.9 \times 10^{-5}$  ( $\tilde{I} = 1\text{mM}$ ) and  $\blacksquare$  for  $I = 3.9 \times 10^{-4}$  ( $\tilde{I} = 10\text{mM}$ )). The dashed lines are a guide to the eye. See Appendix F for details of the line tension calculation.

Figure 6.6 shows the line tension for the case in which the contact angle was changed using route (ii) for two values of the ionic strength and  $T^* = 0.8T_c^*$ . In this case, only small surface charge values ( $\sigma = 1 \times 10^{-4} - 2 \times 10^{-3}$ ) were considered. Therefore small contact angles which are obtained for large surface charges were not studied. The reason for this is that in order to avoid the contribution from the corners of the integration box, these corners should be placed far away from all the interfaces such that the density profiles in the regions where the corners are placed are bulk-like (see Appendix F and Sec. 6.2). To achieve the later for small contact angles is more difficult in the case of the electrolyte solution than in the pure solvent, mainly due to the density distributions of  $\pm$ -ions. Figure 6.7 (b) shows density maps for the solvent  $\varrho_0(\bar{x}, \bar{z})$  and the  $\pm$ -ions  $\varrho_{\pm}(\bar{x}, \bar{z})$  for  $\sigma = 8 \times 10^{-3}$  ( $\tilde{\sigma} = 0.8\mu\text{C}/\text{cm}^2$ ). The density in the liquid bulk is  $\varrho_{\pm} = I = 3.9 \times 10^{-5}$  ( $\tilde{I} = 1\text{mM}$ ). One can see that for the positive ions in the liquid phase the density profile looks bulk-like only in a very small portion of the calculation box, which makes difficult the use of the integration box in Fig. F.1 and the procedure described in Appendix F for the calculation of the line tension. Moreover one can see in Fig. F.2, which shows examples of the dependence of the value of the line tension for different box sizes and two different surface charge densities, that the amplitude of the variations in the value of the line tension increases when the surface charge density  $\sigma$  increases. Figure 6.6 (a) shows that for small surface charge densities the value of the line tension depends weakly on the ionic strength  $I$ . However, as the surface charge density increases, the line tension  $\tau$



increases faster for  $I = 3.9 \times 10^{-5}$  ( $\tilde{I} = 1\text{mM}$ ) than for  $I = 3.9 \times 10^{-4}$  ( $\tilde{I} = 10\text{mM}$ ). This is related to the fact that due to screening for  $I = 3.9 \times 10^{-4}$  ( $\tilde{I} = 10\text{mM}$ ) a larger value of the surface charge is needed to produce the same contact angle than for  $I = 3.9 \times 10^{-5}$  ( $\tilde{I} = 1\text{mM}$ ) (see Fig. 6.6 (b)).

#### 6.4.1 Density distributions close to the three phase contact line

The microscopic structure of the electrolyte solution close to the TPCL is illustrated as density maps in Fig. 6.7 for  $I = 3.9 \times 10^{-5}$  ( $\tilde{I} = 1\text{mM}$ ),  $T^* = 0.8T_c^*$  and two values of the surface charge density  $\sigma = 1 \times 10^{-4}$  ( $\tilde{\sigma} = 0.01\mu\text{C}/\text{cm}^2$ ) and  $\sigma = 8 \times 10^{-4}$  ( $\tilde{\sigma} = 0.8\mu\text{C}/\text{cm}^2$ ). The contact angles are  $\vartheta \approx 47.5^\circ$  for  $\sigma = 1 \times 10^{-4}$  and  $\vartheta \approx 28.3^\circ$  for  $\sigma = 8 \times 10^{-4}$ . Apart from the difference in contact angle and the density of anions and cations in the vicinity of the wall due to the difference in surface charge density  $\sigma$ , one can see that for larger values of the surface charge the density distributions of  $\pm$ -ions differ significantly from the bulk values for a larger distance with respect to the substrate position.

Figures 6.8 and 6.9 show the charge density  $\varrho_c(\bar{x}, \bar{z}) = \varrho_+(\bar{x}, \bar{z}) - \varrho_-(\bar{x}, \bar{z})$ , the local ionic strength  $I(\bar{x}, \bar{z}) = \frac{1}{2}(\varrho_+(\bar{x}, \bar{z}) + \varrho_-(\bar{x}, \bar{z}))$  and the electrostatic potential  $\phi(\bar{x}, \bar{z}) = \beta e \tilde{\phi}(\bar{x}, \bar{z})$  for the same parameters as in Fig. 6.7. For small surface charge density  $\sigma$  (see Fig. 6.8) the charge density  $\varrho_c(\bar{x}, \bar{z})$  has a region in the gas close to the liquid-gas interface where  $\varrho_c(\bar{x}, \bar{z})$  is less negative than  $\varrho_c(-\infty, \bar{z})$ . If one takes a path from the gas side at constant and small  $\bar{z}$ , the charge density  $\varrho_c(\bar{x}, \bar{z})$  is constant in the gas phase far away from the liquid-gas interface, increases upon approaching the liquid-gas interface from the gas side, drops to a very low value on the liquid side of the liquid-gas interface and ultimately increases towards a constant value in the liquid phase. This charge separation in the vicinity of the liquid-gas interface and the TPCL is caused by the difference in the local permittivity of the solvent  $\varepsilon(\varrho_0(\bar{x}, \bar{z}))$  which is higher in the liquid phase (see Eq. 6.4). On the other hand, the structure of the local ionic strength  $I(\bar{x}, \bar{z})$  profiles for constant  $\bar{z}$ , which interpolates from the value in the gas phase to the value in the liquid phase, is almost independent of  $\bar{z}$ . The electrostatic potential  $\phi(\bar{x}, \bar{z})$ , which is related to the charge density through Poisson's Eq. (6.6), does not follow the liquid-gas interface but bends away from it. Moreover, there is an electrostatic potential difference between the liquid and the gas phases in the vicinity of the TPCL. For large surface charge density  $\sigma$  (see Fig. 6.9), the high concentration of charge in the vicinity of the substrate in the gas phase screens in few layers the surface charge of the substrate. This is in contrast to the case of small surface charge for which the charge density  $\varrho_c(\bar{x}, \bar{z})$  decays more slowly to zero (see Fig. 6.8). This difference is due to the nonlinear character of Poisson's equation used in this work (see Eq. (6.6)); for small values of the surface charge density  $\sigma$  its

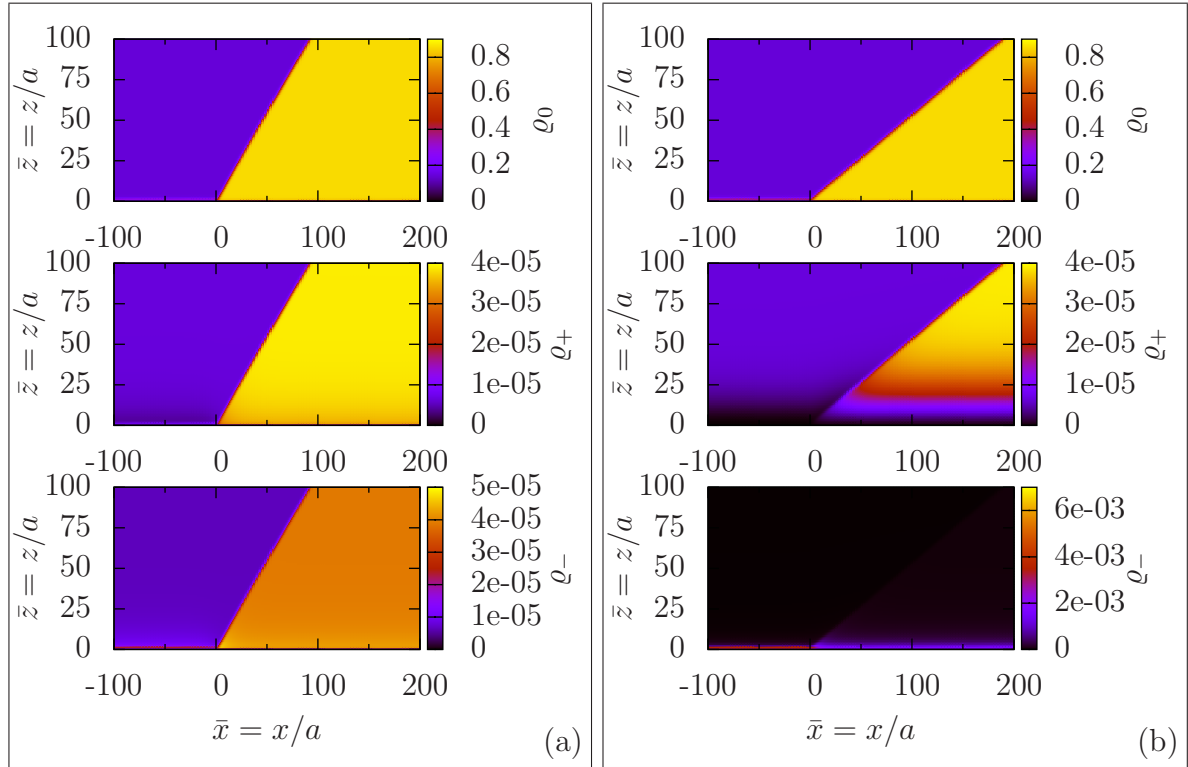


Figure 6.7: Density distributions of the solvent  $\rho_0(\bar{x}, \bar{z})$ , the cations  $\rho_+(\bar{x}, \bar{z})$  and the anions  $\rho_-(\bar{x}, \bar{z})$  for  $\sigma = 1 \times 10^{-4}$  ( $\tilde{\sigma} = 0.01 \mu\text{C}/\text{cm}^2$ ) in (a) and  $\sigma = 8 \times 10^{-3}$  ( $\tilde{\sigma} = 0.8 \mu\text{C}/\text{cm}^2$ ) in (b). The contact angle in (a) is  $\vartheta \approx 47.5^\circ$  and in (b)  $\vartheta \approx 28.3$ . The substrate is positively charged, therefore the high (low) density of negative (positive) ions in its vicinity. Note that the density distribution of the positive ions  $\rho_+$  in the liquid for  $\sigma = 8 \times 10^{-3}$  ( $\tilde{\sigma} = 0.2 \mu\text{C}/\text{cm}^2$ ) (see (b)) needs more layers to achieve its bulk value  $I = 3.9 \times 10^{-5}$  ( $\tilde{I} = 1\text{mM}$ ) than it needs for  $\sigma = 1 \times 10^{-4}$  ( $\tilde{\sigma} = 0.01 \mu\text{C}/\text{cm}^2$ ).

solution is close to the solution of the linearized equation in which the number densities of  $\pm$ -ions decay exponentially to its bulk values with the Debye length  $\kappa$  of the bulk phase. In contrast, for large surface charge density  $\sigma$  both the density distributions of  $\pm$ -ions and the electrostatic potential  $\phi$  deviate significantly from the linear solution in the vicinity of the substrate and the exponential decay is only valid far away from it. The nonmonotonic variation of  $\rho_c(\bar{x}, \bar{z})$  in the vicinity of the liquid-gas interface from the gas side is not observed for this value of  $\sigma$ , however, there is a decrease in the vicinity of the liquid-gas interface from the liquid side. This qualitative difference in the charge density in the vicinity of the TPCL results in a different behavior of the electrostatic potential. In this case, the liquid-gas interface is visible for small  $\bar{z}$  and the difference of the values of the electrostatic potential in the liquid and in the gas phases is not as pronounced as for smaller surface charge densities (see Fig. 6.8). For both cases far away from the substrate

the charge density  $\varrho_c(\bar{x}, \bar{z})$  and the electrostatic potential  $\phi(\bar{x}, \bar{z})$  go to zero and the local ionic strength goes to  $I = 3.9 \times 10^{-5}$ , i.e., their bulk values.

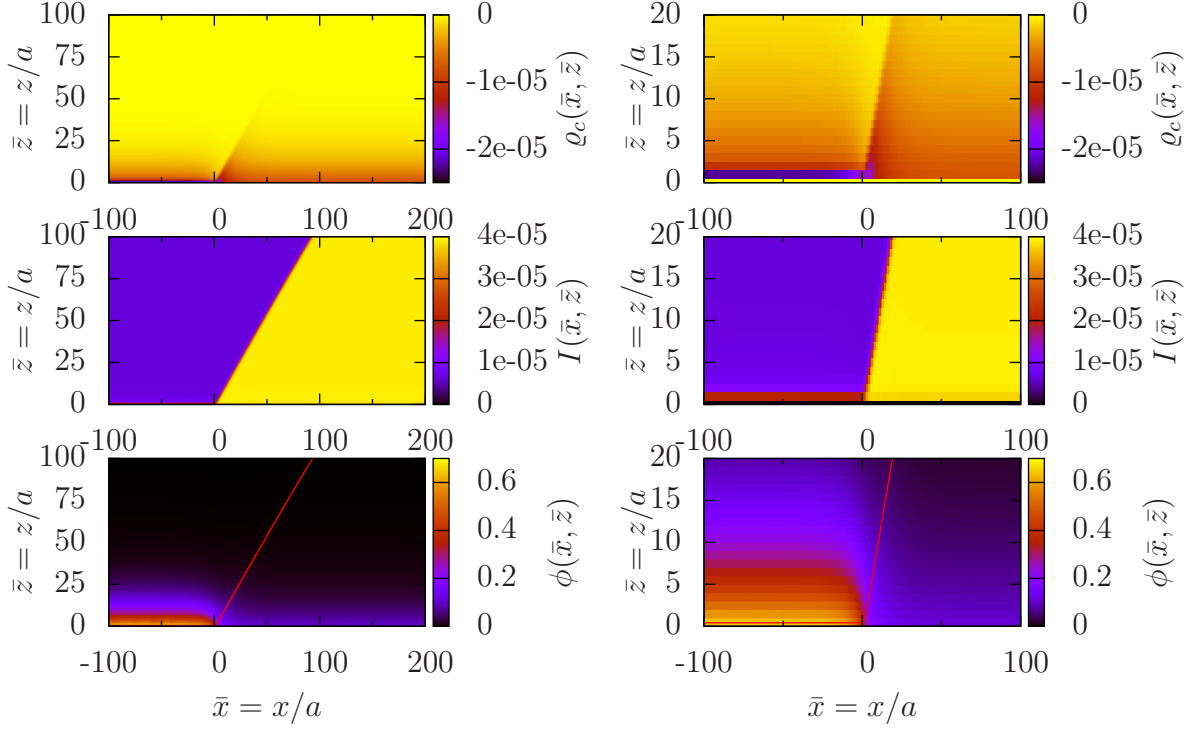


Figure 6.8: Charge density  $\varrho_c(\bar{x}, \bar{z}) = \varrho_+(\bar{x}, \bar{z}) - \varrho_-(\bar{x}, \bar{z})$ , local ionic strength  $I(\bar{x}, \bar{z}) = \frac{1}{2} (\varrho_+(\bar{x}, \bar{z}) + \varrho_-(\bar{x}, \bar{z}))$  and electrostatic potential  $\phi(\bar{x}, \bar{z}) = \beta e \tilde{\phi}(\bar{x}, \bar{z})$  for  $\sigma = 1 \times 10^{-4}$  ( $\tilde{\sigma} = 0.01 \mu\text{C}/\text{cm}^2$ ). The contact angle is  $\vartheta \approx 47.5^\circ$ . The red line in the plot for the electrostatic potential shows the position of the liquid-gas interface profile  $\ell(\bar{x})$  calculated using Eq. (6.7). The plots on the right show close-ups of the plots on the left in the vicinity of the TPCL.

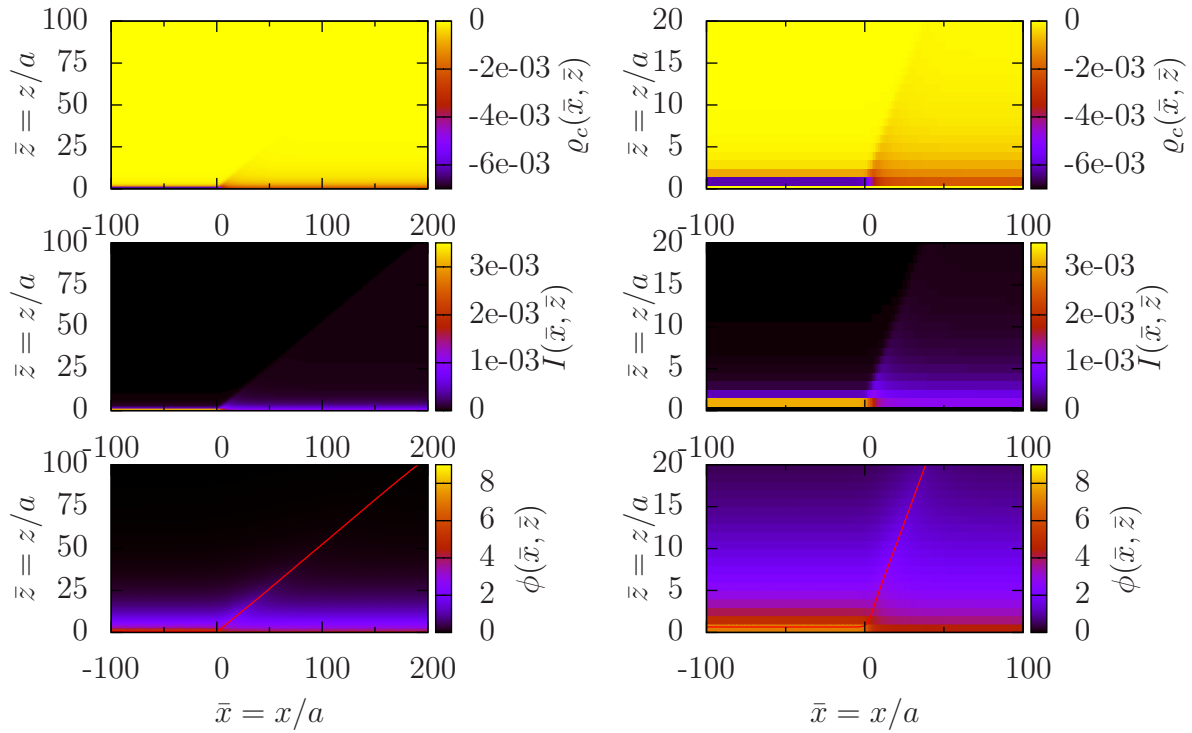


Figure 6.9: Charge density  $\rho_c(\bar{x}, \bar{z}) = \rho_+(\bar{x}, \bar{z}) - \rho_-(\bar{x}, \bar{z})$ , local ionic strength  $I(\bar{x}, \bar{z}) = \frac{1}{2}(\rho_+(\bar{x}, \bar{z}) + \rho_-(\bar{x}, \bar{z}))$  and electrostatic potential  $\phi(\bar{x}, \bar{z}) = \beta e \tilde{\phi}(\bar{x}, \bar{z})$  for  $\sigma = 8 \times 10^{-3}$  ( $\tilde{\sigma} = 0.8 \mu\text{C}/\text{cm}^2$ ). The contact angle is  $\vartheta \approx 28.3^\circ$ . The red line in the plot for the electrostatic potential shows the position of the liquid-gas interface profile  $\ell(\bar{x})$  calculated using Eq. (6.7). The plots on the right show close-ups of the plots on the left in the vicinity of the TPCL.

# Chapter 7

## Conclusions and outlook

The purpose of this thesis has been to investigate wetting phenomena in electrolyte solutions by means of classical density functional theory. To this end, the wetting behavior of a lattice (see Chap. 3) and a continuum (see Chap. 4) model for an electrolyte solution in contact with a charged substrate has been investigated. As a second issue, the phenomenon of electrowetting for a vertical parallel plate capacitor in contact with two immiscible fluids, where at least one of the two is an electrolyte solution, has been analyzed in Chap. 5. Lastly, the influence of the substrate surface charge and of the ionic strength on the fluid structure in the vicinity of the three phase contact line (TPCL) and on the line tension of the lattice model for an electrolyte solution has been investigated (see Chap. 6). Within these density functional theory approaches both bulk and inhomogeneous fluids were studied within the same framework. This is important because an investigation of wetting requires an accurate knowledge of the bulk properties because they are used as boundary conditions for the inhomogeneous calculations. Moreover, the calculations for the inhomogeneous systems, i.e., substrate-fluid and liquid-gas interfaces, were used as boundary conditions in the calculations of the TPCL structure.

In Chap. 3, a lattice-gas model for an electrolyte in contact with a charged substrate was studied. The pure, i.e., salt-free, solvent was first investigated, providing a reference system relative to which the influence of the electrostatic interaction could be compared. The results for the salt-free case were in good agreement with previous studies [190, 191]. The effective interface potential  $\omega(l)$ , which facilitates the transparent identification of the order of the wetting transition, has been calculated numerically. In the next step, the effects of the ionic strength and of the surface charge density  $\sigma$  on the order and on the transition temperature of the wetting transition have been analyzed quantitatively. Concerning the order of the transition it was found that electrostatic forces induce a first-order wetting transition, even for very small surface charges. Within the lattice model,

for  $\sigma = 0$  the transition is second order and occurs at the same temperature as in the salt-free case. For  $\sigma \neq 0$  the wetting transition temperature decreases as the surface charge is increased for fixed ionic strength.

In Chap. 4, an improvement over the approximation of step-like varying density profiles has been implemented in order to derive analytic expressions for the effective interface potential  $\omega(\ell)$  of electrolyte solutions near charged walls. The analysis of the analytical expressions for the effective interface potential revealed that, in the case of short-ranged solvent-solvent and solvent-wall interactions, wetting transitions in the presence of electrostatic interactions are typically first order. This result could be explained in terms of the competition between the two characteristic length scales in the system, i.e., the bulk correlation length  $\xi$  in the wetting liquid phase and the Debye length  $1/\kappa$ . If  $1/\kappa > 2\xi$ , which is typically the case for dilute electrolyte solutions away from (bulk) critical points, a wetting transition at two-phase coexistence is always first order irrespective of its order in the pure, i.e., salt-free, solvent. The same result has been obtained in Chap. 3. However, the analysis of the analytical expressions for the effective interface potential provided a transparent rationale for the pre-eminence of first-order wetting in electrolyte solutions in terms of competing length scales. Moreover, if in those systems in addition long-ranged solvent-solvent and solvent-wall interactions, which favor a critical wetting transition, are present, our analysis reveals the possibility of a wetting scenario which actually corresponds to a sequence of two wetting transitions: first an electrostatically induced (i.e.,  $1/\kappa > 2\xi$ ) discontinuous jump between two finite wetting film thicknesses which upon raising the temperature is followed by a continuous divergence of the wetting film thickness  $\ell$ .

The effect of ions and the surface charge on pure solvents which exhibit first-order wetting transitions was not considered in Chaps. 3 and 4. This is an open and important question because first-order wetting transitions are more common in real systems than second-order ones. This question can be addressed within the lattice model by including for example the effect of long-ranged fluid-fluid and substrate-fluid interactions. On the other hand, within the continuum model this question has to be addressed numerically due to the fact that the analytical expressions for the effective interface potential derived in Chap. 4 are valid only for thick wetting films and the behavior of the effective interface potential for thin films, which is important for first-order wetting transitions, is missing.

In Chap. 5, the electrowetting equation was derived for Pellat's setup of a vertical parallel plate capacitor. The analysis of this equation led to effectively four length scales corresponding to the Debye lengths in both fluids, the thickness of the substrate, and the film thickness, which serve to classify various relevant experimental situations,

e.g., uncoated metal electrodes, hydrophilic or hydrophobic dielectric substrates, or fluids comprising water+oil systems or immiscible electrolyte solutions. By considering limiting cases of general interest it has been found that for uncoated metal electrodes and wetting of hydrophobic dielectric substrates by water in an oil environment, the electrowetting number, i.e., the term in the electrowetting equation which carries the dependence on the applied voltage, within the present density functional approach agrees with that within the electrocapillarity picture as well as with numerous experimental studies. However, a significantly reduced tendency of electrowetting has been predicted here as compared to the predictions within the electrocapillarity approach for electrowetting on hydrophilic dielectric substrates or situations with both fluids being immiscible electrolyte solutions. Due to a lack of experimental data, verification of these predictions is an open issue.

Finally, in Chap. 6 the TPCL and the line tension for the electrolyte solution have been studied for the lattice model in Chap. 3. The behavior for the line tension was found to agree with the predicted behavior for systems with short-ranged interactions. However, the lattice model was found not to be the most appropriate model for the calculation of the line tension due to numerical errors and due to the dependence of the liquid-gas surface tension and of the line tension on the underlying lattice structure. Therefore, the study in Chap. 6 is regarded as a first-step in the microscopic calculation of line tensions in electrolyte solutions which has to be compared with results for other models. Unfortunately, however, such results are not yet available. Moreover, important questions such as the behavior of the line tension upon approaching the wetting transition and the effect of large surface charge density of the substrate on the line tension could not be addressed within the present theory; they deserve to be studied in the future by using for instance a continuum model. Nevertheless, within the lattice model it was possible to calculate the structure of the fluid in the vicinity of the contact line and analyze the effect of the surface charge density of the substrate on the charge density distribution within the fluid and on the electrostatic potential.





# Appendix A

## Bulk correlation length of the pure solvent

In the case of a bulk pure solvent ( $I = 0$ ), the density functional  $\Omega_0$  given by Eq. (3.10) reduces to

$$\beta\Omega_0^{(p)}[\varrho_0(\mathbf{r})] = \int d^3r \left\{ \varrho_0(\mathbf{r})(\ln(\varrho_0(\mathbf{r})) - \beta\mu_{\varrho_0}) + (1 - \varrho_0(\mathbf{r})) \ln(1 - \varrho_0(\mathbf{r})) + \chi(T)\varrho_0(\mathbf{r})(1 - \varrho_0(\mathbf{r})) + \frac{\chi(T)}{6} (\nabla\varrho_0(\mathbf{r}))^2 \right\}. \quad (\text{A.1})$$

If one considers a spatially uniform equilibrium state  $\varrho_0$ , the corresponding two-point correlation function  $G(r) = \varrho_0^2 h(r) = \varrho_0^2(g(r) - 1)$  is obtained from  $G(r) = G(\mathbf{r}, \mathbf{0})$ , with the inverse  $G^{-1}(\mathbf{r}, \mathbf{r}') = \frac{\delta^2\Omega}{\delta\varrho_0(\mathbf{r})\delta\varrho_0(\mathbf{r}' )}$ , where  $\int d^3r'' G(\mathbf{r}, \mathbf{r}'') G^{-1}(\mathbf{r}'', \mathbf{r}') = \delta(\mathbf{r} - \mathbf{r}')$  [162]. From Eq. (A.1) one obtains

$$G^{-1}(\mathbf{r}, \mathbf{r}') = \delta(\mathbf{r} - \mathbf{r}') \left( \frac{1}{\varrho_0} + \frac{1}{1 - \varrho_0} - 2\chi(T) \right) - \frac{\chi(T)}{3} \nabla^2 \delta(\mathbf{r} - \mathbf{r}'). \quad (\text{A.2})$$

The corresponding Fourier transform,  $\hat{G}^{-1}(k) = \int d^3r G^{-1}(\mathbf{r}, \mathbf{r}') e^{-i\mathbf{k}\cdot(\mathbf{r}-\mathbf{r}')}$  with dimensionless  $\mathbf{k}$ , is given by

$$\hat{G}^{-1}(k) = \frac{\chi(T)}{3} \left( \frac{1}{\xi^2} + k^2 \right), \quad (\text{A.3})$$

where Eq. (4.18) has been used.  $\hat{G}(k)$ , which is proportional to the static structure factor, can be written in the form

$$\hat{G}(k) = \frac{\frac{3\xi^2}{\chi(T)}}{1 + (k\xi)^2} = \frac{\hat{G}(0)}{1 + (k\xi)^2}. \quad (\text{A.4})$$

This allows one to identify  $\xi$  with the bulk correlation length. For a discussion of the structure in the presence of ions (Eq. (3.10)) see Ref. [21].

In a similar way for the case with long-ranged interaction between solvent particles (see Eq. (4.49))

$$G^{-1}(\mathbf{r}, \mathbf{r}') = \delta(\mathbf{r} - \mathbf{r}') \left( \frac{1}{\varrho_0} + \frac{1}{1 - \varrho_0} - 2\chi(T) + \frac{\beta\pi^2 A_f}{4} \right) - \frac{\chi(T)}{3} \nabla^2 \delta(\mathbf{r} - \mathbf{r}'). \quad (\text{A.5})$$

Therefore the bulk correlation length  $\xi$  for this case is given by

$$\begin{aligned} \frac{1}{\xi^2} &= \frac{3}{\chi(T)} \left( \frac{1}{\varrho_0} + \frac{1}{1 - \varrho_0} - 2\chi(T) + \frac{\pi^2 \beta A_f}{4} \right), \\ &= \frac{\frac{3}{\tilde{\chi}(T)} \left( \frac{1}{\varrho_0} + \frac{1}{1 - \varrho_0} - 2\tilde{\chi}(T) \right)}{1 + \frac{\pi^2 \beta A_f}{8\tilde{\chi}(T)}} \end{aligned} \quad (\text{A.6})$$

with  $\tilde{\chi}(T) = \chi(T) - \pi^2 \beta A_f / 8$ .

# Appendix B

## Double parabola approximation for the pure solvent

The double parabola approximation (DPA) has been widely used in the context of wetting phenomena in order to obtain analytically tractable density functionals [216–223]. Within this approximations, the grand canonical functional for the pure solvent, i.e.,  $\varrho_{\pm} = 0$  and  $\mathbf{D}(\mathbf{r}, [\varrho_{\pm}]) = 0$  (see Eq. (3.10)) is given by

$$\frac{\beta\Omega_{\text{DPA}}[\varrho_0(z)]}{A} = \int dz \left\{ F_{\text{DPA}}(\varrho_0(z)) + \frac{\chi(T)}{6} \left( \frac{d\varrho_0(z)}{dz} \right)^2 - \varrho_0(z)\beta\mu_0 \right\} - \beta h_1 \varrho_0(z=0) + \beta \frac{g}{2} (\varrho_0(z=0))^2 \quad (\text{B.1})$$

with

$$F_{\text{DPA}}(\varrho_0) = C(T) \begin{cases} (\varrho_0 - \varrho_{0,l}(T))^2, & \varrho_0 > \frac{1}{2}(\varrho_{0,l}(T) + \varrho_{0,g}(T)) \\ (\varrho_0 - \varrho_{0,g}(T))^2, & \varrho_0 < \frac{1}{2}(\varrho_{0,l}(T) + \varrho_{0,g}(T)), \end{cases} \quad (\text{B.2})$$

where  $\varrho_{0,l}(T)$  and  $\varrho_{0,g}(T)$  are, respectively, the (temperature dependent) liquid and gas bulk densities at coexistence, and  $C(T)$  is fixed later in order to render the bulk correlation length. Upon construction, the DPA requires an underlying theory which provides expressions for the bulk densities and the curvature of the local free energy density at coexistence [216–223]. For brevity the temperature dependence is not indicated in the present notation. Within this approach, for a given profile  $\varrho_0(z)$  the assigned film thickness  $\ell_{\text{DPA}}$  is defined as

$$\varrho_0(z = \ell_{\text{DPA}}) = \frac{1}{2}(\varrho_{0,l} + \varrho_{0,g}). \quad (\text{B.3})$$

Minimization of the functional in Eq. (B.1) leads to

$$\varrho''_{0,\text{DPA}}(z) = \begin{cases} \frac{6C}{\chi}(\varrho_{0,\text{DPA}}(z) - \varrho_{0,l}) - \beta\mu_0, & \varrho_{0,\text{DPA}}(z) > \frac{1}{2}(\varrho_{0,l} + \varrho_{0,g}) \\ \frac{6C}{\chi}(\varrho_{0,\text{DPA}}(z) - \varrho_{0,g}) - \beta\mu_0, & \varrho_{0,\text{DPA}}(z) < \frac{1}{2}(\varrho_{0,l} + \varrho_{0,g}) \end{cases} \quad (\text{B.4})$$

with the boundary conditions

$$\begin{aligned} \frac{\chi}{3}\varrho'_{0,\text{DPA}}(0) &= \beta(-h_1 + g\varrho_{0,\text{DPA}}(0)), \\ \varrho_{0,\text{DPA}}(\ell_{\text{DPA}}) &= \frac{1}{2}(\varrho_{0,l} + \varrho_{0,g}), \\ \varrho_{0,\text{DPA}}(\infty) &= \varrho_{0,g}. \end{aligned} \quad (\text{B.5})$$

At two-phase coexistence  $\mu_0 = 0$  (as for the pure solvent case, i.e.,  $\varrho_{\pm} = 0$ , in the present model given by Eq. (4.2)) and Eq. (B.4) reduces to

$$\varrho''_{0,\text{DPA}}(z) = \begin{cases} \frac{6C}{\chi}(\varrho_{0,\text{DPA}}(z) - \varrho_{0,l}), & \varrho_{0,\text{DPA}}(z) > \frac{1}{2}(\varrho_{0,l} + \varrho_{0,g}) \\ \frac{6C}{\chi}(\varrho_{0,\text{DPA}}(z) - \varrho_{0,g}), & \varrho_{0,\text{DPA}}(z) < \frac{1}{2}(\varrho_{0,l} + \varrho_{0,g}). \end{cases} \quad (\text{B.6})$$

Comparison with Eq. (4.17) leads to  $C = \chi/(6\xi^2)$ . Equation (B.6) together with the boundary conditions in Eq. (B.5) yields

$$\varrho_{0,\text{DPA}}(z) = \begin{cases} C_1 \exp(z/\xi) + C_2 \exp(-z/\xi) + \varrho_{0,l}, & 0 \leq z \leq \ell_{\text{DPA}} \\ C_3 \exp(-z/\xi) + \varrho_{0,g}, & z \geq \ell_{\text{DPA}} \end{cases} \quad (\text{B.7})$$

where

$$\begin{aligned} C_1 &= \frac{\frac{\varrho_{0,g} - \varrho_{0,l}}{2} \left( \beta g + \frac{\chi}{3\xi} \right) - \beta(h_1 - g\varrho_{0,l}) \exp(-\ell_{\text{DPA}}/\xi)}{\left( \beta g + \frac{\chi}{3\xi} \right) \exp(\ell_{\text{DPA}}/\xi) + \left( \frac{\chi}{3\xi} - \beta g \right) \exp(-\ell_{\text{DPA}}/\xi)}, \\ C_2 &= \frac{\frac{\varrho_{0,g} - \varrho_{0,l}}{2} \left( \frac{\chi}{3\xi} - \beta g \right) + \beta(h_1 - g\varrho_{0,l}) \exp(\ell_{\text{DPA}}/\xi)}{\left( \beta g + \frac{\chi}{3\xi} \right) \exp(\ell_{\text{DPA}}/\xi) + \left( \frac{\chi}{3\xi} - \beta g \right) \exp(-\ell_{\text{DPA}}/\xi)}, \\ C_3 &= \frac{\varrho_{0,l} - \varrho_{0,g}}{2} \exp(\ell_{\text{DPA}}/\xi). \end{aligned} \quad (\text{B.8})$$

The comparison between Eqs. (4.24) and (B.7) shows that the coefficients  $\hat{A}_l$ ,  $\hat{B}_l$ , and  $\hat{B}_g$  there play the same role as the coefficients  $C_1$ ,  $C_2$ , and  $C_3$ , respectively, here. At

coexistence and for  $\ell = \ell_{\text{DPA}}$  in Eq. (4.31) one obtains

$$\begin{aligned}
 C_1 &= A_l(1 + \mathcal{O}(\exp(-\ell_{\text{DPA}}/\xi))), \\
 C_2 &= B_l(1 + \mathcal{O}(\exp(-\ell_{\text{DPA}}/\xi))), \\
 C_3 &= B_g(1 + \mathcal{O}(\exp(-\ell_{\text{DPA}}/\xi))),
 \end{aligned}
 \tag{B.9}$$

i.e., the relative difference between the coefficients of the profiles in Eq. (4.24) and in Eq. (B.7) is exponentially small for film thicknesses  $\ell = \ell_{\text{DPA}} \gg \xi$  large compared to the bulk correlation length.



# Appendix C

## First-order perturbation theory for including the long-ranged interactions

The total grand canonical functional is given by

$$\Omega[\varrho_0(\mathbf{r}), \varrho_{\pm}(\mathbf{r})] = \Omega_0[\varrho_0(\mathbf{r}), \varrho_{\pm}(\mathbf{r})] + \Delta\Omega[\varrho_0(\mathbf{r})] \quad (\text{C.1})$$

with  $\Omega_0[\varrho_0(\mathbf{r}), \varrho_{\pm}(\mathbf{r})]$  given by Eq. (3.10) whereas  $\Delta\Omega[\varrho_0(\mathbf{r})]$  is given by Eq. (4.50) and depends only on  $\varrho_0(\mathbf{r})$ . A dimensionless coupling parameter  $\lambda \in [0, 1]$  is chosen such that for  $\lambda = 0$  the perturbation  $\Delta\Omega$  is absent and for  $\lambda = 1$  the perturbation is fully present. The perturbed grand canonical functional is

$$\Omega_{\lambda}[\varrho_0(\mathbf{r}), \varrho_{\pm}(\mathbf{r})] = \Omega_0[\varrho_0(\mathbf{r}), \varrho_{\pm}(\mathbf{r})] + \lambda\Delta\Omega[\varrho_0(\mathbf{r})], \quad (\text{C.2})$$

where  $\lambda$  acts as an amplitude multiplying both  $w(|\mathbf{r} - \mathbf{r}'|)$  and  $V(\mathbf{r})$  (see Eq. (4.50)). The equilibrium densities  $\varrho_{0,\lambda}(\mathbf{r})$  and  $\varrho_{\pm,\lambda}(\mathbf{r})$  minimize  $\Omega_{\lambda}$ :

$$\frac{\delta\Omega_{\lambda}}{\delta\varrho_0(\mathbf{r})}[\varrho_{0,\lambda}(\mathbf{r}), \varrho_{\pm,\lambda}(\mathbf{r})] = 0, \quad \frac{\delta\Omega_{\lambda}}{\delta\varrho_{\pm}(\mathbf{r})}[\varrho_{0,\lambda}(\mathbf{r}), \varrho_{\pm,\lambda}(\mathbf{r})] = 0. \quad (\text{C.3})$$

Furthermore, the equilibrium densities  $\varrho_0^{(0)}(\mathbf{r}) \equiv \varrho_{0,\lambda=0}(\mathbf{r})$  and  $\varrho_{\pm}^{(0)}(\mathbf{r}) \equiv \varrho_{\pm,\lambda=0}(\mathbf{r})$  which minimize  $\Omega_0[\varrho_0(\mathbf{r}), \varrho_{\pm}(\mathbf{r})]$  are known (see Sec. 4.1).

In order to proceed the equilibrium densities  $\varrho_{0,\lambda}(\mathbf{r})$  and  $\varrho_{\pm,\lambda}(\mathbf{r})$  are written as power

series in terms of  $\lambda$ ,

$$\begin{aligned}\varrho_{0,\lambda}(\mathbf{r}) &= \sum_{n=0}^{\infty} \lambda^n \varrho_0^{(n)}(\mathbf{r}) = \varrho_0^{(0)}(\mathbf{r}) + \mathcal{O}(\lambda), \\ \varrho_{\pm,\lambda}(\mathbf{r}) &= \sum_{n=0}^{\infty} \lambda^n \varrho_{\pm}^{(n)}(\mathbf{r}) = \varrho_{\pm}^{(0)}(\mathbf{r}) + \mathcal{O}(\lambda),\end{aligned}\tag{C.4}$$

and perform a functional Taylor expansion of the grand canonical potential  $\Omega_{\lambda}[\varrho_{0,\lambda}(\mathbf{r}), \varrho_{\pm,\lambda}(\mathbf{r})]$  around  $\varrho_0^{(0)}(\mathbf{r})$ ,  $\varrho_{\pm}^{(0)}(\mathbf{r})$ :

$$\begin{aligned}\Omega_{\lambda}[\varrho_{0,\lambda}(\mathbf{r}), \varrho_{\pm,\lambda}(\mathbf{r})] &= \Omega_0 \left[ \varrho_0^{(0)}(\mathbf{r}) + \left( \varrho_{0,\lambda}(\mathbf{r}) - \varrho_0^{(0)}(\mathbf{r}) \right), \varrho_{\pm}^{(0)}(\mathbf{r}) + \left( \varrho_{\pm,\lambda}(\mathbf{r}) - \varrho_{\pm}^{(0)}(\mathbf{r}) \right) \right] \\ &\quad + \lambda \Delta \Omega \left[ \varrho_0^{(0)}(\mathbf{r}) + \left( \varrho_{0,\lambda}(\mathbf{r}) - \varrho_0^{(0)}(\mathbf{r}) \right) \right] \\ &= \Omega_0[\varrho_0^{(0)}(\mathbf{r}), \varrho_{\pm}^{(0)}(\mathbf{r})] + \lambda \Delta \Omega[\varrho_0^{(0)}(\mathbf{r})] \\ &\quad + \int d^3r \left\{ \frac{\delta \Omega_0[\varrho_0(\mathbf{r}), \varrho_{\pm}(\mathbf{r})]}{\delta \varrho_0(\mathbf{r})} \Bigg|_{\varrho_0^{(0)}(\mathbf{r}), \varrho_{\pm}^{(0)}(\mathbf{r})} (\varrho_{0,\lambda}(\mathbf{r}) - \varrho_0^{(0)}(\mathbf{r})) \right. \\ &\quad + \frac{\delta \Omega_0[\varrho_0(\mathbf{r}), \varrho_{\pm}(\mathbf{r})]}{\delta \varrho_+(\mathbf{r})} \Bigg|_{\varrho_0^{(0)}(\mathbf{r}), \varrho_{\pm}^{(0)}(\mathbf{r})} (\varrho_{+,\lambda}(\mathbf{r}) - \varrho_+^{(0)}(\mathbf{r})) \\ &\quad \left. + \frac{\delta \Omega_0[\varrho_0(\mathbf{r}), \varrho_{\pm}(\mathbf{r})]}{\delta \varrho_-(\mathbf{r})} \Bigg|_{\varrho_0^{(0)}(\mathbf{r}), \varrho_{\pm}^{(0)}(\mathbf{r})} (\varrho_{-,\lambda}(\mathbf{r}) - \varrho_-^{(0)}(\mathbf{r})) \right\} + \mathcal{O}(\lambda^2) \\ &= \Omega_0[\varrho_0^{(0)}(\mathbf{r}), \varrho_{\pm}^{(0)}(\mathbf{r})] + \lambda \Delta \Omega[\varrho_0^{(0)}(\mathbf{r})] + \mathcal{O}(\lambda^2) \\ &= \Omega_{\lambda}[\varrho_0^{(0)}(\mathbf{r}), \varrho_{\pm}^{(0)}(\mathbf{r})] + \mathcal{O}(\lambda^2)\end{aligned}\tag{C.5}$$

with  $\varrho_{0,\lambda}(\mathbf{r}) - \varrho_0^{(0)}(\mathbf{r}) = \mathcal{O}(\lambda)$  and  $\varrho_{\pm,\lambda}(\mathbf{r}) - \varrho_{\pm}^{(0)}(\mathbf{r}) = \mathcal{O}(\lambda)$  (see Eq. (C.4)). In Eq. (C.5) the first derivatives vanish because  $\varrho_0^{(0)}$  and  $\varrho_{\pm}^{(0)}$  minimize  $\Omega_0$ . Hence  $\Omega_{\lambda=1}[\varrho_{0,\lambda=1}(\mathbf{r}), \varrho_{\pm,\lambda=1}(\mathbf{r})] \approx \Omega_{\lambda=1}[\varrho_0^{(0)}(\mathbf{r}), \varrho_{\pm}^{(0)}(\mathbf{r})] = \Omega[\varrho_0^{(0)}(\mathbf{r}), \varrho_{\pm}^{(0)}(\mathbf{r})]$  up to second order in  $\lambda$ .



# Appendix D

## Coefficients for the effective interface potential in the presence of long-ranged interactions

The effective interface potential for the model with long-ranged interaction (Sec. 4.2) is calculated by following the procedure described in Sec. 4.1. The double integrals in Eq. (4.50) have been evaluated by performing an asymptotic expansion for  $\ell \rightarrow \infty$ . The analytic expressions for the coefficients in Eq. (4.58) are given by (see Appendix E)

$$a_1(T) = \frac{(\varrho_{0,l} - \varrho_{0,g})}{2} \beta(u_3 \varrho_w - t_3 \varrho_{0,l}) \quad (\text{D.1})$$

and

$$b_1(T) = \frac{\beta(\varrho_{0,l} - \varrho_{0,g})}{3} \left( \varrho_w u_4 - 3t_3 \varrho_{0,l} d_w + 3\xi t_3 \exp\left(-\frac{d_w}{\xi}\right) \left( \frac{\beta(h_1 - g\varrho_{0,l})}{\beta g + \frac{\chi(T)}{3\xi}} \right) \right). \quad (\text{D.2})$$

The coefficients  $a_1$  and  $b_1$  can be compared with the general expressions obtained in Ref. [215] within a systematic study of wetting transitions of a simple one-component fluid, inter alia including the presence of van der Waals tails. There the effective interface potential is expressed in terms of the interfacial profiles which emerge as a consequence of wetting phenomena, i.e., the wall-liquid and the free liquid-gas interface for wetting of the wall-gas interface. Within that approach the effective interface potential at coexistence is given by

$$\omega(\ell) = \sum_{k=2}^4 a_k \ell^{-k} + \mathcal{O}(\ell^{-5} \ln \ell) \quad (\text{D.3})$$

where

$$a_2 = \frac{1}{2}(\varrho_{0,l} - \varrho_{0,g})(\varrho_w u_3 - \varrho_{0,l} t_3), \quad (\text{D.4})$$

$$a_3 = a_3^{(0)} - 2a_2 d_{lg}^{(1)}, \quad (\text{D.5})$$

and

$$a_4 = a_4^{(0)} - 3a_3 d_{lg}^{(1)} + 3a_2 [d_{lg}^{(2)} - 2(d_{lg}^{(1)})^2], \quad (\text{D.6})$$

with

$$a_3^{(0)} = \frac{1}{3}(\varrho_{0,l} - \varrho_{0,g})[\varrho_w u_4 - \varrho_{0,l}(t_4 + 3t_3 d_{wl}^{(1)})] \quad (\text{D.7})$$

and

$$a_4^{(0)} = \frac{1}{4}(\varrho_{0,l} - \varrho_{0,g})[\varrho_w u_5 - \varrho_{0,l}(t_5 + 4t_4 d_{wl}^{(1)} + 6t_3 d_{wl}^{(2)})]. \quad (\text{D.8})$$

The coefficients  $t_3$ ,  $t_4$  for the present model are given by Eqs. (4.53) and (4.54);  $d_{wl}^{(i)}$  and  $d_{lg}^{(i)}$  are moments of the wall-liquid interface profile  $\varrho_{0,wl}(z)$  and of the free liquid-gas interface profile  $\varrho_{0,lg}(z)$ , respectively:

$$d_{wl}^{(i)} = i \int_0^\infty dz z^{i-1} \left[ 1 - \frac{\varrho_{0,wl}(z)}{\varrho_{0,l}} \right], \quad i = 1, 2, \quad (\text{D.9})$$

and

$$d_{lg}^{(i)} = \frac{i}{\varrho_{0,l} - \varrho_{0,g}} \int_{-\infty}^\infty dz z^{i-1} [\varrho_{0,lg}(z) - \varrho_{0,lg}^{sk}(z)], \quad i = 1, 2. \quad (\text{D.10})$$

The wall-liquid and the free liquid-gas interface profile can be calculated within our approach by following a procedure analogous to the one described in Sec. 4.1. To this end, in the case of the wall-liquid interface for the pure solvent, the Taylor expansion up to second order of the local part of the functional in Eq. (3.10) with  $\varrho_\pm = 0$  and  $\mathbf{D} = 0$ , is performed about  $\varrho_{0,wl}(z) = \varrho_{0,l}\Theta(z - d_w)$  for  $z \geq 0$  where  $\Theta(x)$  is the Heaviside function. This leads to the wall-liquid density profile

$$\varrho_{0,wl}(z) = \left( \varrho_{0,l} + \frac{\beta(h_1 - g\varrho_{0,l})}{\beta g + \frac{\chi(T)}{3\xi}} \exp(-z/\xi) \right) \Theta(z - d_w). \quad (\text{D.11})$$

Within the approximation discussed in Appendix C, this expression, obtained from minimizing  $\Omega_0$  and shifting by  $d_w$ , is inserted into the general expression in Eq. (D.9) corresponding to  $\Delta\Omega$  and yields

$$d_{wl}^{(1)} = d_w - \frac{\beta\xi(h_1 - g\varrho_{0,l})}{\varrho_{0,l} \left( \beta g + \frac{\chi(T)}{3\xi} \right)} \exp(-d_w/\xi). \quad (\text{D.12})$$

As expected, Eq. (D.12) respects the expected property that in the sharp-kink limit (i.e, vanishing interfacial width  $\xi$ )  $d_{wl}^{(1)}$  reduces to  $d_w$ . With this result Eq. (D.2) can be rewritten as  $b_1(T) = (\beta/3)(\varrho_{0,l} - \varrho_{0,g}) \left( \varrho_w u_4 - 3t_3 \varrho_{0,l} d_{wl}^{(1)} \right)$ . For the free liquid-gas interface, the functional in Eq. (A.1) is considered. All integrals extend over a macroscopic volume. The following boundary conditions  $\varrho_{0,lg}(z \rightarrow -\infty) = \varrho_{0,l}$  and  $\varrho_{0,lg}(z \rightarrow \infty) = \varrho_{0,g}$  are imposed. Accordingly, the Taylor expansion up to second order of the local part of the functional is performed about the sharp-kink profile

$$\varrho_{0,lg}^{sk}(z) = \begin{cases} \varrho_{0,l}, & z < 0, \\ \varrho_{0,g}, & z > 0. \end{cases} \quad (\text{D.13})$$

The resulting liquid-gas density profile based on  $\Omega_0$  is

$$\varrho_{0,lg}(z) = \begin{cases} \varrho_{0,l} + \frac{\varrho_{0,g} - \varrho_{0,l}}{2} \exp(z/\xi), & z < 0, \\ \varrho_{0,g} + \frac{\varrho_{0,l} - \varrho_{0,g}}{2} \exp(-z/\xi), & z > 0. \end{cases} \quad (\text{D.14})$$

Again, within the approximation discussed in Appendix C, this profile stemming from  $\Omega_0$  is inserted into the general expression in Eq. (D.10), which is based on  $\Delta\Omega$ , and renders

$$d_{lg}^{(1)} = 0. \quad (\text{D.15})$$

Inserting Eqs. (4.53), (4.54), (D.12), and (D.15) into Eqs. (D.4) and (D.5) one obtains (with  $t_4 = 0$ )

$$\beta a_2 = a_1 \quad \text{and} \quad \beta a_3 = b_1. \quad (\text{D.16})$$

This leads to the satisfactory statement that if the general results in Ref. [215] for the effective interface potential are applied to the present model one finds the same effective interface potential as the one obtained directly within the present model.



# Appendix E

## Derivation of the effective interface potential for the model with long-ranged interactions

The derivation of  $\omega(\ell)$  in Eq. (4.58) follows the same procedure as described in Sec. 4.1. A Taylor expansion up to second order of the local part of the functional in Eq. (4.49) about the sharp-kink profile in Eq. (4.10) shifted by  $d_w$  and the sharp-kink profile in Eq. (4.11) with the bulk state being determined by Eq. (E.3) is performed. From this expansion one obtains an approximate variational functional  $\hat{\Omega}_{lr}$  for the model with long-ranged interactions. By subtracting the bulk contribution  $\Omega_{b,lr}$  of the gas phase one

obtains the surface contribution  $\Omega_{s,lr}$  to this variational functional:

$$\begin{aligned}
\beta\Omega_{s,lr}(\ell, [\Delta\varrho_0, \Delta\varrho_{\pm}]) &= \frac{\beta\left(\hat{\Omega}_{lr}(\ell, [\Delta\varrho_0(z), \Delta\varrho_{\pm}(z)]) - V\Omega_{b,lr}(\varrho_{0,g}, 0)\right)}{A} \\
&= \beta\ell\left[\Omega_{b,lr}(\varrho_{0,l}, I) - \Omega_{b,lr}(\varrho_{0,g}, 0)\right] - \beta d_w\Omega_{b,lr}(\varrho_{0,l}, I) \\
&\quad + \int_{d_w}^{\ell} dz \left\{ \frac{\chi(T)}{6} \left(\frac{d}{dz}\Delta\varrho_0(z)\right)^2 + \frac{1}{2}(\Delta\varrho_0(z))^2 \left(\frac{1}{\varrho_{0,l}} + \frac{1}{1-\varrho_{0,l}} - 2\chi(T)\right) \right\} \\
&\quad + \int_{\ell}^{\infty} dz \left\{ \frac{\chi(T)}{6} \left(\frac{d}{dz}\Delta\varrho_0(z)\right)^2 + \frac{1}{2}(\Delta\varrho_0(z))^2 \left(\frac{1}{\varrho_{0,g}} + \frac{1}{1-\varrho_{0,g}} - 2\chi(T)\right) \right\} \\
&\quad - \beta h_1\varrho_{0,l} - \beta h_1\Delta\varrho_0(d_w) + \beta\frac{g}{2}(\varrho_{0,l} + \Delta\varrho_0(d_w))^2 \\
&\quad - \frac{1}{2}\varrho_{0,l}^2\beta\left(\mathbf{I}_0^{(\ell,d_w)} + \mathbf{I}_0^{(\ell,\infty)}\right) + \varrho_{0,l}\varrho_{0,g}\beta\mathbf{I}_0^{(\ell,\infty)} - \frac{1}{2}\varrho_{0,g}^2\beta\mathbf{I}_0^{(\infty,\ell)} \\
&\quad - \varrho_{0,l}\beta\mathbf{I}_2^{(\ell,d_w)} - (\varrho_{0,l} - \varrho_{0,g})\beta\left(\mathbf{I}_2^{(\ell,\infty)} - \mathbf{I}_2^{(\infty,\ell)}\right) - \varrho_{0,g}\beta\mathbf{I}_2^{(\infty,d_w)} \\
&\quad + \frac{1}{2}\beta\left(\mathbf{I}_3^{(\ell,\ell)} + \mathbf{I}_3^{(\ell,\infty)} + \mathbf{I}_3^{(\infty,\ell)} + \mathbf{I}_3^{(\infty,\infty)}\right) \\
&\quad + \varrho_{0,l}\varrho_w\beta\int_{d_w}^{\ell} dz V(z) + \varrho_w\beta\mathbf{I}_1^{(\ell)} + \varrho_{0,g}\varrho_w\beta\int_{\ell}^{\infty} dz V(z) + \varrho_w\beta\mathbf{I}_1^{(\infty)} \\
&\quad + \int_0^{\ell} dz \left\{ \frac{1}{2I} \sum_{i=\pm} (\Delta\varrho_i(z))^2 + \frac{2\pi l_B}{\varepsilon_l} (D(z, [\Delta\varrho_{\pm}]))^2 \right\},
\end{aligned} \tag{E.1}$$

where  $d_w$  describes the excluded volume due to the repulsive part of the substrate potential  $V(z)$  given by Eq. (4.48) and

$$w(|z - z'|) = \frac{\pi A_f}{2[(z - z')^2 + 1]^2}. \tag{E.2}$$

The bulk grand canonical potential density  $\Omega_{b,lr}$  per  $k_B T$  is given by

$$\begin{aligned}
\beta\Omega_{b,lr}(\varrho_0, \varrho) &= \varrho_0(\ln(\varrho_0) - \beta\mu_{\varrho_0}) + (1 - \varrho_0)\ln(1 - \varrho_0) + \chi(T)\varrho_0(1 - \varrho_0) \\
&\quad + \frac{1}{2}\varrho_0^2 \int_{-\infty}^{\infty} dx w(|x|) + 2\varrho(\ln(\varrho) - 1) - \beta\mu_I\varrho + \varrho(V_+(\varrho_0) + V_-(\varrho_0)).
\end{aligned} \tag{E.3}$$

$\mathbf{I}_0$ ,  $\mathbf{I}_1$ ,  $\mathbf{I}_2$ , and  $\mathbf{I}_3$  are abbreviations for the following types of integrals:

$$\mathbf{I}_0^{(u_2, v_2)} = \int_{u_1}^{u_2} dz \int_{v_1}^{v_2} dz' w(|z - z'|), \tag{E.4}$$

$$\mathbf{I}_1^{(u_2)} = \int_{u_1}^{u_2} dz V(z)\Delta\varrho_0(z), \tag{E.5}$$

$$I_2^{(u_2, v_2)} = \int_{u_1}^{u_2} dz \int_{v_1}^{v_2} dz' \Delta \varrho_0(z) w(|z - z'|), \quad (\text{E.6})$$

and

$$I_3^{(u_2, v_2)} = \int_{u_1}^{u_2} dz \int_{v_1}^{v_2} dz' \Delta \varrho_0(z) \Delta \varrho_0(z') w(|z - z'|). \quad (\text{E.7})$$

The integrals in Eqs. (E.5)-(E.7) are evaluated at two-phase coexistence using the solutions for  $\Delta \varrho_0(z)$  obtained in Sec. 4.1 (see Eqs. (4.24) and (4.31)). For the present purpose only the asymptotic behavior of these integrals in the limit  $\ell \rightarrow \infty$  is necessary. Using Eqs. (4.24) and (4.48),  $I_1^{(\ell)}$  can be written as

$$\begin{aligned} I_1^{(\ell)} &= - \int_{d_w}^{\ell} dz \left[ \sum_{i \geq 3} \frac{u_i}{z^i} \right] \left[ A_l \exp(z/\xi) + B_l \exp(-z/\xi) \right] \\ &= -A_l \int_{d_w}^{\ell} dz \left[ \sum_{i \geq 3} \frac{u_i}{z^i} \right] \exp(z/\xi) - B_l \int_{d_w}^{\ell} dz \left[ \sum_{i \geq 3} \frac{u_i}{z^i} \right] \exp(-z/\xi). \end{aligned} \quad (\text{E.8})$$

Asymptotic approximations for the integrals in Eq. (E.8) are obtained via integrating by parts repeatedly:

$$\begin{aligned} \int_{d_w}^{\ell} dz \frac{\exp(z/\xi)}{z^3} &= \frac{\xi \exp(\ell/\xi)}{\ell^3} - \frac{\xi \exp(d_w/\xi)}{d_w^3} + 3\xi \int_{d_w}^{\ell} dz \frac{\exp(z/\xi)}{z^4}, \\ &= \frac{\xi \exp(\ell/\xi)}{\ell^3} + \mathcal{O}(\ell^{-4} \exp(\ell/\xi)), \quad \ell \gg d_w, \end{aligned} \quad (\text{E.9})$$

and

$$\int_{d_w}^{\ell} dz \frac{\exp(-z/\xi)}{z^3} = \int_{d_w}^{\infty} dz \frac{\exp(-z/\xi)}{z^3} - \int_{\ell}^{\infty} dz \frac{\exp(-z/\xi)}{z^3} \quad (\text{E.10})$$

with

$$\begin{aligned} \int_{\ell}^{\infty} dz \frac{\exp(-z/\xi)}{z^3} &= \frac{\xi \exp(-\ell/\xi)}{\ell^3} - 3\xi \int_{\ell}^{\infty} dz \frac{\exp(-z/\xi)}{z^4}, \\ &= \frac{\xi \exp(-\ell/\xi)}{\ell^3} + \mathcal{O}(\ell^{-4} \exp(\ell/\xi)), \quad \ell \gg d_w. \end{aligned} \quad (\text{E.11})$$

Here and in the following the properties

$$\int_a^{\ell+b} dz \frac{P_1(z)}{P_2(z)} \exp(z/\xi) \stackrel{\ell \rightarrow \infty}{\simeq} \frac{c_1}{c_2} \xi \ell^{n_1 - n_2} \exp(\ell/\xi)$$

and

$$\int_{\ell+a}^{\infty} dz \frac{P_1(z)}{P_2(z)} \exp(-z/\xi) \stackrel{\ell \rightarrow \infty}{\simeq} \frac{c_1}{c_2} \xi \ell^{n_1 - n_2} \exp(-\ell/\xi)$$

for two polynomials  $P_1(z)$  and  $P_2(z)$  of degrees  $n_1$  and  $n_2$  with the leading coefficients  $c_1$

and  $c_2$ , respectively, of the leading terms which follows from L'Hôpital's rule.

For convenience, the expressions in Eq. (4.31) are written as

$$\begin{aligned} A_l &= A_1 \exp(-\ell/\xi), \\ B_l &= B_1 \exp(-\ell/\xi) + B_2, \\ B_g &= -A_1 \exp(\ell/\xi) + B_1 \exp(-\ell/\xi) + B_2, \end{aligned} \tag{E.12}$$

with

$$\begin{aligned} A_1 &= \frac{\varrho_{0,g} - \varrho_{0,l}}{2}, \\ B_1 &= \frac{\left(\frac{\chi(T)}{3\xi} - \beta g\right) (\varrho_{0,g} - \varrho_{0,l})}{2 \left(\beta g + \frac{\chi(T)}{3\xi}\right)}, \\ B_2 &= \frac{\beta(h_1 - g\varrho_{0,l})}{\beta g + \frac{\chi(T)}{3\xi}}. \end{aligned} \tag{E.13}$$

Collecting only algebraic terms up to the order  $1/\ell^3$ , one obtains for  $I_1^{(\ell)}$

$$I_1^{(\ell)} = -\frac{\xi A_1 u_3}{\ell^3} + \mathcal{O}\left(\frac{1}{\ell^4}\right). \tag{E.14}$$

Analogously, for  $I_1^{(\infty)}$  one has

$$\begin{aligned} I_1^{(\infty)} &= -\int_{\ell}^{\infty} dz \left[ \sum_{i \geq 3} \frac{u_i}{z^i} \right] B_g \exp(-z/\xi) \\ &= \frac{\xi A_1 u_3}{\ell^3} + \mathcal{O}\left(\frac{1}{\ell^4}\right). \end{aligned} \tag{E.15}$$

In order to calculate integrals of the type  $I_2$  Eq. (E.2) is first integrated using the various integration limits appearing in Eq. (E.1) so that

$$\int_{-\infty}^{d_w} dz' w(|z - z'|) = \frac{\pi A_f}{4} \left[ \frac{\pi}{2} - \arctan(z - d_w) - \frac{z - d_w}{(z - d_w)^2 + 1} \right], \tag{E.16}$$

$$\int_{\ell}^{\infty} dz' w(|z - z'|) = \frac{\pi A_f}{4} \left[ \arctan(z - \ell) + \frac{z - \ell}{(z - \ell)^2 + 1} + \frac{\pi}{2} \right], \tag{E.17}$$

and

$$\int_{d_w}^{\ell} dz' w(|z - z'|) = \frac{\pi A_f}{4} \left[ \arctan(z - d_w) + \frac{z - d_w}{(z - d_w)^2 + 1} - \arctan(z - \ell) - \frac{z - \ell}{(z - \ell)^2 + 1} \right]. \tag{E.18}$$



Using Eqs. (4.24) and (E.16) one can write  $I_2^{(\ell, d_w)}$  as

$$\begin{aligned}
I_2^{(\ell, d_w)} &= \frac{\pi A_f}{4} \int_{d_w}^{\ell} dz \left[ \frac{\pi}{2} - \arctan(z - d_w) - \frac{z - d_w}{(z - d_w)^2 + 1} \right] \left[ A_l \exp(z/\xi) + B_l \exp(-z/\xi) \right] \\
&= \frac{\pi A_f}{4} A_l \left[ \frac{\xi \pi}{2} (\exp(\ell/\xi) - \exp(d_w/\xi)) - \xi \exp(\ell/\xi) \arctan(\ell - d_w) \right. \\
&\quad \left. + \xi \exp(d_w/\xi) \int_0^{\ell - d_w} dy \frac{\exp(y/\xi)}{y^2 + 1} - \exp(d_w/\xi) \int_0^{\ell - d_w} dz \frac{y \exp(y/\xi)}{y^2 + 1} \right] \\
&\quad + \frac{\pi A_f}{4} B_l \left[ \frac{-\xi \pi}{2} (\exp(-\ell/\xi) - \exp(-d_w/\xi)) + \xi \exp(-\ell/\xi) \arctan(\ell - d_w) \right. \\
&\quad \left. - \xi \exp(-d_w/\xi) \int_0^{\ell - d_w} dy \frac{\exp(-y/\xi)}{y^2 + 1} - \exp(-d_w/\xi) \int_0^{\ell - d_w} dy \frac{y \exp(-y/\xi)}{y^2 + 1} \right], \tag{E.19}
\end{aligned}$$

where the integration variable has been changed to  $y = z - d_w$ . Asymptotic approximations for the integrals in Eq. (E.19) are obtained via integrating by parts repeatedly:

$$\begin{aligned}
\int_0^{\ell - d_w} dz \frac{\exp(z/\xi)}{z^2 + 1} &= \frac{\xi \exp((\ell - d_w)/\xi)}{(\ell - d_w)^2 + 1} - \xi + \frac{2(\ell - d_w)\xi^2 \exp((\ell - d_w)/\xi)}{((\ell - d_w)^2 + 1)^2} \\
&\quad + \xi^2 \int_0^{\ell - d_w} dz \frac{6z^2 - 2}{(z^2 + 1)^3} \exp(z/\xi), \tag{E.20} \\
&= \frac{\xi \exp((\ell - d_w)/\xi)}{\ell^2} + \frac{2(d_w \xi + \xi^2) \exp((\ell - d_w)/\xi)}{\ell^3} \\
&\quad + \mathcal{O}(\ell^{-4} \exp(\ell/\xi)), \quad \ell \gg d_w,
\end{aligned}$$

$$\begin{aligned}
\int_0^{\ell - d_w} dz \frac{z \exp(z/\xi)}{z^2 + 1} &= \frac{\xi(\ell - d_w) \exp((\ell - d_w)/\xi)}{(\ell - d_w)^2 + 1} - \frac{\xi^2 \exp((\ell - d_w)/\xi)}{(\ell - d_w)^2 + 1} + \xi^2 \\
&\quad + \frac{2((\ell - d_w)\xi)^2 \exp((\ell - d_w)/\xi)}{((\ell - d_w)^2 + 1)^2} - \frac{6(\ell - d_w)\xi^3 \exp((\ell - d_w)/\xi)}{((\ell - d_w)^2 + 1)^2} \\
&\quad + \frac{8((\ell - d_w)\xi)^3 \exp((\ell - d_w)/\xi)}{((\ell - d_w)^2 + 1)^3} \\
&\quad + \int_0^{\ell - d_w} dz \frac{6(z^4 - 6z^2 + 1)}{(z^2 + 1)^4} \xi^3 \exp(z/\xi), \\
&= \xi \exp((\ell - d_w)/\xi) \left( \frac{1}{\ell} + \frac{d_w}{\ell^2} + \frac{d_w^2 - 1}{\ell^3} \right) + \frac{\xi^2 \exp((\ell - d_w)/\xi)}{\ell^2} \\
&\quad + \frac{2\xi^2(d_w + \xi) \exp((\ell - d_w)/\xi)}{\ell^3} + \mathcal{O}(\ell^{-4} \exp(\ell/\xi)), \quad \ell \gg d_w, \tag{E.21}
\end{aligned}$$

and

$$\int_0^{\ell-d_w} dz \frac{\exp(-z/\xi)}{z^2+1} = \int_0^\infty dz \frac{\exp(-z/\xi)}{z^2+1} - \int_{\ell-d_w}^\infty dz \frac{\exp(-z/\xi)}{z^2+1} \quad (\text{E.22})$$

with

$$\begin{aligned} \int_{\ell-d_w}^\infty dz \frac{\exp(-z/\xi)}{z^2+1} &= \frac{\xi \exp(-(\ell-d_w)/\xi)}{(\ell-d_w)^2+1} - \frac{2(\ell-d_w)\xi^2 \exp(-(\ell-d_w)/\xi)}{((\ell-d_w)^2+1)^2} \\ &\quad + \int_{\ell-d_w}^\infty dz \frac{6z^2-2}{(z^2+1)^3} \xi^2 \exp(-z/\xi) \\ &= \frac{\xi \exp(-(\ell-d_w)/\xi)}{\ell^2} + \frac{2\xi(d_w-\xi) \exp(-(\ell-d_w)/\xi)}{\ell^3} \\ &\quad + \mathcal{O}(\ell^{-4} \exp(-\ell/\xi)), \quad \ell \gg d_w, \end{aligned} \quad (\text{E.23})$$

and

$$\int_0^{\ell-d_w} dz \frac{z \exp(-z/\xi)}{z^2+1} = \int_0^\infty dz \frac{z \exp(-z/\xi)}{z^2+1} - \int_{\ell-d_w}^\infty dz \frac{z \exp(-z/\xi)}{z^2+1} \quad (\text{E.24})$$

with

$$\begin{aligned} \int_{\ell-d_w}^\infty dz \frac{z \exp(-z/\xi)}{z^2+1} &= \frac{\xi(\ell-d_w) \exp(-(\ell-d_w)/\xi)}{(\ell-d_w)^2+1} + \frac{\xi^2 \exp(-(\ell-d_w)/\xi)}{\ell^2+1} \\ &\quad - \frac{2((\ell-d_w)\xi)^2 \exp(-(\ell-d_w)/\xi)}{((\ell-d_w)^2+1)^2} \\ &\quad - \frac{6(\ell-d_w)\xi^3 \exp(-(\ell-d_w)/\xi)}{((\ell-d_w)^2+1)^2} \\ &\quad + \frac{8((\ell-d_w)\xi)^3 \exp(-(\ell-d_w)/\xi)}{((\ell-d_w)^2+1)^3} \\ &\quad - \xi^3 \int_{\ell-d_w}^\infty dz \frac{6(z^4-6z^2+1)}{(z^2+1)^4} \exp(-z/\xi), \\ &= \xi \exp(-(\ell-d_w)/\xi) \left( \frac{1}{\ell} + \frac{d_w}{\ell^2} + \frac{d_w^2-1}{\ell^3} \right) - \frac{\xi^2 \exp(-(\ell-d_w)/\xi)}{\ell^2} \\ &\quad + \frac{2\xi^2(\xi-d_w) \exp(-(\ell-d_w)/\xi)}{\ell^3} + \mathcal{O}(\ell^{-4} \exp(-\ell/\xi)), \quad \ell \gg d_w. \end{aligned} \quad (\text{E.25})$$

Additionally, for  $\ell \gg d_w$  one has

$$\frac{\pi}{2} - \arctan(\ell-d_w) = \frac{1}{\ell} + \frac{d_w}{\ell^2} + \frac{d_w^2-1/3}{\ell^3} + \mathcal{O}\left(\frac{1}{\ell^4}\right). \quad (\text{E.26})$$

Note that Eqs. (E.20) and (E.21) contain terms which increase exponentially with  $\ell$ . However, these two integrals are multiplied by  $A_\ell$  which decays exponentially with  $\ell$  (see

Eqs. (E.8) and (E.12)).

Collecting constants and algebraic terms up to the order  $1/\ell^3$ , for  $I_2^{(\ell, d_w)}_{(d_w, -\infty)}$  one obtains

$$\begin{aligned} I_2^{(\ell, d_w)}_{(d_w, -\infty)} &= \frac{A_f \pi B_2}{4} \exp(-d_w/\xi) \left( \frac{\xi \pi}{2} - \xi \int_0^\infty dy \frac{\exp(-y/\xi)}{y^2 + 1} - \int_0^\infty dy \frac{y \exp(-y/\xi)}{y^2 + 1} \right) \\ &+ \frac{\pi A_f \xi A_1}{6\ell^3} + \mathcal{O}\left(\frac{1}{\ell^4}\right). \end{aligned} \quad (\text{E.27})$$

Similarly,  $I_2^{(\infty, d_w)}_{(\ell, -\infty)}$  can be written as

$$\begin{aligned} I_2^{(\infty, d_w)}_{(\ell, -\infty)} &= \frac{\pi A_f}{4} \int_\ell^\infty dz \left[ \frac{\pi}{2} - \arctan(z - d_w) - \frac{z - d_w}{(z - d_w)^2 + 1} \right] B_g \exp(-z/\xi) \\ &= -\frac{\pi A_f \xi A_1}{6\ell^3} + \mathcal{O}\left(\frac{1}{\ell^4}\right). \end{aligned} \quad (\text{E.28})$$

Using Eqs. (4.24) and (E.17) one can write  $I_2^{(\ell, \infty)}_{(d_w, \ell)}$  as

$$\begin{aligned} I_2^{(\ell, \infty)}_{(d_w, \ell)} &= \frac{\pi A_f}{4} \int_{d_w}^\ell dz \left[ \arctan(z - \ell) + \frac{z - \ell}{(z - \ell)^2 + 1} + \frac{\pi}{2} \right] \left[ A_l \exp(z/\xi) + B_l \exp(-z/\xi) \right] \\ &= \frac{\pi A_f}{4} A_l \left[ \frac{\xi \pi}{2} (\exp(\ell/\xi) - \exp(d_w/\xi)) + \xi \exp(d_w/\xi) \arctan(\ell - d_w) \right. \\ &\quad \left. - \xi \exp(\ell/\xi) \int_0^{\ell - d_w} dy \frac{\exp(-y/\xi)}{y^2 + 1} - \exp(\ell/\xi) \int_0^{\ell - d_w} dz \frac{y \exp(-y/\xi)}{y^2 + 1} \right] \\ &+ \frac{\pi A_f}{4} B_l \left[ \frac{-\xi \pi}{2} (\exp(-\ell/\xi) - \exp(-d_w/\xi)) - \xi \exp(-d_w/\xi) \arctan(\ell - d_w) \right. \\ &\quad \left. + \xi \exp(-\ell/\xi) \int_0^{\ell - d_w} dy \frac{\exp(y/\xi)}{y^2 + 1} - \exp(-\ell/\xi) \int_0^{\ell - d_w} dy \frac{y \exp(y/\xi)}{y^2 + 1} \right], \end{aligned} \quad (\text{E.29})$$

where the integration variable has been changed to  $y = \ell - z$ . Using Eqs. (E.20)-(E.26) one obtains asymptotically

$$\begin{aligned} I_2^{(\ell, \infty)}_{(d_w, \ell)} &= \frac{A_f \pi A_1}{4} \left( \frac{\xi \pi}{2} - \xi \int_0^\infty dy \frac{\exp(-y/\xi)}{y^2 + 1} - \int_0^\infty dy \frac{y \exp(-y/\xi)}{y^2 + 1} \right) \\ &+ \frac{A_f \xi \pi B_2}{6\ell^3} \exp(-d_w/\xi) + \mathcal{O}\left(\frac{1}{\ell^4}\right). \end{aligned} \quad (\text{E.30})$$

Similarly,  $I_2^{(\infty, \ell)}$  can be written as (see Eqs. (4.24) and (E.18))

$$\begin{aligned}
I_2^{(\infty, \ell)} &= \int_{\ell}^{\infty} dz \frac{\pi A_f}{4} \left[ \arctan(z-d_w) + \frac{z-d_w}{(z-d_w)^2+1} - \arctan(z-\ell) - \frac{z-\ell}{(z-\ell)^2+1} \right] \times \\
&\quad \times \left[ B_l - A_l \exp(2\ell/\xi) \right] \exp(-z/\xi) \\
&= \frac{\pi A_f}{4} \left[ B_l - A_l \exp(2\ell/\xi) \right] \left[ \xi \arctan(\ell - d_w) \exp(-\ell/\xi) \right. \\
&\quad + \xi \exp(-d_w/\xi) \int_{\ell-d_w}^{\infty} dy \frac{\exp(-y/\xi)}{y^2+1} + \exp(-d_w/\xi) \int_{\ell-d_w}^{\infty} dy \frac{y \exp(-y/\xi)}{y^2+1} \\
&\quad \left. - \xi \exp(-\ell/\xi) \int_0^{\infty} dy' \frac{\exp(-y'/\xi)}{y'^2+1} - \exp(-\ell/\xi) \int_0^{\infty} dy' \frac{y' \exp(-y'/\xi)}{y'^2+1} \right], \tag{E.31}
\end{aligned}$$

where the integration variables have been changed to  $y = z-d_w$  and  $y' = z-\ell$ , respectively. Using Eqs. (E.20)-(E.26), this leads to the asymptotic behavior

$$\begin{aligned}
I_2^{(\infty, \ell)} &= -\frac{A_f \pi A_1}{4} \left( \frac{\xi \pi}{2} - \xi \int_0^{\infty} dy \frac{\exp(-y/\xi)}{y^2+1} - \int_0^{\infty} dy \frac{y \exp(-y/\xi)}{y^2+1} \right) \\
&\quad + \frac{\pi A_f \xi A_1}{6\ell^3} + \mathcal{O}\left(\frac{1}{\ell^4}\right). \tag{E.32}
\end{aligned}$$

Integrals of the type  $I_3$  can be written as (see Eqs. (4.24) and Eqs. (E.2))

$$\begin{aligned}
I_3^{(\ell, \ell)} &= \frac{A_f \pi}{2} \left\{ A_l^2 \int_{d_w}^{\ell} dz \int_{d_w}^{\ell} dz' \frac{\exp(z/\xi) \exp(z'/\xi)}{[(z-z')^2+1]^2} \right. \\
&\quad + 2A_l B_l \int_{d_w}^{\ell} dz \int_{d_w}^{\ell} dz' \frac{\exp(z/\xi) \exp(-z'/\xi)}{[(z-z')^2+1]^2} \\
&\quad \left. + B_l^2 \int_{d_w}^{\ell} dz \int_{d_w}^{\ell} dz' \frac{\exp(-z/\xi) \exp(-z'/\xi)}{[(z-z')^2+1]^2} \right\}, \tag{E.33}
\end{aligned}$$

$$I_3^{(\infty, \infty)} = \frac{A_f \pi}{2} B_g^2 \int_{\ell}^{\infty} dz \int_{\ell}^{\infty} dz' \frac{\exp(-z/\xi) \exp(-z'/\xi)}{[(z-z')^2+1]^2}, \tag{E.34}$$

$$\begin{aligned}
I_3^{(\ell, \infty)} &= \frac{A_f \pi}{2} \left\{ A_l B_g \int_{d_w}^{\ell} dz \int_{\ell}^{\infty} dz' \frac{\exp(z/\xi) \exp(-z'/\xi)}{[(z-z')^2+1]^2} \right. \\
&\quad \left. + B_l B_g \int_{d_w}^{\ell} dz \int_{\ell}^{\infty} dz' \frac{\exp(-z/\xi) \exp(-z'/\xi)}{[(z-z')^2+1]^2} \right\}, \tag{E.35}
\end{aligned}$$

and

$$\begin{aligned} \mathbf{I}_3^{(\infty, \ell)} = \frac{A_f \pi}{2} \left\{ A_l B_g \int_{\ell}^{\infty} dz \int_{d_w}^{\ell} dz' \frac{\exp(-z/\xi) \exp(z'/\xi)}{[(z-z')^2 + 1]^2} \right. \\ \left. + B_l B_g \int_{\ell}^{\infty} dz \int_{d_w}^{\ell} dz' \frac{\exp(-z/\xi) \exp(-z'/\xi)}{[(z-z')^2 + 1]^2} \right\}, \end{aligned} \quad (\text{E.36})$$

with  $\mathbf{I}_3^{(\ell, \infty)} = \mathbf{I}_3^{(\infty, \ell)}$ . The double integrals can be reduced to single ones as follows:

$$\begin{aligned} \int_{u_1}^{u_2} dz \int_{v_1}^{v_2} dz' \frac{\exp(z/\xi) \exp(z'/\xi)}{[(z-z')^2 + 1]^2} &= \int_{u_1}^{u_2} dz \exp(2z/\xi) \int_{v_1}^{v_2} dz' \frac{\exp((z'-z)/\xi)}{[(z-z')^2 + 1]^2} \\ &\stackrel{(y:=z'-z)}{=} \int_{u_1}^{u_2} dz \exp(2z/\xi) \int_{v_1-z}^{v_2-z} dy \frac{\exp(y/\xi)}{[y^2 + 1]^2} \\ &= \frac{\xi}{2} \left[ \exp(2z/\xi) \int_{v_1-z}^{v_2-z} dy \frac{\exp(y/\xi)}{[y^2 + 1]^2} \right] \Big|_{z=u_1}^{z=u_2} \\ &\quad - \frac{\xi}{2} \int_{u_1}^{u_2} dz \exp(2z/\xi) \left[ -\frac{\exp((v_2-z)/\xi)}{[(v_2-z)^2 + 1]^2} \right. \\ &\quad \left. + \frac{\exp((v_1-z)/\xi)}{[(v_1-z)^2 + 1]^2} \right] \\ &\stackrel{(y:=z-v_2,1)}{=} \frac{\xi}{2} \left[ \exp(2z/\xi) \int_{v_1-z}^{v_2-z} dy \frac{\exp(y/\xi)}{[y^2 + 1]^2} \right] \Big|_{z=u_1}^{z=u_2} \\ &\quad + \frac{\xi}{2} \left[ \exp(2z/\xi) \int_{u_1-z}^{u_2-z} dy \frac{\exp(y/\xi)}{(y^2 + 1)^2} \right] \Big|_{z=v_1}^{z=v_2}, \end{aligned} \quad (\text{E.37})$$

$$\begin{aligned} \int_{u_1}^{u_2} dz \int_{v_1}^{v_2} dz' \frac{\exp(-z/\xi) \exp(-z'/\xi)}{[(z-z')^2 + 1]^2} &= -\frac{\xi}{2} \left[ \exp(-2z/\xi) \int_{v_1-z}^{v_2-z} dy \frac{\exp(-y/\xi)}{(y^2 + 1)^2} \right] \Big|_{z=u_1}^{z=u_2} \\ &\quad - \frac{\xi}{2} \left[ \exp(-2z/\xi) \int_{u_1-z}^{u_2-z} dy \frac{\exp(-y/\xi)}{(y^2 + 1)^2} \right] \Big|_{z=v_1}^{z=v_2}, \end{aligned} \quad (\text{E.38})$$

and

$$\begin{aligned}
\int_{u_1}^{u_2} dz \int_{v_1}^{v_2} dz' \frac{\exp(z/\xi) \exp(-z'/\xi)}{[(z-z')^2+1]^2} &= \left[ z \int_{v_1-z}^{v_2-z} dy \frac{\exp(-y/\xi)}{[y^2+1]^2} \right] \Big|_{z=u_1}^{z=u_2} \\
&+ \left[ \int_{u_1-z}^{u_2-z} dy (y+z) \frac{\exp(y/\xi)}{[y^2+1]^2} \right] \Big|_{z=v_1}^{z=v_2} \\
&= \left[ z \int_{v_1-z}^{v_2-z} dy \frac{\exp(-y/\xi)}{[y^2+1]^2} \right] \Big|_{z=u_1}^{z=u_2} \\
&+ \left[ z \int_{u_1-z}^{u_2-z} dy \frac{\exp(y/\xi)}{[y^2+1]^2} \right] \Big|_{z=v_1}^{z=v_2} \\
&+ \left[ \int_{u_1-z}^{u_2-z} dy \frac{y \exp(y/\xi)}{[y^2+1]^2} \right] \Big|_{z=v_1}^{z=v_2}.
\end{aligned} \tag{E.39}$$

Inserting these expressions into Eqs. (E.33)-(E.35) leads to

$$\begin{aligned}
I_{3(d_w, d_w)}^{(\ell, \ell)} &= \frac{A_f \pi}{2} \left\{ A_l^2 \xi \left[ \exp(2\ell/\xi) \int_0^{\ell-d_w} dy \frac{\exp(-y/\xi)}{(y^2+1)^2} - \exp(2d_w/\xi) \int_0^{\ell-d_w} dy \frac{\exp(y/\xi)}{(y^2+1)^2} \right] \right. \\
&+ 2A_l B_l \left[ (\ell-d_w) \left( \int_0^{\ell-d_w} dy \frac{\exp(-y/\xi)}{(y^2+1)^2} + \int_0^{\ell-d_w} dy \frac{\exp(y/\xi)}{(y^2+1)^2} \right) \right. \\
&- \left. \left. \int_0^{\ell-d_w} dy \frac{y \exp(-y/\xi)}{(y^2+1)^2} - \int_0^{\ell-d_w} dy \frac{y \exp(y/\xi)}{(y^2+1)^2} \right] \right. \\
&+ \left. B_l^2 \xi \left[ -\exp(-2\ell/\xi) \int_0^{\ell-d_w} dy \frac{\exp(y/\xi)}{(y^2+1)^2} + \exp(-2d_w/\xi) \int_0^{\ell-d_w} dy \frac{\exp(-y/\xi)}{(y^2+1)^2} \right] \right\}, \tag{E.40}
\end{aligned}$$

$$I_{3(\ell, \ell)}^{(\infty, \infty)} = \frac{A_f \pi}{2} B_g^2 \xi \exp(-2\ell/\xi) \int_0^\infty dy \frac{\exp(-y/\xi)}{(y^2+1)^2}, \tag{E.41}$$

and

$$\begin{aligned}
I_{3(d_w, \ell)}^{(\ell, \infty)} &= \frac{A_f \pi}{2} \left\{ A_l B_g \left[ \ell \left( \int_0^\infty dy \frac{\exp(-y/\xi)}{(y^2+1)^2} - \int_0^{\ell-d_w} dy \frac{\exp(-y/\xi)}{(y^2+1)^2} \right) \right. \right. \\
&+ \left. \int_0^{\ell-d_w} dy \frac{y \exp(-y/\xi)}{(y^2+1)^2} - d_w \int_{\ell-d_w}^\infty dy \frac{\exp(-y/\xi)}{(y^2+1)^2} \right] \\
&+ B_l B_g \frac{\xi}{2} \left[ \exp(-2d_w/\xi) \int_{\ell-d_w}^\infty dy \frac{\exp(-y/\xi)}{(y^2+1)^2} \right. \\
&+ \left. \left. \exp(-2\ell/\xi) \left( \int_0^{\ell-d_w} dy \frac{\exp(y/\xi)}{(y^2+1)^2} - \int_0^\infty dy \frac{\exp(-y/\xi)}{(y^2+1)^2} \right) \right] \right\}. \tag{E.42}
\end{aligned}$$

Note the following relations:

$$\begin{aligned}
A_l^2 &= A_1^2 \exp(-2\ell/\xi) \\
A_l B_l &= A_1 B_1 \exp(-2\ell/\xi) + A_1 B_2 \exp(-\ell/\xi) \\
A_l B_g &= A_1 B_1 \exp(-2\ell/\xi) + A_1 B_2 \exp(-\ell/\xi) - A_1^2 \\
B_l^2 &= B_1^2 \exp(-2\ell/\xi) + 2B_1 B_2 \exp(-\ell/\xi) + B_2^2 \\
B_l B_g &= B_1^2 \exp(-2\ell/\xi) + 2B_1 B_2 \exp(-\ell/\xi) - A_1 B_2 \exp(\ell/\xi) + B_2^2 - A_1 B_1 \\
B_g^2 &= B_1^2 \exp(-2\ell/\xi) + 2B_1 B_2 \exp(-\ell/\xi) - 2A_1 B_2 \exp(\ell/\xi) \\
&\quad + A_1^2 \exp(2\ell/\xi) + B_2^2 - 2A_1 B_1.
\end{aligned} \tag{E.43}$$

Accordingly one obtains

$$\begin{aligned}
&\frac{1}{2} \left( \mathbf{I}_3^{(\ell,\ell)} + \mathbf{I}_3^{(\ell,\infty)} + \mathbf{I}_3^{(\infty,\ell)} + \mathbf{I}_3^{(\infty,\infty)} \right) \\
&= \frac{A_f \pi}{2} \left\{ \frac{A_l^2 \xi}{2} \left[ \exp(2\ell/\xi) \int_0^{\ell-d_w} dy \frac{\exp(-y/\xi)}{(y^2+1)^2} \right. \right. \\
&\quad \left. \left. - \exp(2d_w/\xi) \int_0^{\ell-d_w} dy \frac{\exp(y/\xi)}{(y^2+1)^2} \right] \right. \\
&\quad \left. - A_1^2 \left[ (\ell-d_w) \int_{\ell-d_w}^{\infty} dy \frac{\exp(-y/\xi)}{(y^2+1)^2} + \int_0^{\ell-d_w} dy \frac{y \exp(-y/\xi)}{(y^2+1)^2} \right] \right. \\
&\quad \left. + A_l B_l \left[ (\ell-d_w) \int_{d_w-\ell}^{\infty} dy \frac{\exp(-y/\xi)}{(y^2+1)^2} - \int_0^{\ell-d_w} dy \frac{y \exp(y/\xi)}{(y^2+1)^2} \right] \right. \\
&\quad \left. + \frac{B_l^2 \xi}{2} \exp(-2d_w/\xi) \int_0^{\infty} dy \frac{\exp(-y/\xi)}{(y^2+1)^2} \right. \\
&\quad \left. + (-A_1 B_1 - A_1 B_2 \exp(\ell/\xi)) \frac{\xi}{2} \times \right. \\
&\quad \left. \times \left[ \exp(-2d_w/\xi) \int_{\ell-d_w}^{\infty} dy \frac{\exp(-y/\xi)}{(y^2+1)^2} \right. \right. \\
&\quad \left. \left. + \exp(-2\ell/\xi) \int_0^{\ell-d_w} dy \frac{\exp(y/\xi)}{(y^2+1)^2} \right] \right. \\
&\quad \left. + \frac{\xi}{2} (A_1^2 \exp(2\ell/\xi) - A_1 B_2 \exp(\ell/\xi) - A_1 B_1) \times \right. \\
&\quad \left. \times \exp(-2\ell/\xi) \int_0^{\infty} dy \frac{\exp(-y/\xi)}{(y^2+1)^2} \right\}.
\end{aligned} \tag{E.44}$$

In order to determine the asymptotic behavior of the integrals in Eqs. (E.40)-(E.42) we repeatedly integrate by parts so that

$$\begin{aligned} \int_0^{\ell-d_w} dy \frac{\exp(y/\xi)}{(y^2+1)^2} &= \frac{\xi \exp((\ell-d_w)/\xi)}{((\ell-d_w)^2+1)^2} - \xi + \xi \int_0^{\ell-d_w} \frac{4y}{(y^2+1)^3} \exp(y/\xi), \\ &= \frac{\xi \exp((\ell-d_w)/\xi)}{\ell^4} + \mathcal{O}(\ell^{-5} \exp(\ell/\xi)), \quad \ell \gg 1, \end{aligned} \quad (\text{E.45})$$

$$\int_0^{\ell-d_w} dy \frac{\exp(-y/\xi)}{(y^2+1)^2} = \int_0^\infty dy \frac{\exp(-y/\xi)}{(y^2+1)^2} - \int_{\ell-d_w}^\infty dy \frac{\exp(-y/\xi)}{(y^2+1)^2} \quad (\text{E.46})$$

with

$$\begin{aligned} \int_{\ell-d_w}^\infty dy \frac{\exp(-y/\xi)}{(y^2+1)^2} &= \frac{\xi \exp(-(\ell-d_w)/\xi)}{((\ell-d_w)^2+1)^2} - \xi \int_{\ell-d_w}^\infty \frac{4y}{(y^2+1)^3} \exp(-y/\xi) \\ &= \frac{\xi \exp(-(\ell-d_w)/\xi)}{\ell^4} + \mathcal{O}(\ell^{-5} \exp(-\ell/\xi)), \quad \ell \gg d_w, \end{aligned} \quad (\text{E.47})$$

and

$$\begin{aligned} \int_{d_w-\ell}^\infty dy \frac{\exp(-y/\xi)}{(y^2+1)^2} &= \frac{\xi \exp((\ell-d_w)/\xi)}{((\ell-d_w)^2+1)^2} - \xi \int_{d_w-\ell}^\infty \frac{4y}{(y^2+1)^3} \exp(-y/\xi) \\ &= \frac{\xi \exp((\ell-d_w)/\xi)}{\ell^4} + \mathcal{O}(\ell^{-5} \exp(\ell/\xi)), \quad \ell \gg d_w. \end{aligned} \quad (\text{E.48})$$

Finally, collecting the leading terms for  $\ell \rightarrow \infty$  one obtains the asymptotic behavior

$$\begin{aligned} &\frac{1}{2} \left( \text{I}_3^{(\ell,\ell)} + \text{I}_3^{(\ell,\infty)} + \text{I}_3^{(\infty,\ell)} + \text{I}_3^{(\infty,\infty)} \right) \\ &= \frac{A_f \pi \xi}{2} \left( A_1^2 + \frac{B_2^2 \exp\left(-\frac{2d_w}{\xi}\right)}{2} \right) \int_0^\infty dy \frac{\exp\left(-\frac{y}{\xi}\right)}{(y^2+1)^2} \\ &\quad - \frac{A_f \pi A_1^2}{2} \left( \frac{1}{2} - \frac{1}{2\xi} \int_0^\infty dy \frac{\exp(-y/\xi)}{y^2+1} \right) + \mathcal{O}\left(\frac{1}{\ell^4}\right). \end{aligned} \quad (\text{E.49})$$

Inserting the results for these integrals (see Eqs. (E.14), (E.15), (E.27), (E.28), (E.30), (E.32), and (E.49)) into Eq. (E.1), one obtains the effective interface potential  $\omega(\ell) = \Omega_{s,lr}(\ell) - \Omega_{s,lr}(\infty)$  given by Eq. (4.58); the index  $lr$  refers to *long-ranged* interactions (Sec. 4.2).



# Appendix F

## Line tension calculation in the lattice model

For the line tension calculation, a box that cuts perpendicularly through all the interfaces has been used (Fig. F.1). As discussed in Ref. [149] this type of box ensures that artificial contributions that scale with the contact line length  $L$  due to the edges of the boxes or to inhomogeneities caused by the boundaries do not arise. However in a lattice model, depending on the contact angle, the boundary that cuts through the liquid-gas interface crosses some of the cells leaving just a fraction of them inside the integration box. In order to calculate the contribution of such cells to the total grand canonical energy in Eq. (6.1) the contribution to the energy if the cell were completely included inside the boundary was multiplied by the fraction of the volume of the cell that is actually inside the box. Moreover the value of the line tension has been computed by using the change in the total grand canonical energy when the size of the box is changed. This is done because the lattice model underneath our calculation creates a dependence of the liquid-gas free interface  $\gamma_{l,g}$  on the contact angle  $\vartheta$  when such interface is tilted as in Fig. F.1 due to the mismatch with the lattice grid underneath.

Consider the configuration shown Fig. F.1. The grand canonical energy per unit length can be written as (see Eq. (2.22))

$$\frac{\Omega^{(1)}}{L} = \Omega_b A^{(1)} + \gamma_{l,g}(\vartheta) \frac{z_1}{\cos \vartheta} + \gamma_{s,l} L_{s,l}^{(1)} + \gamma_{s,g} L_{s,g}^{(1)} + \tau \quad (\text{F.1})$$

for the dashed line box (1) that cuts the liquid-gas interface at the coordinate point  $(x_1, z_1)$  marked by a dot and the number (1) in Fig. F.1. Here  $A^{(1)} = A^{(1)} a^2$  is the area of the dashed line box, such that  $V = A^{(1)} L$  is the volume of the fluid inside the box and  $L_{s,l}^{(1)} = L_{s,l}^{(1)} a$  and  $L_{s,g}^{(1)} = L_{s,g}^{(1)} a$  are the linear extensions of the substrate-liquid and

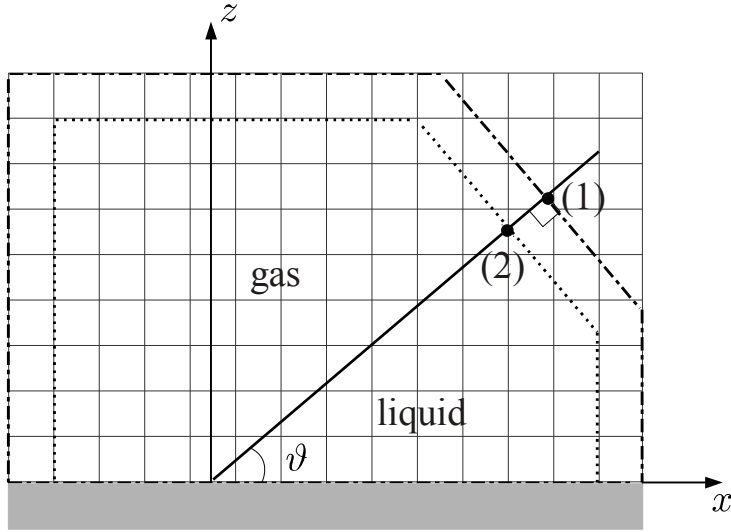


Figure F.1: Geometry for the calculation of the line tension. The Euler-Lagrange equations in Eq. (6.5) are solved via an iterative algorithm in a rectangular box. However, for the calculation of the line tension a box (dashed and dotted lines) that cuts perpendicularly through all the interfaces and encloses the three-phase contact line has been used. The dots (1) and (2) mark the coordinate points  $(x_1, z_1)$  and  $(x_2, z_2)$ , respectively, where the integration boxes intersect the liquid-gas interface. The system is translationally invariant in the  $y$ -direction. Note that the boundary cutting through the liquid-gas interface crosses some of the cells leaving just a fraction of each of them inside the integration box. The contribution of these cells to the total grand canonical energy was computed by multiplying the total contribution of each of these cells by the volume of the cell that is inside the integration box.

substrate-gas interfaces in the  $x$ -direction. Analogously for the dotted line box (2) one has

$$\frac{\Omega^{(2)}}{L} = \Omega_b A^{(2)} + \gamma_{l,g}(\vartheta) \frac{z_2}{\cos \vartheta} + \gamma_{s,l} L_{s,l}^{(2)} + \gamma_{s,g} L_{s,g}^{(2)} + \tau \quad (\text{F.2})$$

Calculating  $\frac{\Delta\Omega}{L\Delta z} = \frac{\Omega^{(1)} - \Omega^{(2)}}{L(z_1 - z_2)}$  one has

$$\frac{\Delta\Omega}{L\Delta z} = \Omega_b \frac{\Delta A}{\Delta z} + \frac{\gamma_{l,g}(\vartheta)}{\cos \vartheta} + \gamma_{s,l} \frac{\Delta L_{s,l}}{\Delta z} + \gamma_{s,g} \frac{\Delta L_{s,g}}{\Delta z}, \quad (\text{F.3})$$

where  $\Delta L_{s,l} = L_{s,l}^{(1)} - L_{s,l}^{(2)}$ ,  $\Delta L_{s,g} = L_{s,g}^{(1)} - L_{s,g}^{(2)}$ , and  $\Delta A = A^{(1)} - A^{(2)}$ . Finally, the line tension is obtained as

$$\tau = \frac{\Omega^{(1)}}{L} - \Omega_b A^{(1)} - z_1 \frac{\Delta\Omega}{\Delta z} + z_1 \Omega_b \frac{\Delta A}{\Delta z} + z_1 \gamma_{s,l} \frac{\Delta L_{s,l}}{\Delta z} + z_1 \gamma_{s,g} \frac{\Delta L_{s,g}}{\Delta z} - \gamma_{s,l} L_{s,l}^{(1)} - \gamma_{s,g} L_{s,g}^{(1)} \quad (\text{F.4})$$

The line tension  $\tau$  was calculated by fixing the intersection of box (1) with the liquid-

gas interface at a value  $\bar{z}_1 = z_1/a \in [30, 40]$  for the pure solvent and  $\bar{z}_1 \in [70, 80]$  for the electrolyte solution and varying the size of box (2) accordingly such that  $\Delta\bar{z} = 1 - 15$ . The procedure is repeated for all  $\bar{z}_1$  integers in the corresponding intervals for the pure solvent and the electrolyte solution. The values of  $L_{s,l}$  and  $L_{s,g}$  are calculated by using the coordinate where the asymptote of the gas-liquid interface intersects the plane  $z = 0$  (see Chap. 6). The size of the rectangular box used to find the equilibrium profiles depends on the contact angle  $\vartheta$ , i.e., for small contact angles a larger extension in the  $x$ -direction is needed. For the pure solvent the smaller size used was  $\bar{L}_x \times \bar{L}_y = 300 \times 60$ , while the bigger was  $1500 \times 60$ . For the electrolyte solution a fixed box size of  $400 \times 100$  was used. Figure F.2 shows the calculated values for the line tension using the above described procedure for the electrolyte solution with  $I = 3.9 \times 10^{-5}$  ( $\tilde{I} = 1mM$ ),  $T^* = 0.8T_c^*$ ,  $u_w/u = 0.69$ , and for two different values of the surface charges density:  $\sigma = 5 \times 10^{-4}$  ( $\tilde{\sigma} = 0.05\mu C/cm^2$ ) (Fig. F.2 (a)) and  $\sigma = 1.8 \times 10^{-3}$  ( $\tilde{\sigma} = 0.18\mu C/cm^2$ ) ( Fig. F.2(b)). One can see that the calculated line tension depends on the size of both integration boxes, i.e, on the coordinates  $(x_1, z_1)$  and  $(x_2, z_2)$  where these boxes intersect the liquid-gas interface (see Fig. F.1), nevertheless the values seem to be distributed around a particular value. In order to determined the value of what in Chap. 6 is called the line tension, the value of  $\Delta\bar{z}$  that produces the smallest variation in the calculated value of the line tension for different  $\bar{z}_1$  is chosen and  $\tau$  is taken to be the mean between the smallest and the largest values of the calculated line tension for that particular  $\Delta\bar{z}$ . Note that the amplitude of the variations in the line tension values increase with increasing  $\sigma$ , i.e., with decreasing contact angle  $\vartheta$ , this can be inferred from the different scale in the vertical axes of Fig. F.2 (a) and (b). The behavior is similar for the other values of the surface charge density considered in Chap. 6. When the surface charge is fixed and the contact angle  $\vartheta$  is changed by changing the temperature, the amplitude of the variations in the value of  $\tau$  increase with increasing temperature  $T^*$ , i.e, with decreasing contact angle  $\vartheta$ .

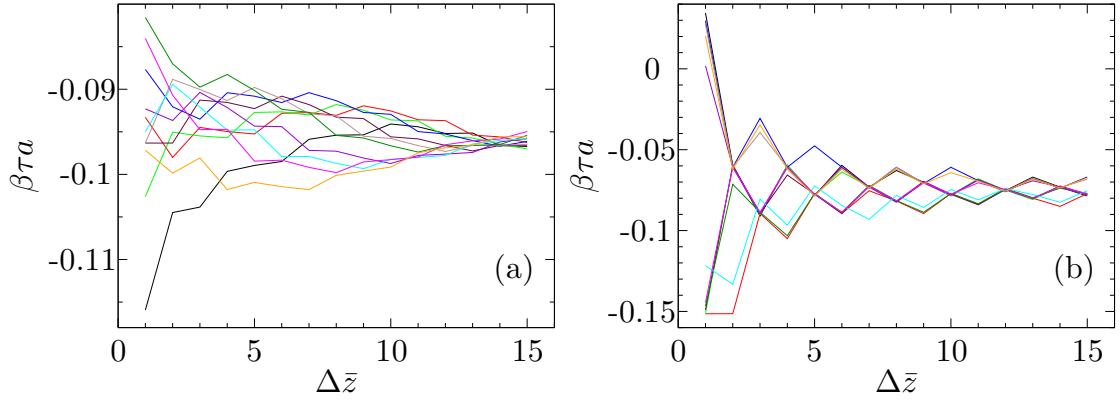


Figure F.2: Line tension  $\tau$  values for an electrolyte solution with  $I = 3.9 \times 10^{-5}$  ( $\tilde{I} = 1mM$ ) at  $T^* = 0.8T_c^*$  for  $\sigma = 5 \times 10^{-4}$  ( $\tilde{\sigma} = 0.05\mu\text{C}/\text{cm}^2$ ) (a) and  $\sigma = 1.8 \times 10^{-3}$  ( $\tilde{\sigma} = 0.18\mu\text{C}/\text{cm}^2$ ) (b). Different colors correspond to different sizes of box (1) in Fig. F.1, i.e., they correspond to different coordinates of the point  $(x_1, z_1)$  where the boundary of the box intersects the liquid-gas interface. The line tension calculated using Eq. (F.4) is plotted as a function of  $\Delta\bar{z} = z_1/a - z_2/a$ , where  $a$  is the lattice constant.

# Bibliography

- [1] P. G. de Gennes, *Rev. Mod. Phys.* **57**, 827 (1985).
- [2] S. Dietrich, in *Phase Transitions and Critical Phenomena*, edited by C. Domb and J. L. Lebowitz (Academic, London, 1988), Vol. 12, p. 1.
- [3] M. Schick, in *Liquids at interfaces*, edited by J. Charvolin, J. F. Joanny, and J. Zinn-Justin (North-Holland, Amsterdam, 1988), p. 415.
- [4] D. Bonn and D. Ross, *Rep. Prog. Phys.* **64**, 1085 (2001).
- [5] D. Bonn, J. Eggers, J. Indekeu, J. Meunier, and E. Rolley, *Rev. Mod. Phys.* **81**, 739 (2009).
- [6] F. Mugele and J.-C. Baret, *J. Phys.: Condensed Matter* **17**, R705 (2005).
- [7] V. Srinivasan, V. K. Pamula, and R. B. Fair, *Lab Chip* **4**, 310 (2004).
- [8] S. K. Cho, H. J. Moon, and C. J. Kim, *J. Microelectromech. Syst.* **12**, 70 (2003).
- [9] B. Berge and J. Peseux, *Eur. Phys. J. E* **3**, 159 (2000).
- [10] R. A. Hayes and B. J. Feenstra, *Nature* **425**, 383 (2003).
- [11] J. N. Israelachvili, *Intermolecular and surface forces*, 2nd ed. (Academic Press, 1991).
- [12] I. Langmuir, *Science* **88**, 430 (1938).
- [13] A. C. Hall, *J. Phys. Chem.* **74**, 2742 (1970).
- [14] B. Derjaguin and N. Churaev, *J. Colloid Interf. Sci.* **49**, 249 (1974).
- [15] R. F. Kayser, *Phys. Rev. Lett.* **56**, 1831 (1986).
- [16] R. Kayser, *J. Phys. (France)* **49**, 1027 (1988).

- [17] N. A. Denesyuk and J.-P. Hansen, *Europhys. Lett.* **63**, 261 (2003).
- [18] N. A. Denesyuk and J.-P. Hansen, *J. Chem. Phys.* **121**, 3613 (2004).
- [19] A. Oleksy and J.-P. Hansen, *Mol. Phys.* **107**, 2609 (2009).
- [20] A. Oleksy and J.-P. Hansen, *J. Chem. Phys.* **132**, 204702 (2010).
- [21] M. Bier, A. Gambassi, and S. Dietrich, *J. Chem. Phys.* **137**, 034504 (2012).
- [22] S. Arrhenius, *Z. Phys. Chem.* **1**, 631 (1887).
- [23] P. W. Debye and E. Hückel, *Physik. Z.* **24**, 185 (1923).
- [24] J. G. Kirkwood and J.C. Poirier, *J. Phys. Chem.* **58**, 591 (1954).
- [25] D.A. McQuarrie, *Statistical mechanics* (Universal Science Books, Sausalito, 2000).
- [26] T. H. Gronwall, V. K. LaMer and K. Sandved, *Physik. Z.* **29**, 358 (1928).
- [27] V. K. LaMer, T. H. Gronwall, L. J. Greiff, *J. Phys. Chem.* **35**, 2245 (1931).
- [28] N. Bjerrum, *Kgl. Dan. Vidensk. Selsk. Mat.-fys. Medd.* **7**, 1 (1926).
- [29] Y. Levin, *Rep. Prog. Phys.* **65**, 1577 (2002).
- [30] L. S. Ornstein and F. Zernike, *Proc. Akad. Sci* **17**, 793 (1914).
- [31] J.-P. Hansen and I.R. McDonald, *Theory of simple liquids*, 3rd ed. (Academic Press, 2006).
- [32] E. Waisman and J. L. Lebowitz, *J. Chem. Phys.* **52**, 4307 (1970).
- [33] E. Waisman and J. L. Lebowitz, *J. Chem. Phys.* **56**, 3086 (1972).
- [34] E. Waisman and J. L. Lebowitz, *J. Chem. Phys.* **56**, 3093 (1972).
- [35] J. L. Lebowitz and J. K. Percus, *Phys. Rev.* **144**, 251 (1966).
- [36] J. S. Høye, J. L. Lebowitz and G. Stell, *J. Chem. Phys.* **61**, 3253 (1974).
- [37] R. J. Fino Leote De Carvalho and R. Evans, *Mol. Phys.* **83**, 619 (1994).
- [38] J. C. Rasaiah and H. L. Friedman, *J. Chem. Phys.* **48**, 2742 (1968).
- [39] P. N. Vorontsov-Veliaminov, A. M. Eliashevich, J. C. Rasaiah and H. L. Friedman, *J. Chem. Phys.* **52**, 1013 (1970).

- [40] A. L. Kholodenko and A. L. Beyerlein, *Phys. Rev. A* **34**, 3309 (1986).
- [41] R. R. Netz and H. Orland, *Europhys. Lett.* **45**, 726 (1999).
- [42] R. R. Netz and H. Orland, *Eur. Phys. J. E* **1**, 203 (2000).
- [43] J.-M. Caillol, *Mol. Phys.* **103**, 1271 (2005).
- [44] A. Ciach and G. Stell, *Int. J. Mod. Phys. B* **19**, 3309 (2005).
- [45] G. Stell, K.C. Wu, and B. Larsen, *Phys. Rev. Lett.* **37**, 1369 (1976).
- [46] M. E. Fisher and Y. Levin, *Phys. Rev. Lett.* **71**, 3826 (1993).
- [47] G. Stell, *J. Stat. Phys.* **78**, 197 (1995).
- [48] Y. Levin and M. E. Fisher, *Physica A* **225**, 164 (1996).
- [49] J.W. Johnson and D. Cubicciotti, *J. Phys. Chem.* **68**, 2235 (1964).
- [50] K.S. Pitzer, M.C.P. de Lima, and D.R. Schreiber, *J. Phys. Chem.* **89**, 1854 (1985).
- [51] M. L. Japas , J. M. H. Levelt. Sengers, *J. Phys. Chem.* **94**, 5361 (1990).
- [52] R. R. Singh and K. S. Pitzer, *J. Chem. Phys.* **92**, 6775 (1990).
- [53] W. Schröer, *Contrib. Plasm. Phys.* **52**, 78 (2012).
- [54] D. N. Card and J. P. Valleau, *J. Chem. Phys.* **52**, 6232 (1970).
- [55] J. C. Rasaiah, D. N. Card and J. P. Valleau, *J. Chem. Phys.* **56**, 248 (1972)
- [56] J.-M. Caillol, D. Levesque and J.-J. Weis, *J. Chem. Phys.* **116**, 10794 (2002).
- [57] Q. Yan and J. J. de Pablo, *J. Chem. Phys.* **116** , 2967 (2002).
- [58] Y. C. Kim, M. E. Fisher, and A. Z. Panagiotopoulos, *Phys. Rev. Lett.* **95**, 195703 (2005).
- [59] D.M. Heyes, *Chem. Phys.* **69**, 155 (1982).
- [60] S.-H. Suh, L. Mier-y-Teran, H.S. White, and H.T. Davis, *Chem. Phys.* **142**, 203 (1990).
- [61] S.-H. Suh, J.-W. Park, K.-R Ha, S.-C. Kim, and J. M. D. Macelroy, *Mol. Simul.* **27**, 387 (2001).

- [62] A. Z. Panagiotopoulos, *J. Phys.: Condens. Matter* **17**, S3205 (2005).
- [63] M. Gouy, *J. Phys.* **4**, 947 (1910).
- [64] D. L. Chapman, *Philos. Mag.* **25**, 475 (1913).
- [65] O. Stern, *Z. Elektrochem.* **30**, 508 (1924).
- [66] *J. Am. Chem. Soc.* **76**, 4819 (1990).
- [67] R. Parsons *Chem. Rev.* **90**, 813 (1990).
- [68] A. J. Bard and L. R. Faulkner, *Electrochemical Methods: Fundamentals and Applications*, 2nd ed. (Wiley, 2000).
- [69] C. W. Outhwaite and L. B. Bhuiyan *J. Chem. Soc. Faraday Trans. II* **79**, 707 (1983).
- [70] S. L. Carnie and G. M. Torrie, *Adv. Chem. Phys.* **56**, 141 (1984).
- [71] L. Mier-y-Teran, S.H. Suh, H.S. White, H.T. Davis, *J. Chem. Phys.* **92**, 5087 (1990).
- [72] L. Mier-y-Teran, Z. Tang, H.T. Davis, L.E. Scriven, H.S. White, *Mol. Phys.* **72**, 817 (1991).
- [73] E. Kierlik and M. L. Rosinberg, *Phys. Rev. A* **44**, 5025 (1991).
- [74] C. N. Patra and S.K. Ghosh, *Phys. Rev. E* **47**, 4088 (1993).
- [75] C. N. Patra and S.K. Ghosh, *J. Chem. Phys.* **100**, 5219 (1994).
- [76] C. N. Patra and S.K. Ghosh, *J. Chem. Phys.* **117**, 8938 (2002).
- [77] T. Goela, C. N. Patra, S. K. Ghosh and T. Mukherjee, *Mol. Phys.* **107**, 19 (2009)
- [78] L. Blum, *Adv. Chem. Phys.* **78**, 171 (1990).
- [79] G. M. Torrie and J. P. Valleau, *Chem. Phys. Lett.* **65**, 343 (1979).
- [80] G. M. Torrie and J. P. Valleau, *J. Chem. Phys.* **73**, 5807 (1980).
- [81] G. M. Torrie and J. P. Valleau, *J. Phys. Chem.* **86**, 3251 (1982).
- [82] D. Boda, W. R. Fawcett, D. Henderson and S. Sokoowski, *J. Chem. Phys.* **116**, 7170 (2002).
- [83] R. R. Netz, *Eur. Phys. J. E* **5**, 189 (2001).



- [84] A. G. Moreira and R. R. Netz, in *Electrostatic effects in soft matter and biophysics*, edited by C. Holm, P. Kékicheff and R. Podgornik (Springer, 2001), p. 367.
- [85] R. D. Rogers, K. R. Seddon, and S. Volkov, Eds. *Green Industrial Applications of Ionic Liquids* (Springer, 2003).
- [86] P. Wasserscheid and T. Welton, Eds. *Ionic Liquids in Synthesis* (Wiley-VCH, Weinheim, Germany, 2007).
- [87] A. A. Koornyshev, *J. Phys. Chem. B* **111**, 5545 (2007).
- [88] M.V. Fedorov and A.A. Kornyshev, *Electrochim. Acta* **53**, 6835 (2008)
- [89] M. Trulsson, J. Algotsson, J. Forsman and C. E. Woodward, *J. Phys. Chem. Lett.* **1**, 1191 (2010).
- [90] M. Z. Bazant, B. D. Storey, and A. A. Kornyshev, *Phys. Rev. Lett.* **106**, 046102 (2011).
- [91] M.T. Alam, M.M. Islam, T. Okajima, and T. Ohsaka, *J. Phys. Chem. C* **111**, 18326 (2007).
- [92] M.M. Islam, M.T. Alam, and T. Ohsaka, *J. Phys. Chem. C* **112**, 16568 (2008).
- [93] V. Lockett, R. Sedev, J. Ralston, M. Horne, and T. Rodopoulos, *J. Phys. Chem. C* **112**, 7486 (2008).
- [94] M. Mezger, H. Schröder, H. Reichert, S. Schramm, J. S. Okasinski, S. Schöder, V. Honkimäki, M. Deutsch, B. M. Ocko, J. Ralston, M. Rohwerder, M. Stratmann, and H. Dosch, *Science* **322**, 424 (2008).
- [95] R. Hayes, S. Z. El Abedin and R. Atkin, *J. Phys. Chem. B* **113**, 7049 (2009).
- [96] S. Perkin, L.Crowhurst, H. Niedermeyer, T. Welton, A. M. Smith and N. N. Gosvami, *Chem. Commun.* **47**, 6572 (2011).
- [97] A. M. Smith, K. R. J. Lovelock and S. Perkin, *Faraday Discuss.* **167**, 279 (2013).
- [98] R. Yamamoto, H. Morisaki, O. Sakata, H. Shimotani, H. Yuan, Y. Iwasa, T. Kimura and Y. Wakabayashi, *Appl. Phys. Lett.* **101**, 053122 (2012).
- [99] M.V. Fedorov and A. A. Koornyshev, *Chem. Rev.* **114**, 2978 (2014).
- [100] M. S. Kilic, M. Z. Bazant, and A. Ajdari, *Phys. Rev. E* **75**, 021502 (2007).

- [101] M. P. Tosi, in *Condensed matter physics aspects of electrochemistry*, edited by M. P. Tosi and A. A. Kornyshev (World Scientific, Singapore, 1991), p. 68.
- [102] J.W. Cahn and J.W. Hilliard, *J. Chem. Phys.* **28**, 258 (1958).
- [103] C. Merlet, B. Rotenberg, P. A. Madden and M. Salanne, *Phys. Chem. Chem. Phys.* **15**, 1578 (2013).
- [104] R. Kjellander , S. Marčelja , R. M. Pashley , J. P. Quirk, *J. Phys. Chem.* **92**, 6489 (1988).
- [105] P. Kékicheff, S. Marčelja, T. J. Senden and V. E. Shubin, *J. Chem. Phys.* **99**, 6098 (1993)
- [106] L. Guldbbrand, B. Jönsson, H. Wennerström and P. Linse, *J. Chem. Phys.* **80**, 2221 (1984).
- [107] B. Svensson and B. Jönsson, *Chem. Phys. Lett.* **108**,580 (1984).
- [108] R. Kjellander, T. Åkesson, B. Jönsson and S. Marčelja, *J. Chem. Phys.* **97**, 1424 (1992).
- [109] A. G. Moreira and R. R. Netz, *Eur. Phys. J. E* **8**, 33 (2002).
- [110] R. Kjellander and S. Marčelja, *Chem. Phys. Lett.* **112**, 49 (1984).
- [111] Y. Burak and D. Andelman, *Phys. Rev. E* **62**, 5296 (2000).
- [112] D. Beysens and D. Estève, *Phys. Rev. Lett.* **54**, 2123 (1985).
- [113] D. Bonn, J. Otwinowski, S. Sacanna, H. Guo, G. Wegdam, and P. Schall, *Phys. Rev. Lett.* **103**, 156101 (2009).
- [114] C. Hertlein, L. Helden, A. Gambassi, S. Dietrich and C. Bechinger, *Nature* **451**, 172 (2008).
- [115] U. Nellen, J. Dietrich, L. Helden, S. Chodankar, K. Nygard, J. F. van der Veen and C. Bechinger, *Soft Matter* **7**, 5360 (2011).
- [116] M. Bier, A. Gambassi, M. Oettel and S. Dietrich, *Europhys. Lett.* **95**, 60001 (2011).
- [117] F. Pousaneh and A. Ciach, *J. Phys.: Condens. Matter* **23**, 412101 (2011).
- [118] F. Pousaneh, A. Ciach and A. Maciolek, *Soft Matter* **10**, 470 (2014).

- [119] S. Samin and Y. Tsori, J. Chem. Phys. **136**, 154908 (2012).
- [120] M. Krech, *Casimir Effect In Critical Systems*, (World Scientific, Singapore, 1994).
- [121] Y. Rosenfeld, J. Chem. Phys. **89**, 4272 (1988).
- [122] Y. Rosenfeld, Phys. Rev. Lett. **63**, 980 (1989).
- [123] G. Lippmann, Ann. Chim. Phys. **5**, 494 (1875).
- [124] M. H. Pellat, C. R. Hebd. Séances Acad. Sci. **119**, 675 (1894).
- [125] M. H. Pellat, C. R. Hebd. Séances Acad. Sci. **121**, 938 (1895).
- [126] M. J. Sparnaay, Surf. Sci. **1**, 213 (1964).
- [127] J. A. M. Sondag-Huethorst and L.G.J. Fokkink, Langmuir **8**, 2560 (1992).
- [128] B. Berge, C. R. Acad. Sci. II **317**, 157 (1993).
- [129] M. Vallet, B. Berge, and L. Vovelle, Polymer **37**, 2465 (1996).
- [130] W. J. J. Welters and L.G.J. Fokkink, Langmuir **14**, 1535 (1998).
- [131] T. D. Blake, A. Clarke, and E.H. Stattersfield, Langmuir **16**, 2928 (2000).
- [132] C. Decamps and J. De Coninck, Langmuir **16**, 10150 (2000).
- [133] A. Quinn, R. Sedev, J. Ralston, J. Phys. Chem. B **107**, 1163 (2003).
- [134] T. B. Jones, K.-L. Wang, and D.-J. Yao, Langmuir **20**, 2813 (2004).
- [135] A. Quinn, R. Sedev, J. Ralston, J. Phys. Chem. B **109**, 6268 (2005).
- [136] D. Klarman and D. Andelman, Langmuir **27**, 6031 (2011).
- [137] R. Sedev, Eur. Phys. J. Special Topics **197**, 307 (2011).
- [138] C. D. Daub, D. Bratko, and A. Luzar, Top. Curr. Chem. **307**, 155 (2012).
- [139] M. Bier and I. Ibagón, Phys. Rev. E **89**, 042409 (2014).
- [140] L. Chen, E. Bonaccorso, Adv. Colloid Interface Sci. **210**, 2 (2014).
- [141] T. B. Jones, K.-L. Wang, and D.-J. Yao, Langmuir **20**, 2813 (2004).
- [142] H. J. J. Verheijen and M. W. J. Prins, Langmuir **15**, 6616 (1999).

- [143] S. Millefiorini, A. H. Tkaczyk, R. Sedev, J. Efthimiadis, and J. Ralston, *J. Am. Chem. Soc.* **128**, 3098 (2006).
- [144] C. Quilliet and B. Berge, *Curr. Opin. Colloid Interface Sci.* **6**, 34 (2001).
- [145] A. Amirfazli, A.W. Neumann, *Adv. Colloid Interface Sci.* **110**, 121 (2004).
- [146] V. Raspal, K. O. Awitor, C. Massard, E. Feschet-Chassot, R. S. P. Bokalawela, and M. B. Johnson, *Langmuir* **28**, 11064 (2012).
- [147] R. Aveyard, J. H. Clint and T. S. Horozova, *Phys. Chem. Chem. Phys.* **5**, 2398 (2003).
- [148] D. Duncan, D. Li, J. Gaydos, A.W. Neumann, *J. Colloid Interface Sci.* **169**, 256 (1995).
- [149] L. Schimmele, M. Napi rkowski, and S. Dietrich, *J. Chem. Phys.* **127**, 164715 (2007).
- [150] J. O. Indekeu, *Physica A* **183**, 439 (1992).
- [151] J. O. Indekeu, *Int. J. Mod Phys B* **8**, 309 (1994).
- [152] A. I. Rusanov, *Surf. Sci. Rep.* **58**, 111 (2005).
- [153] R. Digilov, *Langmuir* **16**, 6719 (2000).
- [154] K. H. Kang, I. S. Kang, and C. M. Lee, *Langmuir* **19**, 9334 (2003).
- [155] T. Chou, *Phys. Rev. Lett.* **87**, 106101 (2001).
- [156] A. Dörr and S. Hardt, *Phys. Rev. E* **86**, 022601 (2012).
- [157] S. Das and S. K. Mitra, *Phys. Rev. E* **88**, 033021 (2013).
- [158] A. Dörr and S. Hardt, *Phys. Fluids* **26**, 082105 (2014).
- [159] P. Hohenberg and W. Kohn, *Phys. Rev.* **136**, B864 (1964).
- [160] W. Kohn and L. J. Sham, *Phys. Rev.* **140**, A1133 (1965).
- [161] N. D. Mermin, *Phys. Rev.* **137**, A1441 (1965).
- [162] R. Evans, *Adv. Phys.* **28**, 143 (1979).
- [163] R. Evans, in *Fundamentals of Inhomogeneous Fluids*, edited by D. Henderson (Marcel Dekker, New York, 1992), p. 85.

- [164] M. Levy, Proc. Natl. Acad. Sci. USA **76**, 6062 (1979).
- [165] W. S. B. Dwandaru and M. Schmidt, Phys. Rev. E **83**, 061133 (2011).
- [166] D. H. Everett, *Basic Principles of Colloid Science*, RSC Paperbacks (The Royal Society of Chemistry, London, 1988).
- [167] M. G. Pollack, R. B. Fair, and A. D. Shenderov, Appl. Phys. Lett. **77**, 1725 (2000).
- [168] O. D. Velev, B. G. Prevo, and K. H. Bhatt, Nature **426**, 515 (2003).
- [169] I. Ibagon, M. Bier, and S. Dietrich, J. Chem. Phys. **138**, 214703 (2013).
- [170] M. Rubinstein and R. H. Colby, *Polymer Physics* (Oxford University Press, 2004).
- [171] J. W. Cahn and J. E. Hilliard, J. Chem. Phys. **28**, 258 (1958).
- [172] H. Nakanishi and M. Fisher, Phys. Rev. Lett. **49**, 1565 (1982).
- [173] C.J.F. Böttcher, *Theory of Electric Polarization* (Elsevier, Amsterdam, 1973).
- [174] T. Aukrust and E. H. Hauge, Phys. Rev. Lett. **54**, 1814 (1985).
- [175] T. Getta and S. Dietrich, Phys. Rev. E **57**, 655 (1998).
- [176] J. D. Jackson, *Classical Electrodynamics*, 3rd ed. (Wiley, New York, 1999).
- [177] M. S. Wertheim, J. Chem. Phys. **55**, 4291 (1971).
- [178] S. L. Carnie and D. Y. C. Chan, J. Chem. Phys. **73**, 2949 (1980).
- [179] J. L. Lebowitz and E. H. Lieb, Phys. Rev. Lett. **22**, 631 (1969).
- [180] E. H. Lieb and J. L. Lebowitz, Adv. Math. **9**, 316 (1972)
- [181] Z. Xu, Phys. Rev. E **87**, 013307 (2013).
- [182] L. Bocquet, E. Trizac, and M. Aubouy J. Chem. Phys. **117**, 8138 (2002).
- [183] C. J. F. Böttcher, O. C. van Belle, P. Bordewijk and A. Rip, *Theory of Electric Polarization: Dielectrics in Static Fields* (Elsevier, Amsterdam, 1973).
- [184] M. Bellac, *Quantum and Statistical Field Theory* (Oxford Science Publications, 1991).

- [185] M. Plischke and B. Bergersen, *Equilibrium Statistical Physics*, 2nd ed. (World Scientific, Singapore, 2006).
- [186] P. M. Chaikin and T. Lubensky, *Principles of Condensed Matter Physics* (Cambridge University Press, 2000).
- [187] S. A. Safran, *Statistical Thermodynamics of Surfaces, Interfaces, and Membranes* (Westview, Boulder, 2003).
- [188] J. Sonnefeld, *Colloids Surf. A* **108**, 27 (1996).
- [189] C. Seah, C. A. Grattoni, and R. A. Dawe, *Fluid Phase Equilib.* **89**, 345 (1993).
- [190] R. Pandit, *Phys. Rev. B* **26**, 5112 (1982).
- [191] R. Pandit and M. Wortis, *Phys. Rev. B* **25**, 3226 (1982).
- [192] K. Binder and D. P. Landau, *Phys. Rev. B* **37**, 1745 (1988).
- [193] K. Binder, D. P. Landau, and S. Wansleben, *Phys. Rev. B* **40**, 6971 (1989).
- [194] M. D. Oliveira and R. B. Griffiths, *Surf. Sci.* **71**, 687 (1978).
- [195] C. Ebner, *Phys. Rev. A* **22**, 2776 (1980).
- [196] C. Ebner, *Phys. Rev. A* **23**, 1925 (1981).
- [197] S. Dietrich and M. Schick, *Phys. Rev. B* **31**, 4718 (1985).
- [198] C. Ebner, W. F. Saam, and A. K. Sen, *Phys. Rev. B* **31**, 6134 (1985).
- [199] J. O. Indekeu, K. Ragil, D. Bonn, D. Broseta, and J. Meunier, *J. Stat. Phys.* **95**, 1009 (1999).
- [200] J. O. Indekeu, *Phys. Rev. Lett.* **85**, 4188 (2000).
- [201] J. Piasecki and E. H. Hauge, *Physica A* **143**, 87 (1987).
- [202] J. O. Indekeu, *Europhys. Lett.* **10**, 165 (1989).
- [203] G. Langie and J. O. Indekeu, *J. Phys. Condens. Matter* **3**, 9797 (1991).
- [204] N. Shahidzadeh, D. Bonn, K. Ragil, D. Broseta, and J. Meunier, *Phys. Rev. Lett.* **80**, 3992 (1998).
- [205] D. E. Sullivan, *Phys. Rev. B* **20**, 3991 (1979).

- [206] D.C. Grahame, *Chem. Rev.* **41**, 441 (1947).
- [207] J. Lyklema, *Fundamentals of interface and colloid science, Vol. I* (Academic Press, London, 1991).
- [208] J. S. Rowlinson and B. Widom, *Molecular Theory of Capillarity* (Dover, Mineola, 2002).
- [209] P.-G. de Gennes, F. Brochard-Wyart, and D. Queré, *Capillarity and Wetting Phenomena* (Springer, New York, 2004).
- [210] L. D. Landau and E.M. Lifshitz, *Fluid mechanics (Volume 6 of Course of Theoretical Physics)* (Elsevier, Amsterdam, 2005).
- [211] H. D. Inerowicz, W. Li, and I. Persson, *J. Chem. Soc. Faraday Trans.* **90**, 2223 (1994).
- [212] C. Kalidas, G. Hefter, and Y. Marcus, *Chem. Rev.* **100**, 819 (2000).
- [213] Y. Marcus, *Chem. Rev.* **107**, 3880 (2007).
- [214] K. H. Kang, *Langmuir* **18**, 10318 (2002).
- [215] S. Dietrich and M. Napiórkowski, *Phys. Rev. A* **43**, 1861 (1991).
- [216] T. Meister and H. Müller-Krumbhaar, *Phys. Rev. Lett.* **51**, 1780 (1983).
- [217] R. Lipowsky, *Z. Phys. B* **55**, 345 (1984).
- [218] R. Hołyst and A. Poniewierski, *Phys. Rev. A* **36**, 5628 (1987).
- [219] M. P. Gelfand and R. Lipowsky, *Phys. Rev. B* **36**, 8725 (1987).
- [220] A. J. Jin and M.E. Fisher, *Phys. Rev. B* **47**, 7365 (1993).
- [221] M. Iwamatsu, *J. Phys.: Condens. Matter* **5**, 7537 (1993).
- [222] A. O. Parry, C. Rascón, N.R. Bernardino, and J.M. Romero-Enrique, *J. Phys.: Condens. Matter* **18**, 6433 (2006).
- [223] A. Wójtowicz and M. Napiórkowski, *J. Phys.: Condens. Matter* **25**, 485007 (2013).
- [224] C. Bauer and S. Dietrich, *Eur. Phys. J. B* **10**, 767 (1999).

- [225] R.-J. Merath, Microscopic calculation of line tensions, doctoral thesis, Universität Stuttgart (2008).
- [226] I. Ibagón, M. Bier and S. Dietrich, *J. Chem. Phys.* **140**, 174713 (2014).



# Curriculum vitae

**Ingrid Carolina Ibagon Pardo**

Born 1986 in Choachí, Colombia

2010-2014 Doctoral studies at Max-Planck-Institut für Intelligente Systeme and IV.Institut für Theoretische Physik, Universität Stuttgart (Stuttgart, Germany)  
Advisors: Prof. Dr. S. Dietrich and Dr. Markus Bier  
Topic: Wetting in electrolyte solutions

2008-2010 Master in Physics at Universidade Federal de Minas Gerais (Belo Horizonte, Brazil)  
Advisor: Prof. Dr. Helio Chacham  
Topic: FeN<sub>4</sub> defects in carbon nanostructures: a comparative study with Fe-porphyrin and Fe-phthalocyanine molecules

2003-2007 Graduation in Physics at Universidad Nacional de Colombia (Bogotá, Colombia)  
Advisor: Ramiro Cardona  
Topic: Electronic structure of iron-porphyrin and its bond with O<sub>2</sub>, CO and CN molecules.